CARNEGIE
INSTITUTION

Annual Report of the Director Geophysical Laboratory

2801 UPTON STREET, NORTHWEST, WASHINGTON, D.C. 20008-3898

1988-1989

For the year July 1, 1988-June 30, 1989
Issued December 1989
Papers from the Geophysical Laboratory
Carnegie Institution of Washington
NO. 2150

Geophysical Laboratory

Washington, District of Columbia

Charles T. Prewitt
Director

Published by: Geophysical Laboratory
2801 Upton St., N.W.
Washington, D.C., 20008-3898
USA

ISSN 0576-792X

December 1989

When used in bibliographic citations, The Annual Report should be cited as follows:

Author, Title, *Annual Report of the Director of the Geophysical Laboratory, Carnegie Instn. Washington, 1988-1989,* Geophysical Laboratory, Washington, D.C., page range, 1989.

GEOPHYSICAL LABORATORY

CONTENTS

INTRODUCTION

This is the second year in which the Annual Report of the Director is published by the Geophysical Laboratory using desktop publishing techniques. I would like to thank the many people who wrote in response to last year's Report telling us that you were glad to see it revived after an absence of several years. We continue to feel that the Report is a very important part of our communication with the scientific community and take pleasure in preparing the scientific articles and sending the Report to those on our mailing list. I again emphasize that the articles in these issues are only progress reports and that you should expect to see the final results published in the refereed scientific literature.

I am pleased to report that the Geophysical Laboratory had a very successful year during 1988-1989, with a wide range of research activity by staff members, postdoctoral fellows, and visitors. Next year, 1990, will be one of great change for the Geophysical Laboratory staff and also for our colleagues at the Department of Terrestrial Magnetism. A new laboratory building is now under construction at the DTM site and we plan to move to this new building during the summer or early fall of 1990. A resolution was passed by the Carnegie Institution of Washington Trustees in May 1986 to "Authorize the President to commission the development of an architectural schematic plan for new construction and renovation of existing structures on the Broad Branch Road site in Washington, DC, appropriate to co-location of the Geophysical Laboratory and the Department of Terrestrial Magnetism." Since that time, we have been involved in devising the general requirements for the building, working with the architectural firm of Peirce, Pierce & Kramer of Cambridge, Massachusetts, to produce a detailed design, and in planning for the actual transfer of equipment and personnel to the new facility. The New Research Building will have about 72,000 gross square feet of floor space, and the present main DTM building will be renovated to contain administrative, library, and auditorium facilities. The present Cyclotron Building will be expanded and refurbished, and will include clean laboratory facilities for use by the geochemists of the two departments. Many of us are sad at having to leave the Upton Street location that has served us so well for 85 years, but the prospect of having an increased amount of modern laboratory space and the great opportunity of expanding our horizons through collaboration with the DTM staff are very appealing.

As this will be the last Annual Report published before the move to DTM takes place, I asked Director Emeritus Hatten S. Yoder, Jr. to write a section for this Report on the history of the Geophysical Laboratory and he agreed to do so. As a relative newcomer to the Lab, I am always impressed when I read or hear about its history and the people who have worked here during the 85 years of its existence. Rather small as research institutions go, the Lab usually has had about fifteen or sixteen

research staff members at any one time along with ten to fifteen Post- and Predoctoral Fellows and visitors.

The Laboratory building itself was constructed for only $75,940 in 1905 and research budgets through the years have been relatively modest. However, the Lab's impact on geoscience has been enormous; I believe this is the result of the Carnegie Institution's policy of letting its scientists pursue their own goals with a minimum of interference. In a time when national research budgets are tight and industrial laboratory managements are requiring more applied research, I think the Carnegie ideal is a very important concept to maintain as an example of what can be done with limited financial support coupled with flexibility and freedom in choosing research topics.

A development of great interest to the Geophysical Laboratory is the recent establishment of the Bayersiches Forschungsinstitut für Experimentelle Geochemie und Geophysik at the Universität Bayreuth. The founding of this institute was influenced greatly by the Geophysical Laboratory experience and its Director, Friedrich Seifert, was a Postdoctoral Fellow and Staff Member here in the 1970s and early 1980s. This initiative has created worldwide interest among geoscientists and is considered to be one of the more exciting developments in the basic earth sciences in recent years. It is interesting to note that when the Geophysical Laboratory was founded early in this century, it was based to a great extent on the experience of German laboratories and institutes. Now it appears that the circle has been completed.

It is with regret that I report that research staff member Peter Bell decided to take early retirement at the end of June 1989. During his 25 years at the Lab, Peter made many contributions in geophysics, mineral physics, and petrology. The collaboration between Bell and Ho-kwang Mao was especially productive and they became known as the world's leading proponents and users of the diamond-anvil cell for ultra-high-pressure research. Peter was a valuable member of our research staff and we will miss his involvement in day-to-day research activities. However, he will retain an official connection with the Lab and will continue to advise and consult with us in his areas of expertise and interest.

IGNEOUS AND METAMORPHIC PETROLOGY - A. FIELD STUDIES

KAAPVAAL SPINEL PERIDOTITES: EVIDENCE OF CRATON ORIGIN

Francis R. Boyd

Continental cratons have mantle roots that extend to depths of at least 200 km, giving cratonic lithosphere a thickness that is two or more times that of oceanic plates. Cratonic lithosphere differs from oceanic in composition as well as in thickness. The garnet peridotites that are the principal components of the Kaapvaal lithosphere, southern Africa, have markedly lower Mg/Si, lower Ca/Al and higher Mg/Fe than do residual oceanic peridotites and their compositional relations are believed to be representative of other cratons (Boyd, 1989). The origin of these differences in structure and composition between cratons and oceanic plates is an important chapter in Earth history.

There are few constraints on the origin of craton roots other than their Archaean age (Richardson *et al.*, 1984). At least two scenarios seem possible. Cratonic nuclei might have developed at oceanic spreading centers and subsequently been underplated by peridotites having compositions similar to Kaapvaal garnet peridotites. If that origin occurred, peridotites now forming the shallow portions of craton roots should have composition typical of oceanic peridotites. Alternatively, the cratonic lithosphere in its entirety may be uniquely different in composition and origin from oceanic lithosphere. In that event, peridotites forming the top of a craton root would have compositions similar to the underlying garnet peridotites.

Evidence required to distinguish between these possible processes of craton development can be obtained by study of the compositional relations of the spinel-facies peridotites that occupy the upper portion of the craton lithosphere. Spinel peridotites are of widespread occurrence in xenolith suites of the Kaapvaal craton, having been collected at over a dozen localities in South Africa and Lesotho. Their proportions in individual xenolith suites vary widely from small to amounts approaching those of garnet peridotites. The relative abundance of spinel peridotites led Carswell *et al.* (1984) to propose that they form a continuous layer at the top of the craton lithosphere, overlying garnet peridotites that are the principal rock type at greater depth.

The depth at which the assemblage Mg-rich garnet + olivine replaces aluminous pyroxene + spinel is the boundary dividing the spinel- and garnet-facies peridotites. This depth is difficult to estimate by thermobarometric methods because many of the peridotites that occur near the top of the lithosphere have failed to equilibrate at relatively low ambient temperatures and

TABLE 1. Mineral and Bulk Analyses for Spinel Peridotite PHN 5254, Premier mine, R. S. A., wt%.

	Bulk*	Olivine	Enstatite	Diopside	Spinel
SiO_2	43.14	40.6	56.7	54.8	0.06
TiO_2	0.05	<0.03	0.05	0.12	0.09
Al_2O_3	1.36	<0.03	2.57	3.34	41.6
Cr_2O_3	0.43	<0.03	0.41	1.21	26.8
Fe_2O_3	2.78	-	-	-	-
FeO	4.21	7.78	5.11	1.40	12.0
MnO	0.12	0.11	0.14	0.07	0.16
MgO	42.47	50.9	35.6	16.4	18.4
CaO	1.53	<0.03	0.65	22.4	<0.03
Na_2O	0.08	n.d.	0.06	1.34	n.d.
K_2O	0.10	n.d.	n.d.	n.d.	n.d.
P_2O_5	0.00	n.d.	n.d.	n.d.	n.d.
NiO	0.27	0.40	0.09	0.06	0.18
LOI	4.53	-	-	-	-
Totals	101.07	99.8	101.4	101.1	99.3
Mg/(Mg + Fe)**	0.919	0.921	0.925	0.954	0.731
Ca/(Ca + Mg)**	-	-	0.013	0.496	-

MODES

Olivine	66.6
Enstatite	25.2
Diopside	6.3
Spinel	1.3

*S. A. Mertzman, analyst
**mole fractions

their pyroxenes are chemically inhomogeneous. Nevertheless, the transition depth can be estimated to be near 50-55 km on the basis of experimental data (Wood and Holloway, 1984). If the base of the crust in the Kaapvaal craton is 40 km, the thickness of a spinel peridotite layer may then be 10-15 km.

A chemical feature that effectively characterizes most Kaapvaal spinel peridotites (Table 1) is that the alumina content of the orthopyroxene is in the range 1.5 - 4 wt %, contrasting with values of 0.7 - 1.0 wt % for the underlying garnet peridotites. Amphibole (pargasite)-bearing spinel peridotites form an exception to this generalization, however, because their alumina contents of orthopyroxene are low, 0.5 - 0.6 wt % (e.g. Boyd, 1971). Spinels are more aluminous than the chromites in garnet facies rocks and there is a positive correlation for the concentration of Al_2O_3 in coexisting spinel and orthopyroxene (Carswell *et al.*, 1984). Diopsides in the spinel peri-

dotites contain somewhat less Cr_2O_3 (average 1.0 wt.%) than is commonly found in diopsides in garnet lherzolites.

Distinctive textural characteristics of the spinel peridotites include an unusually coarse grain size, commonly 1-2 cm. The enstatite in almost all specimens have thin exsolution lamellae, presumed to be clinopyroxene. The igneous age of the spinel peridotites, like that of the garnet peridotites, may be Archaean, but the age of the exsolution is not known. The spinel characteristically forms symplectites (Dawson and Smith, 1975) with olivine and pyroxene as well as amphibole and mica; this habit contrasts markedly with the bleb-like texture of primary spinels in peridotite xenoliths in basaltic volcanics. Two specimens from the Premier mine have the textural characteristics of spinel peridotites but contain small amounts of fine-grained interstitial garnet; these are taken to be transitional between the spinel and garnet facies.

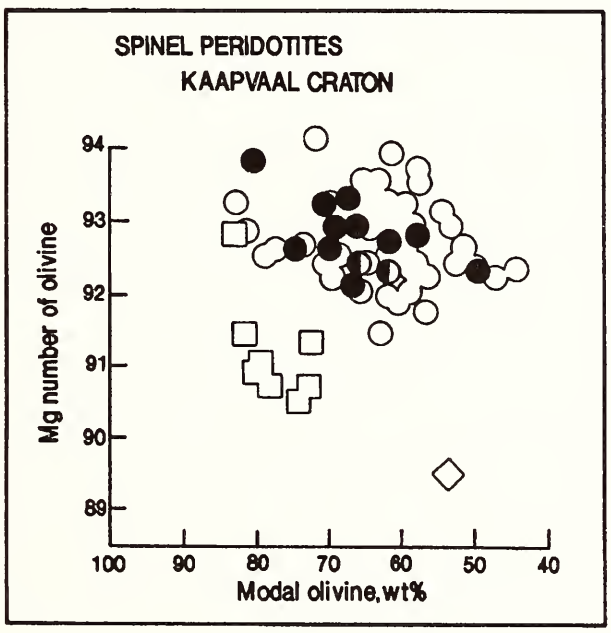

FIG. 1. Compositional data for Kaapvaal spinel peridotites (solid circles) and transitional rocks (half solid circles) compared with data for low-temperature, Kaapvaal garnet peridotites (open circles), oceanic residues (open squares), and pyrolite (open diamond). Most of the spinel peridotites are from the Premier mine but samples from Kimberley, Frank Smith and Letseng are included. Sources of data for the oceanic residues and garnet peridotites are listed in Boyd (1989) and the pyrolite composition is from Ringwood (1979). Modes for the Kaapvaal rocks were calculated from the mineral and bulk analyses. Analytical samples for the bulk analyses were approximately 0.5 kg and were analyzed by S. A. Mertzman.

Insights to the origin of the spinel peridotites can be obtained by comparing their bulk compositions with those of cratonic garnet peridotites and oceanic peridotites. A plot of the modal abundance of olivine against mg number [mg number = Mg/(Mg + Fe)] for either olivine or the whole rock does an excellent job of discriminating oceanic residues and craton-forming, low-temperature garnet peridotites (Fig. 1). The oceanic harzburgites represented by abyssal peridotites and ophiolite tectonites have 70-80% olivine and mg numbers predominantly in the range 0.905-0.915. The cratonic peridotites from the Kaapvaal are enstatite-rich with 20-45% modal enstatite, 40-80% modal olivine and mg numbers of 0.920 - 0.935.

Points for the Kaapvaal spinel peridotites superimposed on plots for low-temperature garnet peridotites and oceanic peridotites clearly overlap the garnet-facies rocks (Fig. 1). These data suggest a common origin for the Kaapvaal peridotites, whether of spinel or garnet facies. The compositional differences between these cratonic peridotites and oceanic residues make it appear unlikely that any large part of the Kaapvaal craton originated as an

oceanic plate. Cratonic peridotites may have formed as bouyant residues of segregated ultramafic liquids at depths of 300-400 km (Boyd, 1989). The circumstances in which these residues floated in a denser, more fertile and largely crystalline mantle and coalesced to form proto-cratons are difficult to clarify. Underplating may have played a role in this process, however, and the spinel peridotites at the top of the cratonic lithosphere might be the oldest rocks in these ancient tectonic blocks.

References

Boyd, F. R., Compositional distinction between oceanic and cratonic lithosphere, *Earth Planet Sci. Lett.*, in press, 1989.

Boyd, F. R., Pargasite - spinel peridotite xenolith from the Wesselton Mine, *Carnegie Instn. Washington Year Book, 70,* 138-142, 1971.

Carswell, D. A., W. L. Griffin, and P. Kresten, Peridotite nodules from the Ngopetsoeu and Lipelaneng kimberlites, Lesotho: a crustal or mantle origin?, in *Kimberlites - II: The Mantle and Crust-Mantle Relationships*, J. Kornprobst, ed., Elsevier, New York, pp. 229-243, 1984.

Dawson, J. B. and J. V. Smith, Chromite - silicate intergrowths in upper-mantle peridotites, *Phys. Chem. Earth, 9,* 339-350, 1975.

Richardson, S. H., J. J. Gurney, A. J. Erlank, and J. W. Harris, Origin of diamonds in old enriched mantle, *Nature, 310*, 198-202, 1984.

Ringwood, A. E., *Origin of the Earth and the Moon*, Springer-Verlag, New York, 1979.

Wood, B. J., and J. R. Holloway, A thermodynamic model for subsolidus equilibria in the system CaO - MgO - Al_2O_3 - SiO_2, *Geochim. Cosmochim. Acta, 48,* 159-176, 1984.

Rare Earth Element Zoning in Pyrope-rich Garnets From Mantle Xenoliths

Donald D. Hickmott

Studies of mantle xenoliths in alkali basalts and kimberlites provide direct evidence concerning the chemical constitution and evolution of the sub-crustal lithosphere and upper asthenosphere. The abundances and isotopic compositions of the rare earth elements have been particularly important in determining the geochemical evolution of these rocks.

Garnet peridotites from the Archeaen Kaapvaal craton can be divided into two texturally and chemically distinct classes, the granular lherzolites and the sheared lherzolites (Boyd and Nixon, 1973). Thermobarometric determinations suggest that the latter equilibrated at higher temperatures (> 1100°C vs. <1100°C) and pressures (> 55 kbar vs. < 55 kbar) than the former (Finnerty and Boyd, 1987). The major elements Na, Al, Ca and Ti are generally enriched in the higher temperature peridotites (Nixon and Boyd, 1973; Boyd and Mertzman, 1987), as are the heavy rare earth elements (HREE) (Shimizu, 1975). Sr and Sc may be enriched in the low-*P-T* suite lherzolites relative to those of the high-*P-T* suite, based on reconstitution of bulk-rock abundances from element concentrations in garnet and clinopyroxene (Shimizu and Allegre, 1978). Low-*P-T* nodules contain more modal enstatite and less olivine than those from the high-*P-T* suite (Boyd and Mertzman, 1987; Boyd, 1989).

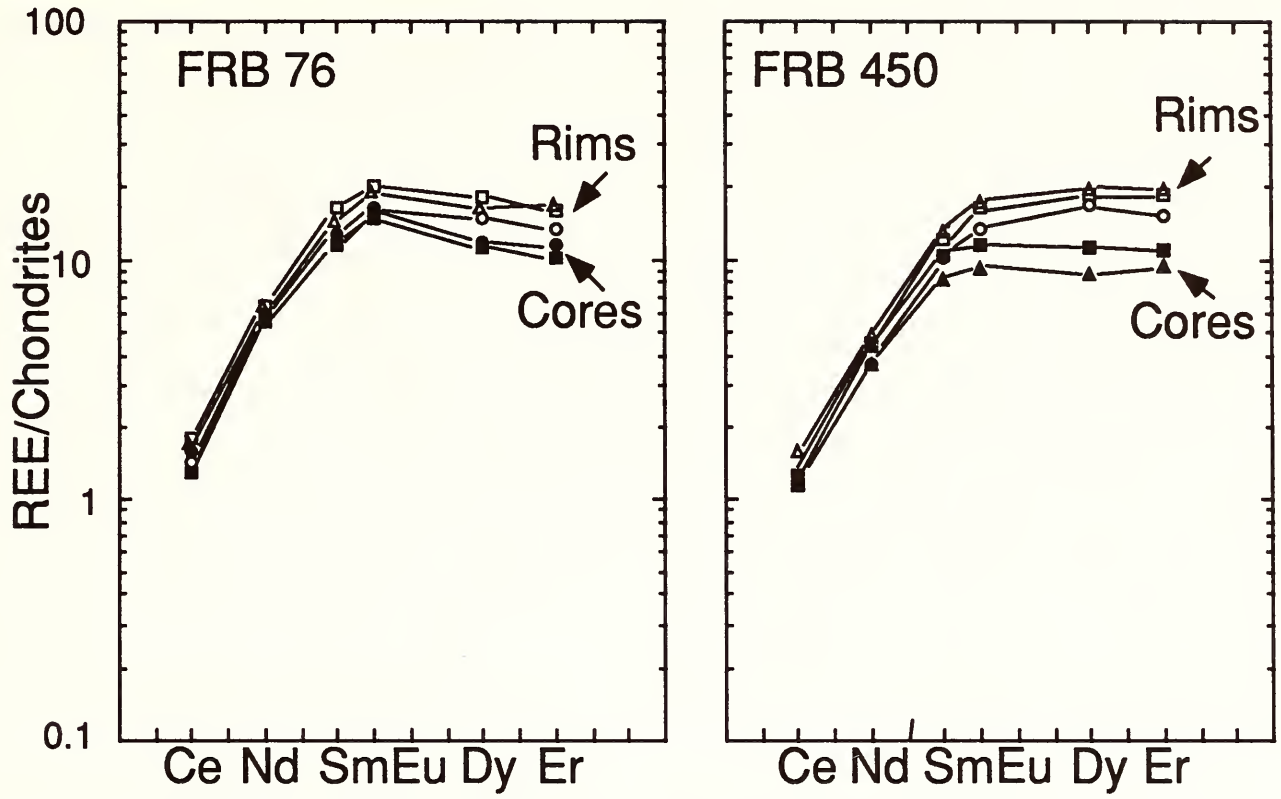

FIG. 2. Rare earth element abundances in two pyrope-rich garnets from the high-*P-T* suite. See Griffin *et al.* (1989) for a description of the petrography and chemistry of these samples. Open symbols - near-rim points; closed symbols - interior points.

The mineral zoning observed in mantle nodules provides constraints on the nature and timing of processes that occurred within the upper mantle prior to eruption of the host magma of a nodule. Smith and co-workers have documented zoning of Ti, Cr, Fe, Na and P in garnets from selected xenoliths from the Kaapvaal craton, South Africa and The Thumb, Colorado Plateau (Smith and Ehrenburg, 1984; Smith and Boyd, 1987; Smith, 1988). Griffin *et al.* (1989) determined that garnets from two samples from Frank Smith kimberlite were characterized by Fe, Ti, Y, Zr and Ga enrichments in their rims relative to their cores. They suggested: 1) that the rim enrichments could be explained by infiltration of an alkalic melt into the mantle rocks; 2) that the enrichments reflected re-equilibration of overgrowths on pre-existing garnet rather than simple diffusional re-equilibration of such garnets; and 3) that the enrichments occurred within a few hundred years prior to eruption of the host kimberlite.

Rare earth element abundances were measured in rims and cores of garnets from the two high-*P-T* suite samples (FRB 76 and FRB 450) previously investigated by Griffin *et al.* (1989) and one low-*P-T* suite garnet (PHN 2302A). The studied garnets from the high-*P-T* samples are from the same nodules, but are not the same crystals as those analyzed by Griffin *et al.* (1989). Analyses were made with a Cameca-IMS-3F ion microprobe with previously analyzed pyrope-rich garnets as standards. Analytical techniques are similar to those described by Shimizu and Richardson (1987). Estimated accuracy of the REE

analyses is ±10%. Yb abundances are not presented due to GdO molecular ion interferences on the Yb mass spectra.

All of the REE investigated in the high-*P-T* samples are enriched in garnet rims relative to garnet cores (Fig. 2). Cerium rises by a small amount (less than 20%), whereas Er rises up to a factor of two; thus HREE/LREE ratios increase from core to rim. In contrast, garnets from lherzolite PHN 2302A from the low-*P-T* suite are HREE enriched and LREE depleted in their rims relative to cores (Fig. 3). Cerium drops up to 70% from roughly 1.7 ppm to 0.4 ppm, whereas Er rises up to a factor of three (0.3 ppm to 1.1 ppm).

The trace element signature of the garnet cores may provide constraints on the nature and evolution of the mantle in the source region of the kimberlites prior to final interaction with a metasomatizing agent, whereas that of the rim may help identify that metasomatic agent. The high LREE abundances of the cores of the high-*P-T* suite garnets relative to chondrites are incompatible with the hypothesis that the rocks are directly residual to magma generation from a chondritic mantle. These samples may have experienced an earlier episode of fluid or melt infiltration prior to their most recent metasomatism. The low abundance of HREE in the core of the low-*P-T* suite garnet suggests that the granular nodules interacted with a LREE-enriched fluid or melt in the absence of garnet prior to subsolidus growth of the garnet cores (Shimizu, 1975). The relatively high modal abundance of garnet in many low-*P-T* nodules may require an episode of metamorphic differentiation subsequent to garnet nucleation.

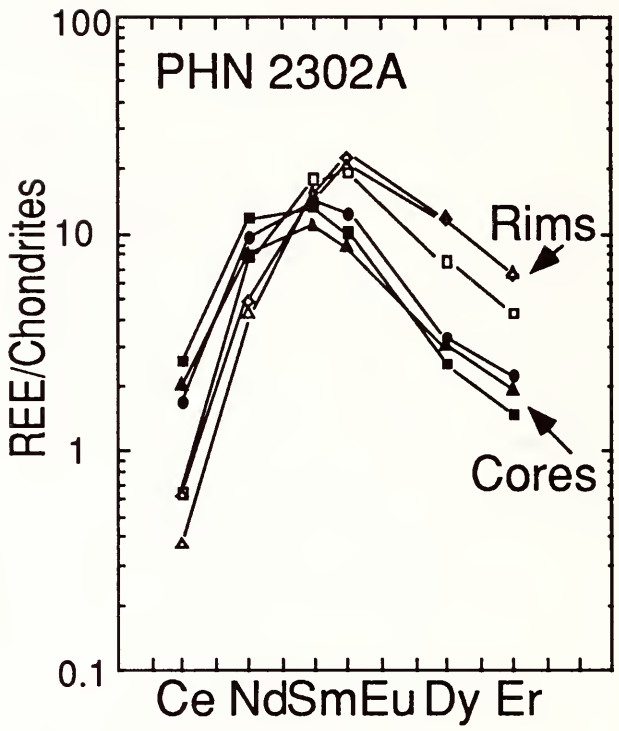

FIG. 3. Rare earth element abundances in a pyrope-rich garnet from the low *P-T* suite. See Boyd (1974), Shimizu (1975) and Shimizu and Allegre (1978) for petrographic and chemical data pertaining to this sample. Open symbols - near-rim points; closed symbols, interior points.

Rare earth element patterns for hypothetical magmatic liquids calculated to be in equilibrium with the rims of the three samples are strongly LREE enriched relative to chondrites (Fig. 4). Selection of alternate sets of partition coefficients for this calculation (i.e., Irving and Frey, 1978) leads to varying absolute REE abundances in calculated liquids, but yield roughly similar REE patterns to those shown. The calculated patterns for both the low-*P-T* and high-*P-T* suite samples are roughly similar in element abundance and slope to each other, although the low-*P-T* garnet may have interacted with a fluid with lower HREE abundance and higher MREE/HREE and MREE/LREE ratios than the high-*P-T* samples. Absolute abundances of the REE in the hypothetical liquids are in approximate agreement with REE abundances of

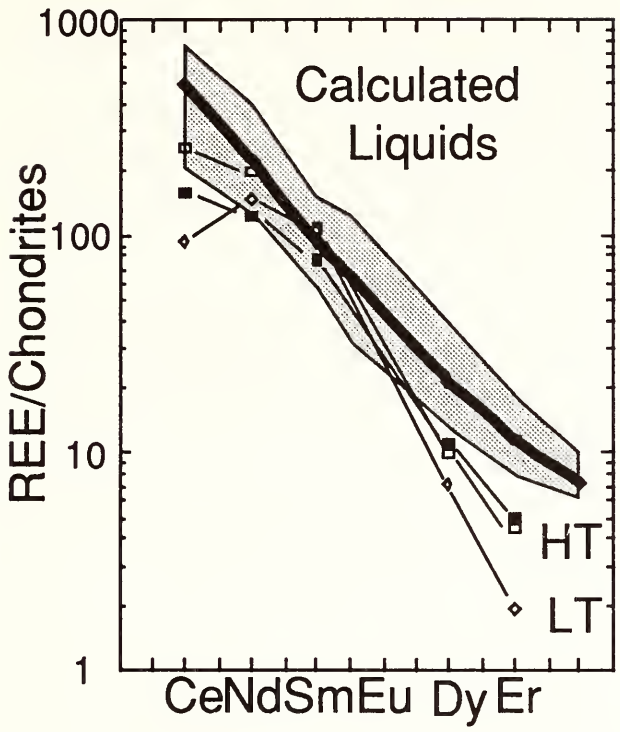

FIG. 4. Magmatic liquids calculated to be in equilibrium with select rim points of zoned, pyrope-rich garnets FRB 76, FRB 450 and PHN 2302A. Partition coefficients of Fujimaki *et al.* (1984) were used in the calculation. Diamond = PHN 2302A; square = FRB 450; open square = FRB 76. Shaded area shows upper- and lower-bounds of kimberlite data reported by Kramers *et al.* (1981). Solid symbols within shaded area is Kramers *et al.* (1981) "average kimberlite".

South African kimberlites (Fig. 4), except for Ce and the HREE, which are depleted relative to most kimberlites.

The simplest explanation for the major and trace element enrichments observed is that the nodules interacted with a melt with kimberlitic affinities. Alkali basalts generally have higher HREE abundances than kimberlites (Menzies *et al.*, 1987); thus, interaction with alkali basalt is unlikely. Hydrous fluid probably does not exist at the depth of origin of these nodules (Smith and Boyd, 1987) and mantle hydrous fluids are generally Ti-poor (Menzies *et al.*, 1987); a hydrous fluid is an unlikely metasomatic agent for the high-*P-T* rocks. The discrepancies between the calculated REE patterns and those observed in kimberlites may be due to 1) inaccurate knowledge of partition coefficients between garnet and melt at the depth in the mantle where these nodules were derived (Kramers *et al.*, 1981), or 2) interaction between the proto-kimberlite and minerals in the mantle prior to interaction with the studied garnets. The large grain-size (> 5 mm diameter) and small diffusion coefficients (Cygan and Lasaga, 1986) of garnets enhance preservation of chemical gradients in this mineral relative to clinopyroxene, olivine and orthopyroxene. It is possible that other minerals in the studied nodules have also interacted with the melt that caused the garnet zoning, even though they are unzoned (Griffin *et al.*, 1989).

Neodymium isotopic studies of lherzolite nodules in kimberlites have been hampered by contamination problems (Richardson *et al.*, 1985; Zindler and Jagoutz, 1988). The most primitive mantle isotopic compositions are frequently determined on the most painstakingly hand-picked and acid washed mineral separates (Richardson *et al.*, 1985; Zindler and Jagoutz, 1988). The present study of REE zoning in mantle garnets suggests that garnet isotopic compositions may also be sensitive to the relative percentages of rim-material and core-material in a given mineral separate. The intermineral isotopic disequilibrium observed in some studies (Allegre *et al.*, 1982) may reflect incomplete infiltrative re-equilibration of the isotopic signatures of garnets relative to co-existing minerals (Smith and Boyd, 1987).

The presence of REE zoning in these garnets suggests that both the trace element

and isotopic signatures of the mantle derived from kimberlitic nodules must be interpreted cautiously. Even in cases where there is no evidence for modal metasomatic effects, recent cryptic metasomatism can be imprinted on older trace element and isotopic signatures. Accurate characterization of mantle chemistry by xenolith studies requires an understanding of the processes that produce element zoning in mantle minerals.

References

Allegre, C. J., Shimizu, N., and D. Rousseau, History of the continental lithosphere recorded by ultramafic xenoliths, *Nature, 296*, 732-735, 1982.

Boyd, F. R., Ultramafic nodules from the Frank Smith Kimberlite Pipe, South Africa, *Carnegie Instn. Washington Year Book, 73*, 285-294, 1974.

Boyd, F. R., Compositional distinction between oceanic and cratonic lithosphere, *Earth Planet. Sci. Lett.*, in press, 1989.

Boyd, F. R., and S. A. Mertzman, Composition and structure of the Kaapvaal lithosphere, southern Africa, in *Magmatic Processes: Physicochemical Principles*, B.O. Mysen, ed., Spec. Pub. No. 1, The Geochemical Society, University Park, PA, pp.13-24, 1987.

Boyd, F. R., and P. H. Nixon, Structure of the upper mantle beneath Lesotho, *Carnegie Instn. Washington Year Book, 72*, 431-446, 1973.

Cygan, R., and A. C. Lasaga, Self-diffusion of magnesium in garnet at 750° to 900°C, *Am. J. Sci., 285*, 328-350, 1985.

Finnerty, A. A., and F. R. Boyd, Thermobarometry for garnet peridotites: basis for the determination of thermal and compositional structure of the upper mantle, in *Mantle Xenoliths*, P. H. Nixon, ed., John Wiley & Sons, New York, pp. 381-402, 1987.

Fujimaki, H., M. Tatsumoto and K. Aoki, Partition coefficients of Hf, Zr, and REE between phenocrysts and groundmasses, in *Proceedings of the 14th Lunar & Planetary Science Conference, Part 2, J. Geophys. Res., 89 Supplement*, pp. B662-B672, 1984.

Griffin, W. L., D. Smith, F. R. Boyd, D.R. Cousens, C. G. Ryan, S. S. Sie, and G. F. Suter, Trace element zoning in garnets from sheared mantle xenoliths, *Geochim. Cosmochim. Acta, 53*, 561-569, 1989.

Irving, A. J., and F. A. Frey, Distribution of trace elements between garnet megacrysts and host volcanic liquids of kimberlitic to rhyolitic composition, *Geochim. Cosmochim. Acta, 42*, 771-787, 1978.

Kramers, J. D., C. B. Smith, N. P. Lock, R. S. Harmon, and F. R. Boyd, Can kimberlites be generated from an ordinary mantle?, *Nature, 291*, 53-65, 1981.

Menzies, M., N. Rogers, A. Tindle, and C. Hawkesworth, Metasomatic and enrichment processes in lithospheric peridotites, an effect of asthenosphere - lithosphere interaction, in *Mantle Metasomatism*, M.A. Menzies & C.J. Hawkesworth, eds., Academic Press, New York, pp. 313-365, 1987.

Richardson, S. H., A. J. Erlank, and S. R. Hart, Kimberlite-borne garnet peridotite xenoliths from old enriched subcontinental lithosphere, *Earth Planet. Sci. Lett., 75*, 116-128, 1985.

Shimizu, N., Rare earth elements in garnets and clinopyroxenes from garnet lherzolite nodules in kimberlites, *Earth Planet. Sci. Lett., 25*, 26-32, 1975

Shimizu, N., and C. J. Allegre, Geochemistry of transition elements in garnet lherzolite nodules in kimberlites, *Contrib. Mineral. Petrol., 67*, 41-50, 1978.

Shimizu, N., and S. H. Richardson, Trace element abundance patterns of garnet inclusions in peridotite - suite diamonds, *Geochim. Cosmochim. Acta, 51*, 755-758, 1987.

Smith, D., Implications of zoned garnets for the evolution of sheared lherzolites: Examples from Northern Lesotho and the Colorado Plateau, *J. Geophys. Res., 93*, 4895-4905, 1988.

Smith, D. and F. R. Boyd, Compositional heterogeneities in a high-temperature lherzolite nodule and implications for mantle processes, in *Mantle Xenoliths*, P.H. Nixon, ed., John Wiley & Sons, New York, pp. 551-561, 1987.

Smith, D., and S. N. Ehrenberg, Zoned minerals in

garnet peridotite nodules from the Colorado Plateau: implications for mantle metasomatism and kinetics, *Contrib. Mineral. Petrol., 86*, 274-285, 1984.

Zindler, A., and Jagoutz, E., Mantle cryptology, *Geochim. Cosmochim. Acta, 52*, 319-333, 1988.

The Earth's Convection Framework: Its Behavior Since the Jurassic and Implications for the Geomagnetic Field

T. Neil Irvine

In last year's Report, a "global convection framework" was defined for the Earth, comprising six "convection centers" at the intersections of three mutually perpendicular great circles. Four of the centers, distributed at 90°-intervals on one great circle, appear to mark axes of upwelling in the Earth's convection system. Three of them are the major volcanic hotspots of Hawaii, Iceland, and the Balleny Islands (the last being affiliated with the McMurdo volcanic province of Antarctica); and the fourth, located next to the Okavango Delta in Botswana, is a seismically active locality that effectively defines the southwest, "geophysical end" of the East African rift valley system. The other two centers are on either side of this circle of four, one in Peru, the second on the edge of Vietnam. Both these regions feature major subduction systems, so the two centers are presumed to represent axes of down-welling. The characteristics of the framework resemble considerably the tomography of the lower mantle, but the most intriguing correlations are with the geomagnetic field (Fig. 5), a matching that suggests that the framework reflects convection in the liquid part of the core as well as the mantle.

When the framework was first conceived, it was thought that its position had probably been constant for some extended period of geological time because the three hotspots traditionally have been included in a global hotspot system that has been relatively stationary for millions of years. Further research has shown, however, that the Earth's magnetic history correlates closely with events of crustal rifting and continental flood basalt magmatism (Fig. 6). In combination with observations that the convection framework appears to be linked to the geomagnetic field, that the Iceland and Balleny centers adjoin mid-ocean rift zones, and that the Okavango center is situated amidst the enormous Karoo basalt floods, this finding suggested that the framework might have moved with time in ways that can be defined by rifting events and flood basalt eruptions. This possibility has been explored, and results extending back to the Middle Jurassic are described below. Through them a convection structure is suggested for the core that may be of interest to specialists in that field.

Movement of the Convection Framework Since the Jurassic

The process of locating the convection framework in the geological past involves two assumptions deriving from its present-day relationships. One is that the arrangement of the six convection centers was always orthogonal; the other is that the Peru and Vietnam centers were always on

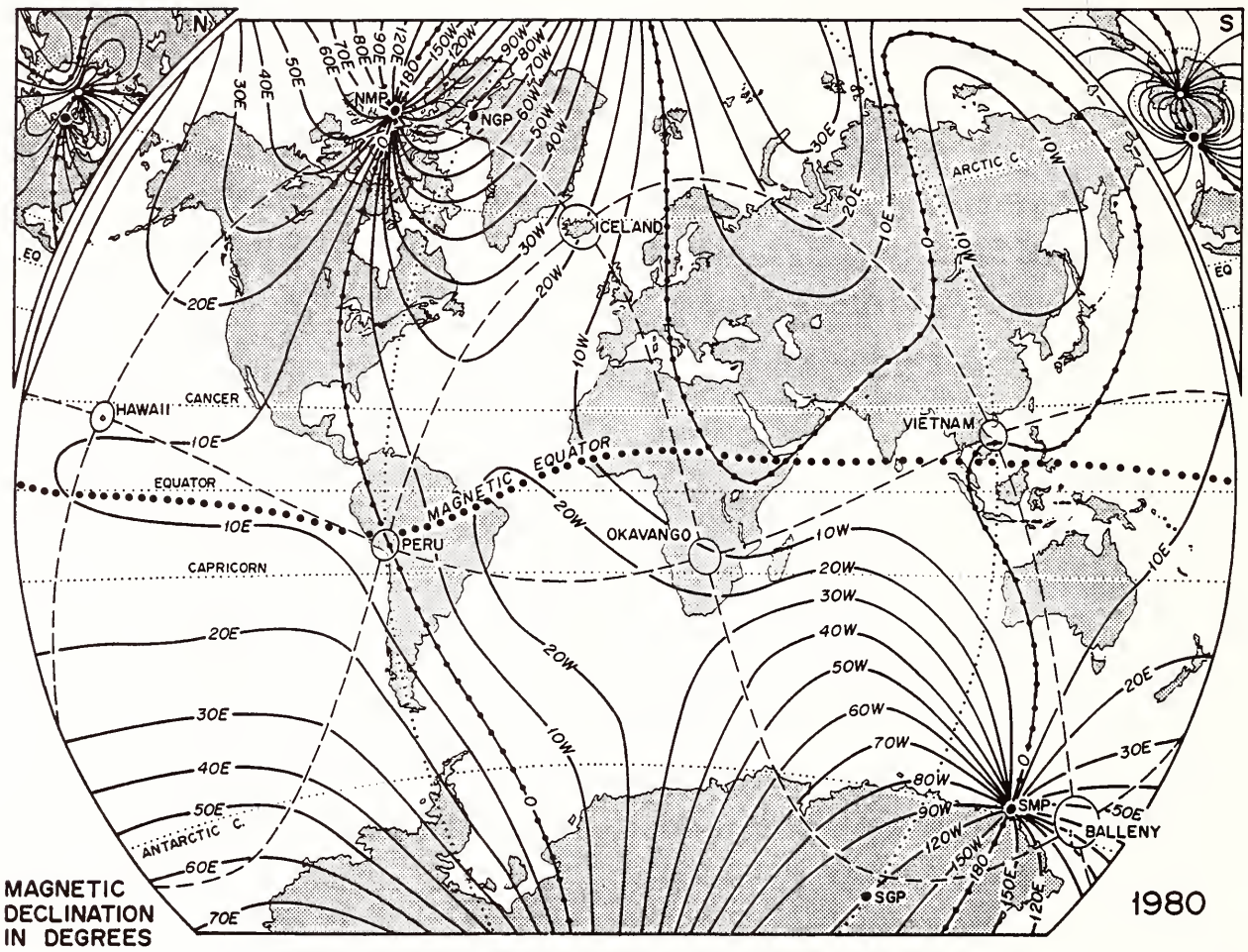

Fig. 5. Map showing the global convection framework superimposed on the Earth's magnetic field (contoured data for 1980 from Fabiano et al., 1983). It is seen that the Peru and Vietnam centers (of downwelling) are almost coincident with the main intersections of the magnetic equator with the lines of zero declination extending from the North and South Magnetic Poles (NMP, SMP). Also, these two centers lie on the meridian (light dotted line) through the North and South Geomagnetic Poles (NGP, SGP; poles of the best-fit dipole field), and the great circle containing the four centers of upwelling (Hawaii, Iceland, Okavango, and Balleny) passes within a few degrees of all four magnetic poles. It might be noted that the large, double-hairpin loop of the line of zero declination extending across Asia is a transitory feature that has shifted widely in historic times because of secular magnetic field variations(see Courtillot and LeMouel, 1988, Fig. 35). Despite this shifting, the intersection of the line with the magnetic equator near Vietnam moved very little.

the magnetic equator. At the present time, the magnetic equator is not coincident with the true equator, but such coincidence is generally assumed in paleomagnetic studies, at least as a time-averaged condition. When it obtains, the combination of the above assumptions additionally implies that the four centers of upwelling are on the same meridian.

Beyond these assumptions, the positioning of the framework requires identification of the centers of upwelling based on events of rifting and volcanism. In this search, a valuable test or criterion derives

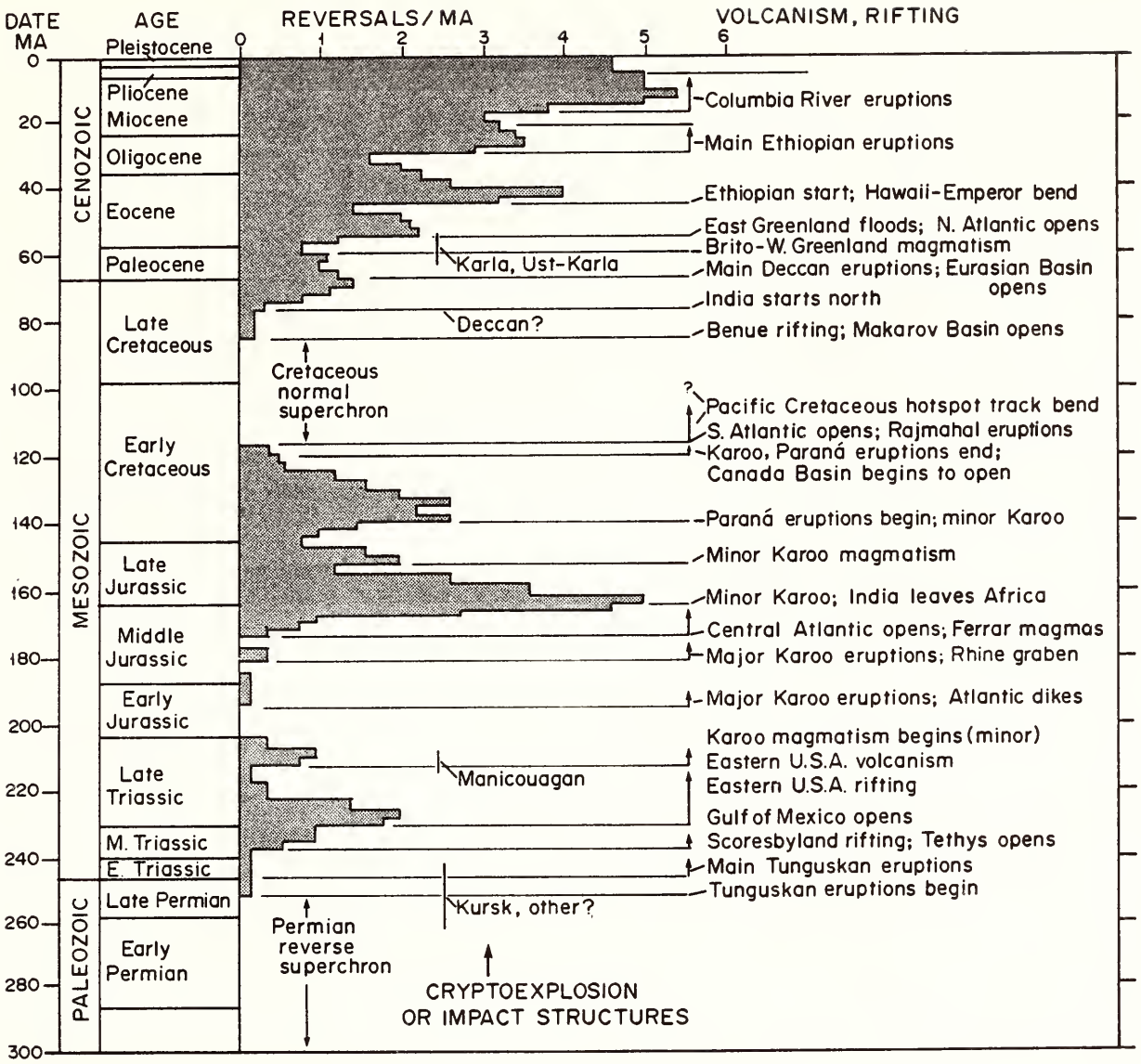

FIG. 6. Correlation of the polarity reversal-frequency histogram for the Earth's magnetic field (Permian to present) with events of crustal rifting and flood basalt magmatism. The histogram is from Creer and Pal (1986); the other information is from many sources, but most notably Erlank (1984), MacDougall (1988), and Vogt and Tucholke (1986). It is seen that all the major changes in reversal frequency are matched by major rifting events or continental flood basalt magmatism. Thus: (1) the episode of frequent reversals through the Triassic began with the eruption of the Tunguskan basalts in Siberia and continued with North American rifting events extending from East Greenland to the Gulf of Mexico; (2) the numerous reversals in the Jurassic and Early Cretaceous seem clearly related to the Karoo and Parana magmatism and the concurrent opening of the South Atlantic; and (3) the steplike increases of reversal frequency from Late Cretaceous through the Miocene successively match (a) the movements of India and the Deccan eruptions, (b) the opening of the North Atlantic and Arctic ocean basins and the related Brito-Arctic magmatism, (c) the rifting of central and eastern Africa and the Ethiopian basalt floods, and (d) the Columbia River basalt eruptions. A few major shock metamorphic (impact or crypto-explosion) structures are indicated for comparison (data from Grieve, 1987) because some investigators believe that geomagnetic reversals are caused by meteorite impacts.

from the orthogonal arrangement of these centers. If one of them is properly located, then the other three would be expected also to be within regions of rifting or volcanism.

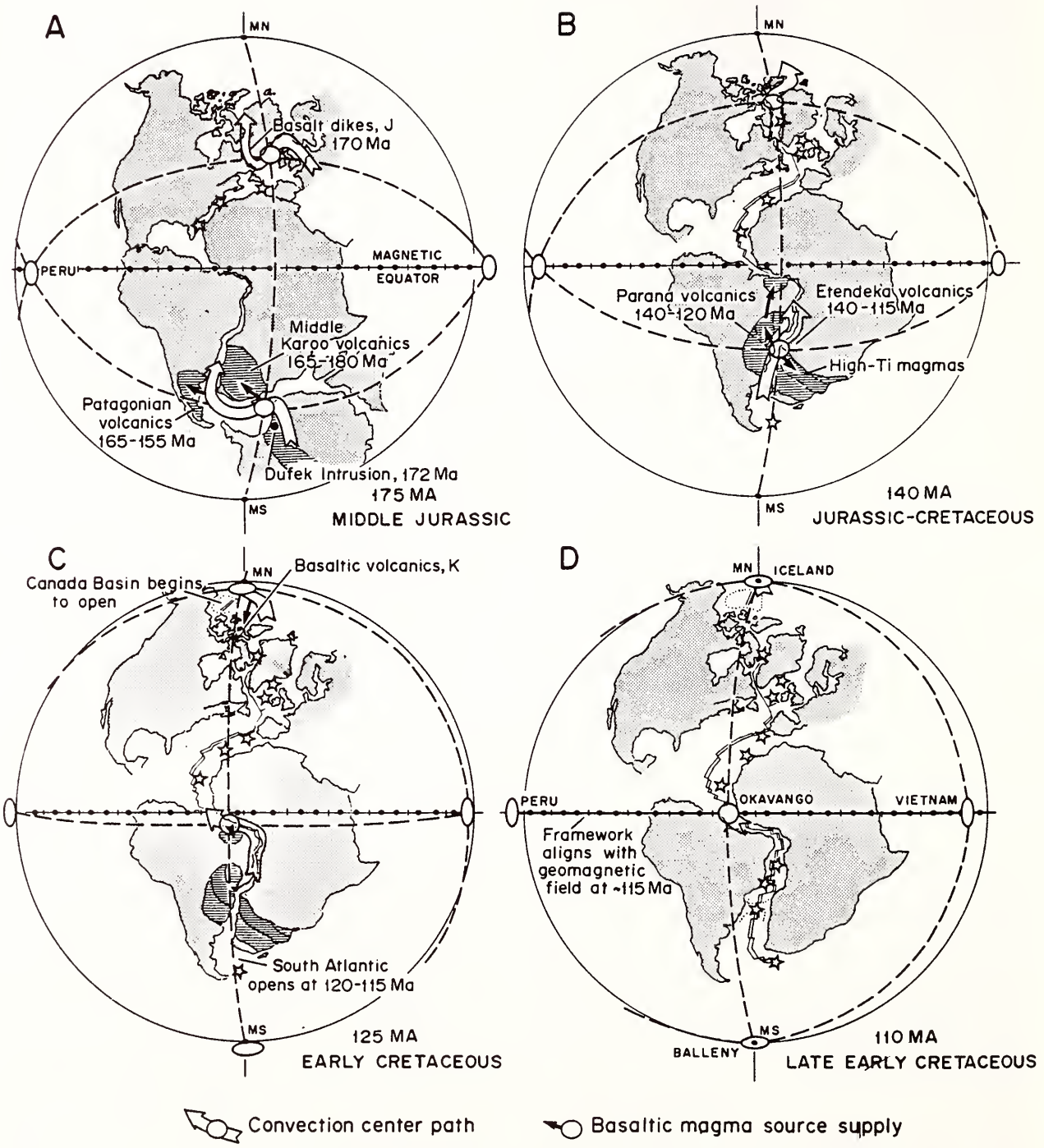
A
MN
Basalt dikes, J
170 Ma
MAGNETIC
EQUATOR
PERU
Middle
Karoo volcanics
165-180 Ma
Patagonian
volcanics
165-155 Ma
Dufek Intrusion, 172 Ma
MS
175 MA
MIDDLE JURASSIC
B
MN
Parana volcanics
140-120 Ma
Etendeka volcanics
140-115 Ma
High-Ti magmas
MS
140 MA
JURASSIC-CRETACEOUS
C
Canada Basin begins
to open
MN
Basaltic volcanics, K
South Atlantic
opens at 120-115 Ma
MS
125 MA
EARLY CRETACEOUS
D
MN
ICELAND
PERU
OKAVANGO
VIETNAM
Framework
aligns with
geomagnetic
field at ~115 Ma
MS
BALLENY
110 MA
LATE EARLY CRETACEOUS
Convection center path
Basaltic magma source supply

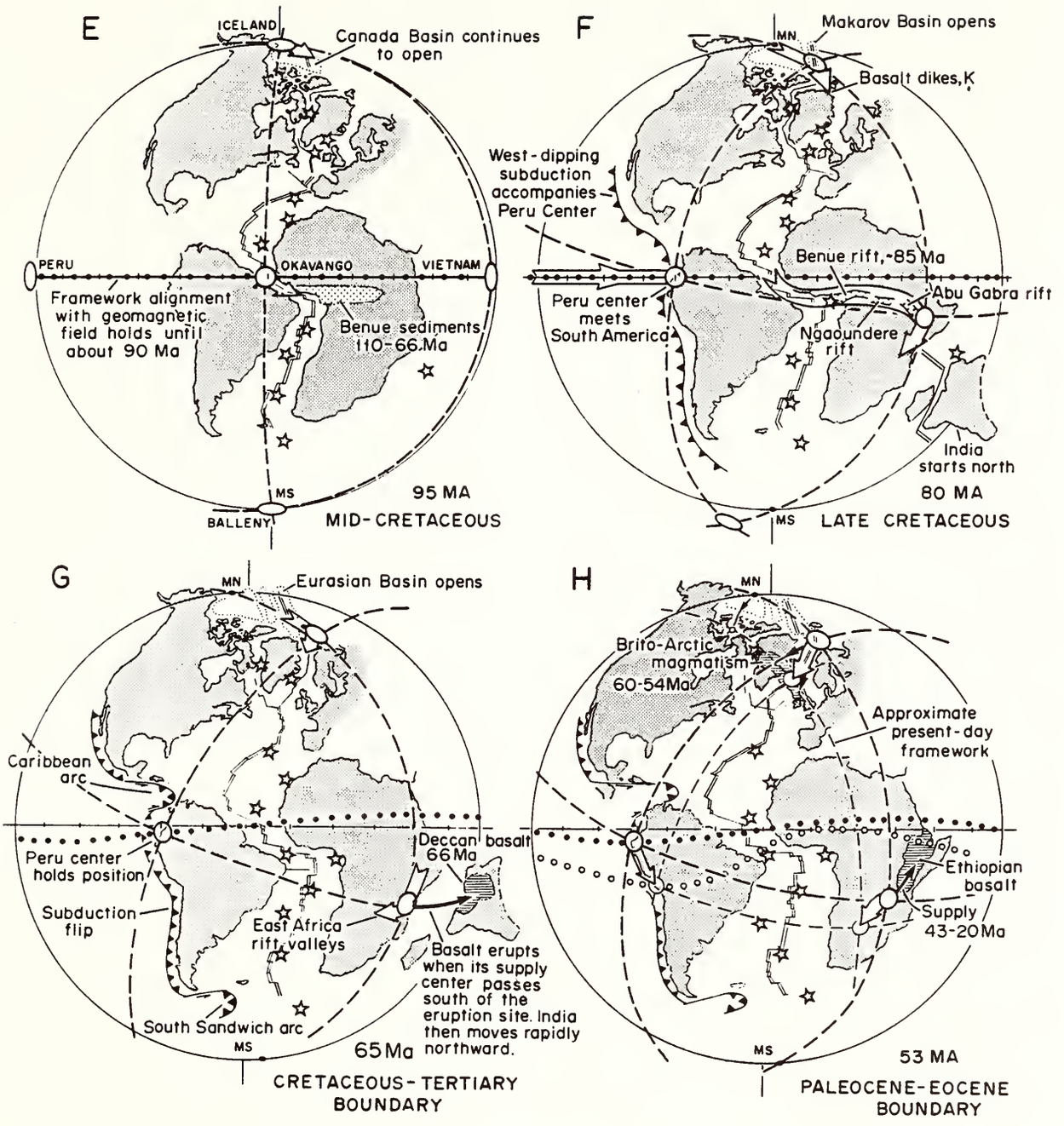

FIG. 7. Paleo-reconstructions on which an attempt is made to position the convection framework with time over the past 175 Ma during the breakup of Gondawana and the opening of the Atlantic. Assumptions are explained in the text. The reconstructions are slightly modified from Sclater *et al.* (1977), principally by the additions of India and Madagascar in maps F and G, and by slight shifting of the magnetic pole positions in maps G and H to bring them into better accord with more recent data from Irving and Irving (1982). Note how this latter change affects the configuration of the magnetic equator in the projection. Other control data are largely from the same sources as Fig. 6. Stars are hotspots. A feature of particular interest in the map sequence is that the convection framework was apparently aligned with the magnetic poles—and presumably, therefore, with the Earth's spin axis—during the time of the Cretaceous superchron (from about 115 to 90 Ma ; cf. Fig. 6) when there were no magnetic reversals. For further discussion, see text.

In the present documentation (Fig. 7), the use of this criterion is limited to a comparison of Iceland and Okavango, because the maps cover only the half of the Earth on which the continents have been mostly concentrated since the Jurassic. A related effect is that the paths of the centers for any interval of time should be mutually compatible within the restrictions of the above assumptions. This effect shows in Fig. 7 in the similarities of the Iceland and Okavango path segments on several maps.

By the Jurassic, the structural bonds between North America and Africa had already been broken, as evidenced by the Late Triassic rift basins of the eastern U.S.A. The concern in Fig. 7, therefore, is primarily with events in the southern and extreme northern parts of the Atlantic. In map A, it is inferred that the Okavango center has just left Antarctica, where the Ferrar dolerite and the large Dufek layered intrusion formed about 178-172 Ma ago. The center then moves westward around the tip of Africa, where Middle Karoo basalts erupted at 178 and 165 Ma, and past Patagonia, where volcanism was extensive between 165 and 155 Ma. During the same period, the Iceland center moves northward from central Europe along the North Sea, where Jurassic volcanism has been reported, and then turns southwest past the Rockall Trough, which was the site of the earliest ocean-floor spreading in the North Atlantic. From there, the center loops back to the northwest past the tip of Greenland, where Jurassic basaltic sills and dikes are found.

During the transition to the Cretaceous in map B, the Okavango center continues northward along the developing rift between South America and Africa as the Parana volcanics formed in Brazil and the Late Karoo and Etendeka volcanics erupted in Africa. The Iceland center concurrently moves up the rift between Canada and Greenland, then hooks westward around Ellesmere Island. From there, it continues in map C past Axel Heiberg Island, where basalt was erupted in the Cretaceous, on to where the Canada basin was soon to open. Meanwhile, the Okavango center has moved north and west to the point where South America and Africa last were joined. A major implication of these paths, of course, is that the centers of upwelling were carving out the future continental blocks.

During the time period of maps D and E, the Iceland center is stationed at the North Pole, where it presumably controlled the opening of the Canada basin. The Okavango center accordingly is positioned on the equator, arbitrarily at a place where the Atlantic could broaden around it. It is notable that the Canada basin has no magnetic stripes (Sweeney, 1983), which implies that it formed during the Cretaceous superchron (see Fig. 6). We thus have an indication that the core convection system was aligned with the Earth's spin axis during this extended period when the geomagnetic field did not reverse. Such a relationship would seem particularly significant to dynamo models for the origin of the geomagnetic field.

The opening of the Canada basin was completed by map F, and the Iceland center then moves successively to the neighboring Makarov and Eurasian basins, which opened in that order—and which are both magnetically striped. To be in accord with

these movements, the Okavango center has to shift rapidly eastward across Africa at latitudes just below the equator. The Benue trough was developing in this region at that time (Browne and Fairhead, 1983). It received marine sediments from about 110 to 65 Ma, and at about 85 Ma (during the Santonian), the existing deposits underwent relatively pronounced deformation. The Okavango center is presumed, therefore, to have passed along the trough at about 85 Ma, ultimately inducing the formation of all three rift zones identified on map F.

Map F also shows the Okavango center turning southward at the East Africa rift valleys. This change of trend is obviously attractive, because it leads along the rift system to the present-day site of Okavango. It might, however, also be justified on other grounds. As the Okavango center reached the rift valleys, the Peru center, following behind 90° to the west, would just have reached South America. The proposition is that its progress was stopped by the continent, hence the Okavango center (and the rest of the convection framework) had to change direction. By the illustrated interpretation, the Peru center was manifest as a west-dipping subduction zone that consumed ocean floor to its east as it moved across the Pacific. But the continent was too buoyant to subduct, hence when it was reached, the subduction system had to "flip" to its present east-dipping configuration, and the Peru center became locked to the continental margin. But if the flipping only occurred where the subduction encountered continental blocks, then as illustrated in map G, two parts of the system that were exceptional could have continued on to the east to become the west-dipping Caribbean and South Sandwich Islands Benioff zones.

In maps G and H, the Iceland and Okavango centers both move southward toward their present locations. Through this period, the Okavango upwelling had to yield, first the Deccan basalts, then the Ethiopian floods, and the Iceland center had to yield the Tertiary magmas of Britain and Greenland. The possibilities relating to these complex events cannot be discussed here, but it is interesting to note that the Deccan eruptions appear to have occurred just when the southward-moving Okavango center passed northward-moving India.

If the analysis presented here has validity, then it demonstrates that the convection framework is potentially a very useful device for relating tectonic and magmatic events in different parts of the world at various times in the geological past. But there obviously are many points on which the analysis might be challenged. Only one question can be addressed here, but it has been the most frequently asked: What about all the other hotspots? Two observations are noted. One is that, among the four centers of upwelling, only Hawaii has a hotspot track that is paralleled by other hotspot tracks. As discussed in last year's report, however, Hawaii apparently plays an extraordinary role in Earth convection in that it appears largely to control the motion of the Pacific Plate—which is where the parallel tracks occur. The other observation is that many (if not all) of the other hotspots might have formed in consequence of the movements of the main centers of upwelling. Thus, for example, as the

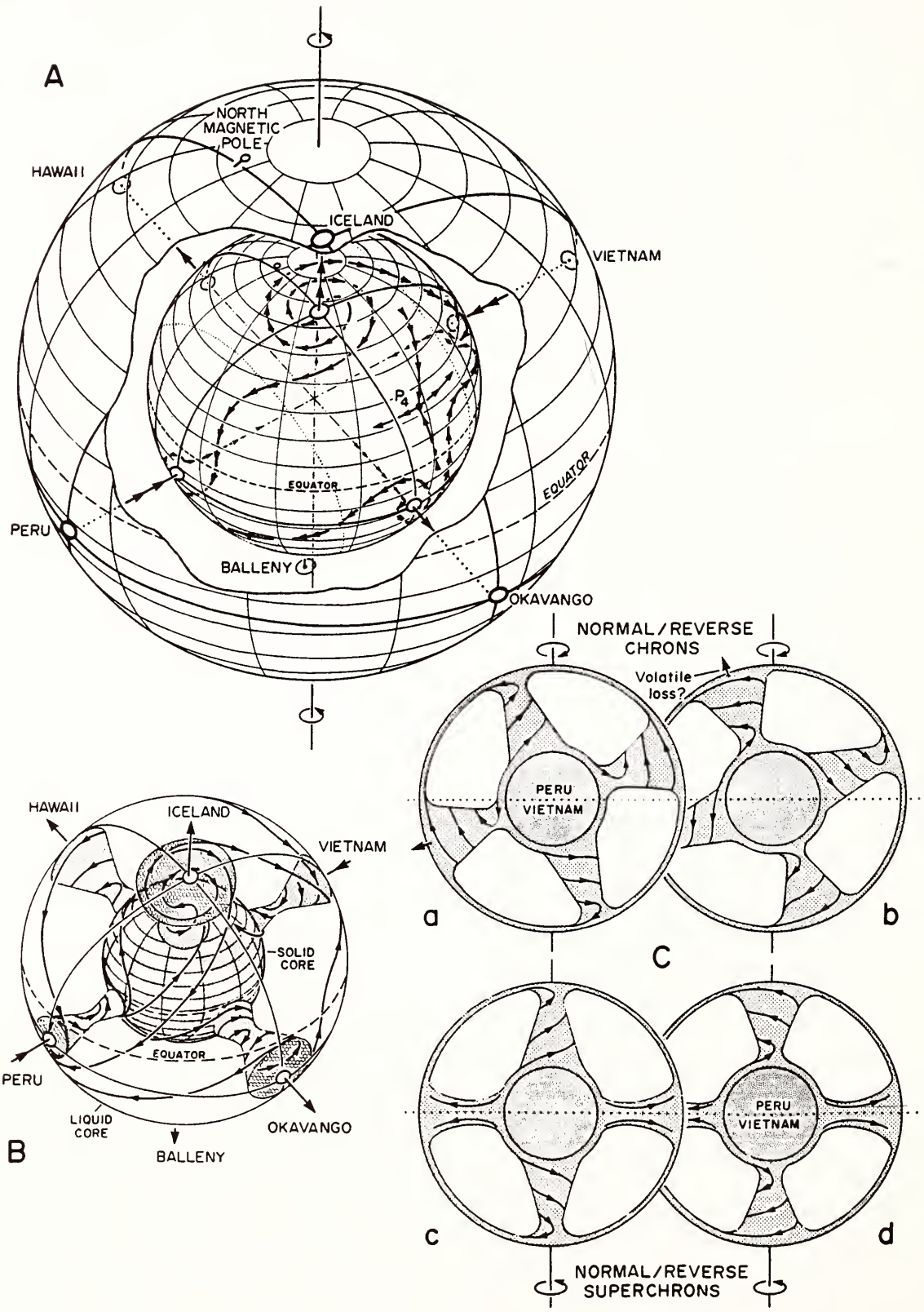

FIG. 8. A suggested convection structure for the Earth's core, based on the convection framework and a fluid dynamics model by Veronis (1959). See text for explanation and discussion.

Okavango center opened the South Atlantic (Fig. 7, A-D), it might also have initiated the volcanic centers at Bouvet, Tristan da Cunha, St. Helena, Ascension, and so on (see Fig. 7).

Core Convection

The suggested core structure (Fig. 8) combines the orthogonal axes of the convection framework with a fluid dynamics model by Veronis (1959) describing the effect of the Coriolis force on a fluid layer heated from below and cooled above. The key feature is that the liquid of the outer core rises and descends at the framework axes by way of spool-shaped vortex structures in which it spirals inward with one sense of rotation to about mid-level in the layer, then switches and spirals outward with the opposite rotation as it completes its transit. When these structures are viewed individually from above, their directions of rotation appear opposite for upwelling and down-welling in the same (northern or southern) hemisphere, and they also appear opposed for either upwelling or down-welling structures in opposite hemispheres. But when the whole core structure is viewed from a single point, as in each diagram in Fig. 8, then the upper (or lower) parts of vortices on opposite sides of the solid inner core are seen actually to have the same rotation. A suggestion that arises here is that, if there were oscillations of the depth at which the flow spiraling reverses, then at any particular time (as illustrated schematically in a relatively extreme way in Fig. 8C), most of the liquid along axial lines through the whole core could be rotating either one way or the other. The proposition is that such oscillatory flow reversals might underlie the polarity reversals of the geomagnetic field.

A further feature of the proposed core structure, portrayed in Fig. 8C (c and d), is that the spiral vortex flow should not occur on convection axes lying in the plane of the equator where the Coriolis force vanishes. Thus, in the analysis of Fig. 7, there should not have been spiraling on the Peru-Vietnam axis (at least until mid-Cenozoic times), nor should it have occurred on the Okavango-Hawaii axis during the Cretaceous superchron. A possible implication of the latter condition is that it had the effect of damping the oscillatory flow reversals suggested above, thereby detering polarity reversals and causing the superchron.

How these various processes might be tied to rifting and volcanism in terms of cause/effect relationships is debatable, but the physical connection is presumably plume activity in the mantle. It would seem also that, if the analysis in Fig. 7 is on the right track, then the inclination of the convection framework relative to the Earth's spin axis is especially critical, perhaps because it influences the planet's rotation characteristics. But this inclination in turn might be controlled by factors such as the interaction or coupling of the convection framework with the continents (as in the case postulated above for the Peru center), by the relative freedom of the lithospheric plates to move without interfering with one another, and by the ease with which the continental blocks can be rifted. A general implication is that the crystallization, cool-

ing, and convection of the core liquid is probably strongly linked to the major tectonic and magmatic events observed at the surface.

References

Browne, S. E, and J. D. Fairhead, Gravity study of the central African rift system: A model of continental disruption, *Tectonophysics, 94,* 187-203, 1983.

Creer, K. M, and P. C. Pal, Geomagnetic reversal spurts and episodes of extraterrestrial catastrophism, *Nature, 320,* 148-150, 1986.

Courtillot, V, and J. L. Le Mouel, Time variations of the Earth's magnetic field: from daily to secular, *Ann. Rev. Earth Planet. Sci., 16,* 389-476, 1988.

Erlank, A. J, Petrogenesis of the Volcanic Rocks of the Karoo Province, *Geol. Soc. S. Africa, Spec. Paper 13,* 1984.

Fabiano, E. B, N. W. Peddie, and A. K. Zunde, The magnetic field of the Earth, U. S. Geol. Surv., Misc. Invest. Series, Map I-1457, 1983.

Grieve, R. A. F., Terrestrial impact structures, *Episodes, 10,* 86, 1987.

Irving, E., and G. A. Irving, Apparent polar wander paths, Carboniferous through Cenozoic, and the assembly of Gondwana, *Geophys. Surveys, 5,* 141-188, 1982.

MacDougall, J. D., *Continental Flood Basalts,* Kluwer, Dordrecht, Netherlands, 1988.

Sweeney, J. F, Arctic seafloor structure and tectonic evolution, *Am. Geophys Un., Geodynamics Series, 2,* 55-64, 1981.

Veronis, G, Cellular convection with finite amplitude in a rotating fluid, *J. Fluid Mechanics, 5,* 311-324, 1959.

Vogt, P. R, and B. E. Tucholke, *The western North Atlantic region,* The Geology of North America, v. M, Geological Society of America, Boulder, Colorado, 696 p., 1986.

Fracture-controlled Fluid Flow During Chlorite-grade Metamorphism at Waterville, Maine

Douglas Rumble, Nicholas H. S. Oliver, and Thomas C. Hoering*

A current controversy in studies of metamorphic rocks concerns the nature and extent of fluid flow during metamorphism. Some researchers have found fluid-rock ratios as high as 17.1 in bedded carbonate metasediments (Hoisch, 1987). Other workers point out, however, that if large ratios are characteristic of an entire metamorphic complex rather than merely pertaining to specific acquifers, difficult questions arise about a feasible source for such vast amounts of fluid (Wood and Walther, 1986). Significant caveats have been issued regarding uncertainties in the magnitude of fluid-rock ratios measured with the reaction progress method (Wood and Graham, 1986). Resolving the controversy is important because of the ramifying effects the putative fluids would have on metamorphic belts. Among the effects that have been claimed are (1) regional alkali metasomatism (Ferry, 1982); (2) regional stable isotope metasomatism (Wickham and Taylor, 1985); (3) advective heat transfer (Chamberlain and Rumble, 1988); and (4) removal of fluid reaction products allowing devolatilization to proceed to completion (Ferry, 1986a).

We are addressing the controversy by testing the hypothesis of fluid flow in the Waterville-Augusta area, Maine. The re-

* Monash University, Dept. of Earth Sciences, Clayton, 3168, Victoria, Australia

gion was chosen for study because it is here that the reaction progress method of estimating fluid-rock ratios was developed and widely applied (Ferry, 1980). The rocks of the area are the focus of a debate about the magnitude of fluid-rock ratios (Wood and Graham, 1986; Ferry, 1986). A practical advantage of the locality is that stratigraphic units strike perpendicularly across metamorphic isograds from chlorite to sillimanite zones (Osberg, 1968). Thus, it is possible to measure metasomatic changes caused by metamorphism with minimal ambiguity.

The reaction progress method of estimating fluid flow developed by Ferry (1980) is best suited to study of metasediments and meta-igneous rocks containing mineral assemblages with low phase rule variance. The method cannot be readily adapted to veins containing assemblages of one or two minerals (e.g. quartz-calcite), however. Ferry's (1980) mapping of fluid flow gives a detailed view of intergranular infiltration of H_2O. But little is known of the role of fracture permeability during metamorphism as recorded by veins. This is a significant lack of knowledge in view of the likelihood that fluid flow through fractures may greatly exceed intergranular infiltration. We decided to investigate fracture permeability by measuring the stable isotope composition of veins and their wall rocks from the Waterville limestone, a member of the Silurian Waterville Formation.

Methodology

Large specimens of 5 to 10 kg are collected showing structural relations of veins and their wall rocks. Hand specimens are slabbed with a rock saw, polished, and stained with Alizarin Red-S and Potassium Ferricyanide. Staining the polished slabs helps to locate and identify carbonate minerals, chiefly calcite and dolomite. Samples weighing 5 to 60 mg (larger amounts for rocks with lower abundances of carbonates) are drilled out with either a 1 or 2 mm diameter, diamond tipped drill. Sample powders are loaded immediately into two-legged reaction vessels for reaction with 100% phosphoric acid at 25°C (McCrea, 1950).

In many chlorite, biotite, and some garnet-grade wall rock samples, calcite and dolomite-ankerite solid solutions are so intimately intergrown that they cannot be physically separated. The simultaneous reaction of both carbonates with phosphoric acid leads to cross-contamination of evolved CO_2. The problem of cross-contamination is usually dealt with by taking a first aliquot of CO_2 released early during reaction as representative of faster reacting calcite; a later aliquot samples slower reacting dolomite (Epstein *et al.*, 1964). Cross-contamination is not a major difficulty in the Waterville samples because the wall rocks are usually either predominantly calcite or dolomite. Samples with both carbonates equally abundant are uncommon. We have found that an aliquot taken at 5 minutes into the reaction gives a reliable value for the $\delta^{18}O$ of calcite from calcite rich rocks. Aliquots taken at 24 and 48 hours give results for dolomite reproducible to ± 0.1 ‰ for dolomite-rich rocks. We do not yet have accurate data on the iso-

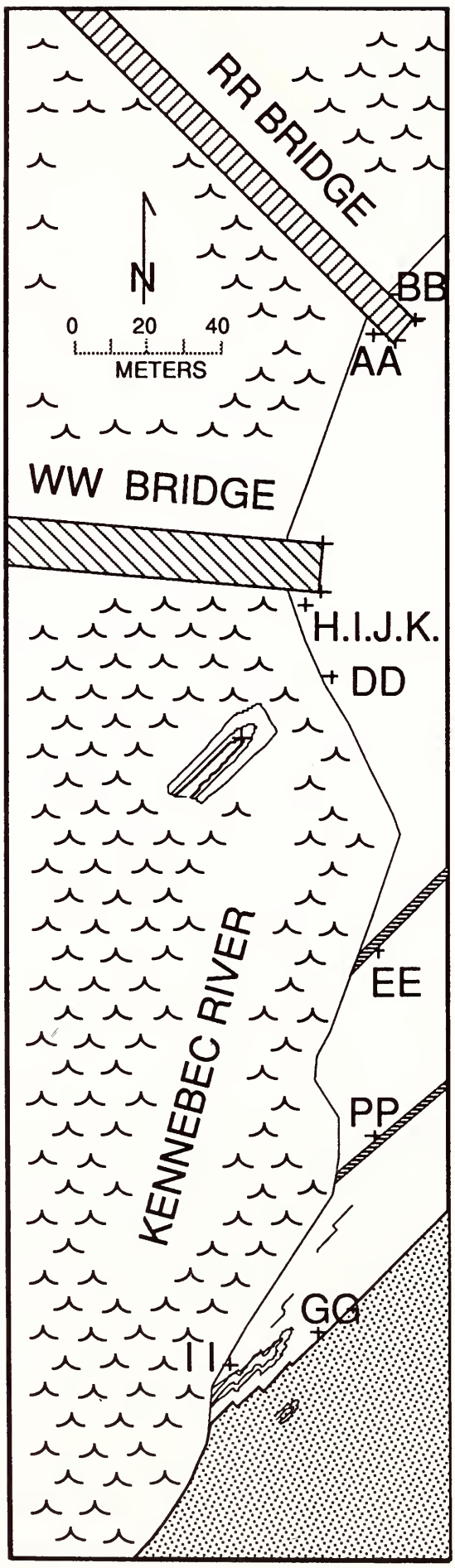

topic compositions of co-existing calcite and dolomite from the same powdered sample. The data presented below on both carbonates from the same hand specimen refers to calcite and dolomite from separate lithologic layers.

Results

We have found evidence of fluid-rock interaction in the outcrops of the Waterville limestone along the east bank of the Kennebec River in Waterville, Maine. Analysis of calcite and dolomite for $\delta^{18}O$ and $\delta^{13}C$ shows that there are cryptic alteration halos around certain veins in which wall rock values have been depleted by 1-2 ‰ in $\delta^{18}O$ and by similar amounts in $\delta^{13}C$. The halos are termed "cryptic" because no mineralogical features have been recognized apart from proximity to veins. In what follows we demonstrate the pre-metamorphic isotopic composition of the limestone and establish its range of isotopic heterogeneity. An account is given of the relative chronology of vein emplacement and the evolution of isotopic values in the veins. These results are used to evaluate the significance of the isotopic alteration halos.

The pre-metamorphic isotopic composition of the Waterville limestone was measured by analyzing vein and wall rock samples taken from localities remote from

FIG. 9. Sample locations and geologic sketch map at Waterville, Maine. Waterville limestone shown in blank with line sketches of refolded isoclinal folds. Graded bedded phyllite is stippled, SE corner of map. Metamorphosed granitic dikes are heavily stippled at localities EE and PP. "WW" denotes Waterville-Winslow bridge.

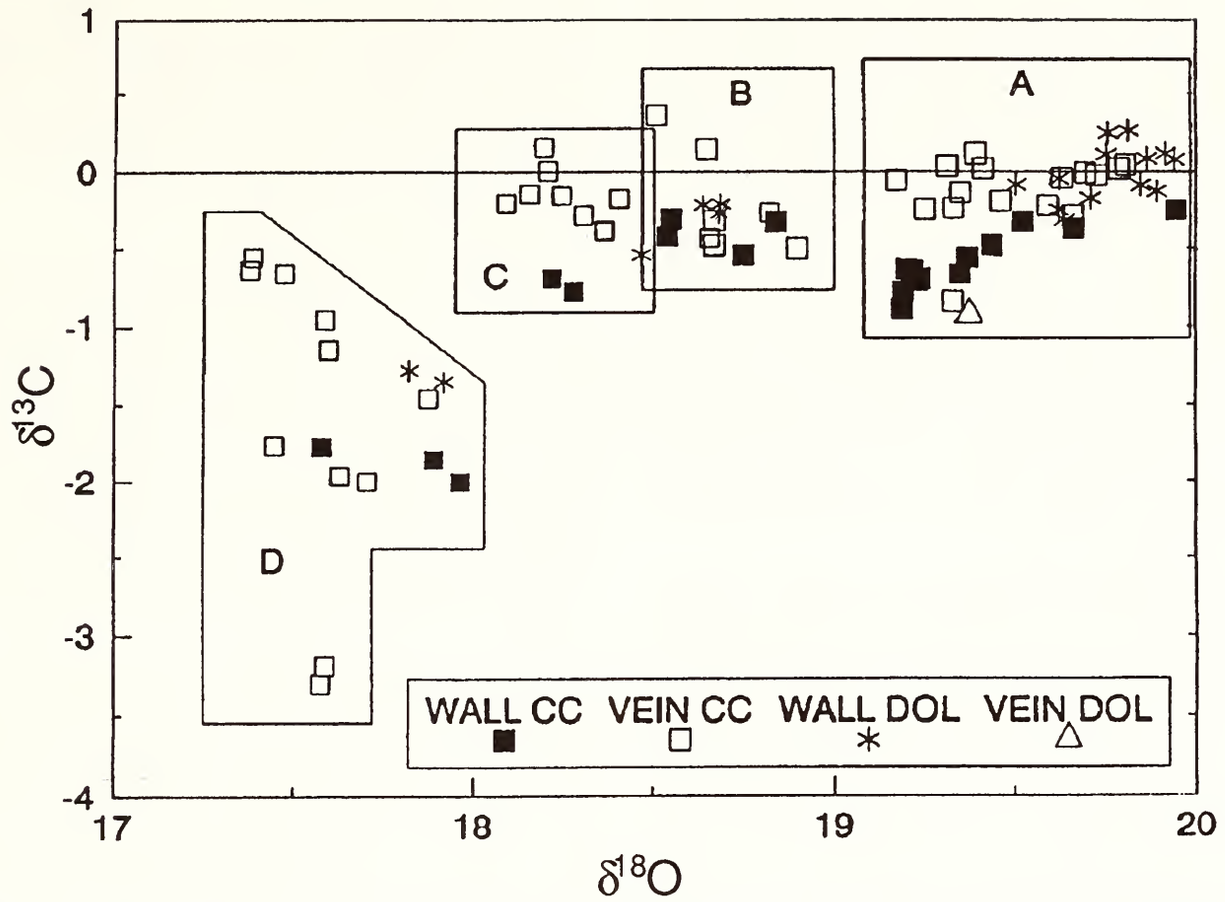

FIG. 10. Plot of $\delta^{13}C$ vs. $\delta^{18}O$. Box A shows compositions of pre-metamorphic limestone at localities H, I, J, and K (Fig. 9). Box B outlines limestone samples taken within 0.1 m of contact with granitic dikes at localities EE and PP. Box C gives analyses of limestone from 0.5 to 7 m from contact with graded bedded phyllite at GG and II. Area D denotes limestones inside alteration halo at localities AA and BB (Fig. 9).

contacts with the metamorphosed granitic dikes and the graded bedded phyllite (Fig. 9, samples H, I, J, K). The $\delta^{18}O$ and $\delta^{13}C$ values are consistently higher than from any other samples analyzed but the $\delta^{18}O$ values are depleted by some 4.0 ‰ in relation to pristine marine limestones (Fig. 10A). There is abundant evidence of fluid flow prior to metamorphism in the form of stylolites and the replacement of current-bedded, clastic calcite grains by fine-grained dolomite. Thus, it is possible that the initial depletion of the limestones in $\delta^{18}O$ occurred during diagenesis. Analysis of individual beds 1-2 cm thick from single hand specimens shows variation of no more than 0.3 ‰ in both $\delta^{18}O$ and $\delta^{13}C$ from bed-to-bed. The effects of proximity to contacts with metamorphosed granitic dikes are depletion in $\delta^{18}O$ by a maximum of 1.0 ‰ but little change in $\delta^{13}C$ (Fig. 10B, samples EE, PP). Samples collected within 1-5 meters of the contact with the graded bedded phyllite are lower in $\delta^{18}O$ by 1.0 ‰ but unchanged in $\delta^{13}C$ (Fig. 10C, samples GG, II). It is concluded that pre-metamorphic values of the limestone ranged from 19.2 to 20.0 ‰ in $\delta^{18}O$ and from -0.9 to +0.3 ‰ in $\delta^{13}C$. Isotopic exchange between limestone and dike rocks or phyllite led to depletion in $\delta^{18}O$ by 1.0 ‰ but little change in $\delta^{13}C$.

The relative chronology of vein emplacement has been established by field observations of the structural relationships

between veins, re-folded isoclinal folds, and granite dikes. The oldest structures are bedding and stratigraphic contacts. These are followed in age by stylolites and dolomitized limestone beds. Beds, contacts, and diagenetic features were subsequently isoclinally folded and intruded by granitic dikes. Both the isoclinal folds and dikes are pre-metamorphic in age (Osberg, 1968). Finally, the area was metamorphosed under greenschist facies conditions and folded along NNE axes.

The oldest (and rarest) vein (V1) discovered is composed of sigmoid black fibres of calcite extending perpendicular from the vein's wall. The vein is isoclinally folded and, therefore, is pre-metamorphic in age. The $\delta^{18}O$ and $\delta^{13}C$ values for the pre-metamorphic vein are 19.2 ‰, and +0.5, respectively. The next youngest group of veins (V2) consist of quartz and calcite. The V2 veins are irregular in shape and size (up to 20 cm in width) and contain isolated fragments of wall rock. Their $\delta^{18}O$ and $\delta^{13}C$ values are typically in the range +19.2 to 19.8 ‰ and -0.8 to +0.2 ‰, respectively, and are closely similar to immediately adjacent wall rock (Fig. 10A). A third group of veins (V3) is made of fibrous calcite with a fringe of muscovite, quartz, and pyrite along the walls. The veins are 0.1 to 1.0 cm thick. They strike NNE and are parallel to the axial surfaces of the minor folds that refold the older, isoclinal folds. The V3 veins have values of 18.1 to 18.5 ‰ in $\delta^{18}O$ and -0.5 to +0.2 ‰ in $\delta^{13}C$ (Fig. 10C). Preliminary results of thin section study suggest that the growth of metamorphic porphyroblasts began after the emplacement of V1 and extended throughout the formation of V3. The youngest veins (V4) contain quartz, calcite, and rare galena, and cross-cut the older veins. The isotopic values of V4 calcites range from +17.4 to 17.6 ‰ ($\delta^{18}O$) and from -3.2 to -2.0 ‰ ($\delta^{13}C$) (Fig. 10D).

There is a systematic trend of depletion in both ^{18}O and ^{13}C from oldest to youngest veins. The values of the V4 veins are similar to some of the wall rocks and veins of the Waterville limestone collected in the staurolite and sillimanite zones. Veins showing values characteristic of V4 have been found in the graded-bedded phyllite, as well.

Cryptic alteration halos have been recognized around V4 veins at the N end of the outcrop (sample locations AA and BB, Fig. 9). The wall rocks consist of current-bedded clastic limestones that have been "dolomitized" parallel to bedding. Calcite-rich beds alternate with dolomitized layers on a scale of 1 to 2 cm. These rocks are indistinguishable in appearance from dolomitized limestones that preserve "pre-metamorphic" isotope values. Both wall rocks and older veins (V2 and V3) have been depleted in $\delta^{18}O$ and $\delta^{13}C$ in halos surrounding V4 veins (Fig. 10D). Isotopic exchange between V4 and its wall rocks appears to be more complete in regard to $\delta^{18}O$ than it is in $\delta^{13}C$. The vein calcites at AA and BB (Fig. 9) with $\delta^{13}C$ values of -1.2 to -0.5 ‰ belong to the V2 and V3 generations (Fig. 10D). Wall rock calcite and dolomite have $\delta^{13}C$ values between -2.0 and -1.2 ‰. The calcite of V4, itself varies in $\delta^{13}C$ from -3.2 to -2.0 ‰ (Fig. 10D). Values of $\delta^{18}O$ in veins and wall rocks, however, extend over a narrow interval from 17.4 to 18.1 ‰.

Calculation of single pass fluid/rock

ratios needed to convert pre-metamorphic wall rock $\delta^{18}O$ and $\delta^{13}C$ values to those observed in the alteration halos gives 2.4 (molar ratio) for ^{18}O and 2.9 (molar ratio) for ^{13}C. In these calculations the fluid composition is assumed to be H_2O-CO_2 [$X(CO_2) = 0.07$ Ferry, 1987] with $\delta^{18}O$ (H_2O) = 14.0 ‰ and $\delta^{13}C$ (CO_2) = -0.6 ‰ (e.g., fluid in equilibrium with most depleted V4 vein calcite at 390°C). The initial and final values of $\delta^{18}O$ for wall rocks are 19.5 and 18.0, respectively, and for $\delta^{13}C$ these values are -0.5 and -2.0 ‰. The fractionation of $^{18}O/^{16}O$ between calcite and H_2O is +3.5 and that of $^{13}C/^{12}C$ between calcite and CO_2 is -2.6 at 390°C (Friedman and O'Neil, 1977). The calculations were made with the equations of Rye and Bradbury (1988, p. 214).

Our results demonstrate that chlorite-grade limestones were penetrated by fluid-filled fractures during the peak-to-waning stages of metamorphism. Fluids infiltrated into wall rocks to a depth of at least 4 cm from vein walls. The fluid/rock ratios calculated from isotopic data for wall rock infiltration are approximately 3.0 by volume, some 8 times greater than the largest ratios estimated by Ferry (1987, outcrop 7), for intergranular infiltration at the same outcrop.

References

Chamberlain, C. P., and D. Rumble, Thermal anomalies in a regional metamorphic terrane: an isotopic study of the role of fluids, *J. Petrol., 29,* 1215-1232, 1988.

Epstein, S., D. L. Graf, and E. T. Degens, Oxygen isotope studies on the origin of dolomite, in *Isotopic and Cosmic Chemistry*, H. Craig, S. L. Miller, and G. Wasserburg, eds., North-Holland, New York, pp. 169-180, 1963.

Ferry, J. M., A case study of the amount and distribution of heat and fluid during metamorphism, *Contrib. Mineral. Petrol., 71,* 373-385, 1980.

Ferry, J. M., Mineral reactions and element migration during metamorphism of calcareous sediments from the Vassalboro Formation, south-central Maine, *Am. Mineral. 68,* 334-354, 1983.

Ferry, J. M., Infiltration of aqueous fluid and high fluid-rock ratios during greenschist facies metamorphism: a reply, *J. Petrol., 27,* 695-714, 1986.

Ferry, J. M., Metamorphic hydrology at 13-km depth and 400-550°C, *Am Mineral., 72,* 39-58, 1987.

Friedman, I., and J. R. O'Neil, Compilation of stable isotope fractionation factors of geochemical interest, *U. S. Geol. Surv. Prof. Paper* 440-K, 12 pp., 1977.

Hoisch, T. D., Heat transport by fluids during Late Cretaceous regional metamorphism in the Big Maria Mountains, southeastern California, *Geol. Soc. Am. Bull. 98,* 549-553, 1987.

McCrea, J. M., On the isotopic chemistry of carbonates and a paleo-temperature scale, *J. Chem. Phys., 18,* 849-857, 1950.

Osberg, O. H., Stratigraphy, structural geology and metamorphism of the Waterville-Vassalboro area, Maine, *Maine Geol. Surv. Bull., 20,* 1968.

Rye, D. M., and H. J. Bradbury, Fluid flow in the crust: an example from a Pyrenean thrust ramp, *Am. J. Sci., 288,* 197-235, 1988.

Wickham, S. M., and H. P. Taylor, Jr., Stable isotope evidence for large scale seawater infiltration in a regional metamorphic terrane: the Trois Seigneurs Massif, Pyrenees, France, *Contrib. Mineral. Petrol., 91,* 122-137, 1985.

Wood, B. J., and C. M. Graham, Infiltration of aqueous fluid and high fluid: rock ratios during greenschist facies metamorphism, *J. Petrol., 27,* 751-761, 1986.

Wood, B. J., and J. V. Walther, Fluid flow during metamorphism and its implications for fluid-rock ratios, in *Fluid Rock Interactions during Metamorphism*, J. V. Walther and B. J. Wood, eds., Springer-Verlag, New York, pp. 89-108, 1986.

The Reaction Progress Method: Quantitative Tests of Petrologic Models on a Microscopic Scale

Craig M. Schiffries

A central problem in petrology is to understand the physical and chemical controls that govern the progress of mineral reactions. It is generally assumed that metamorphic mineral reactions are driven by variations in temperature and pressure, and that metamorphism is nearly isochemical except for the loss or gain of volatiles. According to a growing school of thought, however, fluid infiltration commonly plays an essential role in driving metamorphic mineral reactions (Newton *et al.*, 1980; Rumble *et al.*, 1982; Ferry, 1986). In contrast to the traditional view of metamorphism, fluid infiltration can cause large-scale chemical mass transfer of non-volatile components. The dichotomy of opinion over the relative importance of the physicochemical variables that govern the progress of metamorphic mineral reactions illustrates the need to develop quantitative tests that can distinguish between alternative petrologic models. The principal purpose of this paper is to demonstrate that the reaction progress method (Thompson *et al.*, 1982; Thompson, 1982; Ferry, 1986) can be used to distinguish between isochemical and metasomatic models for the origin of myrmekite (Fig. 11). The isochemical model (Schwantke, 1909) is analogous to the traditional view of metamorphism because the mineralogical changes occur in response to variations in temperature and pressure at constant bulk composition. The metasomatic replacement model (Becke, 1908; Sederholm, 1916) is analogous to fluid infiltration models of metamorphism because the mineral reactions occur in response to fluid-rock interactions.

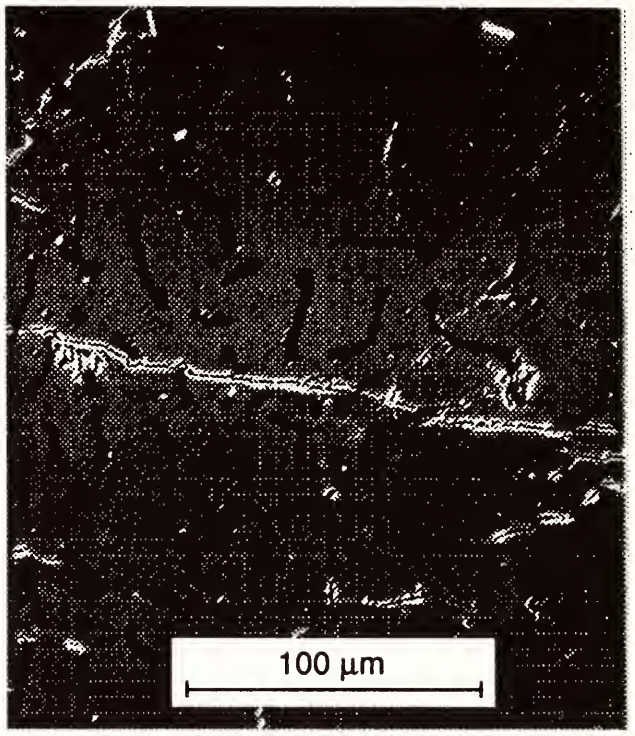

Fig. 11. BSE image of calcic myrmekite from the Bushveld Complex. The vermicular intergrowth consists of quartz (black) and calcic plagioclase (grey).

Myrmekite has been studied by petrologists since the 19th century (Michel-Lévy, 1874-75), and the extensive literature is reviewed by Ashworth (1972) and Phillips (1974). Myrmekite is commonly defined as a descriptive, nongenetic term that refers to vermicular intergrowths of quartz and plagioclase. The intergrowths discussed in this paper consist of quartz and plagioclase, but they are referred to as 'calcic myrmekite' because they are distinctly different from the type of myrmekite that has been widely discussed in the literature (Table 2). It appears that calcic myrmekite

TABLE 2. Comparison between calcic myrmekite and typical myrmekite

	Calcic Myrmekite	Typical Myrmekite
Occurrence	anorthositic and gabbroic rocks	granitic rocks and quartzo-feldspathic gneisses
Alkali Feldspar	generally absent	generally present
Plagioclase Composition	$An_{myr} > An_{host}$	$An_{myr} < An_{host}$

has been frequently overlooked and is a common accessory feature in anorthositic and gabbroic rocks (Schiffries and Dymek, 1985; Dymek and Schiffries, 1987). Calcic myrmekite comprises minerals that are intergrown on a length-scale of approximately 10 μm (Fig. 11), and precise measurements of modal composition cannot be obtained by standard point-counting techniques. Micro-modal data were obtained by inversion of broad-beam electron microprobe analyses and by image processing of digitized BSE photomicrographs. Mineral compositions were determined by conventional electron microprobe techniques.

The metasomatic model for the origin of calcic myrmekite involves an open system reaction in which the host plagioclase is replaced by an intergrowth of quartz and relatively calcic plagioclase. The replacement process can be represented by a single net-transfer reaction:

$$\underset{\text{albite}}{2NaAlSi_3O_8} + \underset{\text{fluid}}{CaNa_{-2}} = \underset{\text{anorthite}}{CaAl_2Si_2O_8} + \underset{\text{qtz}}{4SiO_2}. \quad (1)$$

The endmember reaction (1) can be rewritten in terms of arbitrary values for the initial and final plagioclase composition:

$$\underset{\text{sodic plag}}{(1+f)Na_{1-i}Ca_iAl_{1+i}Si_{3-i}O_8} + \underset{\text{fluid}}{(f-i)CaNa_{-2}} =$$

$$\underset{\text{calcic plag}}{(1+i)Na_{1-f}Ca_fAl_{1+f}Si_{3-f}O_8} + \underset{\text{qtz}}{4(f-i)SiO_2}, \quad (2)$$

where $i = [n_{Ca}/(n_{Ca}+n_{Na})]_{initial}$, $f = [n_{Ca}/(n_{Ca}+n_{Na})]_{final}$, and $f > i$. An advantage of writing the net-transfer reaction in this form is that the stoichiometric reaction coefficients are expressed in terms of the initial (host) and final (myrmekite) plagioclase composition. The production of quartz by reaction (2) is coupled with a progressive increase in the anorthite content of the plagioclase.

The replacement model can be tested by comparing measurements of reaction progress that monitor changes in mineral composition and modal proportions. Reaction progress, ξ, is defined for an arbitrary unit of rock as:

$$\xi = \Delta n_x / \nu_x \quad (3)$$

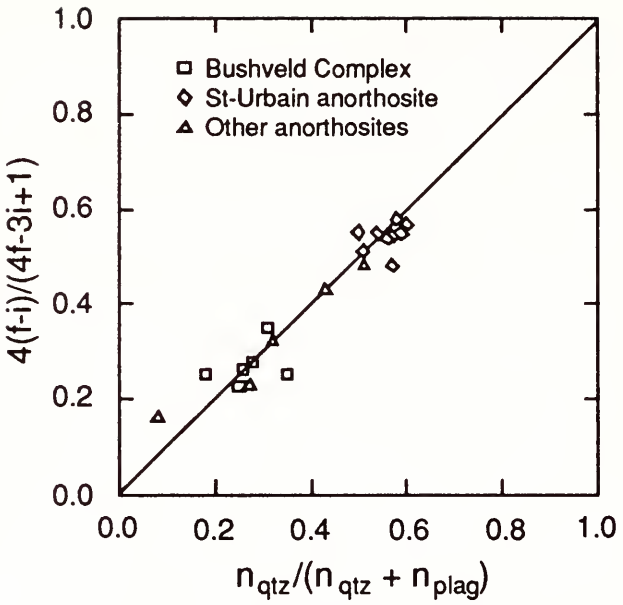

FIG. 12. A test of the metasomatic replacement model.

where Δn_x is the change in the number of moles of species, x, per unit of rock that results from the progress of a given chemical reaction, ν_x is the stoichiometric reaction coefficient of species, x, and the sign of ν_x is positive for the reaction products and negative for the reactants. Two expressions for reaction progress of equation (2) are:

$$\xi = \Delta n_{qtz}/4(f-i) \quad (3a)$$

$$\xi = \Delta n_{plag}/(1+i) \quad (3b)$$

where n_{plag} refers to the number of moles of calcic plagioclase on the right hand side of reaction (2). The initial assemblage does not contain either quartz or calcic plagioclase and therefore $\Delta n_{qtz} = n_{qtz}$ and $\Delta n_{plag} = n_{plag}$. Rearrangement of equations (3a) and (3b) yields:

$$n_{qtz}/(n_{qtz}+n_{plag}) = 4(f-i)/(4f-3i+1) \quad (4)$$

Equation (4) provides a test of the replacement model that is based on two independent sets of data (mineral composition and modal abundance). Fig. 12 shows there is excellent agreement between the empirical data and the relationship predicted by equation (4), providing strong support for the replacement model for the origin of calcic myrmekite.

The isochemical model is based on the assumption that myrmekite forms by exsolution of quartz from the "Schwantke molecule" ($Ca_{0.5}\square_{0.5}AlSi_3O_8$), which is essentially a feldspar that contains excess silica in solid solution. The isochemical model can be represented by the following end-member reaction:

$$2Ca_{0.5}\square_{0.5}AlSi_3O_8 = CaAl_2Si_2O_8 + 4SiO_2, \quad (5)$$
Schwantke anorthite qtz

where myrmekite consists of a vermicular intergrowth of the product minerals. Reaction (5) can be rewritten for an arbitrary initial composition:

$$Na_{1-f}Ca_f\square_f Al_{1+f}Si_{3+3f}O_{8+8f}$$
Schwantke-albite solid solution

$$= Na_{1-f}Ca_fAl_{1+f}Si_{3-f}O_8 + (4f)SiO_2. \quad (6)$$
plagioclase qtz

In contrast to the replacement model, the composition of plagioclase produced by the isochemical process is independent of the composition of plagioclase in the host rock. Two expressions for the progress of reaction (6) are:

$$\xi = n_{qtz}/4f, \quad (7a)$$

$$\xi = n_{plag}. \quad (7b)$$

Combination of equations (7a) and (7b) yields:

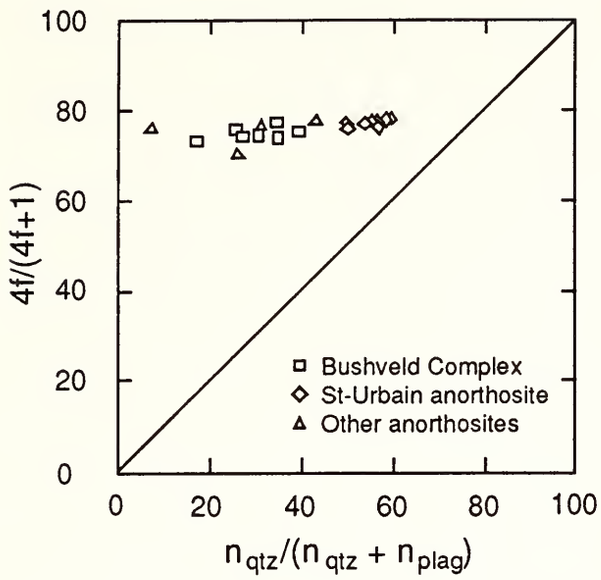

FIG. 13. A test of the isochemical exsolution model

$$n_{qtz}/(n_{qtz}+n_{plag}) = 4f/(4f+1). \quad (8)$$

Equation (8) provides a test of the isochemical exsolution model and Fig. 13 shows that the empirical data are inconsistent with this model.

Alternative models for the origin of calcic myrmekite have been tested through the coordinated application of two microanalytical techniques that monitor changes in mineral composition and modal abundance on a sub-millimeter scale. The data are in agreement with the metasomatic replacement model but are not consistent with the isochemical exsolution model. Similar applications of the reaction progress method may provide a powerful tool for testing petrologic models on a microscopic scale.

References

Ashworth, J. R., Myrmekites of exsolution and replacement origins, *Geol. Mag., 109*, 45-62, 1972.

Becke, F., Über Myrmekit, *Tschermaks Mineral. Petrogr. Mitt., 27*, 377-390, 1908.

Dymek, R. F., and C. M. Schiffries, Calcic myrmekite: Possible evidence for the involvement of water during the evolution of andesine anorthosite from St-Urbain, Quebec, *Can. Mineral., 25*, 291-319, 1987.

Ferry, J. M., Reaction progress: A monitor of fluid-rock interaction during metamorphic and hydrothermal events, in *Fluid-Rock Interactions During Metamorphism*, J. V. Walther and B. J. Wood, eds., Springer-Verlag, New York, 89-108, 1986.

Michel-Lévy, A., De quelques characteres microscopiques des roches anciennes acides, consideres dans leurs relations avec l'age des èruptions, *Soc. Géol. France Bull., 3rd series, 3*, 199-236, 1874-75.

Newton, R. C., J. V. Smith, and B. F. Windley, Carbonic metasomatism, granulites, and crustal growth, *Nature, 288*, 45-50, 1980.

Phillips, E. R., Myrmekite—one hundred years later, *Lithos, 7*, 181-194, 1974.

Rumble, D., J. M. Ferry, T. C. Hoering, and A. J. Boucot, Fluid flow during metamorphism at the Beaver Brook fossil locality, New Hampshire, *Am. J. Sci., 282*, 886-919, 1982.

Schiffries, C. M., and R. F. Dymek, Calcic myrmekite in gabbroic and anorthositic rocks, *Geol. Soc. Am. Abstr. Program., 17*, 709, 1985.

Schwantke, A., Die Beimischung von Ca im Kalifeldspat und die Mymrekitbildung, *Centralbl. Mineral.*, 311-316, 1909.

Sederholm, J. J., On synantectic minerals and related phenomena, *Comm. Geol. Finlande Bull., 153*, 1-148, 1916.

Thompson, J. B., Reaction space: An algebraic and geometric approach, *Rev. Mineral., 10*, 33-51, 1982.

Thompson, J. B., Jr., J. Laird, and A. B. Thompson, Reactions in amphibolite, greenschist, and blueschist, *J. Petrol., 23*, 1-27, 1982.

Liquid-Absent Aqueous Fluid Inclusions

Craig M. Schiffries

A wide variety of geological phenomena are governed by interactions between fluids and rocks at elevated temperatures and pressures. Studies of fluid inclusions provide important constraints on the chemical composition of crustal fluids and the physical conditions of fluid-rock interactions. Raman spectra and microthermometric data are reported here for a new class of aqueous fluid inclusions that is characterized by the absence of a liquid phase at 20°C. The inclusions hold special interest because they display the following properties: (1) Although they do not contain a liquid phase at 20°C, the inclusions homogenize to an aqueous liquid at elevated temperatures; (2) Initial melting occurs at a reaction point (+29°C), rather than a eutectic point as commonly assumed (T_E = -52°C for the system $CaCl_2$ - NaCl - H_2O); (3) Ice is absent in the subsolidus assemblage despite the high-H_2O contents of the inclusions. At room temperature, most of the water occurs as structurally bound H_2O in hydrate minerals and a relatively small amount occurs in a low-density vapor phase; (4) The most abundant daughter minerals in the subsolidus assemblage are antarcticite ($CaCl_2 \cdot 6H_2O$) and a second hydrate that may be a new mineral; (5) The fluid compositions fall outside the compositional limits defined by previous studies of natural fluid inclusions. The inclusions described here occur in quartz from a mafic pegmatoid in the Bushveld Complex. Similar inclusions probably occur in other geological environments, but they may be overlooked or misinterpreted because their solidus temperature is above 20°C.

At room temperature, the liquid-absent aqueous inclusions consist of birefringent hydrates (~60 to 70 volume percent), halite (less than 10 volume percent), and a low density vapor (~20 to 30 volume percent). Raman spectroscopy was used to identify hydrate daughter minerals that are difficult to distinguish by optical microscopy (Dubessy *et al.*, 1982). Experimental conditions of the micro-Raman optical system are similar to those described by Hemley *et al.* (1987). The most abundant phase in the subsolidus assemblage has asymmetric Raman bands at 1660 and 3430 cm^{-1} that are indicative of the bending and stretching modes, respectively, of structural water in antarcticite. The presence of a second hydrate daughter mineral in the subsolidus assemblage is indicated by an additional peak at 1620 cm^{-1} (Fig. 14). The second hydrate has not been positively identified, but the most likely possibility is a polymorph of $CaCl_2 \cdot 4H_2O$. A preliminary study of synthetic compounds indicates that at least one polymorph of $CaCl_2 \cdot 4H_2O$ has a Raman peak at approximately 1620 cm^{-1}. None of the $CaCl_2 \cdot 4H_2O$ polymorphs is currently recognized as a mineral species.

Microthermometric measurements were performed with a USGS-type, gas-flow, heating-cooling stage (Fluid Inc.) mounted on a petrographic microscope. Initial melting occurs at approximately +29°C and a large fraction of liquid (more than 25 volume percent) is present at 30°C in some inclusions. It appears that antarcticite melts

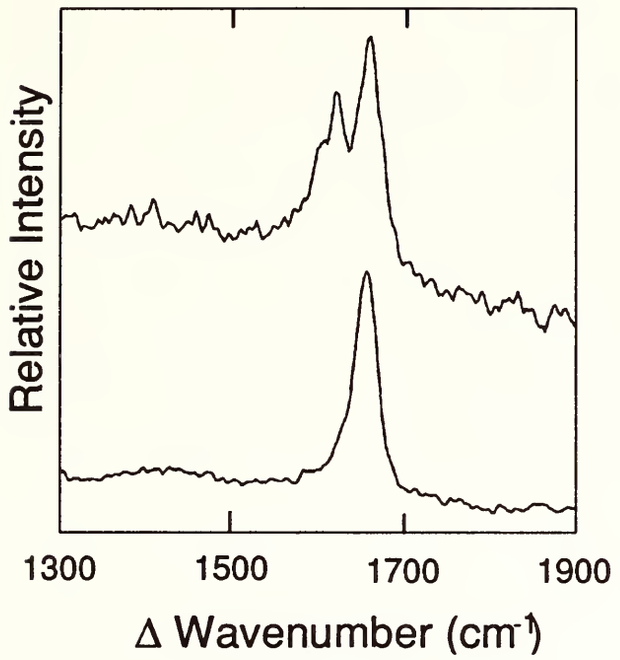

FIG. 14. Micro-Raman spectra (OH-bending mode region) of hydrate daughter minerals at 20°C. The position and shape of the Raman band at 1660 cm^{-1} in the bottom spectrum are consistent with the spectrum of antarcticite. The presence of a second hydrate daughter mineral in the subsolidus assemblage is suggested by an additional Raman band at 1620 cm^{-1} (top spectrum). The mineral responsible for the peak at 1620 cm^{-1} has not been positively identified, but the most likely possibility is a polymorph of $CaCl_2 \cdot 4H_2O$. The Raman band at 1660 cm^{-1} in the top spectrum may reflect contributions from both antarcticite and $CaCl_2 \cdot 4H_2O$.

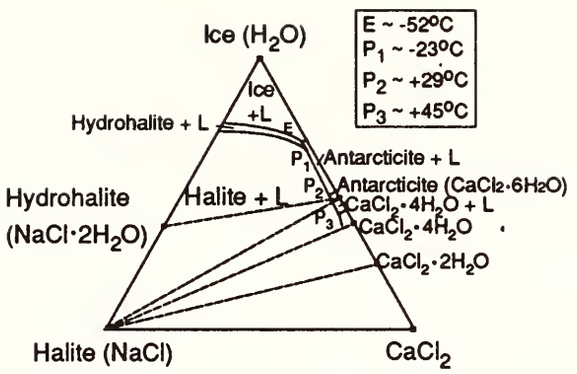

FIG. 15. Provisional vapor-saturated, liquidus diagram for the system $CaCl_2$-NaCl-H_2O (after Brass, 1980; Crawford, 1981; Oakes *et al.*, 1988; Vanko *et al.*, 1988; Zhang and Frantz, 1989). Boundaries of the $CaCl_2 \cdot 4H_2O$ liquidus are based on extrapolations that are consistent with the Alkemade theorem, Schreinemakers rules and the binary $CaCl_2$-H_2O phase diagram. The liquidus fields for antarcticite and $CaCl_2 \cdot 4H_2O$ have been enlarged for clarity. Subsolidus assemblages are indicated by dashed lines. The location of reaction point P_2 relative to the subsoludus join between antarcticite and hydrohalite is uncertain, but the point lies above the join between $CaCl_2 \cdot 4H_2O$ and hydrohalite. For the assemblage ice + hydrohalite + antarcticite, the first equilibrium melt forms at -52°C at the ternary eutectic (*E*). For the assemblage halite + hydrohalite + antarcticite, the first equilibrium melt forms at approximately -22°C at P_1. For the assemblage halite + antarciticte + $CaCl_2 \cdot 4H_2O$, the first equilibrium melt forms at approximately +29°C at P_2.

incongruently at the initial melting temperature and the inclusions subsequently consist of $CaCl_2 \cdot 4H_2O$(?) and vapor. With increasing temperature, the final hydrate [$CaCl_2 \cdot 4H_2O$(?)] rapidly diminishes in size and melts at +32° to +38°C. Halite is present in some inclusions [T_m(halite) = 199±26°C] and it is probably metastably absent in other inclusions. Further heating causes the vapor bubble to shrink and the inclusions homogenize to an aqueous liquid.

The phase equilibria can be interpreted in terms of the vapor-saturated, liquidus diagram for the system $CaCl_2$ - NaCl - H_2O (Fig. 15; see also Brass, 1980; Crawford, 1981; Oaks et al., 1988; Vanko *et al.*, 1988; Zhang and Frantz, 1989). For the subsolidus assemblage antarcticite + $CaCl_2 \cdot 4H_2O$ + halite, the first equilibrium melt forms at approximately +29°C at reaction point P_2. At P_2 antarcticite melts incongruently. to $CaCl_2 \cdot 4H_2O$ and an aqueous liquid. With increasing temperature, the composition of the liquid evolves along the cotectic boundary between halite and $CaCl_2 \cdot 4H_2O$ until the latter phase melts completely at 32° to 38°C. The composition of the liquid subsequently migrates across the halite liquidus until T_m(halite). Previous studies (*e.g.* Crawford, 1981; Vanko *et al.*, 1989) indicate that most fluid inclusions in the system

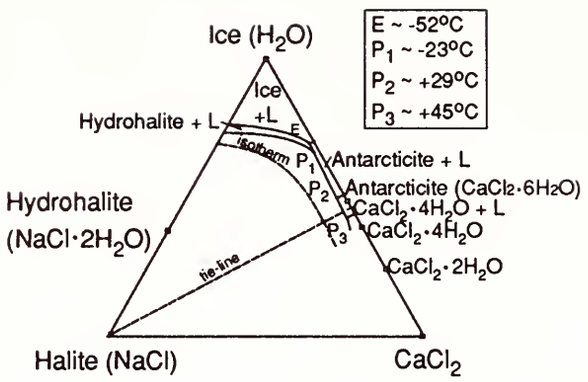

FIG. 16. The bulk composition of the fluid lies at the intersection of the T_m(halite) isotherm, and the tie-line between halite and the point on the halite-$CaCl_2 \cdot 4H_2O$ cotectic that corresponds to $T_m(CaCl_2 \cdot 4H_2O)$.

$CaCl_2$ - NaCl - H_2O exhibit the following melting behavior: the subsolidus assemblage consists of ice + hydrohalite + antarcticite; initial melting occurs at the eutectic point (E); and antarcticite is consumed at the eutectic temperature (-52°C). Given the topology of the phase diagram (Fig. 15), small variations in bulk composition may result in large differences in the subsolidus mineral assemblage, the initial melting temperature, the equilibrium melting sequence, and the phase ratios at 20°C (Schiffries, in preparation).

In theory, the bulk composition of the inclusions discussed here can be determined from two measurements: (1) $T_m(CaCl_2 \cdot 4H_2O)$ in the presence of a cotectic liquid plus halite and vapor and (2) T_m(halite) in the presence of liquid and vapor. By neglecting the mass of the vapor, the bulk composition lies at the intersection of the halite dissolution isotherm, and the tie-line between halite and the point on the halite - $CaCl_2 \cdot 4H_2O$ cotectic corresponding to $T_m(CaCl_2 \cdot 4H_2O)$ (Fig. 16). In practice, the bulk composition cannot be determined precisely by this technique because there are uncertainties in the location of the halite - $CaCl_2 \cdot 4H_2O$ cotectic and the halite dissolution isotherms in the relevant part of the phase diagram. Despite uncertainties in the liquidus diagram, the subsolidus assemblage indicates that the compositions of these inclusions fall outside the compositional limits defined by previous studies of natural fluid inclusions. The fluids are characterized by a high Ca/Na ratio and a very high concentration (greater than 52 wt %) of total dissolved solids.

References

Brass, G. W., Stability of brines on Mars, *Icarus, 42*, 20-28, 1980.

Crawford, M. L., Phase equilibria in aqueous fluid inclusions, in *Short Course in Fluid Inclusions: Applications to Petrology*, L. S. Hollister, and M. L. Crawford, eds., Short Course Handbook 6, Mineral Assoc. Canada, Ottawa, pp. 75-100, 1981.

Dubessy, J. D., D. Audeoud, R. Wilkins, and C. Kosztilanyi, The use of the Raman micro-probe MOLE in the determination of the electrolytes dissolved in the aqueous phase of fluid inclusions, *Chem. Geol., 37*, 137-150, 1982.

Hemley, R. J., P. M. Bell, and H. K. Mao, Laser techniques in high-pressure geophysics, *Science, 237*, 605-612, 1987.

Oakes, C.S., R.J. Bodnar, and J. M. Simonson, Phase equilibria in the system NaCl - $CaCl_2$ - H_2O: The ice liquidus, *Geol. Soc. Am. Abstr. Progm., 20*, A390, 1988.

Vanko, D. A., R. J. Bodnar, and S. M. Sterner, Synthetic fluid inclusions: VIII. Vapor-saturated halite solubility in part of the system NaCl-$CaCl_2$-H_2O, with application to fluid inclusions from oceanic hydrothermal systems, *Geochim. Cosmochim. Acta, 52*, 2451-2456, 1988.

Zhang, Y. G., and J. D. Frantz, Experimental determination of the compositional limits of immiscibility in the system $CaCl_2$-H_2O-CO_2 at high temperatures and pressures using synthetic fluid inclusions, *Chem. Geol., 74*, 289-308, 1989.

IGNEOUS AND METAMORPHIC PETROLOGY - B. EXPERIMENTAL STUDIES

OXYGEN FUGACITY AND EVAPORATION PHASE RELATIONS IN THE SOLAR NEBULA

*Bjorn O. Mysen and Ikuo Kushiro**

Characterization of the pressure (P) - temperature (T) - oxygen fugacity [$f(O_2)$] phase relations that govern evaporation, condensation and melting relations in the system CaO - MgO - Al_2O_3 - TiO_2 - SiO_2 is of interest because this system contains most of the refractory minerals (perovskite, corundum, spinel, hibonite and calcium dialuminate) expected to form at the highest temperatures during rock-forming processes in the early solar nebula. Principal evidence for this suggestion is the phase assemblages in Ca-, Al-rich inclusions (CAI's) in carbonaceous chondrites (see MacPherson *et al.*, 1988 for review).

The suggested $f(O_2)$ range during rock-forming processes in the early solar nebula is from about 5 orders of magnitude below to perhaps 2 orders of magnitude above that defined by the iron-wustite (IW) oxygen fugacity buffer (e.g., Fegley, 1985; Brett and Sato, 1984; Kozul *et al.*, 1986). It is possible that partial or complete reduction of metal cations (Si^{4+}, Al^{3+}, Ca^{2+}, Ti^{4+}, and Mg^{2+}) in the system may take place in the lowest portion of this $f(O_2)$ range. Thus, the phase relations in the early solar nebula will be affected by the oxygen fugacity. Experimental determination of phase relations as a function of $f(O_2)$ is reported here.

The Knudsen Cell technique (Knudsen, 1909) has been used to measure vapor pressures of the phase assemblages (with modifications and calibrations described by Mysen and Kushiro, 1988). The samples were contained in Mo and C Knudsen cells. Through interaction between the sample containers (Mo and C) and the oxide starting materials, $f(O_2)$-values at or near the Mo - MoO_2 and C - CO - CO_2 buffers were defined This $f(O_2)$ range covers that from near the highest oxygen fugacities recorded from intrinsic oxygen fugacity measurements of chondrites (1-2 orders of magnitude above the IW buffer; Brett and Sato, 1984; Kozul *et al.*, 1986) to about two orders of magnitude above the $f(O_2)$ suggested for the primordial solar nebula (5-6 orders of magnitude below the IW buffer; Fegley, 1985).

The melting and vaporous phase relations of the high-temperature refractory aluminates and perovskite are distinctly dependent on the $f(O_2)$ (Fig. 17). Not only do the P - T coordinates of the vaporous boundaries change as the $f(O_2)$ is lowered, but in the case of the most important phases such as spinel ($MgAl_2O_4$), hibonite ($CaO{\bullet}6Al_2O_3$) and perovskite ($CaTiO_3$), the vaporous phase also changes as a function of $f(O_2)$ at pressures below the triple point

* Address: Geological Institute, University of Tokyo, Hongo-Tokyo 113, Japan

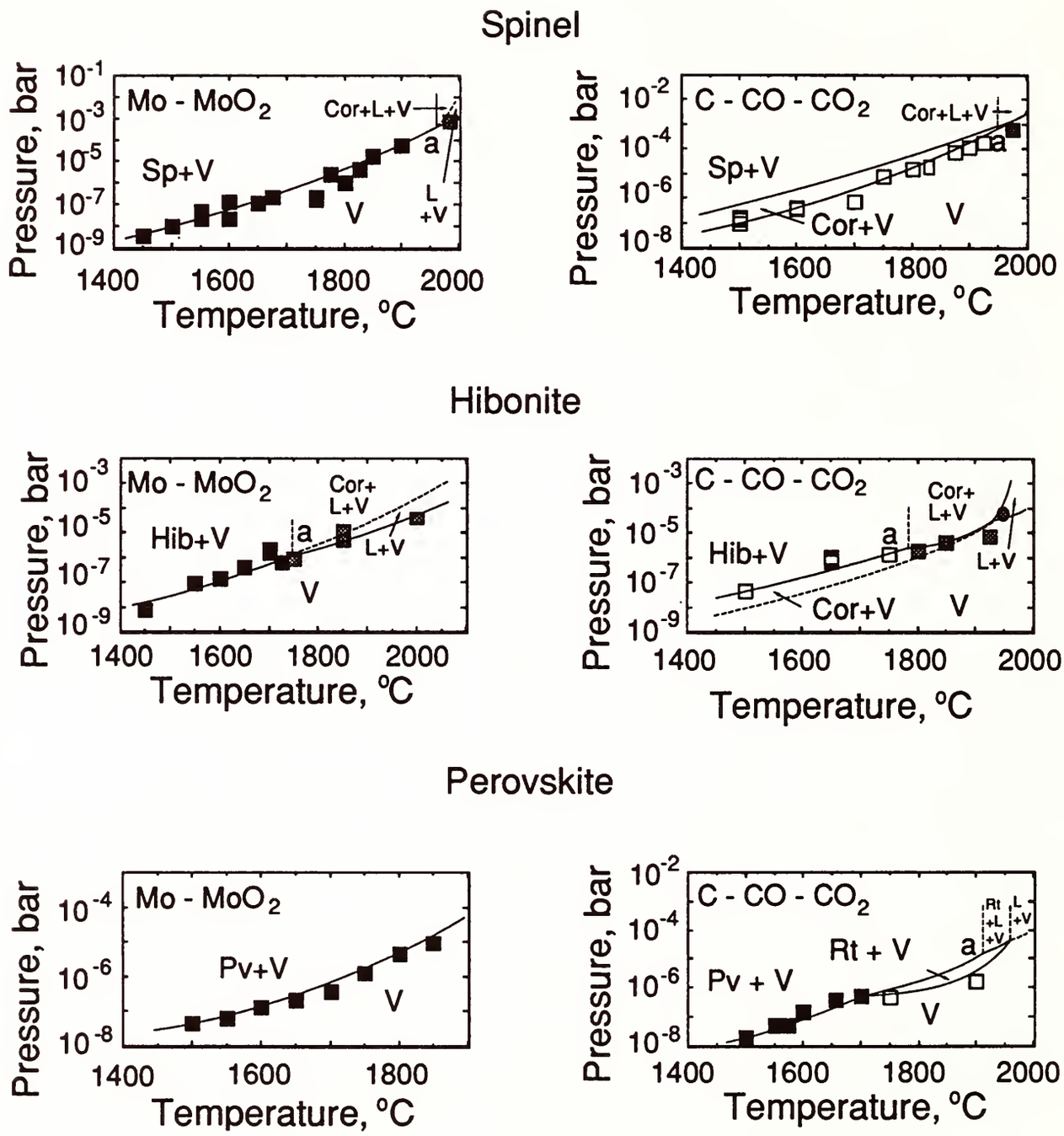

FIG. 17. Pressure - temperature trajectories of phase relations in the systems $MgAl_2O_4$, $CaO{\bullet}6Al_2O_3$ and $CaTiO_3$ at the $f(O_2)$ of the Mo - MoO_2 and C - CO - CO_2 oxygen fugacity buffers. Abbreviations: Sp - spinel, Cor - corundum, Hib - hibonite, Pv - perovskite, Rt - rutile, L - liquid, V - Vapor. Closed symbols represent experimental points along a vaporous with congruent evaporation, grey symbols show the vaporous of liquid-bearing assemblages, and open symbols represent incongruent evaporation phase relations.

(marked *a* in Fig. 17). Whereas spinel, hibonite and perovskite are the vaporous phases at the high $f(O_2)$ (Mo - MoO_2), at the lower $f(O_2)$ (C - CO - CO_2), corundum (for the aluminates) or a TiO_2 phase (for perovskite starting material, probably rutile) becomes the vaporous phase.

These changes in vaporous phase relations result from partial reduction of Ca^{2+} and Mg^{2+} in the vapor. From the slopes of the vapor pressure ($\ln P_v$) versus absolute temperature ($1/T$) for the CaO and MgO

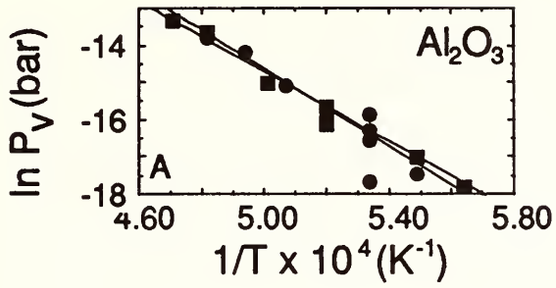

	• C - CO - CO_2		■ Mo - MoO_2	
	ΔH	ΔS	ΔH	ΔS
Al_2O_3	466	110	405	80
MgO	411	115	332	67
CaO	530	159	349	54

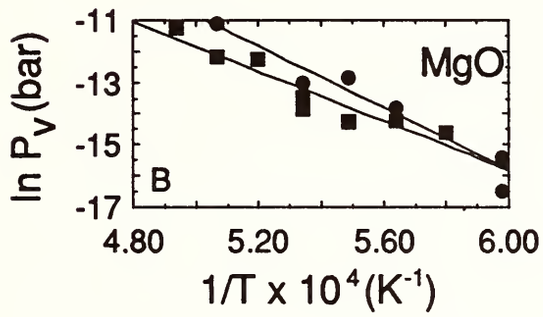

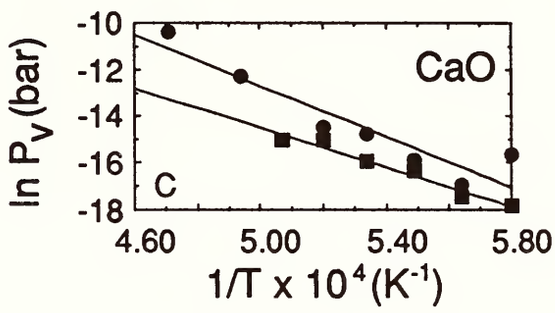

FIG. 18. Vapor pressure (natural logarithm, ln P_v) versus temperature ($1/T$) for the systems Al_2O_3, CaO and MgO at the $f(O_2)$ of the Mo - MoO_2 and C - CO - CO_2 oxygen fugacity buffers. Thermodynamic parameters pertinent to evaporation are also shown.

system (Fig. 18) it is evident that both the entropy, ΔS, and enthalpy, ΔH, of evaporation increases with the reduced $f(O_2)$. The effect of $f(O_2)$ on the corundum vaporous relations is significantly less.

The increased ΔH and ΔS values of evaporation of CaO and MgO with decreasing $f(O_2)$ (Fig. 18) can be rationalized by suggesting increased dissociation in the vapor by lowering the $f(O_2)$ (e. g., Ca, Mg, O_2 and O). At the $f(O_2)$ of the Mo-MoO_2 buffer, the evaporation reaction is:

$$MgO(s) \Leftrightarrow MgO(v), \quad (1)$$

with a ΔH of evaporation of 331 KJ/mol (Fig 18). From the data of Dowart *et al.* (1964) about 50% of the MgO(v) will be in the elemental state at the log $f(O_2)$ of the C-CO-CO_2 buffer. The resulting reduction of the activity of Mg^{2+} most likely is the explanation of incongruent evaporation of spinel at the latter $f(O_2)$, whereas spinel evaporates congruently at the $f(O_2)$ of the Mo - MoO_2 buffer.

Similar reasoning can be applied to evaporation of lime (CaO) at the two different oxygen fugacities. Analogous species (Ca, CaO, O and O_2) exist in the vapor from this system as in the Mg-O system. The ΔH for the reaction:

$$CaO(v) + O(v) \Leftrightarrow Ca(v) + O_2(v), \quad (2)$$

is 117 KJ/mol (Dowart *et al.*, 1964). From the data in Fig. 18, this enthalpy would imply essentially complete dissociation of CaO(v) to Ca(v) and O_2(v) as the oxygen fugacity is reduced from that of the Mo - MoO_2 buffer to that of the C - CO - CO_2 buffer. The consequent reduction in Ca^{2+} activity in the vapor (probably can explain

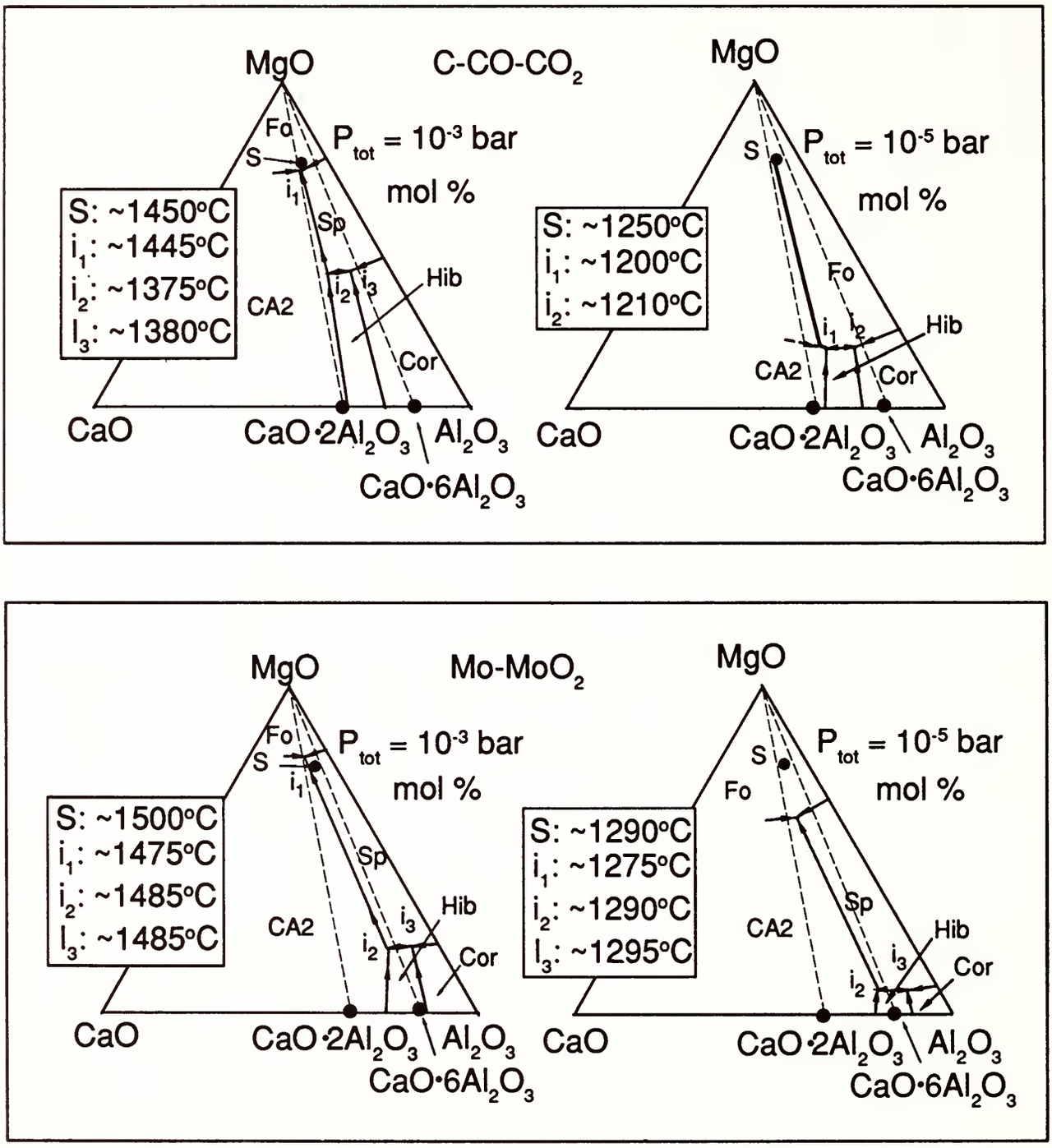

FIG. 19. Vaporous surfaces in the system CaO - MgO - Al_2O_3 - SiO_2 at 10^{-3} bar (A,C) and 10^{-5} bar (B, D) total pressure. *S* denotes solar CaO/MgO/Al_2O_3 (from Anders and Ebihara, 1982). SiO_2 content is that of the solar abundance. Temperatures of various invariant points and the vaporous surface temperatures of *S* are indicated in the inserts. The overall dilution in the gas is about 10^4 (solar dilution). Abbreviations: Cor - corundum, Sp spinel, Pe - periclase, CA2 - calcium dialuminate, Hib - hibonite, Fo - forsterite. Oxygen fugacity is at that of the C-CO-CO_2 (A,B) and Mo - MoO_2 (C,D) buffer.

the change from congruent to incongruent evaporation of hibonite and perovskite ($CaTiO_3$) as the $f(O_2)$ is lowered.

From the evaporation data reported here and elsewhere (Mysen, 1988; Mysen and Kushiro, 1988), vaporous surfaces in the system CaO - MgO - Al_2O_3 - SiO_2 with Mg/Si = 1 have been calculated (Fig. 19) under the assumption of ideal mixing in the gas phase and with the proportion of oxide

components relative to an inert gas diluent equal to that of the solar nebula (~10^4; Anders and Ebihara, 1982). The condensation and evaporation sequences are strongly affected by $f(O_2)$. For example, spinel is only stable at high pressure, or high $f(O_2)$, or both. The occurrence of spinel-rich CAI's may indicate that such conditions existed in the solar nebula. Corundum and hibonite-rich phase assemblages probably required either low total pressure (less than ~10^{-5} bar), or that the $f(O_2)$ was at or below that of the C - CO - CO_2 oxygen buffer during their formation. For example, reheating and partial evaporation of materials rich in organic carbon will take place with $f(O_2)$ near that of the C - CO - CO_2 buffer. With this low oxygen fugacity, the evaporation process yields a residue enriched in aluminum relative to that of the starting material.

In the early solar nebula where temperatures and pressures probably increased toward its center, the experimentally determined phase relations lead to the suggestion of an overall increase in (Mg + Ca)/Al in the condensates with decreasing distance to the Sun. This trend may be retained in the bulk composition of the planets today.

References

Anders, E., and M. Ebihara, Solar system abundances of the elements, *Geochim.Cosmochim. Acta, 46*, 2363-2380, 1982.

Brett, R., and M. Sato, Intrinsic oxygen fugacity measurements on seven chondrites, a pallasite and a tektite and the redox state of meteorite parent bodies, *Geochim. Cosmochim. Acta, 48*, 111-120, 1984

Dowart, J., G. Exsteen, and G. Verhaegen, Mass spectrometric determination of the dissociation energy of thermocouples MgO, CaO, SrO and Sr_2O*, *Trans. Faraday Soc., 60,* 1920-1933, 1964.

Fegley, B., Oxidation state indicators of the solar nebula, *Lunar Planet. Sci. XVI,* 232-233, 1985.

Kozul, J., G. C. Ulmer, and R. Hewins, Allende inclusions are oxidized!, *EOS, 67*, 300, 1986.

Mysen, B. O., Rock - forming processes in the early solar nebula: Phase relations in the system CaO - MgO - Al_2O_3 - SiO_2 to 2000°C and 10^{-1} bar, *Annual Report of the Director of the Geophysical Laboratory, Carnegie Instn. Washington, 1987-1988,* Geophysical Laboratory, Washington, D. C. , 69-76, 1988.

Mysen, B. O., and I. Kushiro, Condensation, evaporation, melting and crystallization in the primitive solar nebula: Experimental data in the system MgO - SiO_2 - H_2 to 10x10^{-9} bar and 1870°C with variable oxygen fugacity, *Am. Mineral., 73*, 1-19, 1988.

Knudsen, M., Die Molekularstromung der Gase durch Offnungen und die Effusion, *Ann. Phys., 28*, 999-1016, 1909.

MacPherson, G. J., D. A. Wark, and J. T. Armstrong, Primitive materials surviving in chondrites: refractory inclusions, in *Meteorites and the Early Solar System*, J. F. Kerridge and M. S. Matthews, eds., The University of Arizona Press, Tucson, pp. 746-807, 1988.

Experimental Determination of Element Partitioning and Calculated Phase relations in the Mg-Fe-Si-O System at High Pressure and High Temperature

Yingwei Fei, Ho-kwang Mao, and Bjorn O. Mysen

The principal components of the Earth's mantle are MgO, FeO and SiO_2. Phase relations in this system are of great interest to geochemists and geophysicists because both the 400 km and the 670 km seismic discon-

tinuities may reflect the phase transformations of olivine (α) to β-phase and of spinel (γ) to perovskite plus magnesiowüstite, respectively.

The phase relations can be established in two ways. One is to determine phase boundaries in *P-T-X* space (e.g. Akimoto, 1987; Katsura and Ito, 1989; Ito and Takahashi, 1989). The other is to determine precisely the phase boundaries of pure phases and the mixing properties of each solid solution. The phase relations in binary or multi-component systems can then be calculated. Solid solutions in the Mg-Fe-Si-O system include (Mg,Fe)O (magnesiowüstite), $(Mg,Fe)_2SiO_4$ (olivine, β-phase, spinel) and $(Mg,Fe)SiO_3$ (pyroxene, ilmenite, perovskite). These solid solutions form four pairs of coexisting phases with magnesiowüstite (Mw), Mw-olivine, Mw-β, Mw-spinel and Mw-perovskite. The solution properties of the individual phase may be derived from the element distribution data by considering the distribution of an element between two solid solutions as an exchangeable reaction (Fei and Saxena, 1986). The purpose of this study is to derive the mixing properties of each solution by determining experimentally the distribution of Mg and Fe between coexisting solid solutions at various pressure and temperature conditions and to establish phase relations in the system.

The experiments are conducted with the piston-cylinder apparatus (up to 50 kbar) (Boyd and England, 1960, 1963), the multi-anvil device (up to 300 kbar) (Liebermann *et al.*, 1986 and Remsberg *et al.*, 1988), and the diamond-anvil cell device (Mao and Bell, 1978). Chemical and structural analytical techniques such as x-ray diffraction, microprobe or SEM and Raman spectroscopy were used to characterize the structure and chemical composition of the samples.

Synthetic olivine and magnesiowüstite solid solutions with different iron contents were used as starting materials. Magnesiowüstite solid solutions were those synthesized by Rosenhauer *et al.* (1976). Olivine solid solutions were synthesized in the piston-cylinder apparatus, with oxide mixtures as starting material, for 48 hours at 1273K and 15 kbar. The synthetic olivines were examined optically and with x-ray diffraction; no oxide remainder was present. The compositions were checked by electron microprobe.

For the Mg-Fe partition experiments with magnesiowüstite and olivine, magnesiowüstite and olivine of suitable compositions were mixed in appropriate proportions (e.g., 2 magnesiowüstite to 3 olivine in most cases). The mixtures were ground to a grain size of less than 3 μm and well homogenized. Two different types of capsules, platinum capsule sealed inside with graphite capsule and molybdenum capsule, were used to test if there was iron loss in the runs. No evidence for iron-loss was found.

The piston-cylinder apparatus was used for experiments below 50 kbar. The multi-anvil device was used for determining distribution coefficients between magnesiowüstite and olivine at 90 kbar and 1723K, between magnesiowüstite and β-phase and between magnesiowüstite and spinel at 150 kbar and 1773K. The multi-cell sample chambers described by Mao *et al.* (1989) were used in the experiments.

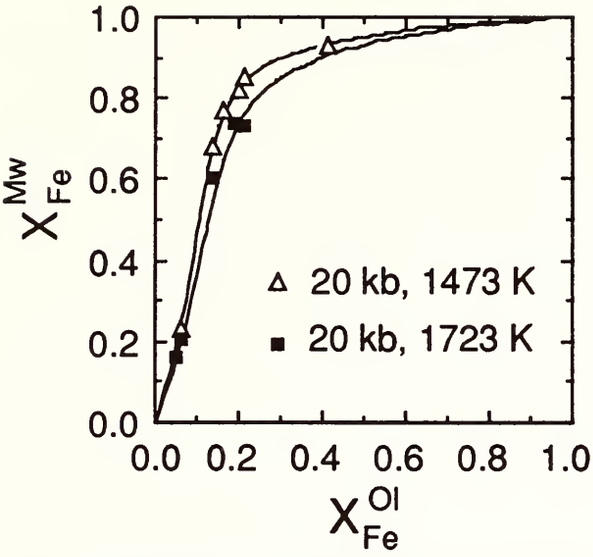

FIG. 20. Distribution of Mg and Fe between coexisting magnesiowüstite (Mw) and olivine (Ol) at a pressure of 20 kbar and at temperatures of 1473K (upper curve) and 1723K (lower curve). Curves are calculated results and symbols represent the experimental data.

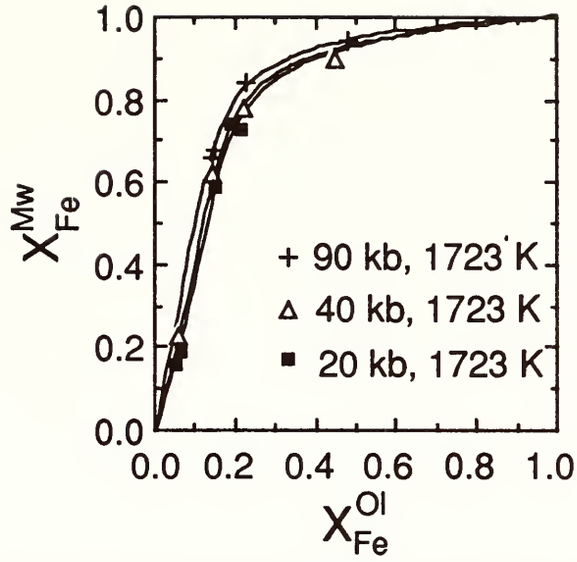

FIG.21. Distribution of Mg and Fe between coexisting magnesiowüstite (Mw) and olivine (Ol) at a temperature of 1723K and at pressures of 20 kbar (lower curve), 40 kbar (middle curve) and 90 kbar.

Figs. 20 and 21 show the temperature and pressure dependences of the Mg-Fe distribution coefficients between magnesiowüstite and olivine. The experimental results show systematic variations of the distribution data with temperature and pressure.

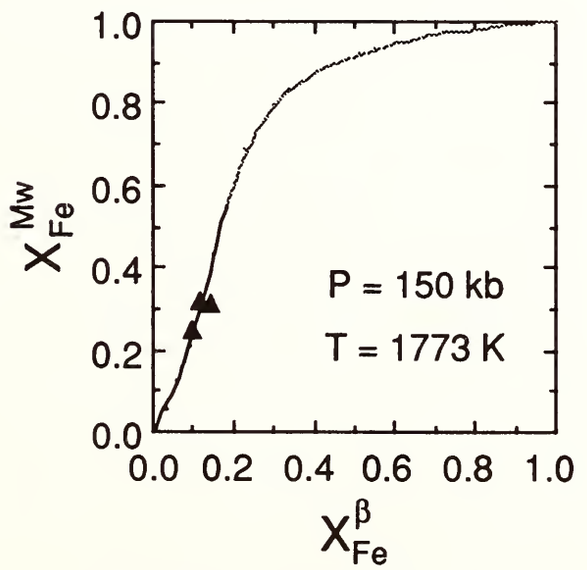

FIG. 22. Distribution of Mg and Fe between coexisting magnesiowüstite (Mw) and β-phase (β) at a pressure of 150 kbar and at a temperature of 1773K. Curves are calculated results and symbols represent the experimental data.

The Mg-Fe distribution coefficients between magnesiowüstite and β-phase or spinel are shown in Figs. 22 and 23. The results by Ito *et al.* (1984) and Yagi *et al.* (1979) are also shown for comparison.

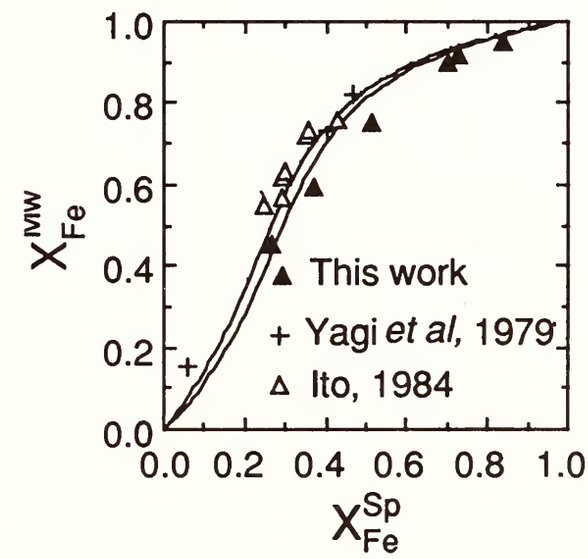

FIG. 23. Distribution of Mg and Fe between coexisting magnesiowüstite (Mw) and spinel (Sp) at a temperature of 1773K and pressures of 150 kbar (lower curve), and at temperature of 1873K and pressure of 200 kbar (upper curve). Curves are calculated results and symbols represent the experimental data.

TABLE 3. Nonideal mixing parameters of solid solutions in the Mg-Fe-Si-O system

Solid solutions	$W_{Mg\text{-}Fe}$ (J/mol)	$W_{Fe\text{-}Mg}$ (J/mol)
Magnesiowüstite	16100	26300 - 5.56T
Olivine (α)	4500 + 0.013P	6500 + 0.013P
β-phase	1000	2000
Spinel (γ)	3900 - 1.10T	3900
Perovskite	4130 - 1.37T + 0.011P	-4050 - 2.45T + 0.015P

To determine the distribution of Mg and Fe between magnesiowüstite and perovskite, olivines (Fo_{85}, Fo_{80} and Fo_{73}) were used as starting materials in the diamond-anvil cell. Olivine with small ruby grains was imbedded in a 250 μm hole drilled in a gasket. The sample was pressurized in the diamond-anvil cell and heated by YAG laser beam. The pressure was measured with the fluorescence technique. The products were examined optically and by x-ray diffraction. The composition of each phase in the assemblage was determined both by x-ray diffraction (the relation between volume and composition using the calibrations of Yagi *et al.*, 1979; Rosenhauer *et al.*, 1976) and by electron microprobe. The lattice parameters of each phase were determined by x-ray diffraction, with gold as internal standard for calibration. The results accord with those determined with the electron microprobe. The results on the Mg-Fe partitioning between magnesiowüstite and perovskite are shown in Fig. 24. These are in agreement with those obtained by Ito *et al.* (1984) and Yagi *et al.* (1979).

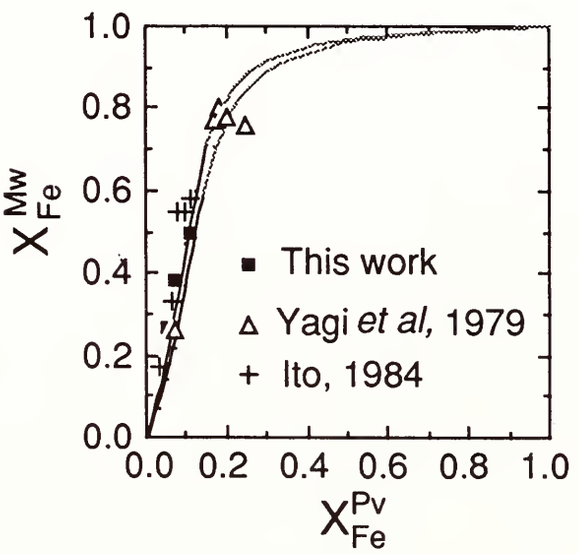

FIG. 24. Distribution of Mg and Fe between coexisting magnesiowüstite (Mw) and perovskite (Pv) at a temperature of 1873K and pressures of 260 kbar (lower curve), and 300 kbar (upper curve). Curves are calculated results and symbols represent the experimental data.

Solution parameters (W_{ij}) for five solid solutions have been obtained by fitting the experimental data simultaneously using the Margules formulation (Table 3). Various calculated Roozeboom diagrams for the exchange of Mg^{2+} and Fe^{2+} between coexisting solid solutions are shown in Figs. 20 - 24.

The solution parameters listed in Table 3 with an internally consistent thermodynamic data set on phases in the system (Fei, 1989) can be used to compute phase relations. Fig. 25 shows computed isothermal phase relations in the binary system Mg_2SiO_4 - Fe_2SiO_4 at temperatures of 1473K and

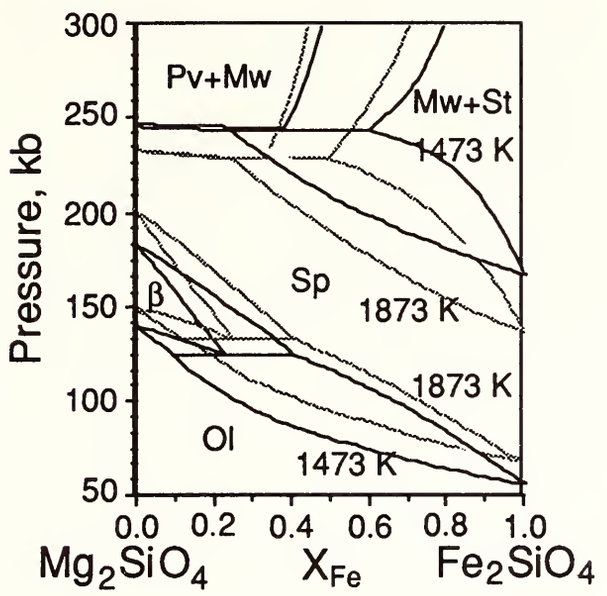

FIG. 25. Calculated isothermal phase relations in the binary system Mg_2SiO_4 and Fe_2SiO_4 at temperatures of 1473K (the heavy lines) and 1873K (the light lines) and pressures to 300 kbar.

1873K and pressures to 300 kbar.

The calculated diagram is in good agreement with those determined by Katsura and Ito (1989) and Ito and Takahashi (1989) in the Mg-rich region and by Akimoto (1987) in the Fe-rich region. The thermodynamic data base evaluated from experimental data can be used not only for reproducing the existing experimental results, but also for interpolation and even extrapolation with caution. It allows us to explore phase relations in the system in various ways. For instance, one may construct phase relations in pressure-temperature space or in pressure-composition space. In the mantle model of peridotitic composition where olivine $(Mg_{0.88}Fe_{0.12})_2SiO_4$ is the major component, the phase diagram of this olivine indicates that the depth and width of the phase transformations of olivine to β-phase and of spinel to perovskite plus magnesiowüstite are compatible with the seismic observation of the 400 km and the 670 km discontinuity, respectively. The density profile of the mantle can be simulated by varying chemical composition along the assumed geotherm. However, to make the comparison between the calculated and observed profiles, at least Ca and Al should be included in the system. Experimental determination and computer simulation of phase relations in the extended system can provide critical constraints for models of the Earth's mantle.

References

Akimoto, S., High-pressure research in geophysics: past, present and future, in *High Pressure Research in Mineral Physics*, M. H. Manghnani and Y. Syono, eds., Terra Scientific Publishing Company (TERRAPUB), Tokyo/American Geophysical Union, Washington, D. C., pp. 1-13, 1987.

Boyd, F. R., and J. L. England, Apparatus for phase-equilibrium measurements at pressures up to 50 kilobars and temperatures up to 1750°C, *J. Geophys. Res.*, *65*, 741-748, 1960.

Boyd, F. R., and J. L. England, Effect of pressure on the melting of diopside, $CaMgSi_2O_6$, and albite, $NaAlSi_3O_8$, in the range up to 50 kilobars, *J. Geophys. Res.*, *68*, 311-323, 1963.

Fei, Y., Thermochemical - thermophysical data on phases in the Mg-Fe-Si-O system: a synthesis of theory and experimental data and computation of phase equilibrium, Ph.D. dissertation, City University of New York, 1989.

Fei, Y., and S. K. Saxena, A thermochemical data base for phase equilibria in the system Fe-Mg-Si-O at high pressure and temperature, *Phys. Chem. Minerals, 13*, 311-324, 1986.

Ito, E., and E. Takahashi, Post-spinel transformations in the system Mg_2SiO_4-Fe_2SiO_4 and some geophysical implications, *J. Geophys. Res.*, in press, 1989.

Ito, E., E. Takahashi, and Y. Matsui, The mineralogy and chemistry of the lower mantle: an implication of the ultrahigh-pressure phase relations

in the system MgO - FeO - SiO_2, *Earth Planet. Sci. Lett.*, *67*, 238-248, 1984.

Katsura, T., and E. Ito, The system Mg_2SiO_4-Fe_2SiO_4 at high pressures and temperatures: precise determination of stabilities of olivine, modified spinel and spinel, *J. Geophys. Res.*, in press, 1989.

Liebermann, R. C., H. Watanabe, T. Gasparik, C. T. Prewitt, and D. J. Weidner, High pressure mineral synthesis in USSA-2000, *EOS*, *67*, 361, 1986.

Mao, H. K., and P. M. Bell, Design and varieties of the megabar cell, *Carnegie Inst. Washington Year Book, 77*, 904-908, 1978.

Mao, H. K., Y. Fei, and T. Gasparik, Multi-cell sample chamber in multi-anvil apparatus - a tool for high-resolution and high-efficiency experimental studies, *EOS*, *70*, 471, 1989.

Remsberg, A. R., J. N. Boland, T. Gasparik, and R. C. Liebermann, Mechanism of the olivine-spinel transformation in Co_2SiO_4, *Phys. Chem. Minerals, 15*, 498-506, 1988.

Rosenhauer, M., H. K. Mao, and E. Woermann, Compressibility of $(Fe_{0.4}Mg_{0.6})O$ magnesiowüstite to 264 kbar, *Carnegie Instn. Washington Year Book, 75*, 513-515, 1976.

Yagi, T., P. M. Bell, and H. K. Mao, Phase relations in the system MgO - FeO - SiO_2 between 150 and 700 kbar at 1000°C, *Carnegie Instn. of Washington Year Book*, *78*, 614-618, 1979.

Partitioning of High Field Strength Elements Among Olivine, Pyroxenes, Garnet and Calc Alkaline Picrobasalt: Experimental Results and An Application

Peter Ulmer

On chondrite- and MORB-normalized trace element plots, the calc-alkaline magmas of convergent plate margins characteristically show depletion of high field strength elements (HFSE) such as Ta, Nb, Zr, Ti, Hf, and Y relative to the alkaline earth and rare earth (REE) elements. This characteristic is widely interpreted as an imprint of a depleted MORB-type source, a possibility that is also consistent with Sr, Nd, and Hf isotopic relationships (e.g., Morris and Hart, 1983; White and Patchett, 1984). On the other hand, the magmas show relatively strong enrichments of highly incompatible elements (notably Ba, K, Rb, Sr, Th) and REE, and these characteristics are frequently attributed to metasomatism of the mantle source by fluids released through dehydration or low-percentage melting of subducting oceanic crustal slabs (Green and Ringwood, 1968; Lambert and Wyllie, 1970; Arculus and Curran, 1972; Green, 1980). The need for metasomatism is perhaps most strongly suggested by modelling results (e.g., Lopez-Escobar *et al.*, 1977) indicating that, for a primordial or chondritic mantle source, simple batch or fractional melting can only yield the observed incompatible element concentrations at degrees of melting too low (2-5%) to be consistent with major element constraints established by experimental studies (e.g., Green, 1973).

The basis of this concept requiring first depletion, then metasomatism of the mantle source is weak, however, in that reliable HFSE partition coefficients have not been available for minerals and liquids of appropriate compositions at appropriate pressure-temperature conditions. In the study described here, the crystal/liquid partition coefficients of Nb, Ta, P, Zr, Hf, Ti, Y, Sc, and V have been determined experimentally for olivine, clinopyroxene (cpx), orthopyroxene (opx), and garnet in equilibrium with a calc-alkaline picrobasaltic melt.

TABLE 4. Summary of the Experimentally Determined Crystal/Liquid Partition Coefficients for High Field Strength Elements.

Element	Garnet	Cpx	Opx	Olivine
Nb	0.07	0.02	≤0.01	≤0.01
Ta	0.04	0.02	≤0.01	≤0.01
P	0.10	0.03	0.03	≤0.01
Zr	0.32	0.03	0.03	0.01
Hf	0.44	0.22	0.14	≤0.01
Ti	0.28	0.18	0.10	0.02
Y	2.11	0.20	≤0.01	≤0.01
Sc	2.27	0.51	0.33	0.16
V	1.57	1.31	0.90	0.06

Partition coefficients were determined experimentally using powders of picrobasalt sample RC158c (Ulmer, 1988) doped with 1 wt % of oxide of the element. The melting experiments for garnet, cpx, and opx were run at 1330°-1340°C at 28 kbar; those for olivine, at 1330°-1350°C at 1 atm with oxygen fugacity close to the NNO buffer.

The picrobasalt (sample RC158c) comes from late dikes in the Tertiary calc-alkaline Adamello batholith of northern Italy. Previous phase-equilibria work showed that the rock probably represents primary magma because its melt is in equilibrium with garnet lherzolite at an upper mantle pressure of 28 kbar (Ulmer, 1988).

Experimental Study

For garnet and the pyroxenes, the HFSE partition coefficients were determined at 28 kbar and 1330°C, conditions approximating the liquidus of the picrobasalt in the upper mantle. Doped powders of the rock were melted in graphite containers sealed in Pt capsules in solid-media, high-pressure apparatus at the Geophysical Laboratory and ETH-Zürich. Standard 12.5 mm and 14 mm talc-*Pyrex*™ assemblies were used. Run products typically consisted of 60-70% melt, as represented by glass and quench products, plus stable, unzoned crystals of cpx, opx, and garnet.

For olivine, the HFSE partitioning had to be determined from 1-atm experiments, because the mineral is not readily stabilized at liquidus conditions at high pressures owing to Fe losses from the melt to the Pt capsules by way of cracks in graphite container and to gains of CO_2 through reaction of the melt with the graphite. The 1-atm experiments were done by the Pt wire loop technique at oxygen fugacities close to the NNO buffer at 1330°C.

Run products from all experiments were analyzed by electron microprobe for major elements and HFSE. No reversals were made, but the approach of the HFSE partitioning to equilibrium was tested by comparing results for runs of 6 and 12 hours. For Zr, P, and Ti, test runs of 51 hours were

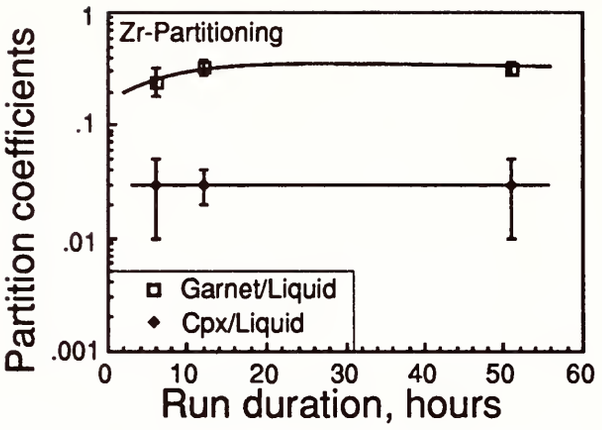

FIG. 26. Variation of the crystal/liquid partition coefficients of Zr for garnet and cpx in picrobasaltic liquid as a function of run duration. The error bars indicate uncertainties for single runs.

also made. With the possible exception of Zr, the partition coefficients were stable in runs longer than 6 hours. The coefficient for Zr showed a slight increase from 6 to 12 hours but was the same after 51 hours as at 12 (Fig. 26).

The determined partition coefficients are summarized in Table 4 and illustrated in Fig. 27. Garnet has the highest partition coefficients, followed by cpx and opx in that order. Solubilities of the HFSE in olivine were barely detectable by the electron microprobe analytical method, so its coefficients are all low; in fact, only those for Sc

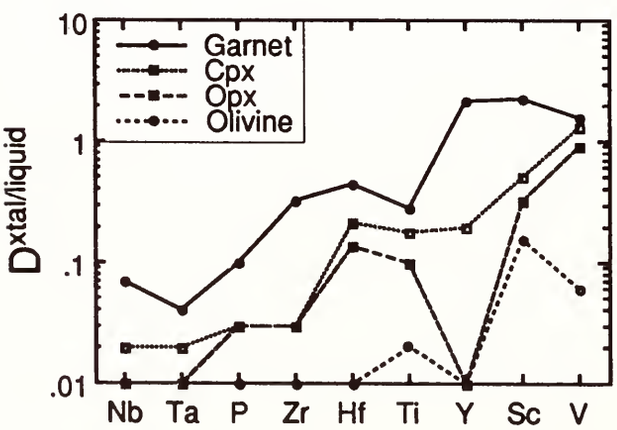

FIG. 27. Experimentally measured coefficients describing the crystal/liquid partitioning of HFSE for garnet, cpx, opx, and olivine in picrobasalt melt.

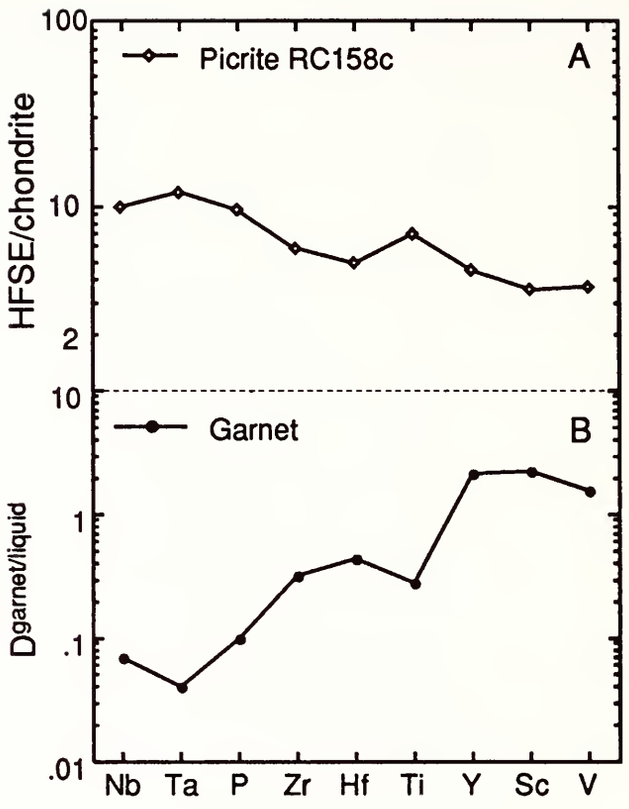

FIG. 28. (A) Variation diagram for natural HFSE abundances in picrobasalt RC158c. Concentrations are chondrite normalized for all elements except Sc and V. Primitive mantle values are from Sun and Nesbitt (1977), Sun (1982), Thompson *et al.* (1982). (B) Crystal/liquid partition coefficients for the HFSE for garnet in picrobasaltic melt.

and V are significant. It is evident that, in the melting of garnet lherzolite, garnet will be the dominant control for all HFSE, but cpx could have a substantial subordinate influence, especially for Hf, Ti, Sc, and V. The opx coefficients are almost as large as the cpx coefficients for P, Zr, Hf, Ti , Sc and V, but the opx value for Y is lower by an order of magnitude.

The partition coefficients for garnet are compared with the chondrite-normalized natural HFSE concentrations of the picrobasalt in Fig. 28. An inverse relationship is revealed, implying strongly that garnet largely controlled the HFSE composition of the picrobasalt magma during partial melting of a garnet lherzolite source.

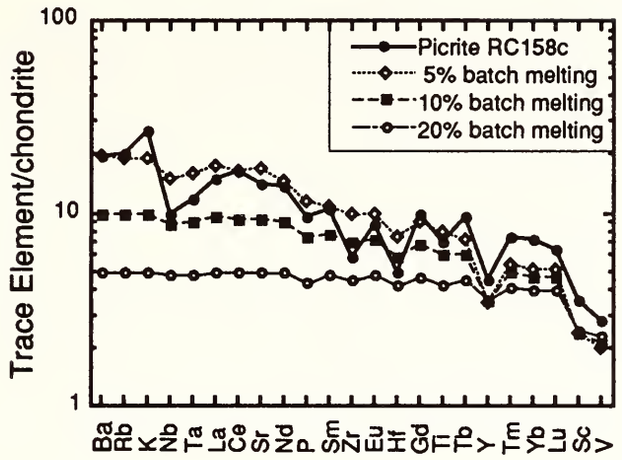

FIG. 29 . The natural trace element pattern of picrobasalt RC158c compared with patterns calculated for melts of a garnet lherzolite source using the simple batch-melting equation of Shaw (1970) and experimental partition coefficients (including those obtained in the present study).

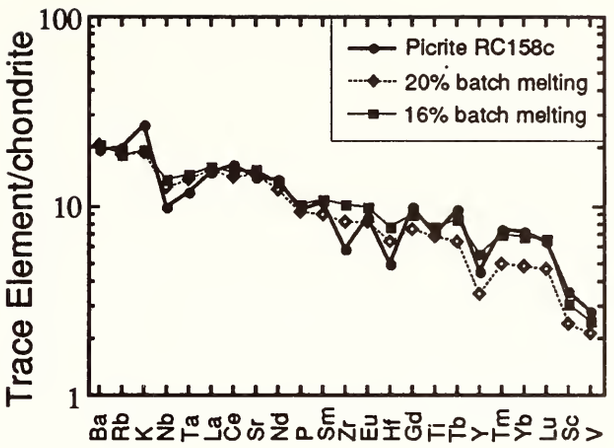

FIG. 30. The natural trace element pattern of picrobasalt RC158c compared with patterns calculated for aggregated liquid from a garnet lherzolite mantle plume using the batch plume melting equation of O'Hara (1985). The curve labeled 20% melting represents a maximum of 20% melting in the center of a plume composed of the same fertile peridotite assumed in the calculations in Fig. 29. The pattern for 16% melting pertains similarly to a plume of less fertile peridotite. For both calculated patterns, the melting maximum represents the stage at which the cpx-content of the source rock was exhausted.

Application

Trace element patterns have been calculated for partial melts of a garnet lherzolite source using the measured HFSE coefficients in combination with published coefficients for other elements (Harrison, 1981; Shimizu and Kushiro, 1974; Irving, 1978; Hanson, 1980; Terakoda and Masuda, 1979; Irving, 1978). Two sets of calculations were made, as illustrated in Figs. 29 and 30.

For Fig. 29, the following conditions were assumed: (1) the source rock was a fertile garnet lherzolite composed of 57% (by weight) olivine, 19% opx, 12% cpx, and 12% garnet; (2) the melting equation was that derived in the experimental study by Ulmer (1988): 0.582 cpx + 0.388 garnet + 0.031 opx <=> 0.075 olivine + 0.925 liquid; and (3) after extraction of the melt, 0.2% liquid remained trapped in the source. The simple, non-modal batch melting equation of Shaw (1970) was used, and partial melting percentages of 5, 10, and 20% were investigated. The cpx content of the source is just exhausted at 20% melting. The model patterns show that the picrobasalt composition can be approximated by the simple batch melting equation only if the percentage of melting is low, of the order of 5% or less. The heavy REE concentrations derived by this equation are too low, and the depletion of the HFSE is also poorly reproduced. This type of melting would indeed require metasomatism of the source to account for the enrichment of the highly incompatible elements and REE.

It is unlikely, however, that the simple batch partial melting equation is appropriate. The mantle source was probably a plumelike structure in which temperature varied both horizontally and vertically; hence the amount of melting probably was not constant. O'Hara (1985) has derived alternative partial melting equations that

describe trace element abundances for aggregated melt from such a regime. The equations are denoted CAPEPM and CAPFPM, acronyms for Complex Aggregated Perfect Equilibrium (or Fractional) Partial Melting. They were modified for present purposes in such a way that melt percentages varied with temperature in accordance with 30 kbar experiments on the picrobasalt (Ulmer, 1988). The melt distribution was approximated by a simple analytical function, and the equation was integrated numerically from the edge of the melting region to its center. The important consequence is that, in the aggregated liquid, the melt from the high-percent-melting central part of the plume mostly controls major element abundances, whereas that from the low-percent-melting fringe mainly controls the trace elements.

Trace element patterns from the O'Hara-type equilibrium (batch) calculations are compared with the natural picrobasalt pattern in Fig. 30. The dotted-line pattern derives from the same parameters used in Fig. 29 for 20% melting at the center of the plume. The broken-line pattern represents a less fertile source containing only 11% cpx and 7% garnet. With it, cpx and garnet are both consumed at approximately 16% melting. The two calculated patterns both match the natural pattern reasonably well, but Zr and, to a lesser extent, Hf, Nb, and Ta, are not closely reproduced. Possible explanations of the discrepancies are:

(1) The measured distribution coefficients for Zr, Hf, Nb, and Ta are too low in consequence of the charge doping. The doped concentrations are 2-4 orders of magnitude larger than the natural abundances of the picrobasalt; thus the distribution coefficients could be outside the range of Henry's law (cf. Mysen, 1978; Harrison; 1981). The reported D-values should be regarded as minimum values.

(2) Some additional mineral might retain these elements in the melting range of the picrobasalt (cf. Sauders *et al.*, 1980; Green, 1981). For example, rutile was observed in picrobasalt charges melted at 35 - 40 kbar at temperatures up to 1150°C.

The O'Hara model does, however, reproduce most of the trace element pattern of the natural calc-alkaline picrobasalt from a chondritic to primitive mantle source without requiring that it be metasomatized. Most particularly, it reproduces the enrichment of LILE and REE and the depletion of the HFSE. The possibility of metasomatism is not ruled out, but much less is necessary than has commonly been contended.

References

Arculus, R. J., and E. B. Curran, The genesis of the calc-alkaline rock suite, *Earth Planet. Sci. Lett., 15*, 255-262,1972.

Green, D. H., Experimental testing of "equilibrium" partial melting of peridotite under water saturated, high-pressure conditions, *Can. Mineral., 14*, 255-268, 1976.

Green, T. H., Experimental evidence for the role of accessory phases in magma genesis, *J. Volcanol. Geotherm. Res., 10*, 405-422, 1981.

Green, T. H., and A. E. Ringwood, Genesis of the calc-alkaline igneous rock suite, *Contrib. Mineral. Petrol., 18*, 269-385, 1968.

Green, T. H., Island arc and continent-building magmatism - A review of petrogenic models based on experimental petrology and geochemistry, *Tectonophysics, 63*, 367-385, 1980.

Irving, A. J., A review of experimental studies of crystal/liquid trace element partitioning, *Geochim. Cosmochim. Acta, 42*, 743-770, 1978.

Hanson, G. N., Rare earth elements in petrogenetic studies of igneous systems, *Ann. Rev. Earth Planet. Sci. Lett., 8*, 371-406, 1980.

Harrison, W. J., and B. J. Wood, An experimental investigation of the partitioning of REE between garnet and liquid with reference to the role of defect equilibria, *Contrib. Mineral. Petrol., 72*, 145-155,1980.

Harrison, W. J., Partition coefficients for REE between garnets and liquids: implications of non-Henry's law behavior for models of basalt origin and evolution, *Geochim. Cosmochim. Acta, 45*, 1529-1544, 1981.

Lambert, J. B., and P. J. Wyllie, Melting in the deep crust and upper mantle and the nature of low-velocity layer, *Phys. Earth Planet. Inter., 3*, 316-322.

Leeman, W. P., The influence of crustal structures on compositions of subduction-related magmas, *J. Volcanol. Geotherm. Res., 18*, 561-598, 1983.

Lopez-Escobar, L. L., A. F. Frey, and M. Vergara, Andesites and High-Alumina basalts from the central-south Chile high Andes: Geochemical evidence bearing on their petrogenesis, *Contrib. Mineral. Petrol., 63*, 199-228, 1977.

Morris, J. D., and S. R. Hart, Isotopic and incompatible element constraints on the genesis of island arc volcanics from Cold Bay and Amak Island, Aleutians, and implications for mantle structure, *Geochim. Cosmochim. Acta, 47*, 2015-2033, 1983.

Mysen, B. O., Experimental determination of nickel partition coefficients between liquid, pargasite, and garnet peridotite minerals and concentration limits of behavior according to Henry's law at high pressure and temperature, *Am. J. Sci., 278*, 217-243, 1978.

O'Hara, M. J., Importance of the 'shape' of the melting regime during partial melting of the mantle, *Nature, 314*, 58-62, 1985.

Shaw, D. M., Trace element fractionation during anatexis, *Geochim. Cosmochim. Acta, 34*, 237-243, 1970.

Shimizu, N., and I. Kushiro, The partitioning of REE between garnet and liquid at high pressures: Preliminary experiments, *Geophys. Res. Lett., 2*, 413-416, 1974.

Sun, S. S., and R. W. Nesbitt, Chemical heterogeneity of the Archean mantle, composition of the Earth and mantle evolution. *Earth Planet. Sci. Lett., 35*, 429-448, 1977.

Sun, S. S., Chemical composition and origin of the Earth's primitive mantle, *Geochim. Cosmochim. Acta, 46*, 179-192, 1982.

Terakoda, Y. and A. Masuda, Experimental study of REE partitioning between diopside and melt under athmospheric pressure, *Geochem. J., 13*, 121-129, 1979.

Thompson, R. N., A. P. Dickin, L. L. Gibson, and M. A. Morrison, Elemental fingerprints of isotopic contamination of Hebridean Palaeocene mantle-derived magmas by Archean Sial, *Contrib. Mineral. Petrol., 79*, 159-168, 1982.

Ulmer, P., High pressure phase equilibria of a calc-alkaline picro-basalt: Implication for the genesis of calc-alkaline magmas, *Annual Report of the Director of the Geophysical Laboratory, Carnegie Instn. Washington, 1987-1988,* Geophysical Laboratory, Washington, D. C., 28-35, 1988.

White, W. M., and J. Patchett, Hf-Nd-Sr isotopes and incompatible element abundances in island arcs: implications for magma origins and crust-mantle evolution, *Earth Planet. Sci. Lett., 67*, 167-185, 1984.

Relationships Between Composition, Pressure and Structure of Depolymerized, Peralkaline Aluminosilicate Melts

Bjorn O. Mysen

The structure of silicate liquids at high temperature and high pressure, and relationships between structure and properties are important to characterize natural magmatic processes. Bulk compositions between depolymerized (nonbridging oxygen per silicon; $NBO/Si > 0$) alkali or alkaline earth silicates and fully polymerized ($NBO/Si = 0$) silica - aluminates represent

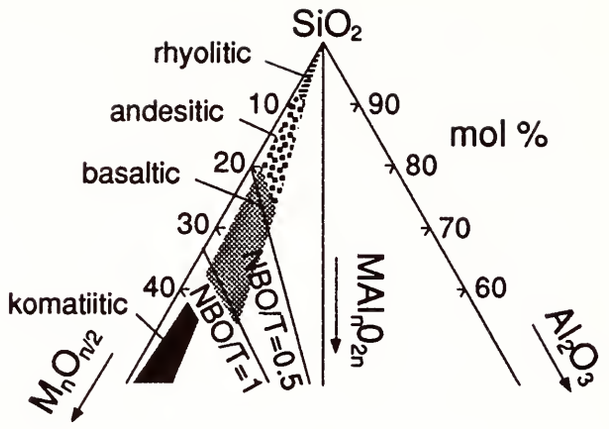

FIG. 36. Approximate fields of major groups natural magmatic liquids in in the system M_2O - Al_2O_3 - SiO_2 (M = K + Na + Ca + Mg + Fe^{2+}) (data from Mysen, 1988).

the structural environment of natural magmatic liquids (see Fig. 36). Their Al/(Al + Si) typically is between 0.2 and 0.3. Alkali metals are the principal cations for charge-balance of tetrahedrally-coordinated Al^{3+} at 1 atmosphere (Mysen, 1988).The exceptions are picrite and komatiite. These melts are less polymerized and often have lower Al/(Al + Si) than other major groups of magmatic melts.

Silicate melts in this composition range (Fig. 36) consist of coexisting structural units characterized by their average number of nonbridging oxygen per tetrahedrally-coordinated cations (*NBO/T*) equal to 0 (TO_2, or Q^4-species), 1(T_2O_5, or Q^3-species), and 2 (TO_3, or Q^2-species; see, for example, Virgo *et al.*, 1980). The equilibrium in such melts is described with the equation (Virgo *et al.*, 1980);

$$T_2O_5\ (Q^3) \Leftrightarrow TO_3\ (Q^2) + TO_2\ (Q^4), \quad (1)$$

where T = Al + Si. The Q^4, Q^3 and Q^2 notations are sometimes used in place of the stoichiometric designations. The superscript in the Q-notation denotes the number of bridging oxygen in the unit.

Physical and chemical properties of natural magmas depend on the properties, detailed structure, and proportions of these individual structural units. The relative abundance of the different structural units is likely to depend on melt polymerization, the ionization potential of charge-balancing and network-modifying cations, Al/(Al + Si), pressure, and temperature (e.g., Mysen *et al.*, 1985; Brandriss and Stebbins, 1988). In order to provide a structural framework for quantitative characterization of the properties of natural magma, it is necessary to characterize the relationships between pressure, temperature, and the compositional variables. In view of the fact that most magmatic processes take place at pressures above 1 atmosphere, it is particularly important to determine these relationships at high pressure.

Raman spectroscopy (Fig. 37) has been used to determine the abundances of individual structural units in the quenched melts. All compositions in this study are on the join $M_2Si_4O_9$ - $M_2(MAl)_4O_9$ (M = K, Na and Li; denoted KS4 - KA4, NS4 - NA4 and LS4 - LA4), with, therefore, *NBO/T* = 0.5 (see Fig. 36). The unit distributions in quenched melts probably reflect those near the glass transition temperature (T_g). One-bar samples were formed by quenching at ~500°C/s in vertical quench-furnaces, whereas high-pressure samples (to 30 kbar) were quenched at ~100°C/s in the solid-media, high-pressure apparatus. The abundances have been determined from calibration of area ratios of (Si,Al) - O stretch bands in the high-frequency envelopes of

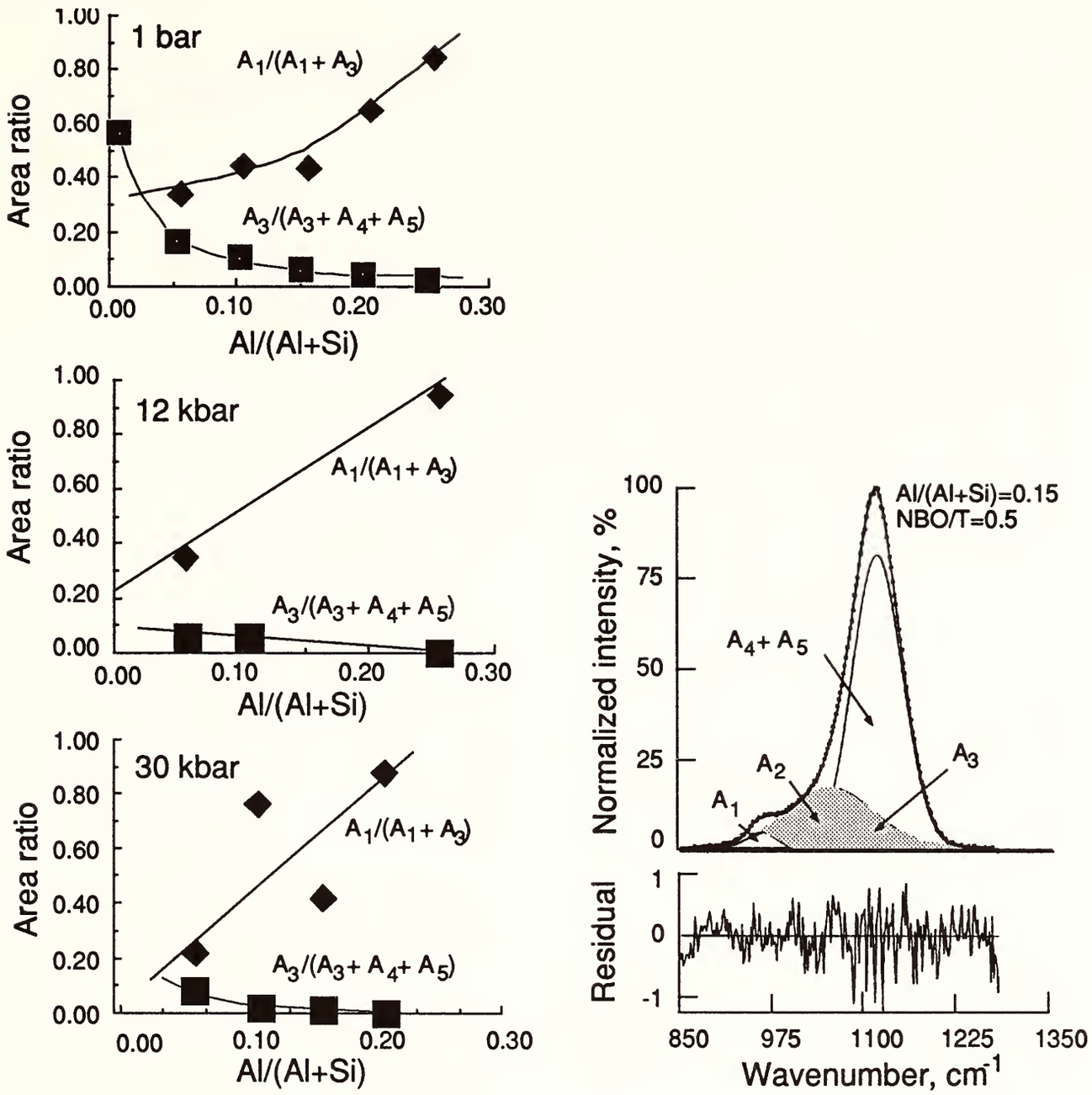

FIG. 37. Relationship between area ratios (as indicated) from Raman spectra of quenched melts on the join $K_2Si_4O_9$ - $K_2(KAl)_4O_9$ at 1 bar, 12 and 30 kbar. The relevant portion of the high-frequency envelope of a typical Raman spectrum with compositional variables as indicated is also shown.

the spectra (Fig. 37). In order to obtain the exact frequencies and areas of individual Raman bands, the spectra were fitted statistically with the method described by Mysen *et al.* (1982). The A_1 is the area of the (Si,Al) - O^- antisymmetric stretch band from TO_3 units and A_3 from T_2O_5 units. The remaining bands, against which these areas are normalized, are from bridging oxygen bonds. The relative errors (from the fitting procedure) in these determinations are between 10 and 20%.

The 1-bar relationship between unit abundances and Al/(Al + Si) is shown in Fig. 38. Substitution of charge-balanced Al^{3+} for Si^{4+} results in a systematic lowering of the abundance of T_2O_5 units together with a concomitant increase in the more po-

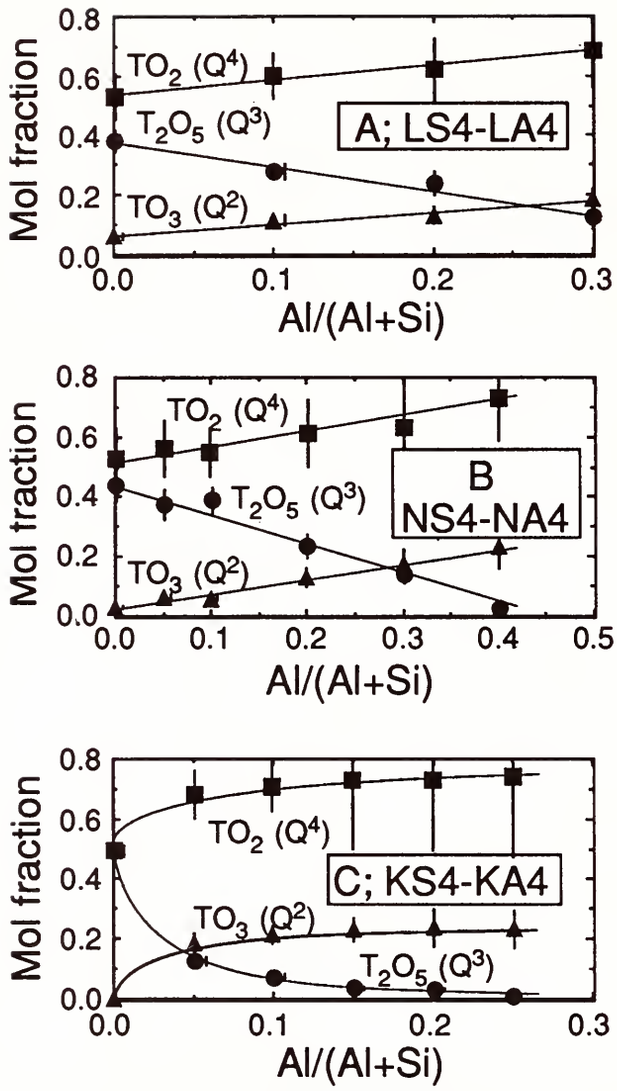

FIG. 38. Mol fraction of structural units in 1-bar, temperature-quenched melts as a function of Al/(Al + Si). A - The join $Li_2Si_4O_9$ - $Li_2(LiAl)_4O_9$ (LS4 - LA4), B - The join $Na_2Si_4O_9$ - $Na_2(NaAl)_4O_9$ (NS4 - NA4), C - The join $K_2Si_4O_9$ - $K_2(KAl)_4O_9$ (KS4 - KA4).

lymerized unit, TO_2 and the less polymerized one, TO_3. The overall degree of polymerization of the melts remains constant ($NBO/T = 0.5$) in this process. Thus, qualitatively, increasing Al/(Al + Si) shifts equation (1) to the right. It is notable, however, that even in the absence of Al^{3+} the larger the ionization potential of the network-modifying cation (Li > Na > K), the mol fractions, $X(TO_2)$ and $X(TO_3)$, are greater, and the $X(T_2O_5)$ is smaller. This observa-

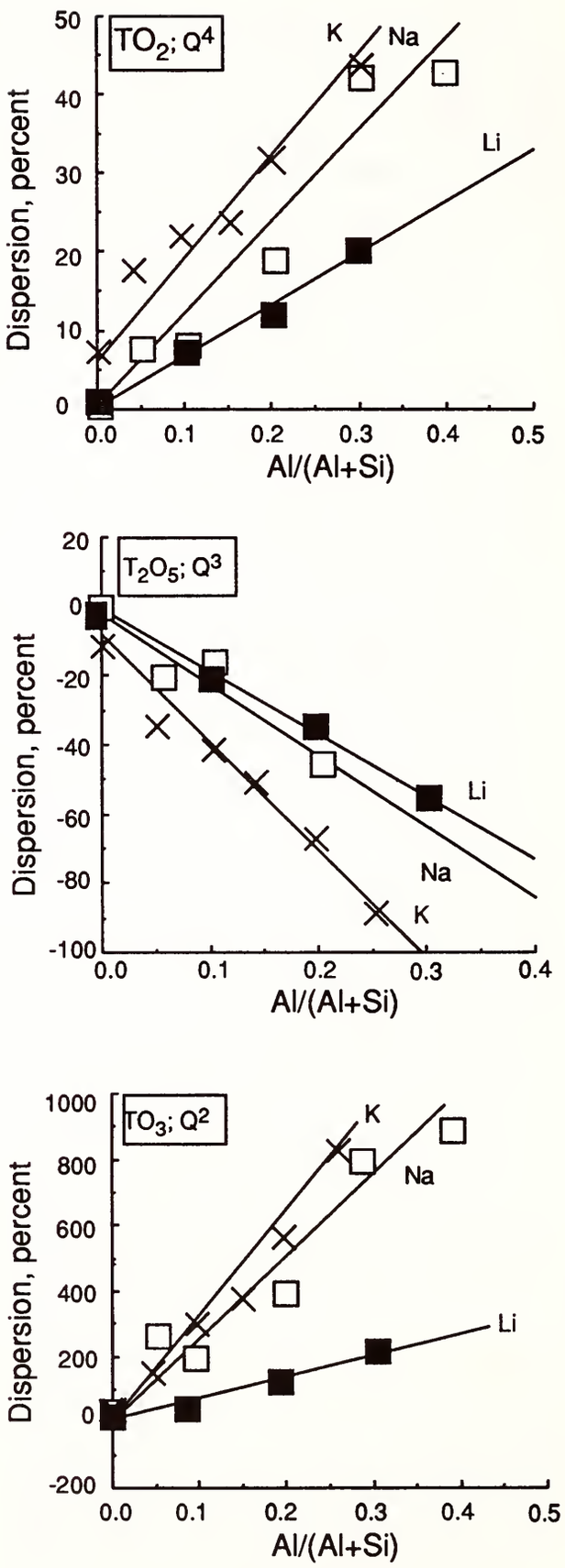

FIG. 39. Dispersion of structural units (as indicated on the panels) as a function of Al/(Al + Si) and the type of network-modifying and charge-balancing cation.

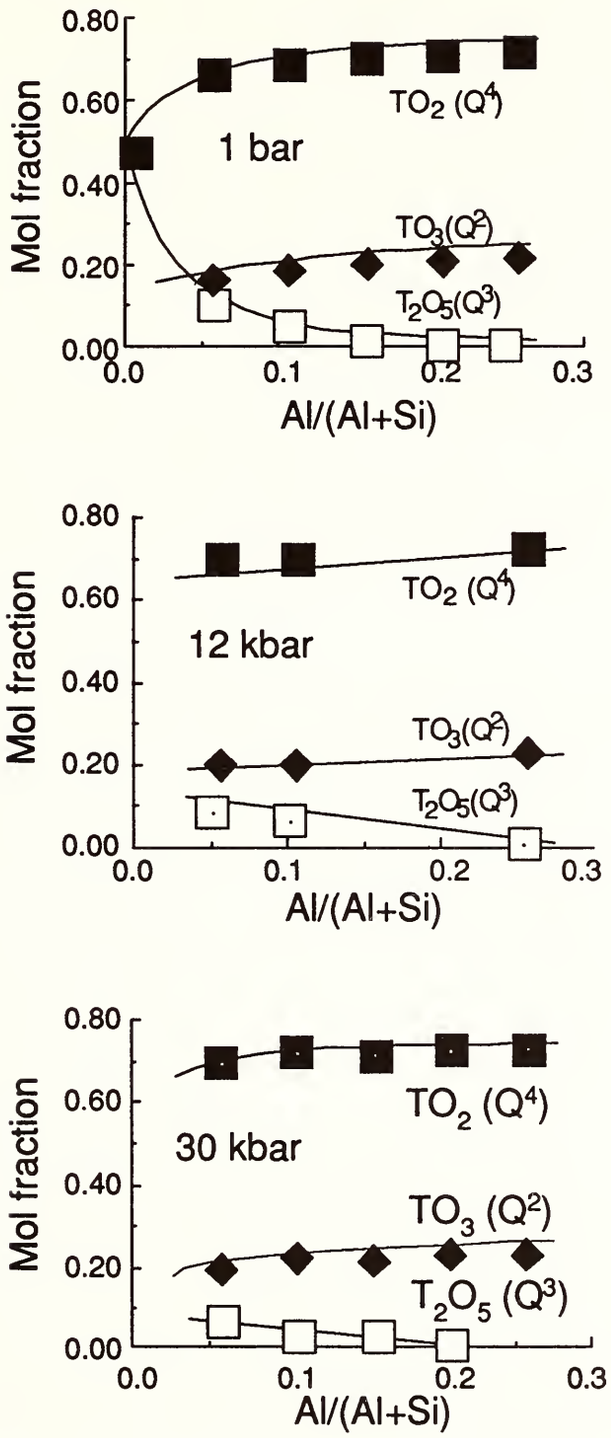

FIG. 40. Mol fraction of structural units in $K_2Si_4O_9$ - $K_2(KAl)_4O_9$ melts as a function of Al/(Al +Si) at the pressures indicated.

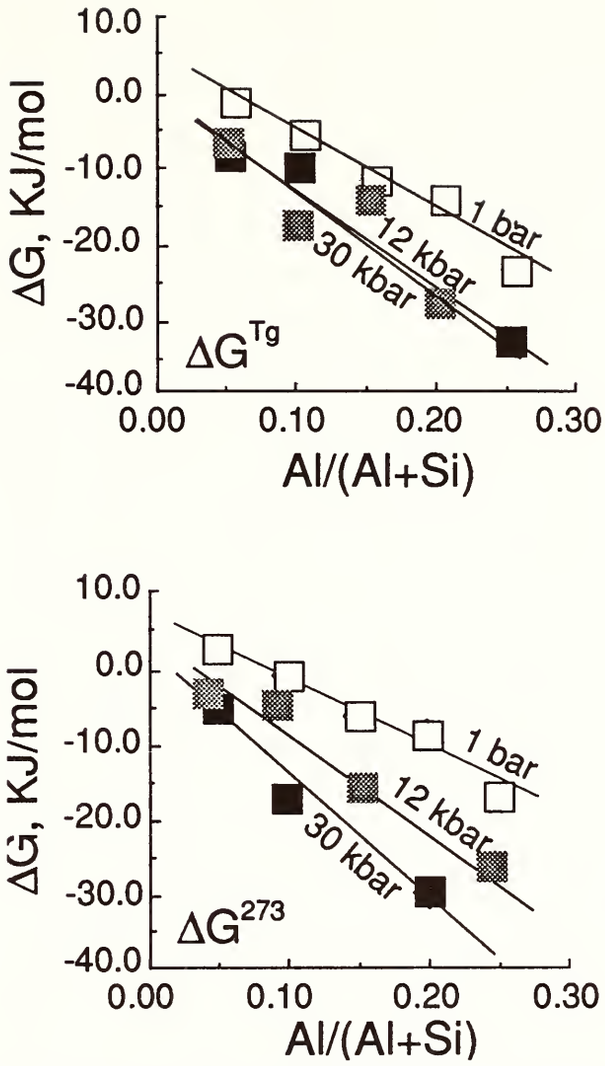

FIG. 41. Free energy (ΔG) for equilibrium (1) at the glass transition temperature (ΔG^{Tg}) and at 273K (ΔG^{273}) for melts on the join $K_2Si_4O_9$ - $K_2(KAl)_4O_9$ as a function of pressure as indicated.

tion accords with results from ^{29}Si NMR spectroscopy of analogous melt compositions (Stebbins, 1987).

For the compositions studied here, the alkali metals also serve to charge-balance Al^{3+} in tetrahedral coordination. It is evident that the influence of Al/Al + Si) on equation (1) at 1 bar also depends on the charge-balancing cation (Fig. 39). The increase (or decrease) in mol fractions of the coexisting structural units, relative to the abundance in the Al-free end-member silicate melts is termed dispersion. The dispersion is more pronounced (K > Na > Li) the smaller the ionization potential of the cation.

The distribution of structural units as a function of Al/(Al + Si) follows the same general trends at high pressure (Fig. 40) as

at 1 bar (Fig. 38) at least for the potassium tetra-aluminosilicate quenched melts. Qualitatively, from the abundance information in Fig. 40, at a given Al/(Al + Si), the $X(T_2O_5)$ tends to be lower at higher pressure, thus indicating a shift of equation (1) to the right. Such a trend has also been suggested for Al-free KS4 quenched melts reported by Dickinson *et al.* (1985).

Under the assumption of ideal mixing of the structural units, the free energy of reaction (1) can be calculated (Fig. 41). Although the viscosity of these melts probably decreases with increasing pressure (Kushiro, 1976), and, therefore, the glass transition temperature probably also decreases (e.g., Rosenhauer *et al.*, 1979). This effect has not been taken into account as the exact relationship between pressure and T_g is not known for these melts. Also shown in Fig. 41 are the free energy data at 273K calculated with the ΔS-value (5 J/mol K) suggested by Stebbins (1989). In light of available high-temperature calorimetric data (see Richet and Bottinga, 1986, for summary), temperature-dependence of ΔCp for equation (1) is not considered.

It is clear (Fig. 41) that not only does the ΔG decrease with increasing Al/(Al + Si) at constant pressure, but increasing pressure generally results in a further decrease in ΔG for all aluminum contents studied. The pressure effect on ΔG for reaction (1) is further enhanced as a function of increasing aluminum content. Thus, as suggested from density measurements on fully polymerized ($NBO/T = 0$) alkali aluminosilicate melts (e.g., Kushiro, 1980), depolymerized ($NBO/T > 0$) aluminosilicate melts become increasingly compressible as Al^{3+} is substituted for Si^{4+} (Fig. 42) at least for the potassium tetra-aluminosilicate compositions.

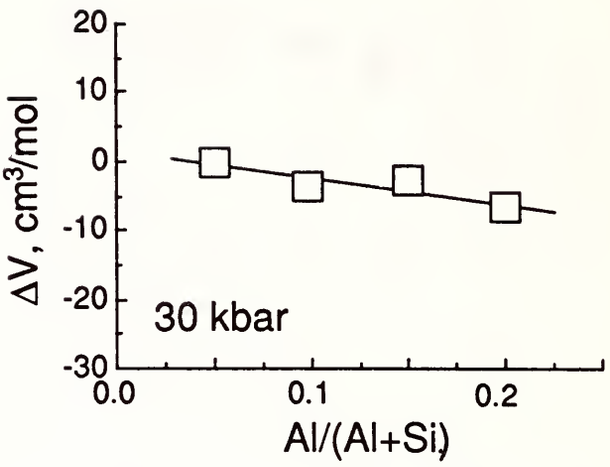

FIG. 42. Volume change, ΔV, for equilibrium (1) at 30 kbar as a function of Al/(Al + Si) for melts on the join $K_2Si_4O_9$ - $K_2(KAl)_4O_9$.

The shift of reaction (1) to the right with increasing ionization potential of the network-modifying cation probably is a result of local electric charge constraints. That is, geometric constraints increasingly tend to prevent neutralization of the negative charge in the anionic network the smaller the network-modifying metal cation. This problem compounds as the NBO/Si of a particular structural unit decreases. Notably, among crystalline alkali silicates, only potassium forms a stable tetrasilicate. Potassium and sodium form stable disilicate crystalline materials, whereas no lithium disilicate is known. In melts where more than one depolymerized structural unit is present, the smaller cations will prefer the least polymerized unit, and, thus, drive, reactions such as (1) to the right.

The aluminum distribution between the structural units is governed by the differences in intertetrahedral angles (α) be-

tween the various units, and will favor the unit with the smallest intertetrahedral angle (Mysen *et al.*, 1985). As $\alpha(TO_2) < \alpha(T_2O_5) < \alpha(TO_3)$ (Furukawa *et al.*, 1981), Al^{3+} will then substitute preferentially for Si^{4+} in the TO_2 units, thus driving equation (1) to the right.

Finally, because the intertetrahedral angle in fully polymerized structural units depends on pressure (Seifert *et al.*, 1983), it is suggested that the compressibility of the individual coexisting units in melts govern the influence of pressure on reaction (1). Among the coexisting units in tetrasilicate and tetra-aluminosilicate melts, the TO_2 structure is much more compressible than either the T_2O_5 or the TO_3 (Bockris and Kojonen, 1960). These compressibility relations have two consequences. First, because $(\partial V/\partial P)_T < 0$ even for Al-free silicate melts, equation (1) shifts to the right. Second, by substituting charge-balanced Al^{3+} for Si^{4+}, the $X(TO_2)$ increases, thus increasing the bulk compressibility. Furthermore, the Al/(Al + Si) in the TO_2 units increases. This increase lengthens the (Si,Al)-O bridging bonds, and the $\alpha(TO_2)$ becomes smaller. This angle is expected to be more compressible. All these factors serve to enhance the bulk melt compressibility. Thus, the observed enhancement of bulk melt compressibility with increasing Al/(Al + Si) would be expected.

The pressure-composition relationships provides a rationale to understand the behavior of natural magmatic liquids under pressure. (i) As indicated in Fig. 36, magmatic liquids become more polymerized with increasing silica, or alumina, or both. Thus, the relative abundance of TO_2 units in the melts increases. As a result, the molar volume and the melt compressibility of magmatic liquids increase in the order komatiite < basalt < andesite < rhyolite. (ii) For basaltic melts, high-aluminum basalt is more compressible than tholeiite even though their *NBO/T* are practically the same (Mysen, 1988). This behavior is the result of the higher Al/(Al + Si) in the high-alumina basalt as compared with tholeiite. This higher Al/(Al + Si) shifts reaction (1) to the right thus enhancing the melt compressibility. (iii) The bulk composition of alkali basalt and tholeiite differs principally in the values of the average ionization potential (Z/r) of the charge-balancing metal cations. The $(Z/r)_{\text{alkali basalt}} < (Z/r)_{\text{tholeiite}}$ with the result that ΔG of reaction (1) for alkali basalt is smaller (more negative) resulting in greater compressibility. Relationships similar to (i-iii) would also be expected for all other melt properties that depend on the abundance and character of bridging oxygen bonds in TO_2 units in the magmatic liquids.

References

Bockris, J. O., and F. Kojonen, The compressibility of certain molten alkali silicates and borates, *J. Am. Chem. Soc., 82*, 4493-4497, 1960.

Brandriss, M. E., and J. F. Stebbins, Effects of temperature on the structures of silicate liquids: ^{29}Si NMR results, *Geochim. Cosmochim. Acta, 52*, 2659-2669, 1988.

Dickinson, J. E., and C. M. Scarfe, Pressure-induced structural changes in $K_2Si_4O_9$ silicate melt, *EOS, 66*, 395, 1985.

Furukawa, T., K. E. Fox, and W. B. White, Raman spectroscopic investigation of the structure of

silicate glasses. III. Raman intensities and structural units in sodium silicate glasses, *J. Chem. Phys., 153*, 3226-3237, 1981.

Kushiro, I., Changes in viscosity and structure of melt of $NaAlSi_2O_6$ composition at high pressures, *J. Geophys. Res., 81*, 6347-6350, 1976.

Kushiro, I., Viscosity, density, and structure of silicate melts at high pressures, and their petrological implications, in *Physics of Magmatic Processes*, R. B. Hargraves, ed., Princeton University Press, Princeton, Ch. 3, 1980.

Mysen, B. O., *Structure and Properties of Silicate Melts*, Elsevier, Amsterdam, 354 pp., 1988.

Mysen, B. O., L. W. Finger, F. A. Seifert, and D. Virgo, Curve-fitting of Raman spectra of amorphous materials, *Am. Mineral., 67*, 686-696, 1982.

Mysen, B. O., D. Virgo, and F. A. Seifert, Relationships between properties and structure of aluminosilicate melts, *Am. Mineral., 70*, 834-847, 1985.

Richet, P., and Y. Bottinga, Thermochemical properties of silicate glasses and liquids: A review, *Rev. Geophys., 24*, 1-26, 1986.

Rosenhauer, M., C. M. Scarfe, and D. Virgo, Pressure dependence of the glass transition temperature in glasses of diopside, albite and sodium trisilicate composition, *Carnegie Instn. Washington, Year Book, 78*, 556-559, 1979.

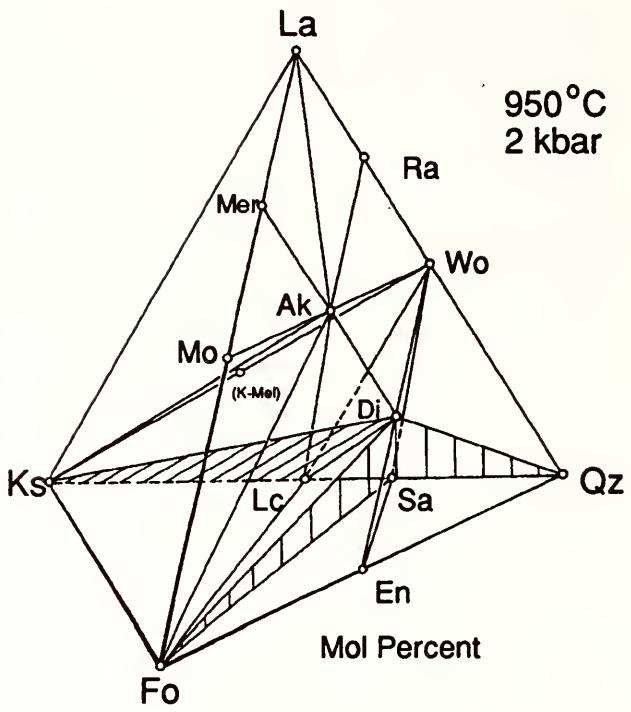

FIG. 31. Potassium analogue of the extended normative, basalt tetrahedron Ks - La - Fo - Qz exhibiting stable joins determined experimentally at 950°C and 2 kbar.

Ak	akermanite	Lc	leucite
Di	diopside	Mer	merwinite
En	enstatite	Mo	monticellite
Fo	forsterite	Ra	rankinite
K-mel	potassium melilite	Sa	sanidine
Ks	kalsilite	Qz	quartz
La	larnite	Wo	wollastonite

IGNEOUS AND METAMORPHIC FACIES OF POTASSIUM-RICH ROCKS: COEXISTING ASSEMBLAGES IN KALSILITE-FORSTERITE-LARNITE-QUARTZ AT 950°C AND 2 KBAR WITH AND WITHOUT H_2O.

Hatten S. Yoder, Jr.

The wide variety of potassium-rich igneous and metamorphic rocks appears to result primarily from the great diversity of bulk composition and from the large number of reactions between phases (Yoder, 1986). The mineralogical complexity of the final products probably results from incomplete or failed reactions as the magmas cool. For this reason an effort was made to establish experimentally a stable array of assemblages with which observed and alternative assemblages could be compared.

The principal minerals involved in *anhydrous* potassium-rich rocks are displayed in Fig. 31. The tetrahedron is the potassium analogue of the extended basalt tetrahedron (Schairer and Yoder, 1964) wherein kalsilite replaces nepheline. The joins connecting coexisting phases were established by experiments at 950°C and P=2 kbar of 5 days duration. Stable assemblages were determined by reacting natural

minerals close to endmember composition, synthetic endmembers, or both, in compatible and incompatible combinations. The experiments were carried out in an internally-heated, gas-media, high-pressure apparatus (Yoder, 1950). Over 60 mixtures of compatible and incompatible phases were reacted to establish the stable joins for both the anhydrous and hydrous tetrahedrons at isothermal, isobaric conditions. The conditions 950°C and 2 kbar were chosen so that there was adequate pressure to stabilize the appropriate hydrous minerals, and at a sufficiently high temperature to be at or near the beginning of melting, yet above the stability of the amphiboles.

To illustrate the strategy in determining these joins under anhydrous and hydrous conditions, the join Di ($CaMgSi_2O_6$) - Ks ($KAlSiO_4$) will be used as an example. (Abbreviations are defined in the caption of Fig. 31).

The reactions investigated that prove that Di-Ks is the stable join are:

$$Fo + 3Lc + 2Ak \rightarrow 4Di + 3Ks \quad (1)$$

$$Fo + 3Lc + 2Ak \xrightarrow{H_2O} 4Di + 3Ks \quad (2)$$

$$Ph + 3Ak + 4Lc \rightarrow 6Di + 5Ks + H_2O \quad (3)$$

$$Mo + Lc \rightarrow Di + Ks \quad (4)$$

$$2Mo + Sa \rightarrow 2Di + Ks \quad (5)$$

$$2Mo + Sa \xrightarrow{H_2O} 2Di + Ks \quad (6)$$

$$12Di + 5\gamma\text{-}Al_2O_3 + 5[K_2O{\cdot}2SiO_2] \rightarrow 12Di + 10Ks \quad (7)$$

$$Do1 + Sa \rightarrow Di + Ks + 2CO_2. \quad (8)$$

The Di-Ks join is critical because it penetrates the common assemblage Mel+Fo+Lc of the katungites. Note that the join is stable under both hydrous and anhydrous conditions. (The hydrous tetrahedron is presented below.) Reactions 4-6 show that monticellite is not stable with either Lc or Sa at these conditions - it is cut by the planes Ak - Ks - Fo and Di - Ks - Fo. Reaction 7 was a test of the alkali-loss problem experienced in the past. To avoid alkali loss, it was usually necessary to use natural minerals close to the end members or well characterized synthetic phases. The last reaction is the well known metamorphic reaction observed at Brome Mt., Quebec, and Hendricksplaats, RSA.

In order to appreciate the value of the tetrahedron and clarify the relationships, the various subtetrahedra are presented in an exploded view in Fig. 32. The subtetrahedral volumes are labelled with the appropriate rock names underlined. The faces and joins have also been labelled where rock names have been assigned. (Alkali-rich rock enthusiasts have, fortunately, missed naming a few of the joins). Beginning at the left, the kalsilite-rich end, the principal mineral assemblage for the melilite mafurites, Mel + Ks + Cpx + Fo, is found. Passing through the mafurites, Ks + Cpx + Fo, one comes to the leucite mafu-

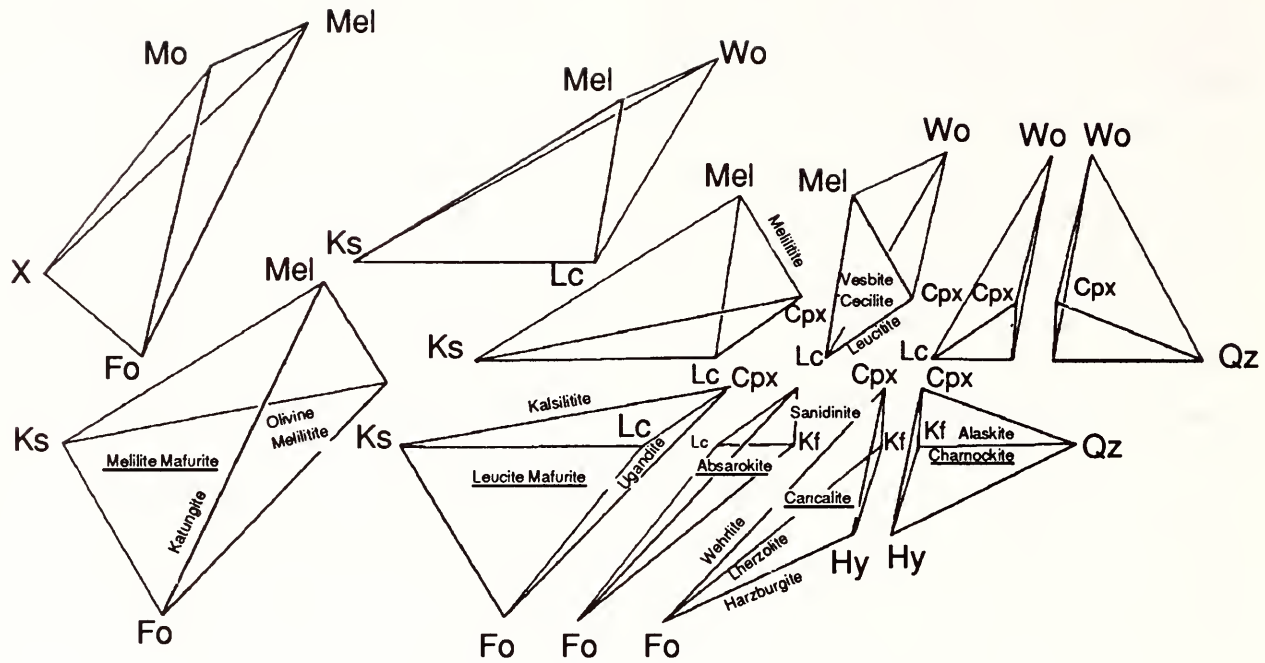

FIG. 32. Exploded view of generalized subtetrahedra in Fig.31 with names of closely related rock types inscribed. Names for four-phase volumes are underlined.

Cpx	clinopyroxene	Mel	melilite
Hy	hypersthene	Ol	olivine
Kf	potassium feldspar		

rites. Then, through the ugandites, Lc + Cpx + Fo, the absarokite assemblage is next encountered. The adjoining assemblages are the cancalites and finally the charnockites. Illustrated in the subtetrahedra on the top row of Fig. 32 are those assemblages of monticellite-bearing rocks related to the kimberlites to be discussed below. Potassium melilite (K-Mel) did not form on the join Ks-Wo under either anhydrous or hydrous conditions at this pressure and temperature. The vesbites, common in the Roman region of Italy, are next exhibited. The two upper subtetrahedra on the right are very rare metamorphic assemblages.

The point to be emphasized is that *all* of these rock types may be stable at the same pressure and temperature under anhydrous conditions. Thermodynamically, all com-

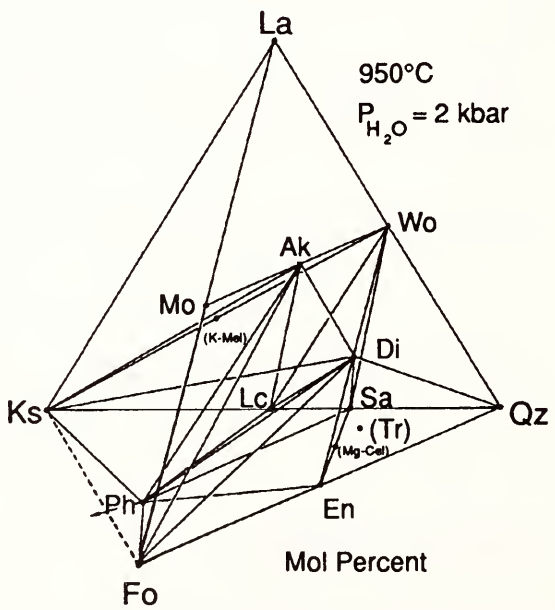

FIG. 33. Potassium analogue of the extended normative basalt tetrahedron Ks - La - Fo - Qz exhibiting stable joins determined experimentally at 950°C with $P(H_2O)$ = 2 kbar.

Mg-Cel	magnesium celadonite
Ph	phlogopite
Tr	tremolite

See Fig. 31 for definition of abbreviations of anhydrous phases.

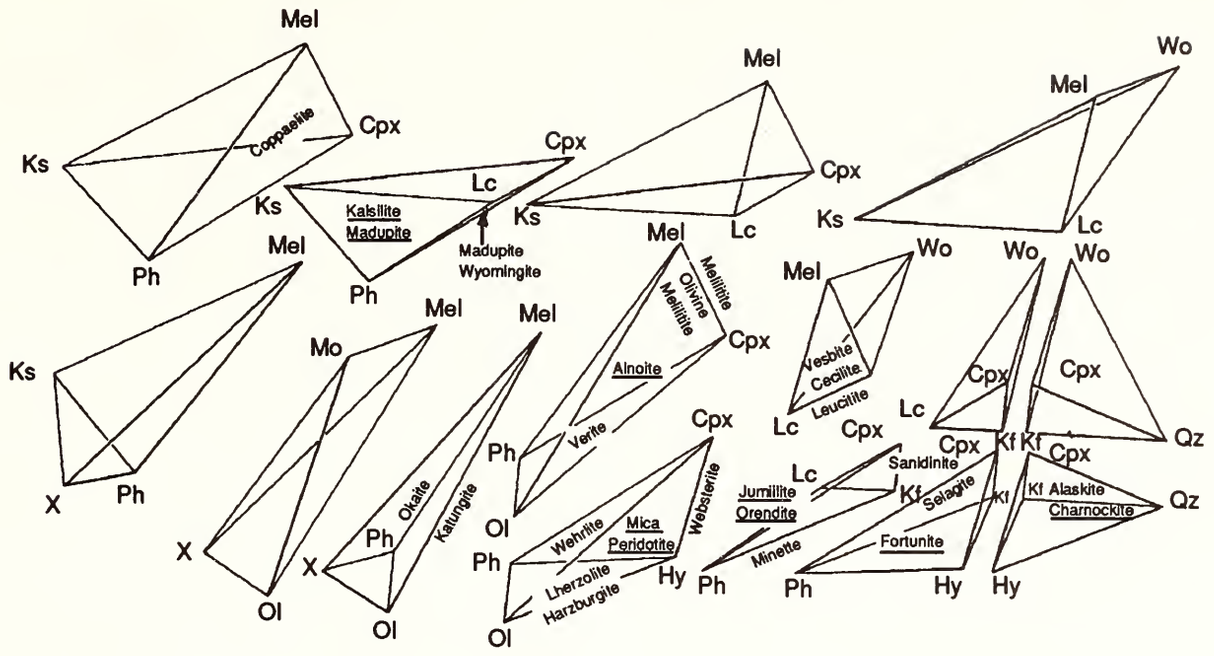

FIG. 34. Exploded view of generalized subtetrahedra by Fig. 33 with names of closely related rock types inscribed. Abbreviations given in Figs. 32 and 33.

positional space must be represented by a stable or metastable assemblage at every pressure and temperature. Displayed is the entire array of *stable* assemblages, which describe a consistent set of rock types and show their compositional relationships.

The hydrous tetrahedron at the same pressure and temperature is displayed in Fig. 33. The anhydrous phases are the same. Phlogopite is the key hydrous phase and joins radiate out to all the principal phases except Qz, Wo, and, contrary to natural occurrences, Mo. Phlogopite is the phase that appears to provide liquid lines of descent through many of the thermal barriers in the flow sheet developed for the anhydrous potassium-rich lavas (Yoder, 1986). The theoretical mica, magnesium celadonite (Mg-Cel), lies on the join Sa - En, but it did not form under the applied conditions. The amphibole tremolite (Tr) lies on the face Di - En - Qz. It is stable only up to 890°C at 2 kbar, and was, therefore, not encountered. On the other hand, tremolite was a useful starting material because joins with other phases penetrated a large number of other planes.

The significance of these stable assemblages, all proven experimentally, can be appreciated in an exploded view of the individual subtetrahedra in the hydrous tetrahedron in Fig. 34. Only six of the previous subtetrahedra in the anhydrous tetrahedron persist. Note again that Mo is cut off from Lc and Sa, whereas Ak is stable with Lc, but not Sa, as observed in natural rocks. The principal mineral assemblages are assigned the names of the most representative rock types. The Italian and African provinces are represented in the upper left two subtetrahedra. One may begin a review of the array of assemblages with the okaites and katungites. These adjoin the alnöites, a major member of the lampro-

phyres. After passing through the verites, one comes to the mica peridotites. These rocks are contiguous with the lamproites, represented by the jumillites and orendites. The lamproites in turn adjoin sequentially the basic and acid charnockites. The incredible array of rock types may be stable at the same pressure and temperature. It is not necessary, therefore, to assign special, exotic pressure and temperature conditions to explain the assemblages represented by kimberlite, lamprophyres, lamproites or charnockites. The critical question to be resolved is how the large range of bulk composition was generated.

Special note should be made of the absence of the join Mo - Phl so critical to the Group I variety of kimberlite. The planes Ak - Ks - X and Ak - Fo - X cut the Mo - Phl join. The X represents a K - Mg-rich fluid, not yet adequately characterized, that is required to account for mass balance. The composition X is of exceptional importance because there appears to be a fluid available for metasomatism that is *complementary* to phlogopite. In other words, phlogopite is an indicator that a metasomatizing solution was produced and is not itself a product of that solution. From this viewpoint, phlogopite may form at the same time the metasomatizing fluid is generated; for example, by reaction of Fo+Ks with H_2O. It will be illuminating to reexamine the textural relations of phlogopite in kimberlites with this concept in mind.

These results are for exactly one pressure, 2 kbar, and one temperature, 950°C. If the temperature is raised or lowered 100°C, another ensemble of assemblages will be generated. In addition, a modest pressure

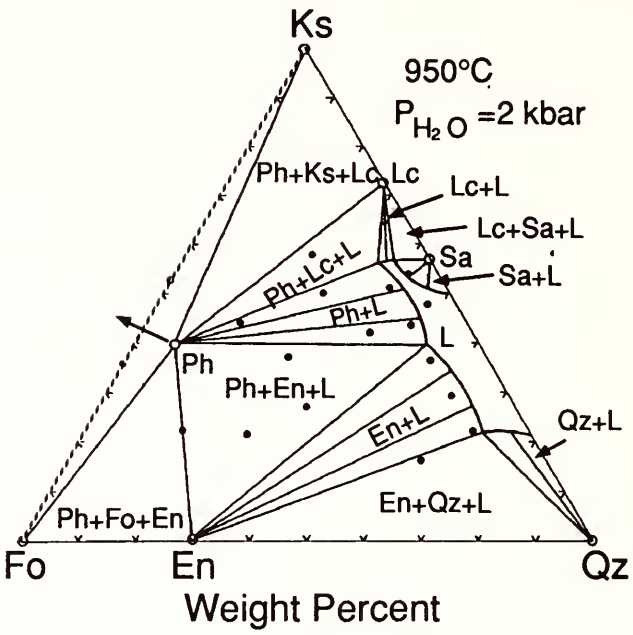

FIG. 35. The system Ks - Fo - Qz at 950°C and $P(H_2O)$ = 1 kbar. Abbreviations as in Figs. 32 and 33. L = liquid.

increase of 5-10 kbar will eliminate melilite, monticellite, and leucite—some of the principal phases in these assemblages.

Melting was not observed in the anhydrous tetrahedron, but melting was observed in the charnockite subtetrahedra under hydrous conditions (Fig. 35). Only the base plane of the tetrahedron is displayed to reduce the complexity. Melting begins near the alaskite join previously investigated by Shaw (1963). All of the major phases except Fo and Ks are on the liquidus. The significance of these observations is that the charnockites and related migmatites may be partially melted while all the other rock types will be in a crystalline state. These results suggest that migmatites, formed in several ways, do not necessarily imply a hot spot—difficult to explain thermally—but may indicate a regional temperature rise where all the surrounding related rock types may remain stable in the solid state. For this reason it

will be necessary in the future to relate igneous facies with ultrametamorphic facies for the entire array of compositions in order to characterize the pressure and temperature.

The results provide a consistent ensemble of assemblages from which compatible and incompatible mineral assemblages in K-rich rocks can be determined. The complexity of the alkaline rocks appears to result primarily from variations in bulk composition, however the large number of potential reactions between phases (Yoder, 1986) contribute to further complexity when the successive reactions are incomplete. Because of the large number of phases in alkaline rocks, the textural relations (e.g., rimming, morphology, and zoning) may be of great importance in revealing the sequence of reactions.

References

Schairer, J. F., and H. S. Yoder, Jr., Crystal and liquid trends in simplified alkali basalts, *Carnegie Instn. Washington Year Book, 63,* 65-74, 1964.

Shaw, H. R., The four-phase curve sanidine - quartz -l iquid - gas between 500 and 4000 bars, *Am. Mineral., 48,* 883-896, 1963.

Yoder, H. S., Jr., High-low quartz inversion up to 10,000 bars, *Trans. Am. Geophys. Union, 31,* 827-835, 1950.

Yoder, H. S., Jr., Potassium-rich rocks: Phase analyses and heteromorphic relations, *J. Petrol., 27,* 1215-1228, 1986.

Techniques for Experimentally Loading and Analyzing Gases and Their Application to Synthetic Fluid Inclusions

John D. Frantz, Yi-gang Zhang, Donald D. Hickmott, and Thomas C. Hoering

Experimental studies of equilibria between minerals and mixed-volatiles under hydrothermal conditions have long been a research focus for many experimentalists. One of the principal difficulties in experimentally investigating reactions between minerals and mixed volatiles under hydrothermal conditions is loading the experimental charges with gas mixtures of known composition. In the past, gas loading was accomplished primarily by the addition of solid compounds that produced volatiles in the experimental charge. For example, silver oxalate was used as a source of carbon dioxide (Holloway *et al.*, 1968); iridium carbonyl, to produce carbon monoxide (Eggler *et al.*, 1979); oxalic acid, as a source of carbon dioxide, water, and hydrogen (Holloway and Reese, 1974); chromium nitride, to produce nitrogen or ammonia if used in conjunction with an external oxygen buffer (Hallam and Eugster, 1976); acetic acid, as a source of carbon dioxide and methane (Seitz *et al.*, 1987; Palmer and Drummond, 1986); and graphite to produce carbon dioxide, carbon monoxide, and methane when used in conjunction with an external oxygen buffer (French, 1966; Eugster and Skippen, 1967). The applications of these procedures have been instrumental in many studies important to our understanding of equilibria be-

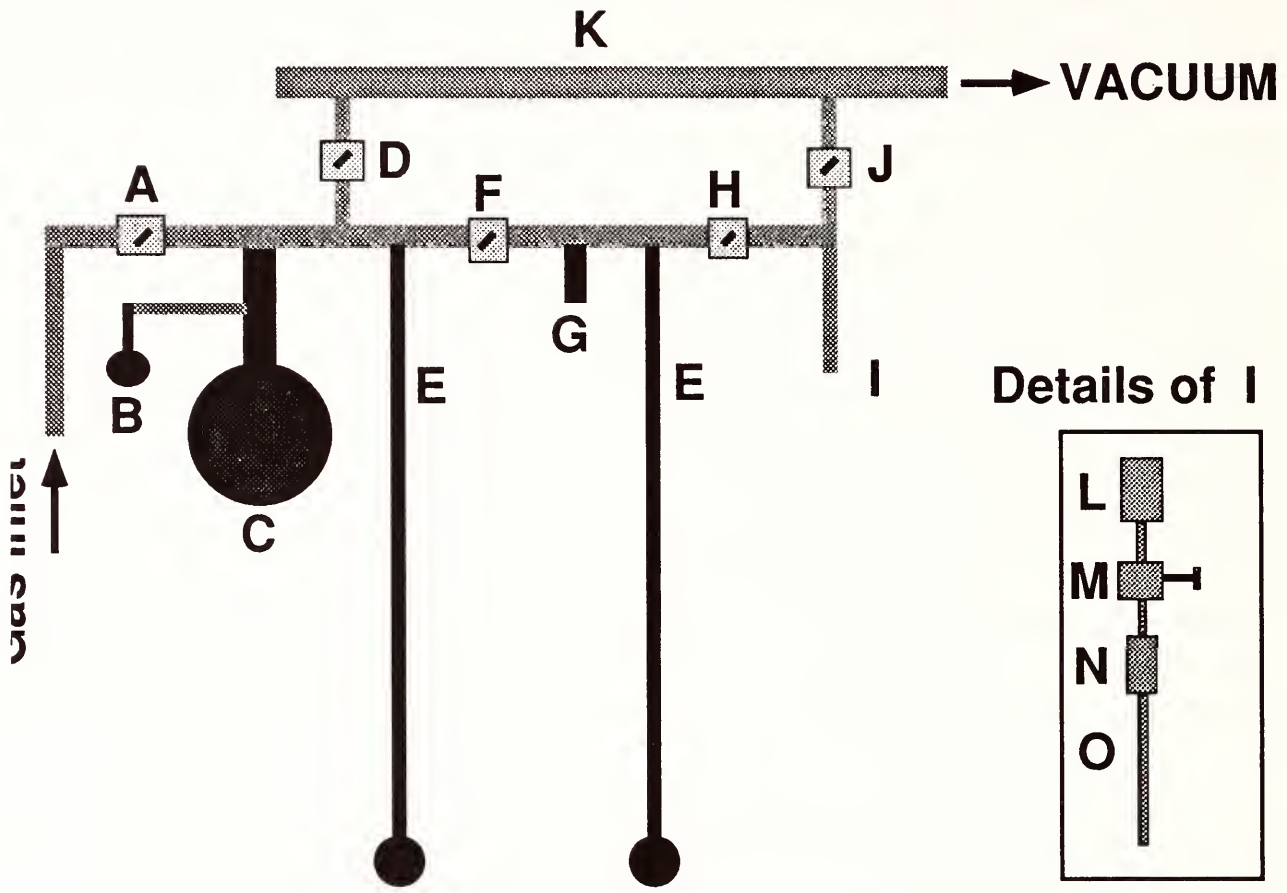

FIG. 43. Gas pipette apparatus. See text for details.

tween metamorphic mineral assemblages and mixed volatiles (Skippen, 1971; Jacobs and Kerrick, 1981).

The use of these compounds, however, has limitations. For example, at temperatures below 700°C, graphite reacts slowly with C-O-H gases (Ziegenbein and Johannes, 1980). Below 600°C, the breakdown of acetic acid is sluggish (Palmer and Drummond, 1986). Chromium nitride does not decompose completely under hydrothermal conditions and thus cannot be used quantitatively to add fixed amounts of gas to an experimental charge. Compounds such as oxalic acid, ammonium oxalate, and ammonium nitrate decompose to yield unwanted gas species such as hydrogen or oxygen (Holloway and Reese, 1974). Continuously variable gas compositions in ternary and quaternary gas mixtures such as the C-O-H and C-O-H-N systems are difficult to achieve by the addition of stoichiometric compounds. For research involving mixed volatiles in synthetic fluid inclusions, a relatively fixed (and known) distribution of gas species must be achieved shortly after the experimental temperature and pressure is reached because inclusions form rapidly, trapping the current fluid compositions. Seitz *et al.* (1987) demonstrated a large variability in the carbon dioxide-methane ratio for different inclusions in the same sample. The synthetic fluid inclusion sample contained carbon dioxide, methane, and water generated by the addition of acetic acid and water to the charge. Due to these limitations, development of a new technique for loading mixed

volatiles in hydrothermal experiments was desirable.

In order to load volatiles quantitatively in experimental hydrothermal charges, a gas pipetting apparatus was constructed of *Pyrex* glass shown in Fig. 43. The system consists of a gas storage section (separated from the rest of the system by valves *A*, *D*, and *F*), a measured gas aliquot section (between valves *F* and *H*), a vacuum manifold *K* with a vacuum gauge, and the sample holder *I*. Gas is first introduced into the gas storage section that consists of a 2000 ml flask *C*, a 100 ml flask *B*, and a mercury manometer *E*. The small flask can be used to purify gases, such as CO_2, which have relatively high condensation temperatures of gas impurities with lower condensation temperatures such as methane, nitrogen, and oxygen. This is accomplished by immersing the small flask in liquid nitrogen and evacuating the system by opening valve *D* and exposing the storage section to the vacuum manifold. In the case of loading gases with low condensation temperatures, gas impurities having high condensation temperatures can be condensed into the cold finger G by immersing it in liquid nitrogen bath with valve *F* open. Valve *F* is then closed, the liquid nitrogen bath is removed, and the gas impurities in the gas aliquot section are evacuated. With valves *A*, *D*, and *H* closed and *F* opened, a small quantity of gas can be introduced into the gas aliquot section. By having previously evacuated this section (using valves *H* and *J*), the pressure of gas introduced into this section can be determined with the second manometer and a cathetometer. After evacuating the sample holder section, the gas aliquot section can then be opened to the sample holder section by opening valve *H* (valve *J* closed). The sample holder consists of a 1/2" *Swagelock*™ union (*L*) with Teflon ferrules (to connect the holder to the 1/2" glass tubing used in the pipette apparatus), a valve (*M*), a 1/4" *Swagelock*™ union with Teflon ferrules (*N*), and a noble-metal capsule with the bottom end welded (*O*). Electronic pressure transducers could be used to replace the above-mentioned mercury manometers.

The volume of the gas aliquot section was calibrated by connecting a glass bulb fitted with a stopcock. The volume of the bulb has been determined accurately by weighing it when filled with mercury and subtracting the weight of the empty volumetric. Then, carbon dioxide gas is allowed to enter both the gas aliquot and sample holder sections with the valve on the calibration volumetric open. After the pressure is measured, the valve on the calibration bulb is closed and both sections are evacuated through the vacuum manifold. Next, the valve on the calibrated volumetric is opened and all the carbon dioxide is transferred into the gas aliquot section by immersing the cold finger (*G*) into liquid nitrogen. After closing valve *H* and allowing the carbon dioxide to warm to room temperature, the pressure on the manometer is again measured. Because we know the volume and the gas pressure that existed in the calibrated volume and we know the final gas pressure of the same quantity of gas in the gas pipette section alone, the volume and the number of moles of gas contained in the gas pipette section can be computed for that particular pressure using

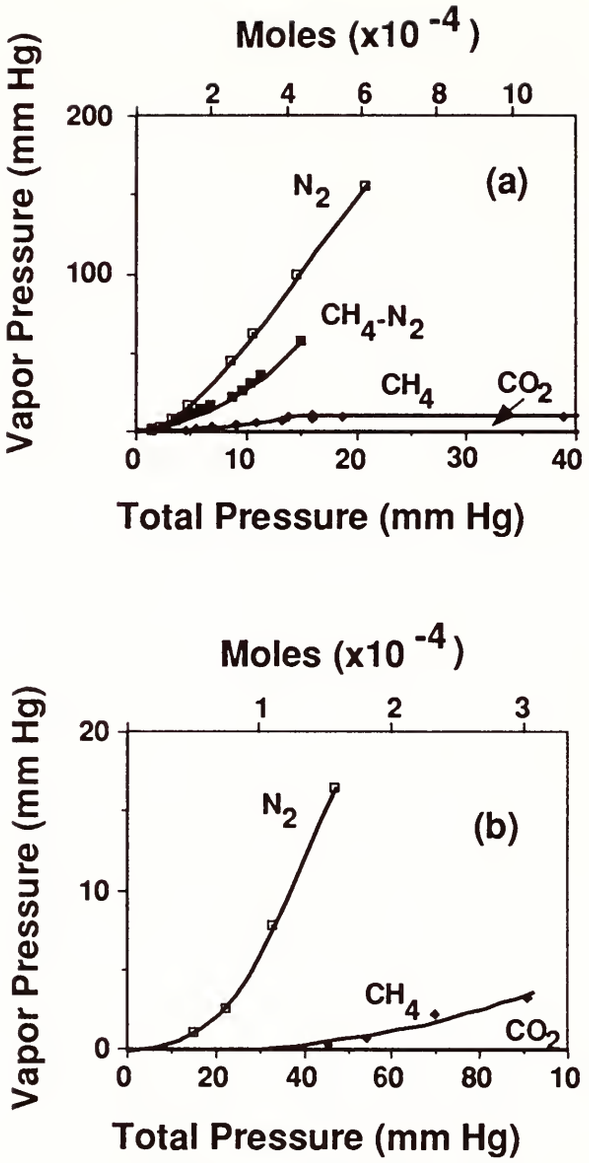

FIG. 44. (a), (b) Vapor pressure of nitrogen, methane, carbon dioxide, and 50-50 mole% methane-carbon dioxide mixture above 38 mg silica gel as a function of the pressure and number of moles of the gases in the measured gas aliquot section of the gas loading apparatus.

the ideal gas law. This calibration was done at a series of pressures because the volume of the manometer contributes to the volume of the gas pipette section.

A quantity of gas in the gas aliquot section is transferred to the experimental capsule by opening valve H to the evacuated sample holder section and drawing the gas into the capsule by immersing it in liquid nitrogen. In the case of carbon dioxide, the resultant vapor pressure above the frozen gas is less than $1x10^{-4}$ mm mercury at -195.8°C and the transfer is complete. In the case of other gases, there may be significant vapor pressure above the condensed gas at liquid nitrogen temperatures. It is well known that solid compounds with pore structures absorb gases strongly at low (liquid nitrogen) temperatures. When dealing with gases having significant vapor pressures at liquid nitrogen temperatures, the adsorbtion by porous solids is advantageous since substantial vapor pressures above the condensed gases at liquid nitrogen temperatures introduce appreciable error. A gel, zeolite, or some other compound that adsorbs gases at cryogenic temperatures is placed in the capsule with the charge. Due to the properties of adsorption of these compounds, the resultant vapor pressures are quite reduced. In Fig. 44a, the vapor pressures above 38 mg of silica gel for nitrogen, methane, carbon dioxide, and methane-nitrogen mixtures are plotted as a function of both the total pressure and the number of moles of the gas or gas mixture contained in the measured gas aliquot section of our apparatus (Fig. 43). In the case of nitrogen, for example, the vapor pressure of liquid nitrogen is 760 mm mercury and quantitative transfer without the use of a gas adsorbing compound is not possible. When nitrogen is adsorbed, however, the vapor pressure is only 6 mm Hg (using 38 mg gel) for 0.0001 mol of the gas (Fig. 44b). In the case of methane, the vapor pressure is even lower. A vapor pressure of less than 1 mm Hg occurs for 0.001 mol of methane, allowing the addition of precisely known quantities of the gas. Addition of more gel will result in lower vapor pres-

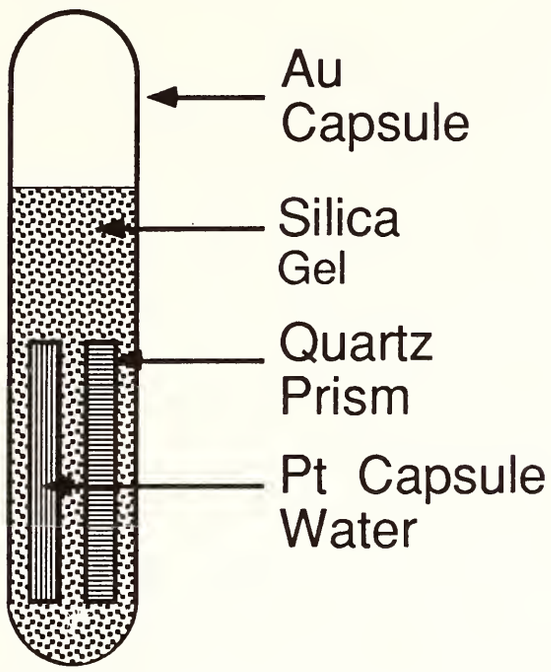

FIG. 45. Experimental capsule detail.

sures and the possibility of adding a larger quantity of gas. This technique can be used for *any mixture* such as carbon dioxide + methane or carbon dioxide + methane + nitrogen containing a non-condensed gas. The use of an adsorbing compound is vital in this case because significant partitioning between the condensed and solidified gases and the coexisting vapor would occur with mixtures comprised of gases with varying vapor pressures at liquid nitrogen temperature. With respect to CO_2 - CH_4 mixtures, best results were obtained by first loading pure carbon dioxide into the capsule. By keeping the capsule at liquid nitrogen temperature, pure methane can then be added. Carbon dioxide appears to freeze before being adsorbed by the gel and thus the capacity of the gel for methane is not reduced by the presence of carbon dioxide. In fact, the resultant vapor pressure is even somewhat less than in the case of pure methane possibly indicating adsorption of methane on solid carbon dioxide.

Water, however, cannot be directly added to the capsule as it may saturate the porous solid. To overcome this problem, a length of 2 or 3 mm platinum tubing is completely filled with water and a section corresponding to the length containing the desired quantity of water is cut and cold welded on both ends using a pinch-off device (Komarneni *et al.*, 1979). This inner capsule is placed in the larger capsule. After the loading procedure is complete, the portion of the capsule containing the experimental charge is cut and cold welded using the pinch-off device and, while the capsule remains in the liquid nitrogen, is electrically welded. A vacuum-tight cold weld is essential as a large amount of air can be drawn into the capsule by the absorbing solid before the capsule is electrically welded. The capsule is then removed from the nitrogen, checked for leaks in water, and placed in the hydrothermal pressure vessel. Such a welded capsule can safely hold 100 bar of pressure. Upon heating, the absorbing solid releases the gases and the inner platinum capsule containing water ruptures, releasing water, producing a mixed volatile fluid of known composition.

A major application of this technique lies in the experimental study of the properties of hydrothermal fluids containing mixed volatiles using synthetic fluid inclusions. In an effort to both test the loading technique described above and to initiate a thorough study of the C-O-H system (discussed in Zhang and Frantz, this Report), synthetic fluid inclusions with fluids containing mixtures of carbon dioxide, methane, and water were grown. Fractured quartz

TABLE 5. Analyses by gas chromatography

	Initial Gas Composition				Measured Gas Composition			
Wt% CH_4	Mol CH_4	Mol CO_2	Mol H_2O	Mol Ratio CH_4/CO_2	Mol CH_4	Mol CO_2	Mol H_2O	Mol Ratio CH_4/CO_2
5	0.000098	0.000175	0.001221	0.560	0.000086	0.000169	-NA-	0.509
10	0.000143	0.000124	0.000843	1.153	0.000131	0.000122	0.0008995	1.074
15	0.000145	0.000083	0.000537	1.747	0.000129	0.000079	0.0005386	1.633
20	0.000169	0.000068	0.000442	2.485	0.000176	0.000066	-NA-	2.667
25	0.000152	0.000047	0.000298	3.234	0.000155	0.000047	0.0002778	3.298

prisms, cold welded platinum capsules containing water, and approximately 75 mg silica gel were placed in thick-walled gold capsules (4.75 mm O.D.; 4.0 mm I.D.) (Fig. 45). The gas pipette was used to load the methane and carbon dioxide. Five different bulk compositions containing 5, 10, 15, 20, and 25 wt% methane were chosen with wt% ratios for CO_2/H_2O of 0.357. The experiments were placed in standard hydrothermal pressure vessels for four days at 600°C and 2000 bar. In order to assure thorough mixing of water and the gases in the tiny cracks of the quartz prism, the pressure vessel was heated at 1000 bar. After reaching the experimental temperature, the vessel was cycled four or five times between 500 and 3000 bar. Further discussion of the synthetic fluid inclusion techniques and the hydrothermal procedures employed in this study are described in Bodnar and Sterner (1987) and Zhang and Frantz (1987, 1989). An *Accuspec*™ *Compac II* gas chromatograph was modified to accept gases released from the gold hydrothermal capsules. The results of these measurements are tabulated in Table 5. The measured number of moles of methane and carbon dioxide are computed based on the measured area as referenced to the least-squares fit of all the data and thus only reflect the internal consistency of the measurements. The mole ratios, however, depend only on the ratio of the measured areas and the instrument calibration using the above mentioned gas standards. The measured values for water were determined by weighing the capsule before puncturing, drying it in a vacuum oven (120°C) after puncturing, reweighing the capsule, and computing the number of moles of H_2O after subtracting the measured weight of the carbon dioxide and methane. The close agreement of these mole ratios between the initial composition and the measured composition demonstrates the precision of both our gas loading and the gas chromatography techniques.

A new gas loading technique has been described by which gases that are non-condensible at room temperature and pressure can be loaded into experimental charges. The method has been successfully demonstrated by growing synthetic fluid

inclusions in C-O-H fluids at high temperatures and pressures analyzing the gases in the capsule by gas chromatography. Experimental studies of mineral-fluid equilibria and other studies involving mixed volatiles at hydrothermal temperatures and pressures should benefit from the development of the gas pipette loading technique.

References

Bodnar, R. J., and S. M. Sterner, Synthetic fluid inclusions, in *Hydrothermal Experimental Techniques*, G. C. Ulmer and H. L. Barnes, eds., John Wiley & Son, New York, pp. 423-458, 1987.

Eggler, D. H., B. O. Mysen, T. C. Hoering, and J. R. Holloway, The solubility of carbon monoxide in silicate melts at high pressures and its effect on silicate phase relations, *Earth and Planetary Sci. Lett., 43*, 321-330, 1979.

Eugster, H. P., and G. B. Skippen, Igneous and metamorphic reactions involving gas equilibria, in *Researches in Geochemistry, 2*, P. H. Abelson, ed., John Wiley and Sons, New York, pp. 492-520, 1967.

French, B. M., Some geological implications of equilibrium between graphite and a C-H-O gas phase at high temperatures and pressures, *Rev. Geophys., 4*, 223-253, 1966.

Hallam, M., and H. P. Eugster, Ammonium silicate stability relations, *Contrib. Mineral. Petrol., 57*, 227-244, 1976.

Holloway, J. R., C. W. Burnham, and G. L. Millhollen, Generation of H_2O-CO_2 mixtures for use in hydrothermal experimentation, *J. Geophys. Res., 73*, 6598-6600, 1968.

Holloway, J. R., and R. L. Reese, The generation of N_2-CO_2-H_2O fluids for use in hydrothermal experimentation I. Experimental method and equilibrium calculations in the C-O-H-N system, *Am. Mineral., 59*, 587-597, 1974.

Jacobs, G. K., and D. M. Kerrick, Devolatilization equilibria in H_2O - CO_2 and H_2O - CO_2 - NaCl fluids: An experimental and thermodynamic evaluation at elevated pressures and temperatures, *Am. Mineral., 66*, 1135-1153, 1981.

Komarneni, S., W. P. Freeborn, and C. A. Smith, Simple cold-weld sealing of noble-metal tubes, *Am. Mineral., 64*, 650-651, 1979.

Palmer, D. A., and S. E. Drummond, Thermal decarboxylation of acetate. Part I. The kinetics and mechanism of reaction in aqueous solution, *Geochim. Cosmochim. Acta, 50*, 813-823, 1986.

Seitz, J. C., J. D. Pasteris, and B. Wopenka, Characterization of CO_2 - CH_4 - H_2O fluid inclusions by microthermometry and laser Raman microprobe spectroscopy: Inferences for clathrate and fluid equilibria, *Geochim. Cosmochim. Acta, 51*, 1651-1663, 1987.

Skippen, G. B., Experimental data for reactions in siliceous marbles, *J. Geol., 70*, 457-481, 1971.

Zhang, Y. G., and J. D. Frantz, Determination of the homogenization temperatures and densities of supercritical fluids in the system NaCl - KCl - $CaCl_2$ - H_2O using synthetic fluid inclusions, *Chem. Geol., 64*, 335-350, 1987.

Zhang, Y. G., and J. D. Frantz, Experimental determination of the compositional limits of immiscibility in the system $CaCl_2$ - CO_2 - H_2O at high temperatures and pressures using synthetic fluid inclusions, *Chem. Geol., 74*, 289-308, 1989.

Ziegenbein, D., and W. Johannes, Graphite in C-O-H fluids: an unsuitable compound to buffer fluid composition at temperatures up to 700°C, *N. Jb. Miner. Abh., 7*, 289-305, 1980.

Investigations of Fluid Properties in the CO_2-CH_4-H_2O System using Synthetic Fluid Inclusions

Yi-gang Zhang and John D. Frantz

High-temperature, high-pressure intergranular fluids in the Earth's mantle and crust have had a profound influence on the evolution and resulting mineral petrogenesis of igneous and metamorphic rock suites. These fluids, mixtures of gases, water, and dissolved electrolytes, exist either as a

supercritical phase or possibly as a mixture of two immiscible phases (Zhang and Frantz, 1989). Of particular importance is the ubiquitous C-O-H system. Its presence has a major influence on the genesis of primary magma in the mantle and subsequent metasomatism resulting from element partitioning between the melt and the fluid (Green *et al*, 1987). Calculation of the oxidation state of the mantle involves multicomponent equilibria between the mineral phases and C-O-H fluids (Saxena, 1989). In the Earth's crust, element partitioning and material transport within C-O-H fluids containing dissolved electrolytes have resulted in the metasomatism of metamorphic mineral assemblages and the formation of ore deposits (Hollister and Burrus, 1976; Wintsche *et. al.* 1981; Ramboz *et. al.*, 1985). Vestiges of ancient C-O-H fluids are commonly found in the incorporation of these components in minerals and in their presence in natural fluid inclusions. The latter represent a unique opportunity to 1) detect the composition of the fugitive volatile phase; 2) to determine the temperature-pressure conditions of the formation of the surrounding mineral; and 3) to understand the evolution of the associated rock suites. Petrologists routinely measure properties of fluid inclusions such as the homogenization temperature along the liquid-vapor curve and, assuming that the volume of the inclusion remains constant with increasing temperature and pressure, use these measurements to delineate the possible temperature-pressure conditions of formation. Measurements such as these require knowledge of *both* the compositions of the inclusions and the PVT properties of the fluids corresponding to those particular compositions.

Due to its obvious importance, the C-O-H has received considerable attention in both experimental and theoretical investigations. For the most part, the studies have been concerned with one of the three binaries: CO_2 - H_2O, CH_4 - H_2O, and CO_2 - CH_4. In the case of the CO_2 - H_2O system, experimental work at high temperatures and pressures has been performed by Franck and Todheide (1959), Todheide and Franck (1963), Takenouchi and Kennedy (1964), Greenwood (1969, 1973), and Schmulovich (1980). The CH_4 - H_2O binary has received less attention with the work of Welsch (1973) being the principle high-temperature, high-pressure study. The CO_2 - CH_4 binary system, important to the chemical industry, has attracted geologists' attention as fluids of this composition have been discovered in natural fluid inclusions (Swanenberg, 1979). The system along with previous experimental work is discussed in Swanenberg (1979), Burrus (1981), and Heyen *et al.*, (1982). No experimental work has been done at high temperatures and pressures for the ternary CO_2 - CH_4 - H_2O system.

With the development of accurate gas-loading techniques (Frantz *et al.*, this Report) combined with synthetic fluid inclusion techniques (Bodnar and Sterner, 1985; Zhang and Frantz, 1987), experimental studies of the C-O-H system are now possible. Experiments producing synthetic fluid inclusions containing water-rich CH_4 - H_2O binary and CO_2 - CH_4 - H_2O ternary fluids were performed at temperatures from 400 to 600°C and at pres-

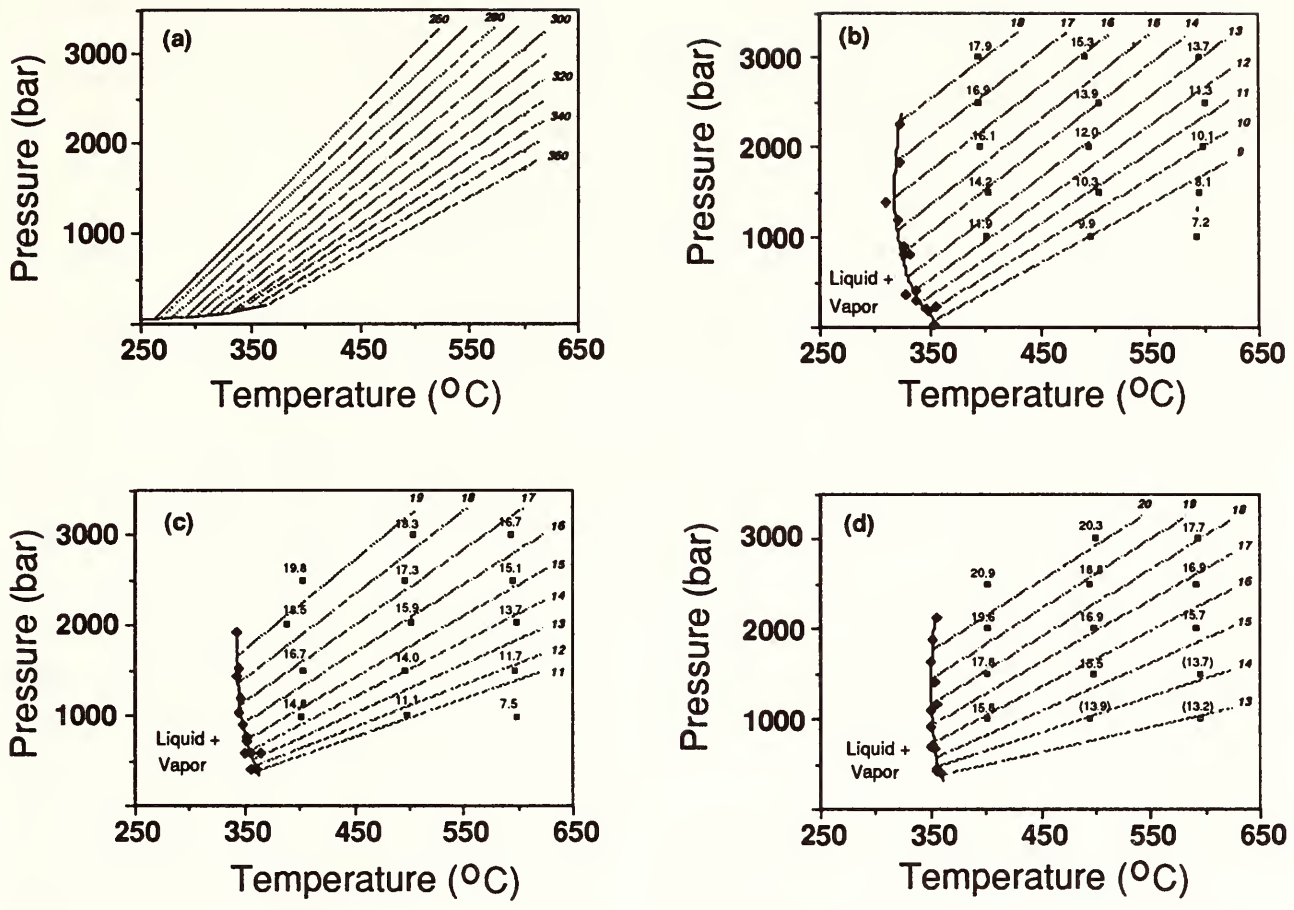

FIG. 46. Plot of the measured clathrate melting temperatures as a function of experimental temperature and pressure for a) H_2O, b) 5.5 mol% CH_4-H_2O, c) 11.0 mol% CH_4-H_2O, and d) 16.5 mol% CH_4-H_2O. The shaded lines represent lines of constant clathrate melting temperature (isochores). The non-italicized numbers refer to the measured clathrate melting temperatures and the italicized numbers refer to the clathrate melting temperatures represented by these lines. The curved lines represent the liquid-vapor curve for that compositional section.

sures from 1000 to 3000 bar. These experiments have resulted in the determination of 1) isochores; 2) liquid-vapor curves; and 3) the melting relations of clathrate as a function of composition.

CH_4-H_2O binary compositions

Lines of constant homogenization temperature and isochores have been extremely useful in natural fluid inclusion studies for the determination of the temperature-pressure history of the host minerals. Zhang and Frantz (1987) determined constant homogenization temperature lines and isochores for fluids in the NaCl - KCl - $CaCl_2$ - H_2O system and found that they could be represented in temperature-pressure space by a series of straight lines described by a simple function of the form;

$$P(\text{bar}) = A_1 + A_2 T(^\circ\text{C}) \qquad (1)$$

The coefficients A_1 and A_2 were functions of the homogenization temperature (T_h), the solute type, and the solute concentration. Using the regression parameters of

TABLE 6. Isochore regression parameters

System	Mol % CO_2	Mol % CH_4	a_1	a_2	a_3	a_4
CH_4-H_2O	—	5.5	3.274 x 10^3	-9.974 x 10^2	4.317 x 10^1	-7.073 x 10^0
	—	11.0	3.528 x 10^3	-6.123 x 10^2	1.760 x 10^1	-2.661 x 10^0
	—	16.5	1.482 x 10^4	-1.919 x 10^3	5.634 x 10^1	-3.500 x 10^1
CO_2-CH_4-H_2O	5.5	5.5	6.011 x 10^3	-1.311 x 10^3	5.135 x 10^1	-7.779 x 10^0
	11.0	5.5	-4.771 x 10^4	6.277 x 10^3	-2.096 x 10_2	1.097 x 10^2
	5.5	11.0	-6.906 x 10^3	9.524 x 10^2	-3.725 x 10^1	2.027 x 10^1

Zhang and Frantz (1987) isochores for pure water for the unary H_2O system are presented as a function of temperature and pressure in Fig. 46a.

Clathrate melting temperatures ranging from 7° to almost 21°C were measured with temperature-cycling techniques and are plotted as a function of the experimental temperature and pressure in Figs. 46b, 46c, and 46d for 5.5, 11.0, and 16.5 mol% CH_4 respectively. The italicized numbers represent experiments in which the inclusions homogenized to vapor rather than liquid. Since the melting temperature of clathrate in the pure CH_4-H_2O system depends only on composition and total inclusion density, they can be used in much the same way as homogenization temperatures were in the salt - H2O system to determine isochores. The data were fit to the following function:

$$P = (a_1 + a_2 T_{mc} + a_3 T_{mc}^2) + (a_4 + a_5 T_{mc} + a_6 T_{mc}^2)T, \quad (2)$$

in which T_{mc} is the clathrate melting temperature. The regression constants of these fits are given in Table 6. Lines of constant clathrate melting temperature or isochores are shown as shaded lines in Figs. 46b, 46c and 46d. The italicized numbers represent the clathrate melting temperatures corresponding to the lines. The slopes of the isochores generally become shallower with increasing concentration of the volatile, but the major change in slope occurs below 5.5 mol%. The liquid-vapor curve for each concentration was computed by solving equation (1) for homogenization pressures using the experimental homogenization temperatures (letting $T=T_h$) and clathrate melting temperatures. The results are shown as diamonds in Figs. 46b, 46c, and 46d. The homogenization pressures are high, with some high density inclusions being greater than 2000 bar. In Fig. 47, our CH_4 - H_2O liquid vapor curve results plotted as solid squares are compared to those of Welsch (1973) shown as shaded curves. The agreement is remarkable considering the different techniques used in the two studies.

The volumetric properties of the CH_4 - CO_2 isochores can be computed using the clathrate melting temperatures in conjunction with the bulk compositions. Bonham

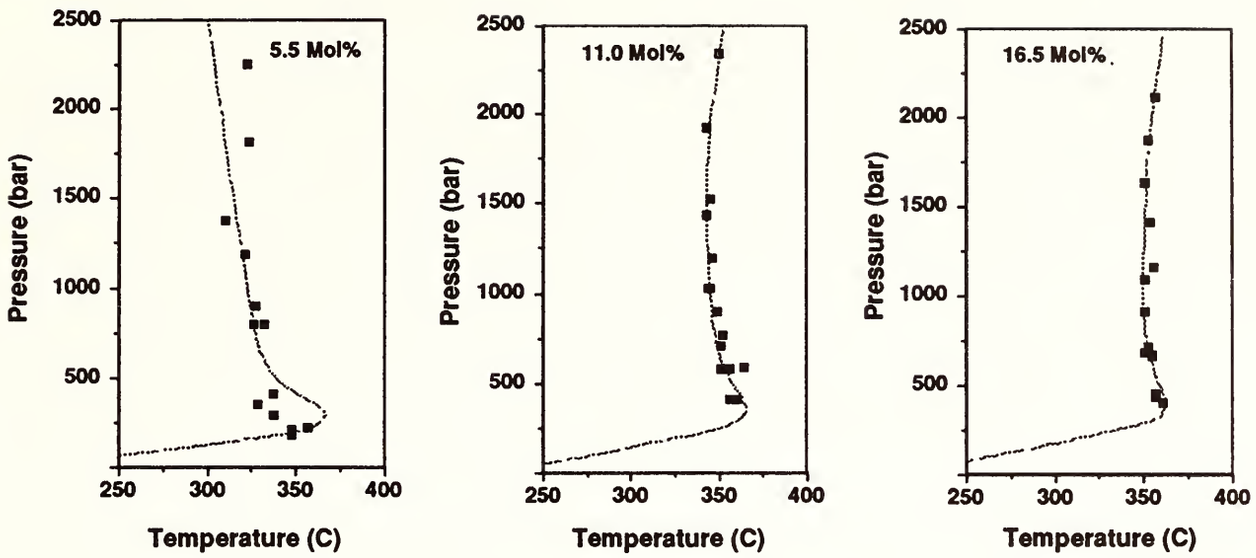

FIG. 47. Comparison of the liquid-vapor curve data of this study (solid squares) with those of Welsh (1973) for 5.5 mol% , 11.0 mol%, and 16.5 mol% CH_4-H_2O.

(1978) demonstrates that the solubility of methane in water at ambient temperatures and pressures to 100 bar is less than 0.2 mol%. The ice melting point measurements made on our methane-water experiments were within 0.1 or 0.2 of 0°C indicating low methane solubility in the liquid phase. Based on this, the vapor phase can be assumed to be composed entirely of methane and the liquid phase, of water and

$$V_{total} = V(H_2O)/(1+1/X) + V(CH_4)/(1+X), \quad (3)$$

where V_{total} is the molar volume of the entire inclusion, $V(CH_4)$ is the molar volume of the vapor phase, $V(H_2O)$ is the molar volume of the liquid phase, and X is the ratio of the number of moles of CH_4 over the number of moles of H_2O. Values for X can be computed from the relative amounts of methane and water introduced into the experimental charge. The clathrate melting temperature can be used to compute the internal pressure of the inclusion at the clathrate melting temperature using the data of Deaton and Frost (1946). Their data appear to be linear when the logarithm of the pressure is plotted against the melting temperature and the computed pressures ranged from 70 to over 200 bar. These values of the internal pressure were used in conjunction with the molar volume data for methane (Angus *et al.*, 1978) and the molar volume data for pure water to compute the total inclusion molar volumes corresponding to our experiments. These are shown as functions of the clathrate melting temperature for 5.5, 11.0, and 16.5 mol% CH_4 in Fig. 48.

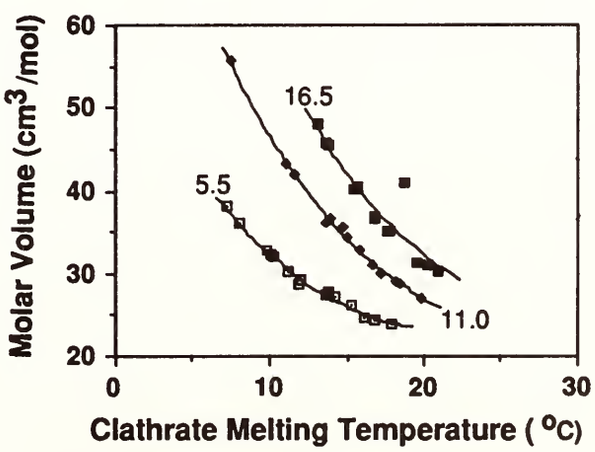

FIG. 48. Plot of the molar volume of 5.5, 11.0, and 16.5 mol% CH_4-H_2O as a function of the clathrate melting temperature.

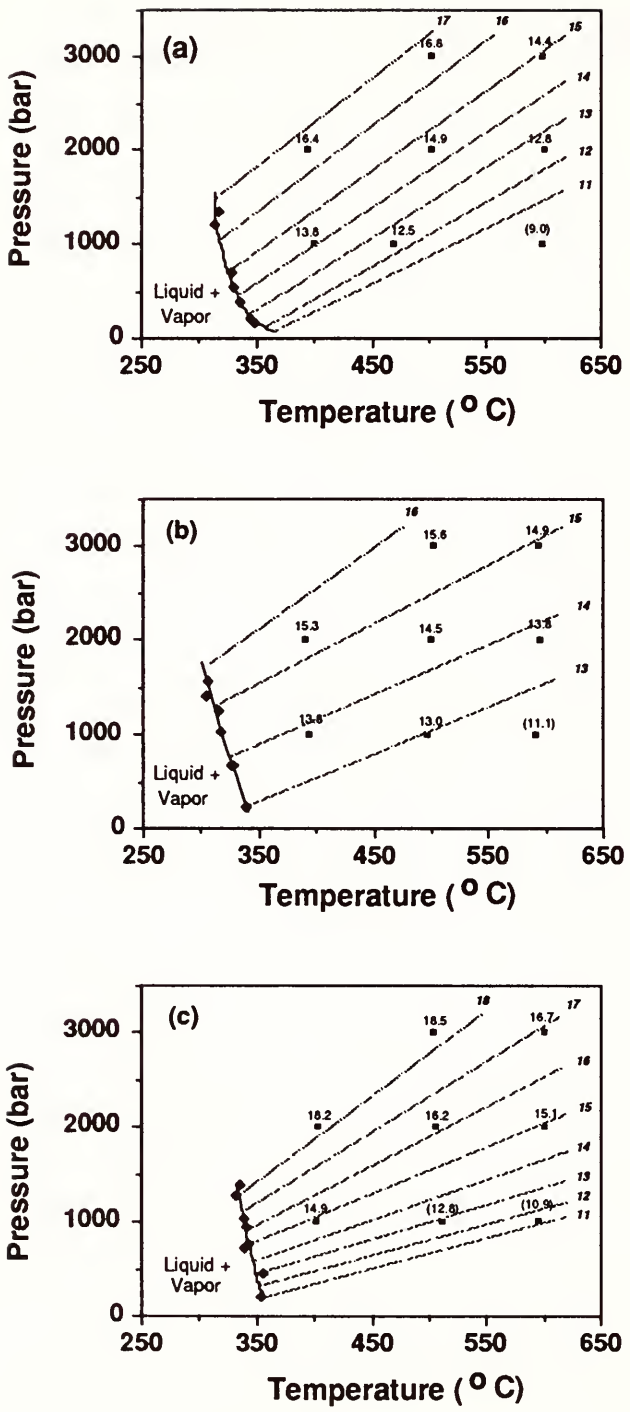

FIG. 49 Plot of the measured clathrate melting temperatures as a function of experimental temperature and pressure for a) 5.5 mol% CO_2 : 5.5 mol% CH_4 , b) 11.0 mol% CO_2 : 5.5 mol% CH_4, and c) 5.5 mol% CO_2 :11 mol% CH_4. The shaded lines represent lines of constant clathrate melting temperature (isochores). The non-italicized numbers refer to the measured clathrate melting temperatures and the italicized numbers refer to the clathrate melting temperatures represented by these lines. The curved lines represent the liquid-vapor curve for that compositional section.

CO_2-CH_4-H_2O ternary compositions

As in the case of the binary CH_4-H_2O system, the clathrate melting temperatures for ternary CO_2-CH_4-H_2O compositions were plotted as a function of the experimental temperature and pressure in an effort to determine the location of lines of constant T_{mc} or isochores (Fig. 49a shows the results for 5.5 mol% CO_2 : 5.5 mol% CH_4; Fig. 49b, for 11.0 mol% CO_2 : 5.5 mol% CH_4; Fig. 49c, for 5.5 mol%CO_2 : 11.0 mol% CH_4). The numbers in parentheses indicate experiments in which the inclusions homogenized to vapor. These data were fit with equation (2) yielding regression coefficients listed in Table 6. Lines of constant clathrate melting temperature calculated from these regressions are shown in Figs. 49a, 49b, and 49c as shaded lines labeled with italicized values of T_{mc}. Despite the limited number of data points for the ternary compositions, it is clear that the slopes of the isochores in Fig. 49a for the 5.5 mol% CO_2 : 11.0 mol% CH_4 are quite similar to those of the 5.5 mol% methane-water binary (Fig. 46b). The 5.5 mol% CO_2 : 11.0 mol% CH_4 (Fig. 49c) has isochores with slopes similar to those of the 11.0 mol% CH_4 - H_2O binary (Fig. 46c). It appears from these observations that the slopes of the isochores as determined from clathrate melting temperatures tend to follow the trends of the CH_4 - H_2O. The locations of the liquid-vapor curves were computed in the same manner as in the case of the CH_4-H_2O binary using the measurements of both the clathrate melting temperatures and the homogenization temperatures in conjunction with equation (2). The

results, plotted as diamonds, are shown on Figs. 49a, 49b, and 49c. Liquid-vapor curves for the 5.5 mol% CO_2 : 5.5 mol% CH_4 and the 11.0 mol% CO_2 : 5.5 mol% CH_4 compositions are *both* almost identical to that of the 5.5 CH_4 - H_2O binary. The liquid-vapor curve for the 5.5 mol% CO_2 : 11.0 mol% CH_4 is very similar to that of the 11.0 mol% CH_4 binary. Even more than in the case of the slopes of the isochores, the positions of the liquid-vapor curves in the portion of the CO_2 - CH_4 - H_2O ternary studied in this investigation closely follow the locations of the CH_4 - H_2O liquid-vapor curves having the same mol% methane.

The synthetic fluid inclusion method combined with the gas-loading techniques of Frantz *et al.* (this Report) have proven quite effective in the determination of the molar volumes, liquid-vapor curves, isochores, and low-temperature phase relations of C-O-H gas mixtures. The fluids produced using these techniques yielded inclusions of extremely homogeneous composition as evidenced by the low standard deviations of the microthermometric measurements for clathrate melting temperature (approximately ±0.1°C). Regressions considering measurements of the clathrate melting temperature or the homogenization temperature as a function of the experimental temperature and pressure yielded sets of isochores which systematically varied as a function of concentration. As the gas concentration increases, the slopes of the sets of isochores tend to become shallower. Molar volumes considerably larger than those of pure water were computed for the isochores using measurements of the clathrate melting temperature The quality of the data permitted the calculation of liquid-vapor curves for the CH_4 - H_2O binaries which are in reasonable agreement with data obtained using large-volume hydrothermal pressure vessels. The presence of methane appears to dominate both the slopes of the isochores and the position of the liquid-vapor curve in the ternary compositions considered in this study.

References

Angus, S., B. Armstrong, and K. M. deReuck, *International Thermodynamic Tables of the Fluid State-5. Methane. IUPAC chemical data series 16*, Pergamon Press, New York 251pp, 1978.

Bodnar, R. J., and S. M. Sterner, Synthetic fluid inclusions in natural quartz, II. Application to PVT studies, *Geochim. Cosmochim. Acta, 49*, 1855-1859, 1985.

Burrus, R. C., Analysis of fluid inclusions: phase equilibria at constant volume, *Am. J. Sci., 281*, 1104-1126, 1981.

Deaton, W. M., and E. M. Frost, Gas hydrates and their relation to the operation of natural pipelines, *U. S. Bur. Mines Monogr., 8*, 103p, 1946.

Franck, E. U., and K. Todheide, Thermische Eigenschaften überkritischer Mischungen von Kohlendioxyd und Wasser bis zu 750 °C und 2000 atm, *Chem. Neue. Folge., 22*, 232-245, 1959.

Green, D. H., T. J. Falloon, and W. R. Taylor, Mantle-derived magma-roles of variable source peridotite and variable C-H-O fluid compositions, in *Magmatic Processes: Physicochemical Principles*, B. Mysen, ed., Spec. Pub. No. 1, The Geochemical Society, University Park, Pennsylvania, pp. 139-154, 1987.

Greenwood, H. J., The compressibility of gaseous mixtures of carbon dioxide and water between 0 and 500 bars pressure and 4500 and 800°C, *Am. J. Sci., 267A*, 191-208, 1969.

Greenwood, H. J., Thermodynamic properties of gaseous mixtures of H_2O and CO_2 between

450°and 800°C and 0 to 500 bars, *Am. J. Sci., 273*, 561-571, 1973.

Heyen, G., C. Ramboz, and J. Dubessy, Simulation des equilibres des phases dans le system CO_2-CH_4 en-dessous de 50°C et de 100 bars, *C. R. Acad. Sci. Paris, 294*, 203-206, 1982.

Hollister, L., and R. C. Burrus, Phase equilibria in fluid inclusions from the Khtada Lake metamorphic complex, *Geochim. Cosmochim. Acta , 40*, 163-176, 1976.

Ramboz, C., D. Schnapper, and J. Dubessy, The P-V-T-X-f(O_2) evolution of H_2O - CO_2 - CH_4-bearing fluid in a wolframite vein: Reconstruction from fluid inclusion studies, *Geochim. Cosmochim. Acta, 49*, 205-219, 1985.

Saxena, S. K., Oxidation state of the mantle, *Geochim. Cosmochim. Acta, 53*, 89-95, 1989.

Swanenberg, H. E. C., Phase equilibria in carbonic system, and their application to freezing studies of fluid inclusions, *Contr. Mineral. Petrol., 68*, 303-306, 1979.

Takenouchi, S., and G. C. Kennedy, The binary system H_2O - CO_2 at high temperatures and pressures, *Am. J. Sci., 262*, 1055-1074, 1964.

Welsch, H., Die Systems Xenon-Wasser und Methan-Wasser bei lohen Drücken und temperature, Ph. D. dissertation, Inst. for Physical Chem., Karlsruhe, 1973.

Wintsche, R. P., A. F. O'Connell, L. Ransom, and M. J. Wiechmann, Evidence for the influence of f(CH_4) on the crystallinity of disseminated carbon in greenschist facies rocks, Rhode Island, USA, *Contr. Mineral. Petrol., 77*, 207-213, 1981.

Zhang, Y. G., and J. D. Frantz, Determination of the homogenization temperatures and densities of supercritical fluids in the system NaCl - KCl - $CaCl_2$ - H_2O using synthetic fluid inclusions, *Chem. Geol., 64*, 335-350, 1987.

Zhang, Y. G., and J. D. Frantz, Experimental determination of the compositional limits of immiscibility in the system $CaCl_2$ - CO_2 - H_2O at high temperatures and pressures using synthetic fluid inclusions, *Chem. Geol., 74*, 289-308, 1989.

A Laser-based Carbon Reduction Technique For Oxygen Isotope Analysis of Silicates and Oxides

*Zachary D. Sharp and James R. O'Neil**

Stable isotope analysis is one of the most valuable geochemical techniques available for constraining the conditions of formation and alteration in most rock types. However, the methods for extracting oxygen from silicates and oxides have remained relatively unchanged over the past 25 years. As a result, large sample sizes are required for analysis and nearly all spatial resolution is lost. Fine-scale variations in the $\delta^{18}O$ of oxides and silicates cannot normally be determined. In comparison, other geochemical techniques have been used successfully to determine major, minor and trace element concentrations, crystal structures, and isotopic compositions (i.e., U-Th-Pb, $^{40}Ar/^{39}Ar$, $\delta^{34}S$) on a μm scale. This report outlines a microanalytical method for $\delta^{18}O$ determinations of selected silicates and oxides using a laser-heated carbon reduction technique.

The natural variations in the $\delta^{18}O$ of minerals is so small that analytical techniques of very high precision are required to distinguish them. Two analytical methods have been developed that are capable of analyzing the $\delta^{18}O$ of oxides and silicates at the high level of precision necessary to discern these small isotopic differences: 1) fluorination and 2) carbon reduction.

Fluorination of minerals at moderate temperatures (200-650°C) liberates O_2

* Dept. of Geological Sciences, University of Michigan, Ann Arbor, MI 48109-1063

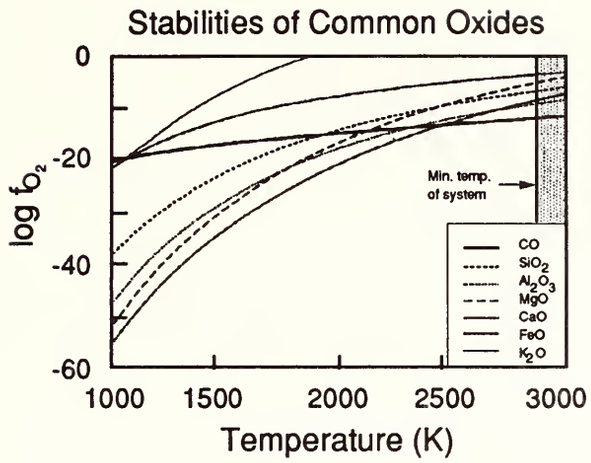

FIG. 50. T-$f(O)_2$ diagram showing the stability of common oxides relative to the elements. The C - CO buffer (thick solid line) crosses below the stability field of all common oxides above 2450K. In the presence of graphite, all oxides will reduce to the elements and carbon monoxide above this temperature. The minimum temperature of the present system (shaded area) is 2890K (melting point of molybdenum). Thermodynamic data are from Chase *et al.* (1985).

which is converted to CO_2 and subsequently analyzed by conventional isotope ratio mass spectrometry. The fluorination method (e.g., Baertschi and Silverman, 1951; Clayton and Mayeda, 1963) is applicable to all but the most refractory minerals, but relatively large sample sizes of 5-30 mg are generally required to obtain accurate and reproducible results. Samples as small as 1 mg can be analyzed only with extreme care and assigning a somewhat arbitrary blank correction (Lee *et al.*, 1980).

The carbon reduction method involves the high temperature (1000-2400°C) reduction of minerals to carbides or native elements and CO with varying amounts of CO_2. The evolved CO is converted to CO_2 and analyzed. This technique has met with partial success (e. g., Schwander, 1953; Clayton and Epstein, 1958), but has been limited, in part, by the difficulty of attaining the high temperatures required for reaction. The traditional carbon reduction technique also requires large sample sizes, a time consuming degassing procedure and is claimed to be unsatisfactory for alkali-bearing minerals (Clayton and Epstein, 1958). This is a result of the volatile alkali metals being oxidized by the evolved CO, which involves a large isotopic fractionation. The laser-based carbon reduction technique allows for reduced sample sizes of 1-3 mg *or less*, and because the heating is so rapid, analyses can be made much more quickly and cleanly than with either the conventional fluorination or carbon reduction method.

The carbon reduction method is based on the fact that all common oxides and silicates will be reduced in the presence of carbon, if sufficient temperatures are reached. For example, quartz and magnetite are reduced by the following reactions, respectively (Clayton and Epstein, 1958):

$$SiO_2 + 3C = SiC + 2\ CO, \qquad (1)$$

$$Fe_3O_4 + 4\ C = 3\ Fe + 4\ CO. \qquad (2)$$

The stabilities of selected common oxides relative to the C - CO - CO_2 buffer are shown as a function of temperature at 1 bar in Fig. 50. Above 2400°C, all common oxides in the presence of graphite should be reduced to either elements or carbides. Temperatures of 2617°C (melting point of molybdenum) are easily achieved with the Nd-YAG laser equipment at the Geophysical Laboratory.

In the present system, samples are prepared by grinding the weighed mineral

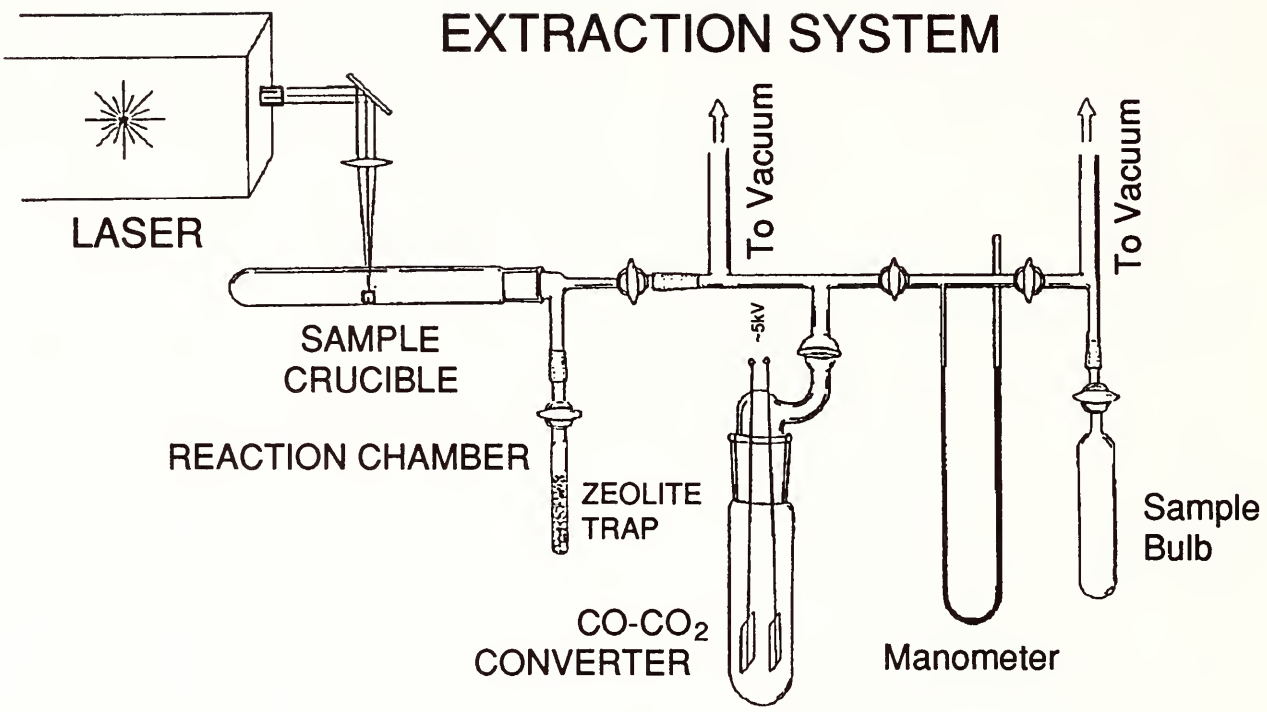

FIG. 51. Laser extraction system. The system consists of a Nd-YAG laser, a sample crucible, a reaction chamber with zeolite trap and a CO - CO_2 converter. During reaction, the CO is collected on the zeolite trap, which is removed from the reaction chamber and placed onto the vacuum line. The CO is then desorbed and converted to CO_2 on the CO - CO_2 converter.

with excess graphite (15-50% over stoichiometric). The mixture is pressed into a pellet 3 mm in diameter to insure intimate contact between the two phases. During laser heating, the graphite absorbs the radiation, heating the entire pellet to extremely high temperatures. To prevent reaction with the sample chamber, the pellet is nested in a 5 mm O.D. graphite crucible which in turn is placed in a platinum crucible holder. The platinum cup is used to prevent direct contact between the hot graphite crucible and the walls of the sample chamber.

The extraction system comprises a laser, a sample crucible, a reaction chamber and a CO - CO_2 converter (Fig. 51). A variable power, 18 watt maximum Nd-YAG laser (λ = 1.064 μm) with a 6X air-objective is used as a heating source. The focal length of this lens is 20 mm with a focused spot of ~10 μm. Although most minerals are transparent to radiation of this wavelength, graphite strongly absorbs the radiation and heats up. The admixed mineral is heated by conduction from the graphite powder. The sample chamber consists of a 20 mm O.D. quartz sample tube with a ground glass joint to admit the sample and a removable zeolite trap (cold finger) equipped with a stopcock (Fig. 51). The reaction chamber containing the sample pellet is evacuated and degassed at 600°C for 1 hour. The sample is gently rastered under the focused laser beam until the sample pellet is entirely reacted. The evolved CO is collected on the cold finger as the reaction proceeds. Thus a high vac-

uum is maintained in the reaction chamber at all times. By keeping the CO fugacity extremely low, there is less chance for the CO to react with reactive alkali metals that may vaporize and plate out on the chamber walls during reaction. The zeolite trap is isolated from the reaction chamber and heated to 300°C to desorb the CO. The CO is then converted to CO_2 with a high voltage electric discharge between two parallel platinum plates (Agget *et al.*, 1965; Rafter, 1967) by the reaction

$$2\,CO = CO_2 + C. \qquad (3)$$

The CO_2 yield is measured manometrically, and the gas is fed to a sample tube.

Isotopic data obtained with the laser-based carbon reduction method are presented in Table 7 and Fig. 52. Analyses of all oxides and some of the silicate minerals examined are in agreement with analyses made with conventional fluorination methods. Refractory minerals such as olivine and kyanite give erratic results and are not amenable to the present carbon reduction technique. Analyses of feldspars are consistently low by 3.3 ± 0.3 ‰. During laser heating, tiny particles of unreacted material are blown out of the graphite crucible along with the evolving CO and consequently yields are generally low, typically 40-60 per cent. Because magnetite reacts at very low temperatures, yields of 100% are achieved. The low yields obtained for the other minerals do not affect the isotopic results. There is no correlation between the % yield of a mineral and the difference between the measured and true isotopic composition of that mineral, as long as feldspar is not included in the correlation.

If the isotopic analyses of feldspars are always low by a constant amount, a correction can be applied to the data in order to bring them into accord with the actual values as is done for carbonates analyzed by the H_3PO_4 technique (McCrea, 1950). It is not clear why the $\delta^{18}O$ values are lower than their accepted values. Clayton and Epstein (1958) first reported a problem with carbon reduction of feldspar. They observed the formation of a metallic mirror on the walls of the glass chamber as the samples were heated. Such mirrors are probably the result of the vaporization of alkalis from the mineral and condensation on the glass walls as metals. As their reactions proceeded, the mirrors lost their metallic finish presumably due to the oxidation of the highly reactive metal by either CO or CO_2. Because the oxidation of the

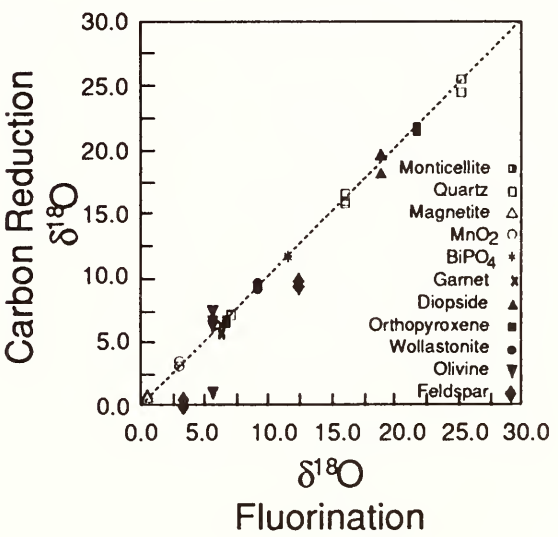

FIG. 52. Comparison between $\delta^{18}O$ values determined with the carbon reduction method and those from the fluorination method. The diagonal line represents perfect agreement between the two methods. The $\delta^{18}O$ values of feldspar determined with the carbon reduction method are consistently 3.3 ‰ light. Olivine and garnet may give erratic results.

TABLE 7. Isotopic composition, sample size and % recovery of various minerals determined with the carbon reduction technique. The $\delta^{18}O$ actual represents either accepted values of isotopic standards or newly measured values using the fluorination method. All data are reported in the ‰ notation relative to SMOW.

Mineral	$\delta^{18}O$ actual	$\delta^{18}O$ measured	Sample Size (mg)	μmole CO_2 recovered	% recovery
Quartz	7.2	7.2	3.6	n.d.	n.d.
	7.2	7.1	3.0	12	23
	7.2	7.1	3.9	25	38
	16.2	15.9	3.2	24	45
	16.2	15.7	2.8	20	42
	16.2	16.5	3.0	7	13
	16.2	16.5	3.3	35	63
	25.3	24.4	2.3	23	59
	25.3	25.4	1.5	n.d.	n.d.
Magnetite	0.6	0.6	1.9	16	100
	0.6	0.8	2.3	20	100
MnO_2	3.1	3.1	2.9	14	34
	3.1	3.5	2.9	18	56
$BiPO_4$	11.7	11.5	3.6	13	55
	11.7	11.7	2.7	8	42
Orthopyroxene	6.8	6.8	3.9	34	77
	6.8	6.4	2.4	16	60
Diopside	19.0	18.0	2.7	18	49
	19.0	19.4	6.6	41	45
	19.0	19.5	4.1	32	56
Wollastonite	9.3	9.1	5.3	18	26
	9.3	9.6	2.4	12	39
	9.3	9.3	4.1	20	38
Garnet	6.4	5.7	4.1	23	46
	6.4	5.8	2.7	14	44
	6.4	6.3	3.0	16	44
Forsterite	5.7	6.0	3.0	n.d.	n.d.
	5.7	7.2	3.2	n.d.	n.d.
	5.7	1.0	1.9	4	13
	5.7	6.4	1.2	4	25

TABLE 7. Continued

Mineral	$\delta^{18}O$ actual	$\delta^{18}O$ measured	Sample Size (mg)	μmole CO_2 recovered	% recovery
Monticellite	22.0	21.5	4.8	20	33
	22.0	21.6	4.5	18	31
	22.0	21.4	4.8	19	31
Feldspar	12.5	9.1	2.7	16	42
	12.5	9.5	2.5	16	46
	3.4	0.3	3.2	13	29
	3.4	-0.2	3.7	17	32
Kyanite	n.d.	7.5	3.6	19	34
	n.d.	8.6	4.0	24	39
CaO	n.d.	25.6	3.3	11	37
	n.d.	25.4	4.9	20	46
Al_2O_3	n.d.	14.4	4.7	24	35
	n.d.	14.2	3.8	23	41
MgO	n.d.	n.d.	3.1	15	39
	n.d.	n.d.	3.4	20	47

metallic mirror is a kinetic rather than equilibrium reaction, carbon oxides containing the light isotope of oxygen should react preferentially. As a result, the residual CO would have a $\delta^{18}O$ value that is higher than the actual value of the alkali-bearing silicate. This expected elevation of the $\delta^{18}O$ values of feldspars was observed by Clayton and Epstein (1958), but with the present carbon reduction technique, the measured $\delta^{18}O$ of the feldspars is lower than the actual value (Table 7). One explanation for the low isotopic values is that the oxygen in the Si-O-Al bonds reacts preferentially to the oxygen in Si-O-Si bonds in the laser-based carbon reduction procedure. The sign and magnitude of this effect is consistent with previous estimates based on relative bond strength (Taylor and Epstein, 1962).

Isotopic analyses of the refractory minerals forsterite, kyanite, and to a lesser extent, garnet are more erratic than those of other minerals, and in the case of olivine, the yields are substantially lower. The oxides that comprise olivine and kyanite (MgO, SiO_2 and Al_2O_3) all react to a uniform extent with reproducible isotopic analyses. The calculated $f(O_2)$ required to reduce forsterite to its elements is higher than for the oxide components, so thermo-

dynamics favors the reduction of olivine over the oxides. Furthermore, olivine melts when radiated by the Nd-YAG laser because the iron linkages absorb radiation at 1.063 μm. The reaction involves a thermodynamically favorable reduction of a melt with graphite, but very little takes place. The erratic $\delta^{18}O$ observed for forsterite, but not monticellite ($CaMgSiO_4$), cannot be explained by preferential reaction of differently bound oxygen. All of the oxygen in olivine is shared between a silicon and M^{2+} cation. There is no isotopic distinction between sites, and therefore, no possible reaction of one site relative to another.

The safety, rapidity and small sample sizes are the primary benefits of the laser-based carbon reduction technique over conventional fluorination. Microvariations in the $\delta^{18}O$ of quartz veins, porphyroblasts and phenocrysts can be measured with this new method. Unfortunately, not all minerals are amenable to the carbon reduction method at this time, but further investigations of the isotopic systematics involving the laser-based carbon reduction technique may lead to a better understanding of high-temperature, rapid kinetic processes that occur during laser heating.

References

Aggett, J., C. A. Burton, T. A. Lewis, D. R. Llewellyn, C. O'Connor, and A. L. Odell, The isotopic analysis of oxygen in organic compounds and in coordination compounds containing organic hazards, *J. Appl. Radiat. Isot., 16*, 165-170, 1965.

Baertschi, P., and S. R. Silverman, The determination of relative abundances of the oxygen isotopes in silicate rocks, *Geochim. Cosmochim. Acta, 1*, 317-328, 1951.

Chase, M. W. Jr., C. A. Davis, J. R. Downey, Jr., D. J. Frurip, R. A. McDonald, and A. N. Syverud, JANAF Thermochemical Tables, 3rd ed., *J. Phys. Chem. Ref. Data, 14*, 1986.

Clayton, R. N., and S. Epstein, The relationship between O^{18}/O^{16} ratios in coexisting quartz, carbonate and iron oxides from various geological deposits, *J. Geol., 66*, 352-371, 1958.

Clayton, R. N., and T. K. Mayeda, The use of bromine pentafluoride in the extraction of oxygen from oxides and silicates for isotopic analysis, *Geochim. Cosmochim. Acta, 27*, 43-52, 1963.

Lee, T., T. K. Mayeda, and R. N. Clayton, Oxygen isotopic anomalies in Allende inclusion HAL, *Geophys. Res. Lett., 7*, 493-496, 1980.

McCrea, J. M., On the isotopic chemistry of carbonates and a paleotemperature scale, *J. Chem. Phys., 18*, 849-857, 1950.

Rafter, T. A., Oxygen isotopic compositions of sulphates - I: A method for extraction of oxygen and its quantitative conversion to carbon dioxide for isotope ratio measurements, *N. Zealand J. Sci., 10*, 493-510, 1967.

Schwander, H., Bestimmung des relativen Sauerstoffisotopen-Verhaltnisses in Silikatgesteinen und -Mineralien, *Geochim. Cosmochim. Acta, 4*, 261-291, 1953.

Taylor, H. P., Jr., and S. Epstein, Relationship between O^{18}/O^{16} ratios in coexisting minerals of igneous and metamorphic rocks, *Geol. Soc. Am. Bull., 73*, 675-694, 1962.

Crystallography - Mineral Physics

Isotope Effects in Dense Solid Hydrogen: Phase Transition in Deuterium at 190 (±20) GPa

Russell J. Hemley and Ho-kwang Mao

Once the exclusive domain of theory, the behavior of hydrogen at ultrahigh pressures is now amenable to direct experimental investigation using ultrahigh-pressure, diamond-anvil techniques (Hemley and Mao, 1988; Mao and Hemley, 1989). The goal of this effort has been the characterization of hydrogen above 100 GPa and testing of theoretical predictions of the insulator-metal transition pressure in this material, currently predicted to occur between 150 and 300 GPa. Recently, we demonstrated that solid hydrogen undergoes a phase transition at 145 GPa and 77K (Hemley and Mao, 1988). Changes in the Raman spectra indicate that the transition may be a structural one between insulating molecular phases, possibly associated with orientational ordering. Recently, we have shown that on further increase in pressure the optical properties of the high-pressure phase change dramatically. Above 200 GPa there is evidence for ground-state electronic excitations at visible wavelengths, and at pressures in the 250 GPa range hydrogen samples are opaque (Mao and Hemley, 1989). These observations have led to the possibility that the transition at 145 GPa may be associated with band overlap. If so, the character of the optical spectra indicate that the gap may be indirect at closure. This interpretation is consistent with theoretical predictions that band overlap may occur below 200 GPa (Friedli and Ashcroft, 1977; Min *et al.*, 1986; Barbee *et al.*, 1989).

An important constraint on the nature of phase transitions in solid hydrogen is provided by the study of isotope effects, which produce a well-known effect on the orientational ordering transformation at low densities (Silvera, 1988). The ordering transformation occurs at significantly lower pressures in D_2 than in H_2 because of the lower rotational constant of the heavier isotope. There is a pronounced isotope effect on the Raman-active vibron. In both hydrogen and deuterium, the frequency of the vibron increases with pressure but then decreases above a critical pressure. In H_2 the critical pressure is 30 GPa whereas in D_2 it is shifted to 50 GPa (Sharma *et al.* 1980). The weaker negative pressure shift of the D_2 vibron is magnified at higher pressures: at 125 GPa, for example, the vibron frequency is 40 cm^{-1} above and 40 cm^{-1} below the zero-pressure values for D_2 and H_2, respectively (Mao *et al.*, 1985). Although these results suggest that the equations of state for the two solids are significantly different at these very high densities, direct measurements at low pressures indicate that the compressibility of the two solids are similar (Mao *et al.*, 1988).

In the present study we have pressur-

ized deuterium to pressures above 250 GPa to examine its vibron shift above the previous limit of 125 GPa (Mao *et al.*, 1985). In particular, we wished to examine possible phase transitions in the region of the transition observed in hydrogen. The experiments were performed using techniques described previously (Hemley and Mao, 1988). The Raman active vibron was measured as a function of pressure, with pressure determined using the ruby fluorescence technique. Because of the use of low-fluorescence diamonds and the high sensitivity of the optical system, time-resolved techniques were not needed to measure the ruby fluorescence spectra. The ruby spectra were measured to pressures of about 240 GPa on the quasihydrostatic pressure scale.

The pressure shift of the Raman-active vibron of molecular deuterium to pressures above 200 GPa is shown in Fig. 53. A single, well-resolved band which decreases in frequency above 50 GPa was observed initially, as in previous studies (Sharma *et al.*, 1980; Mao *et al.*, 1985). Above 100 GPa, the negative pressure shift of the vibron, measured here at 77 K, converged with that measured previously at room temperature to 125 GPa, and continued smoothly to higher pressures. At 190 (±20) GPa, however, a second, broader peak appeared 130 (±5) cm^{-1} below that of the first. The two peaks coexisted over a small pressure interval with the intensity of the new peak growing at the expense of the first with increasing pressure. With further increase in pressure, the higher frequency peak completely disappeared. The second peak continued to decrease in frequency

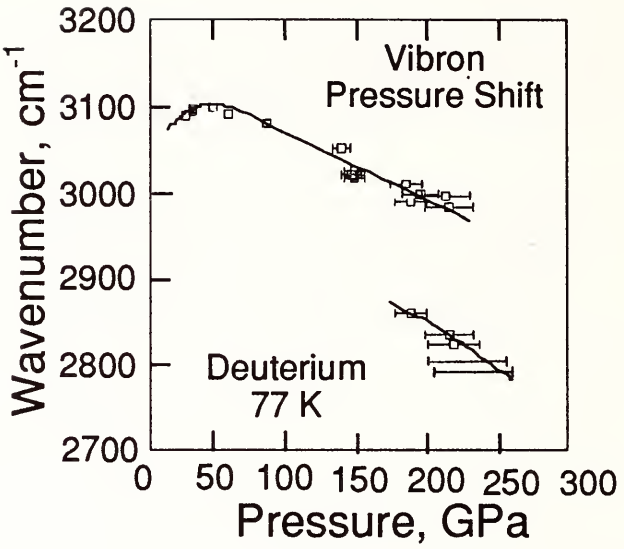

FIG. 53. Pressure shift of the Raman-active vibron of molecular deuterium to ultra-high pressures. The second, lower frequency vibron first appeared at a ruby pressure of 190 (± 20) GPa. The two peaks coexisted over a pressure interval of approximately 20 GPa, with an average separation of 130 cm^{-1} between them. The width of the mixed phase region is likely to reflect the magnitude of pressure gradients in the sample across the laser spot (~5 mm in diameter). Similar effects were observed in hydrogen.The error bars for the higher pressure points include the uncertain-ties arising from the broadness of the ruby R_1 peaks and from pressure calibration (hydrostatic versus quasihydrostatic). The pressure could not be measured directly for the two highest pressure spectra. At these pressures, the sample had completely transformed to the high pressure phase, as evidenced by the single peak present in the measured spectra.

with increasing pressure; at the highest pressures attained, the frequency of the peak was 2793 cm^{-1}. The pressures could not be determined reliably above 240 GPa as a result of the decrease in the ruby fluorescence intensity. We estimate that the maximum pressure reached on the deuterium was 240-280 GPa (see Mao and Hemley, 1989).

The appearance of the second, broader vibron, and coexistence of the two peaks over a small pressure interval, strongly resembles that recently observed in hydro-

gen. However, there are some notable differences in the two isotopes that bear further analysis. First, despite the uncertainties in pressure, the data clearly indicate that the transition in deuterium occurs at a higher pressure than that in hydrogen (190 versus 145 GPa). Second, the vibron discontinuity is larger (130 versus 105 cm^{-1} for hydrogen). The weaker pressure dependence of the vibron in deuterium has been noted previously (Mao *et al.* 1985). The transition in deuterium occurred when the vibron reached a value of 2990 cm^{-1}, which is close to its zero-pressure value; in contrast the transition in hydrogen occurred when the vibron was approximately 100 cm^{-1} below its zero-pressure value.

The more pronounced pressure dependence of the vibron frequency for hydrogen indicates that the molecules in this solid are significantly more anharmonic than in deuterium at a given pressure (density). Ashcroft (1988) has argued that the different pressure dependencies of the vibron frequencies may arise from large differences in zero-point energy for the two isotopes. If the phase transitions in the two isotopes involve the same crystal structures, it is possible that the differences in zero-point energy may also be responsible for the higher phase transition pressures for the heavier isotope. Moreover, since the difference in zero-point energy for the two isotopes is expected to be comparable to the energy differences between different structures, it is also possible that the two isotopes crystallize in different structures at high pressures and have a different series of phase transitions in the molecular solid prior to metallization. Finally, recent theoretical calculations indicate that band overlap should occur in the molecular phase as low as 150 GPa (see Mao and Hemley, 1989). At the point of band overlap, electron density will be removed from the molecular bonds to conduction states, causing a decrease in the frequency of the molecular vibron. The magnitude of this frequency shift could therefore provide useful constraints on possible band overlap in the molecular phase.

References

Ashcroft, N. W., Quantum liquid metals: the physics of dense hydrogen, *Z. Phys. Chemie, 156,* 41-51, 1988.

Barbee, T. W., A. Garcia, M. L. Cohen, and J. L. Martins, Theory of high-pressure phases of hydrogen, *Phys. Rev. Lett., 62,* 1150-1153, 1989.

Friedli, C., and N. W. Ashcroft, Combined representation method for use in band structure calculations: application to highly compressed hydrogen, *Phys. Rev. B, 16,* 662-672, 1977.

Hemley, R. J., and H. K. Mao, Phase transition in solid molecular hydrogen at ultra-high pressure, *Phys. Rev. Lett. 61,* 857-860, 1988.

Mao, H. K., and R. J. Hemley, Optical studies of hydrogen above 200 gigapascals: evidence for metallization by band overlap, *Science, 244,* 1462-1465, 1989.

Mao, H. K., P. M. Bell, and R. J. Hemley, Ultrahigh pressures: optical observations and Raman measurements of hydrogen and deuterium to 1.47 Mbar, *Phys. Rev. Lett., 55,* 99-102, 1985.

Mao, H. K., A. P. Jephcoat, R. J. Hemley, L. W. Finger, C. S. Zha, R. M. Hazen, and D. E. Cox, Synchrotron x-ray diffraction measurements of single-crystal hydrogen to 26.5 gigapascals, *Science, 239,* 1131-1134, 1988.

Min, B. I., H. J. F. Jansen, and A. J. Freeman, Pressure-induced electronic and structural phase transitions in solid hydrogen, *Phys. Rev. B, 33,*

6383-6390, 1986.
Sharma, S. K., H. K. Mao, and P. M. Bell, Raman measurements of deuterium in the pressure range of 8-537 kbar at room temperature, *Carnegie Instn. Washington Year Book, 79*, 358-364, 1980.
Silvera, I. F., The phase diagram and excitations in solid hydrogen: prospects for metallization, in *Simple Molecular Systems at Very High Densities*, A. Polian, P. Loubeyre, and N. Boccara, eds., Plenum, New York, pp. 33-46, 1988.

The Effect of Pressure, Temperature, and Composition on the Lattice Parameters and Density of $(Fe,Mg)SiO_3$ - Perovskites to 30 GPa

*Ho-kwang Mao, Russell J. Hemley, Jinfu Shu, Liang-chen Chen, Andrew P. Jephcoat, Yan Wu, and William A. Bassett**

Information on the physical properties (density, bulk modulus, and lattice parameters) of the $MgSiO_3$-perovskite as a function of pressure, temperature and Fe-Mg composition is of fundamental importance for a realistic model of the lower mantle. Although there is a growing body of data on these properties from high pressure single-crystal and polycrystalline x-ray diffraction (Yagi *et al.*, 1982; Kudoh *et al.*, 1987; Knittle and Jeanloz, 1987; Ross and Hazen, 1989), from Brillouin scattering measurements (Yeganeh-Haeri and Weidner, 1989) and from theoretical calculations (Hemley *et al.*, 1987; Wolf and Bukowinski, 1987), little is known about the properties of perovskite at higher pressures. Indeed, the equation of state of the orthorhombic perovskite has not been studied above 13 GPa under hydrostatic pressure conditions; hydrostatic pressure is necessary for distinguishing the compressibility of individual lattice parameters. Previous quasihydrostatic measurements on the elasticity of the perovskite were made at ambient conditions or at pressures far below the stability field of the perovskite, which could cause samples to behave abnormally. Thermal expansion data for $(Fe,Mg)SiO_3$-perovskite were collected at ambient pressure by Knittle *et al.* (1986). No measurements have yet been carried out at simultaneous high-pressure and high-temperature conditions. The effects of Fe/Mg ratio on the equation of state or the perovskite, which is crucial for the determination of the iron content in the mantle, has also not been studied experimentally nor theoretically.

Polycrystalline x-ray diffraction in the megabar diamond-anvil cell with an external resistance heater can reach the stability field of the perovskite and cover the pressure range of the lower mantle. A high degree of hydrostaticity and high resolution in the diffraction measurements are necessary for observing changes in orthorhombic distortion and for determining a precise equation of state for the perovskites. The present paper reports the development of a new technique for such experiments .

The silicate perovskite samples were synthesized from synthetic pyroxenes by laser-heating at 40 GPa in diamond-anvil cells (Mao *et al.*, 1977). The perovskite sample formed a disc-shaped polycrystalline aggregate, 150 mm diameter and 20 to 50 mm thick and gold was used as a high-

* Department of Geological Sciences, Cornell University, Ithaca, NY 14853

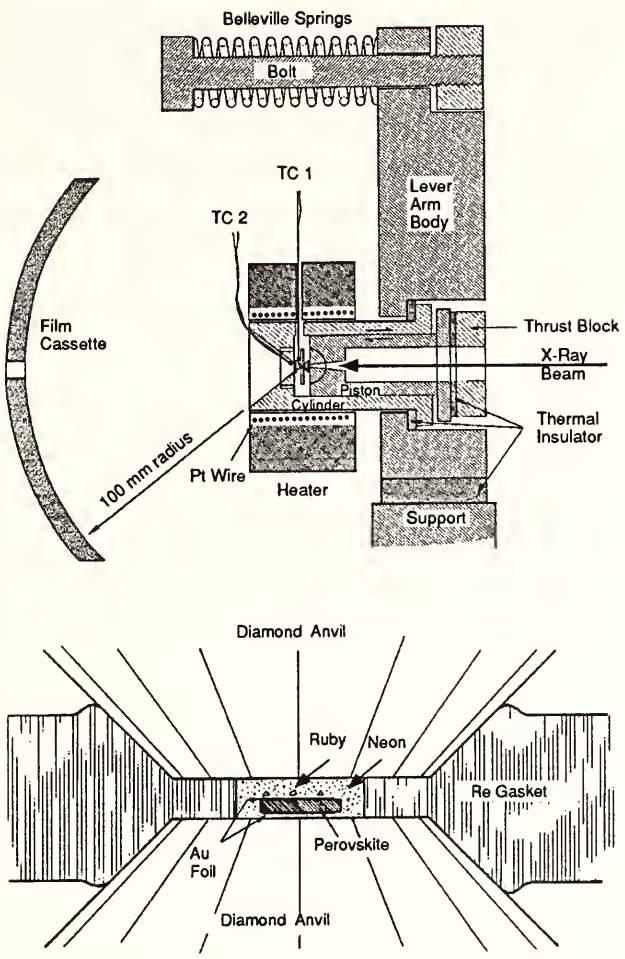

FIG. 54. (a) The diamond-anvil cell with external heater; (b) Sample configuration

temperature high-pressure calibrant (Jamieson *et al.*, 1982; Ming *et al.*, 1983). Several ruby grains, 2-5 mm size, were placed on top of the perovskite sample as an ambient-temperature high-pressure calibrant (Mao *et al.*, 1986). The sample chamber was then filled with neon gas at 200 MPa and ambient temperature in a high-pressure gas-loading device (Jephcoat *et al.*, 1987). In the present experiment, a sleeve-shaped platinum-wire heater with a shell of ceramic insulator was fit around the extruded portion of piston-cylinder (Fig. 54). Temperatures were measured with two chromel - alumel thermocouples, mounted on the diamond anvils. The temperature difference between the two thermocouples was normally less than the uncertainty of the thermocouple (~2 K) at 900K.

One of the major difficulties in studying the $(Fe,Mg)SiO_3$-perovskite by polycrystalline x-ray diffraction techniques arises from the fact that the diffraction pattern consists primarily of many groups of multiplets (Yagi *et al.*, 1977). The separation of the peaks within each multiplet is typically only ~ 1%. In order to obtain accurate measurement of the lattice parameters, it is necessary to resolve these multiplets by high-resolution techniques. Monochromatic synchrotron x-ray radiation currently provides the highest possible resolution for polycrystalline diffraction. In the present study, we used a wiggler beamline at Cornell High Energy Synchrotron Source (CHESS); a sagittal single-crystal monochromator was used to provide focused 16.1 keV x-ray radiation. The diffraction patterns were recorded using film techniques. In order to increase the angular resolution, we replaced the commonly used 50-mm radius film cassette for diamond cell with a newly designed 100-mm radius cassette. Example of diffraction patterns are shown in Fig. 55.

The orthorhombic distortion of the $(Fe,Mg)SiO_3$-perovskites is clearly revealed by the splitting of single diffraction lines of the cubic structure into doublets or triplets in the orthorhombic structure. The most intense triplet consists of the 020, 112, and 200 diffraction lines (Fig. 55), which are equivalent to the 110 diffraction peaks of the cubic perovskite. By monitoring the splitting of these triplets at high pressure and temperatures, the change of orthor-

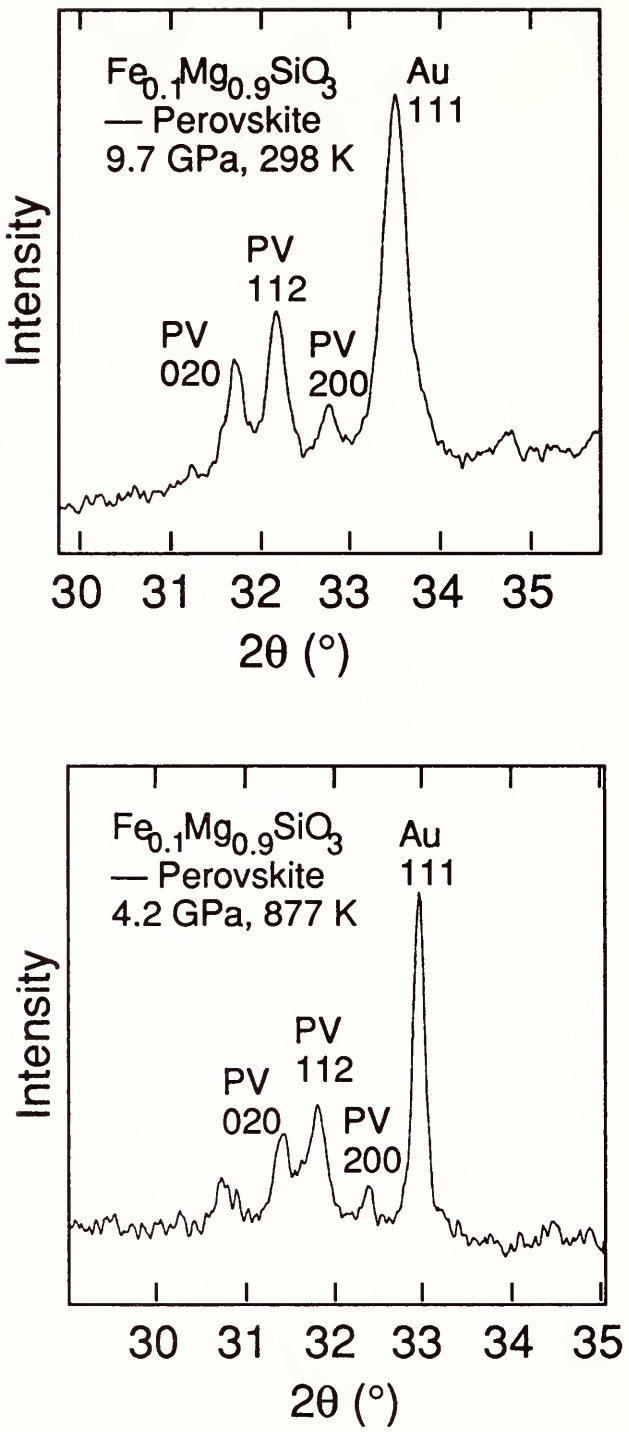

FIG. 55. (a,b) Diffraction patterns of (Fe,Mg)SiO_3-perovskite at 9.7 GPa and 298 K and at 4.2 GPa and 877 K.

hombic distortion can be obtained directly. The lattice parameters and unit cell volumes of the (Fe,Mg)SiO_3-perovskites determined at high pressures and 298 K in this manner are listed in Table 8.

Pressures measured on the gold and ruby scales were in good agreement, and were averaged (standard deviation, 0.2 GPa) to yield the reported pressures in Table 8. Pressures were also determined by the volume compression and *P-V* equation of state of neon (Hemley *et al.*, 1989).

The compressibilities of the three $Fe_xMg_{1-x}SiO_3$ perovskites with x = 0, 0.1, and 0.2 determined from the present study are indistinguishable (Table 8). The three sets of data were combined for a least-squares fit of a second-order Murnaghan equation of state (Murnaghan, 1944);

$$V/V_o = [1 + (K_o'P/K_o)]^{-1/K_o'} \quad (1)$$

$$K = -(\partial P/\partial \ln V)_T = K_o + K_o'P, \quad (2)$$

where V, K, and K' are molar volume, bulk modulus, and pressure derivative of the bulk modulus; the subscript zero denotes the parameters at zero pressure. Two-parameter, least-squares fitting yielded K_o = 275(±8) GPa and K_o' = 3.7 (±0.8). How-

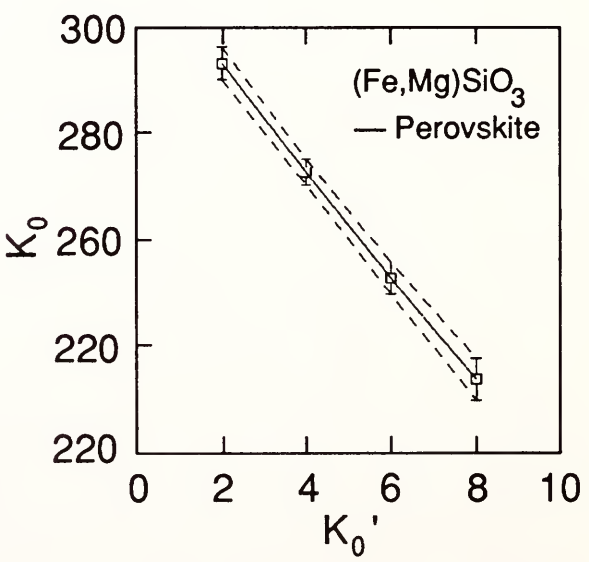

FIG. 56. Dependence of K_o on fixed K'_o for the 298 K isotherm of (Fe,Mg)SiO_3 perovskites.

TABLE 8. Lattice Parameters and Unit-Cell Volume of $Fe_xMg_{1-x}SiO_3$-Perovskite up to 30 GPa (298 K).

P, GPa	*a*, Å	*b*, Å	*c*, Å	*V*, Å³	a/a_o	b/b_o	c/c_o	V/V_o
x=0.0								
3.86	4.753	4.911	6.875	160.46	0.9947	0.9962	0.9966	0.9876
6.29	4.736	4.895	6.852	158.84	0.9911	0.9931	0.9932	0.9776
13.3	4.707	4.869	6.793	155.69	0.9851	0.9877	0.9847	0.9582
x=0.1								
2.50	4.768	4.916	6.881	161.30	0.9972	0.9971	0.9965	0.9908
9.69	4.726	4.883	6.819	157.37	0.9885	0.9903	0.9875	0.9667
13.5	4.707	4.867	6.796	155.70	0.9844	0.9871	0.9842	0.9564
18.6	4.683	4.848	6.761	153.51	0.9795	0.9832	0.9792	0.9430
27.2	4.648	4.815	6.690	149.73	0.9721	0.9765	0.9689	0.9197
x= 0.2								
5.13	4.770	4.905	6.857	160.41	0.9944	0.9940	0.9925	0.9810
13.3	4.713	4.868	6.795	155.87	0.9826	0.9864	0.9835	0.9532
20.3	4.689	4.846	6.750	153.37	0.9776	0.9820	0.9769	0.9379
29.6	4.642	4.807	6.688	149.24	0.9679	0.9740	0.9680	0.9126

ever, since the total range of volume compression in the present study was only 9%, the data were better used to constrain only one parameter by fixing K_o'. The dependence of K_o on the fixed K_o' is shown in Fig. 56. The preferred value is $K_o = 272.5(\pm 2.4)$ GPa when $K_o' = 4$ is assumed. The curve and data are plotted in Fig. 57. When a second-order Birch equation of state (Birch, 1952) is used instead of the Murnaghan equation to fit the data, we obtained $K_o = 273.4(\pm 2.4)$ GPa with fixed $K_o' = 4$. Within the present range of compression, the Murnaghan and Birch equations are indistinguishable.

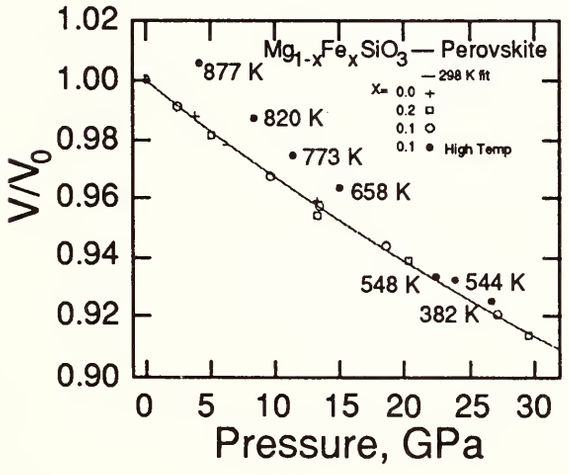

FIG. 57. *P-V-T* relations for $Fe_xMg_{1-x}SiO_3$ perovskites. Open squares (x=0.2), open circles (x=0.1) and crosses (x=0) are measurements at 298 K. Solid circles (x=0.1) are high-pressure data at high temperatures as marked next to the data points. The solid curve is the 298 K isotherm.

A similar least-squares fit for the isothermal compression data of the three lattice parameters yields:

$$b_{ao} = 1.291(0.02)GPa^{-1}, K'a_o = 11.4;$$

$$b_{bo} = 1.053(0.011)GPa^{-1}, K'b_o = 13.9;$$

TABLE 9. Lattice Parameters and Unit-Cell Volume of $Fe_{0.1}Mg_{0.9}SiO_3$-Perovskite at High Pressures and Temperatures.

P, GPa	T, K	a, Å	b, Å	c, Å	V, Å^3	a/a_o	b/b_o	c/c_o	V/V_o
7.2	298	4.648	4.815	6.690	149.73	0.9721	0.9765	0.9689	0.9197
26.8	382	4.661	4.802	6.696	150.46	0.9749	0.9777	0.9698	0.9243
23.9	544	4.665	4.830	6.730	151.63	0.9757	0.9795	0.9746	0.9315
22.5	548	4.668	4.829	6.735	151.81	0.9762	0.9793	0.9755	0.9325
15.1	658	4.737	4.872	6.790	156.72	0.9908	0.9881	0.9834	0.9627
11.4	773	4.745	4.894	6.829	158.56	0.9923	0.9925	0.9890	0.9740
8.38	820	4.770	4.908	6.863	160.66	0.9975	0.9954	0.9939	0.9869
4.19	877	4.794	4.937	6.916	163.72	1.0027	1.0014	1.0016	1.0057

TABLE 10. Zero-Pressure Bulk Modulus and Linear Compressibilities of $Fe_xMg_{1-x}SiO_3$ Perovskite at 298 K.

$K_o^{(Ref)}$ GPa	K'_o	b_{ao}	b_{bo} TPa^{-1}	b_{co} TPa^{-1}	P_{max} TPa^{-1}	P_{media} GPa	Sample	x
246[1]	—	1.31	1.20	1.56	0	—	single xl.	0
247[2]	4	1.41	1.07	1.57	10	M-E-W	single xl.	0
254[3]	4	1.30	1.04	1.24	13	M-E, Ne	single xl.	0
258[4]	4	1.58	1.19	1.10	7	M-E	powder	0
266[5]	3.9	—	—	—	112	none	powder	0.12
272[6]	4	1.29	1.05	1.33	30	Ne	powder	0, 0.1, 0.2

(l) Adiabatic bulk modulus and compressibilities measured with Brillouin scattering technique,
(2)-(6) Isothermal moduli and compressibilities determined by fitting *P-V-a-b-c* data measured with x-ray diffraction techniques.

M-E: methanol ethanol mixture; -H: -water.

Reference

(1) Yeganeh-Haeri *et al.* (1989)
(2) Kudoh *et al.* (1987)
(3) Ross and Hazen (1989)
(4) Yagi *et al.*(1982)
(5) Knittle and Jeanloz (1987)
(6) Present study

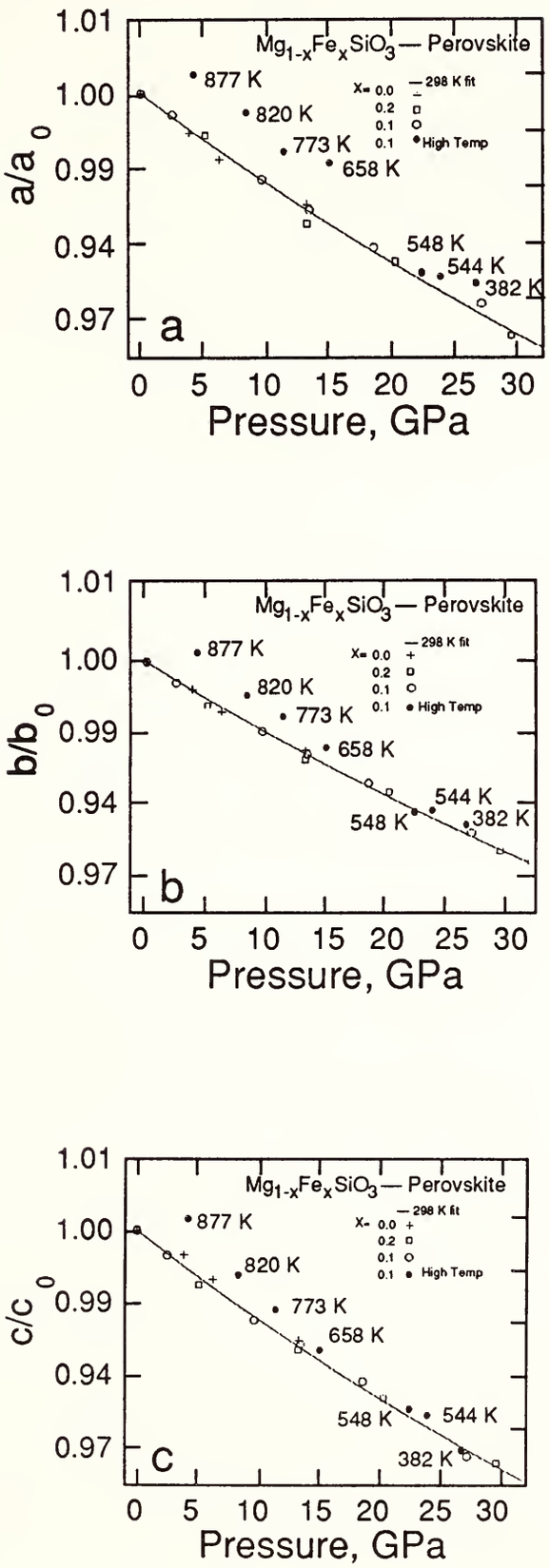

FIG. 58. Compression of lattice parameters. (a) a. (b) b. (c) c. See Fig. 57 for notation.

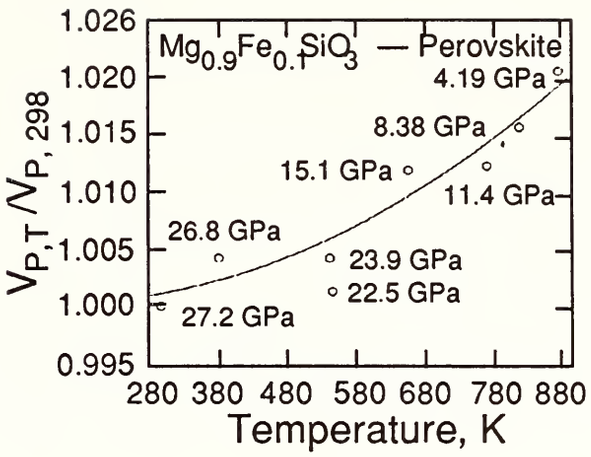

FIG. 59. Thermal expansion, $V_{p,T}/V_{p,298}$, as a function of temperature at various pressures. The value of P is marked at each data point.

$$b_{co} = 1.330(0.018)GPa^{-1}\ K' c_o = 11.0;$$

$$b_x = -(\partial lnx/\partial lP)_T$$

The three compression curves and data points are plotted in Fig. 58A-C.

A study for simultaneous high P-T diffraction measurements was also conducted for $Fe_{0.1}Mg_{0.9}SiO_3$ perovskite. At temperatures above 500K, however, the gold standard tended to anneal to larger crystals. The effect can be seen in Fig. 55, in which the 298 K diffraction peak of gold is broad due to the small grain size, and the 877K peak of gold is sharpened. The results of lattice parameters and volume as a function of pressure and temperature were listed in Table 9 and plotted in Fig. 58. The thermal expansion as a function of temperature at various pressures is plotted in Fig. 59.

The orthorhombic $(Fe,Mg)SiO_3$ perovskite has the axial ratio $a:b:c$ = 0.97:1:1.41, which differs from the equivalent ratio of the ideal cubic perovskite,

1:1:1.41, mainly in that the *a* axis is 3 % smaller. The present results clearly show that the orthorhombic $(Fe,Mg)SiO_3$ perovskite is elastically anisotropic with the *b* axis being the least compressible, ~25 % less compressible than *a* or *c*. The compressibilities of *a* and *c* are similar, with c slightly more compressible. With such differential compressibilities, the difference between *a* and *b* becomes even larger and the structure becomes more distorted at higher pressures. Results from other studies of linear compressibilities of lattice parameters of $(Fe,Mg)SiO_3$ perovskite are listed in Table 10 for comparison.

Nonhydrostatic pressure has major effect on the relative compressibilities of the lattice parameters. Pressure conditions in the diffraction measurements of Yagi *et al.* (1982) became clearly nonhydrostatic between 7.5 and 9 GPa, and thus only data below 7.5 GPa were used for the calculations of the compressibility. The pressure conditions in the measurements of Knittle and Jeanloz (1987) were nonhydrostatic. The relative axial compressibility would be different from the hydrostatic one. In addition, without the resolution to separate the orthorhombic splitting of the equivalent cubic diffraction peaks, relative compressibilities of lattice parameters could not be accurately determined.

In summary, the differences in K_o among various studies are larger than the claimed uncertainty in each study, but are much smaller than those typically observed in other materials when compared with measurements from different laboratories. It is also important to emphasize that although the extrapolated zero-pressure parameters are useful for comparisons with low-pressure data, they do not carry any specific significance in high-pressure experiments. Since the purpose of studying the $(Fe,Mg)SiO_3$ perovskite for solid-earth geophysics is to assess its role in the lower mantle, the more important parameters are the density and bulk modulus of perovskite with the appropriate composition above 20 GPa. These parameters were measured directly in the present study.

References

Birch, F., Elasticity and constitution of the Earth's interior, *J. Geophys. Res., 57*, 227-286, 1952.

Hemley, R. J., M. D. Jackson, and R. G. Gordon, Theoretical study of the structure, lattice dynamics, and equations of state of perovskite-type $MgSiO_3$ and $CaSiO_3$, *Phys. Chem. Minerals, 14*, 2-12, 1987.

Hemley, R. J., C. S. Zha, A. P. Jephcoat, H. K. Mao, L. W. Finger, and D. E. Cox, X-ray diffraction and equation of state of solid neon to 110 GPa, *Phys. Rev. B, 39*, 11820-11827, 1989.

Ito, E., and D. J. Weidner, Crystal growth of $MgSiO_3$ perovskite, *Geophys. Res. Lett., 11*, 464-466, 1986.

Jamieson, J. C., J. N. Fritz, and M. H. Manghnani, Pressure measurement at high temperature in x-ray diffraction studies: Gold as a primary standard, in *High-Pressure Research in Geophysics*, S. Akimoto, and M. H. Manghnani, eds., Reidel Publ., Boston, pp. 27-48, 1982.

Jephcoat, A. P., H. K. Mao, and P. M. Bell, Operation of the megabar diamond-anvil cell, in *Hydrothermal Experimental Techniques*, G. C. Ulmer and H. L. Barnes, eds., Wiley-Interscience, New York, Chapter 11, pp. 469-506, 1987.

Knittle, E., and R. Jeanloz, Synthesis and equation of state of $(Mg,Fe)SiO_3$ perovskite to over 100 gigapascals, *Science, 235*, 668-670, 1987.

Knittle, E., R. Jeanloz, and G. L. Smith, The thermal expansion of silicate perovskite and stratification of the Earth's mantle, *Nature*, 319, 214-216, 1986.

Kudoh, Y., E. Ito, and H. Takeda, Effect of pressure on the crystal structure of perovskite-type $MgSiO_3$. *Phys. Chem. Minerals, 14,* 1987.

Mao, H. K., T. Yagi, and P. M. Bell, Mineralogy of the Earth's deep mantle: quenching experiments on mineral compositions at high pressures and temperature, *Carnegie Instn. Washington Year Book, 76,* 502-504, 1977.

Mao, H. K., J. Xu, and P. M. Bell, Calibration of the ruby pressure gauge to 800 kbar under quasihydrostatic conditions, *J. Geophys. Res., 91,* 4673-4676, 1986.

Ming, L. C., M. H. Manghnani, S. B. Qadri, E. F. Skelton, J. C. Jamieson, and J. Balogh, Gold as a reliable internal pressure calibrant at high temperatures, *J. Appl. Phys., 54*, 4390-4397, 1983.

Murnaghan, F. D., The compressibility of media under extreme pressures, *Proc. Nat. Acad. Sci. USA, 30*, 244-247, 1944.

Ross, N. L., and R. M. Hazen, High-pressure crystal chemistry of $MgSiO_3$ perovskite, *Phys. Chem. Minerals, 16*, 415-420, 1989.

Wolf, G., and M. Bukowinski, Theoretical study of the structural properties and equations of state of $MgSiO_3$ and $CaSiO_3$ perovskites: implications for lower mantle composition, in *High-Pressure Research in Mineral Physics,* M. H. Manghnani and Y. Syono, eds., Terra Scientific Publishing Company (TERRAPUB), Tokyo/ American Geophysical Union, Washington, D. C., pp. 313-331, 1987.

Yagi, T., H. K. Mao, and P. M. Bell, Crystal structure of $MgSiO_3$ perovskite, *Carnegie Instn. Washington Year Book, 76*, 516-519, 1977.

Yagi, T., H. K. Mao, and P. M. Bell, Hydrostatic compression of perovskite-type $MgSiO_3$, in *Advances in Physical Geochemistry, Vol. 2*, S. K.. Saxena, ed., Springer-Verlag, New York, pp. 317-325, 1982.

Yeganeh-Haeri, A., D. J. Weidner, and E. Ito, Elasticity of $MgSiO_3$ in the perovskite structure, *Science, 243,* 787- 789, 1989.

Single Crystal X-ray Diffraction Study of A New Hydrous Silicate, Phase E

*Yasuhiro Kudoh, Larry W. Finger, Robert M. Hazen, Charles T. Prewitt, and Masami Kanzaki**

Ringwood and Major (1967) investigated the system MgO - SiO_2 - H_2O at pressures between 10 and 18 GPa and at temperatures from 600 to 1100°C. They discovered three new phases denoted A, B and C and suggested phase B as a probable host mineral for H_2O in the deep mantle. Subsequently, Yamamoto and Akimoto (1974) reported the discovery of phase D with chemical composition close to that of chondrodite $Mg(F,OH)_2{\cdot}2Mg_2SiO_4$. Among these, phase B is known to have a temperature-pressure stability field higher than the others (Akimoto and Akaogi, 1980) but its Mg/Si ratio is 3.0 (Finger *et al.*, 1989). More recently Kanzaki (1989) investigated phase relations in the system MgO - SiO_2 - H_2O up to 15 GPa and 1500°C using a uniaxial split-sphere multi-anvil apparatus and discovered a new phase that was synthesized at 1000°C pressures higher than 13 GPa, which he denoted phase E. This hydrous silicate phase has an Mg/Si ratio less than 2, close to that of the mantle.

In this paper we report the crystal structural and crystal chemical aspects of phase E, which is a potential host for H_2O in the mantle transition zone.

* University of Alberta, Edmonton, Alberta, Canada

Experimental Results

Phase E (Kanzaki, 1989) was synthesized at 15 GPa and 1000°C using a uniaxial split-sphere multi-anvil apparatus. The starting material was a stoichiometric mixture of high-purity SiO_2 and $2Mg(OH)_2$. A single crystal with approximate dimensions 160x110x40 μm was used for x-ray diffraction. x-ray photographs indicated systematic absences of reflections with $-h+k+l = 3n$ for hkl, which is consistent with a rhombohedral space group, indicating that the space group of phase E is either $R3m$, $R3$ or $R\bar{3}m$. Intensity statistics did not indicate a definite conclusion as to whether the crystal has center of symmetry or not. The cell constants determined by means of a four-circle diffractometer, using 14 reflections of with 2θ from 26-36°, with a wavelength of 0.7093 Å were $a = 2.959(1)$ Å, c=13.844(2) Å, $V = 104.98(6)$ Å^3. They are close to those refined from powder diffraction data [a=2.9701(1) Å, c=13.842(1) Å, $V = 106.05(4)$ Å^3]. Electron microprobe analysis of the specimen at 12 sampling points showed homogeneous chemical composition with MgO 48.4 wt.%, SiO_2 40.1 wt.% (no other element was detected), yielding a total of 88.6. When closest-packing of oxygen atoms is assumed, the short axis allows only one oxygen atom per layer in the a_1-a_2 plane and the length of the c axis allows six oxygen layers; therefore, there are six oxygen atoms per unit cell. If the difference of the total weight is ascribed to H_2O, the formula is calculated to be $Mg_{2.27}Si_{1.26}H_{2.40}O_6$. Crystal structure analysis is now in progress.

Since phase E was observed co-existing with stishovite in run products of a silica-rich starting material (Kanzaki, 1989), phase E is considered to have a stability field corresponding to the mantle transition zone. Phase E has geophysical importance because it is a hydrous phase with a chemical composition close to that of the mantle. Its density, 2.89 g/cm^3, is rather low, however.

The composition of phase E can be derived from a brucite starting point with a cell content of $Mg_3(OH)_6$. If a magnesium atom is removed, silicon atoms in tetrahedral coordination can be placed over this vacancy. The two possible reactions are:

$$Mg(OH)_2 + Si^{4+} \Leftrightarrow SiO_2 + Mg^{2+} + 2H^+, \quad (1)$$

which corresponds to a single Si per Mg removed, or

$$2Mg(OH)_2 + 2Si^{4+} \Leftrightarrow MgSi_2O_4^{2+} + Mg^{2+} + 4H^+, \quad (2)$$

which results when two Si are involved. The measured composition corresponds to 1.73 Si atoms added for each Mg removed from the hypothesized starting position, which indicates that both mechanisms apply; however, the second one is more important. From the diffraction data, it is obvious that these substitutions result in short-range order. Although clusters of defects are expected, the size of the cluster does not result in diffuse scattering with appreciable intensity. Long-term x-ray photographs indicate the existence of diffuse maxima with the a axis seven times longer and the c axis doubled, as compared to the subcell.

References

Akimoto, S., and M. Akaogi, The system Mg_2SiO_4 - MgO - H_2O at high pressures and temperatures-possible hydrous magnesian silicates in the mantle transition zone, *Phys. Earth Planet. Inter., 23,* 268-275, 1980.

Finger, L. W., J. Ko, R. M. Hazen, T. Gasparik, R. J. Hemley, C. T. Prewitt, and D. J. Weidner, Water in the upper mantle: crystal chemistry of phase B and a new anhydrous magnesium silicate, *Nature,* in review.

Kanzaki, M., High pressure phase relations in the system MgO - SiO_2 - H_2O, *EOS, 70,* 508, 1989.

Ringwood, A. E., and A. Major, High-pressure reconnaissance investigations in the system Mg_2SiO_4 - MgO - H_2O, *Earth Planet. Sci. Lett., 2,* 130-133, 1967.

Yamamoto, K., and S. Akimoto, The system MgO - SiO_2 - H_2O at high pressures and temperatures-stability field for hydroxyl-chondrodite, hydroxyl-clinohumite and 10 Å -phase, *Am. J. Sci., 277,* 288-312, 1977.

Spectroscopic Evidence for a new New High-pressure Magnesium Silicate Phase

James D. Kubicki and Russell J. Hemley

Experimental constraints on the mineralogy of the lower mantle have mainly been obtained from high-pressure phases that are quenchable to ambient pressure and temperature (Yagi *et al.*, 1979). A series of experiments have been started using the laser-heated, diamond-anvil cell and micro-Raman spectroscopy to investigate the possible existence of non-quenchable phases under lower mantle conditions. Micro-Raman spectroscopy was employed to probe the sample after melting and quenching at high pressure. With micro-Raman spectroscopy, it is possible to study any heterogeneities in the sample that may be induced by laser-heating. The *in situ* nature and spatial resolution of the technique are ideally suited for identification of small amounts of non-quenchable high-pressure phases.

Approximately 1 weight percent platinum black was mixed and ground with $MgSiO_3$ glass to absorb Nd-YAG laser-radiation (1.06 mm line). The sample was compressed to 35 GPa at room temperature and the Raman spectra measured (Fig. 60). The platinum fluoresces under the argon laser (514.5 nm line) thereby reducing the signal-to-noise ratio, and obscuring the broad band between 800 and 1100 cm^{-1} observed in previous spectra (Kubicki *et al.*, 1987). The sample was then heated with a Nd-YAG laser. Regions exposed to the highest temperatures (estimated to be above 2000K) formed rounded spots more transparent than the surrounding unheated

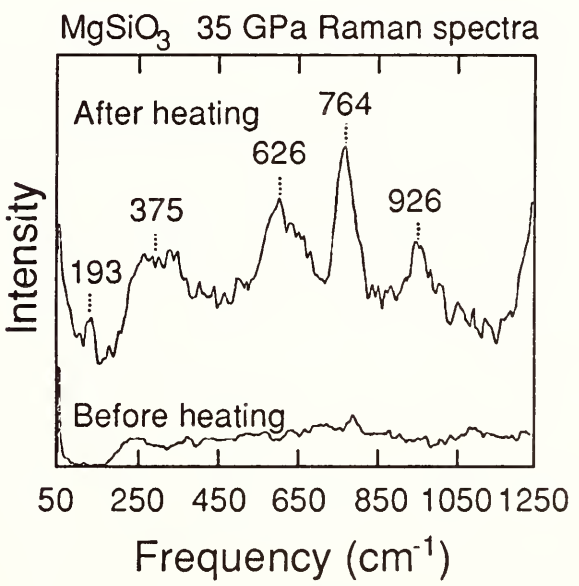

Fig. 60. Raman spectrum of $MgSiO_3$ glass mixed with Pt black at 35 GPa before laser-heating and after heating with Nd/YAG laser and *in situ* quenching. A linear, sloping baseline due to platinum fluorescence has been subtracted from both spectra.

regions. Platinum was also concentrated around the inner boundary between the heated and unheated region. From these observations we conclude that melting has occurred at the most intensely heated regions. Heating to lower temperatures was also performed to drive subsolidus transformations such as the crystallization of $MgSiO_3$-perovskite. In this case, the heated region was visibly darker than either the starting material or melted regions and the Raman spectra are identifiable as $MgSiO_3$-perovskite (Hemley *et al.*, 1989).

The Raman spectrum of the melted and quenched sample (Fig. 60) is significantly different from the unheated sample. Five major peaks (193, 375, 626, 764, and 926 $cm^{-1)}$ appear in the spectrum. These were not present before laser-heating. These peaks also became sharper and more intense with time under the argon-laser radiation used to measure the Raman spectrum. Spectra were also measured upon decompression. Broad bands centered at 631 and 997 cm^{-1} from $MgSiO_3$ glass (Kubicki *et al.*, 1987) and peaks of $MgSiO_3$-perovskite were observed. No unassigned peaks exist in the spectrum of the heated region after decompression that could be attributed to the high-pressure, laser-heated spectrum.

There are several possible explanations for the spectrum induced by laser-heating. The unidentified spectrum may be of a glass quenched from the high-pressure melt. In this case, the spectrum of the glass melted at high-pressure would be very different from the glass compressed at room temperature (Kubicki *et al.*, 1987). The sharpness of the Raman peaks, however, indicate some degree of crystalline order. Crystallites may have formed under the very rapid heating and quenching conditions of the experiment. Very fine-grained crystals (i.e., less than 1 mm) and poorly crystalline materials exhibit peak-broadening effects associated with the breakdown of crystalline selection rules (Hemley *et al.*, 1986). The fact that the new peaks become more intense and sharper with time under the argon laser suggests that annealing or recrystallization has taken place resulting from a small degree of heating of the sample by the argon laser. Under these high-temperature and rapid quench conditions, the possibility of crystallizing a metastable phase also exists. Another possibility is that the high-temperature and pressure conditions of the experiment caused a reaction between the $MgSiO_3$ glass and the Pt black. Formation of a platinum-magnesium silicate under the experimental conditions can not be ruled out.

Raman frequencies of silicates at high-pressure are compared with this new spectrum in Table 11. Although certain peaks may be correlated with known phases, no combination of Raman peaks for phases previously measured will explain the entire spectrum. For example, the peaks at 193 and 626 cm^{-1} may be correlated with the high-pressure Raman spectra of stishovite and $MgSiO_3$-perovskite, respectively (Table 11); but the other peaks of stishovite and $MgSiO_3$-perovskite at 35 GPa are not present in this spectrum. The intensity pattern of the spectrum is also broadly similar to that of stishovite. The structure of the phase may have features in common with other high-pressure silicates, such as octahedral Si, which gives rise to these similar Raman

TABLE 11. Comparison of Raman frequencies for stishovite, $MgSiO_3$-perovskite, orthoenstatite, and the spectrum of this study all at 35 GPa (s, strong; m, moderate;w, weak; vw, very weak; b, broad).

$MgSiO_3$ Orthoenstatite[a]	Stishovite[b]	$MgSiO_3$-Perovskite[c]	This Study
—	195 m	—	193 w
265 w	—	342 w	—
360 w	—	353 w	375 b
—	—	454 w	—
525 m	—	464 s	—
—	647 m	646 s	626 b
—	—	648 vw	—
770 s	855 s	—	764 s
1140 m	969 w	1040 vw	926 m

[a]Kubicki (unpublished data)

[b]Hemley (1987)

[c]Hemley *et al.* (1989)

features. The overall crystal structure, however, must be different to account for all the peaks observed. It is not known if the $MgSiO_3$-phases melt congruently at high pressures so the new phase may be enriched in either Mg or Si relative to $MgSiO_3$. In addition, high temperature gradients present during laser-heating could have altered the composition of the sample locally due to the Soret effect (Heinz and Jeanloz, 1987). The heterogeneity of the sample in this laser-heated region also allows the possibility of a combination of phases giving rise to this Raman spectrum.

The spectrum most probably arises from a previously unidentified phase that appears to be non-quenchable from high pressures. Also, it has been demonstrated that micro-Raman spectroscopy, used in combination with the laser-heated, diamond-anvil cell, is a useful technique for probing the possible existence of non-quenchable, high-pressure phases. Future work to analyze the structure of newly identified phases should be carried out with *in situ,* high-pressure X-ray diffraction and TEM techniques.

References

Hemley, R. J., H. K. Mao, and E. C. T. Chao, Raman spectrum of natural and synthetic stishovite, *Phys. Chem. Min., 13*, 285-290, 1986.

Hemley, R. J., Pressure dependence of Raman spectra of SiO_2 polymorphs: Quartz, coesite, and stishovite, in *High-Pressure Research in Mineral Physics,* M. H. Manghnani and Y. Syono, eds., Terra Scientific Publishing Co. (TERRAPUB), Tokyo/American Geophysical Union, Washington, D. C., 1987.

Hemley, R. J., R. E. Cohen, A. Yeganeh-Haeri, H.

K. Mao, D. J. Weidner, and E. Ito, Raman spectroscopy and lattice dynamics of $MgSiO_3$-perovskite at high pressure, in *Perovskite: A Structure of Great Interest to Geophysics and Materials Science,* A. Navrotsky and D. A. Weidner, eds., Am. Geophys. Union, Washington, D. C, pp. 35-53, 1989.

Heinz, D. L. and R. Jeanloz, Measurement of the melting curve of $Mg_{0.9}Fe_{0.1}SiO_3$ at lower mantle conditions and its geophysical implications, *J. Geophys. Res., 92,* 11437-11444, 1987.

Kubicki, J. D., R. J. Hemley, and H. K. Mao, *In situ,* high-pressure Raman spectroscopy of $MgSiO_3$, $CaSiO_3$, and $CaMgSi_2O_6$ glasses, (abstract) *EOS, Trans. Am. Geophys. Union, 68,* 1456, 1987.

Yagi, T., P. M. Bell, and H. K. Mao, Phase relations in the system MgO - FeO - SiO_2 between 150 and 700 kbar at 1000°C, *Carnegie Instn. Washington Year Book, 78,* 614-618, 1979.

Compression and Polymorphism of $CaSiO_3$ at High Pressures and Temperatures

Liang-chen Chen, Ho-kwang Mao, and Russell J. Hemley

Introduction

Numerous experimental studies have determined high pressure properties of magnesium and iron-magnesium silicates, but much less information is available on those of $CaSiO_3$ at under upper and lower mantle conditions. Ringwood and Major (1967) found a high pressure modification of $CaSiO_3$(I) (wollastonite) at about 3 GPa. The structure was analyzed by Trojer (1969) and found to be related to walstromite. Later, Liu and Ringwood (1975) measured *in situ* x-ray diffraction from laser heated $CaSiO_3$ at about 16 GPa and obtained a diffraction pattern consistent with the cubic perovskite. Further, they showed that the phase reverted to a glass on release from high pressure; this observation was confirmed in later diamond-anvil studies (Mao *et al.*, 1977). Further information on the properties of $CaSiO_3$ at high pressure has been obtained from theoretical calculations in which only the perovskite-type phase has been examined (Hemley *et al.*, 1987). The present study was undertaken to investigate phase transitions and pressure-volume equation of state of $CaSiO_3$ up to conditions equivalent to those at the core-mantle boundary. We have also studied the phase transitions at low pressure (<15 GPa) and examined the range of stability of the low-pressure polymorphs. A new phase named $CaSiO_3$(III) has been identified. In addition, we have investigated the onset of vitrification of $CaSiO_3$-perovskite decompression below its stability field.

Experimental Methods and Results

In the first set of experiments, natural $CaSiO_3$(I) (Wollastonite) ground and mixed with 1% platinum black was used as a starting material. The samples were loaded in the diamond-anvil cell, and were heated with the Nd-YAG laser ($\lambda = 1.06\mu m$) after each pressure increment. Powder x-ray diffraction data were collected using a sealed tube MoK_α source and film techniques with a camera radius of about 50 mm. Pressures were measured with the ruby fluorescence technique.

The diffraction data demonstrate that following increasing pressure and heating,

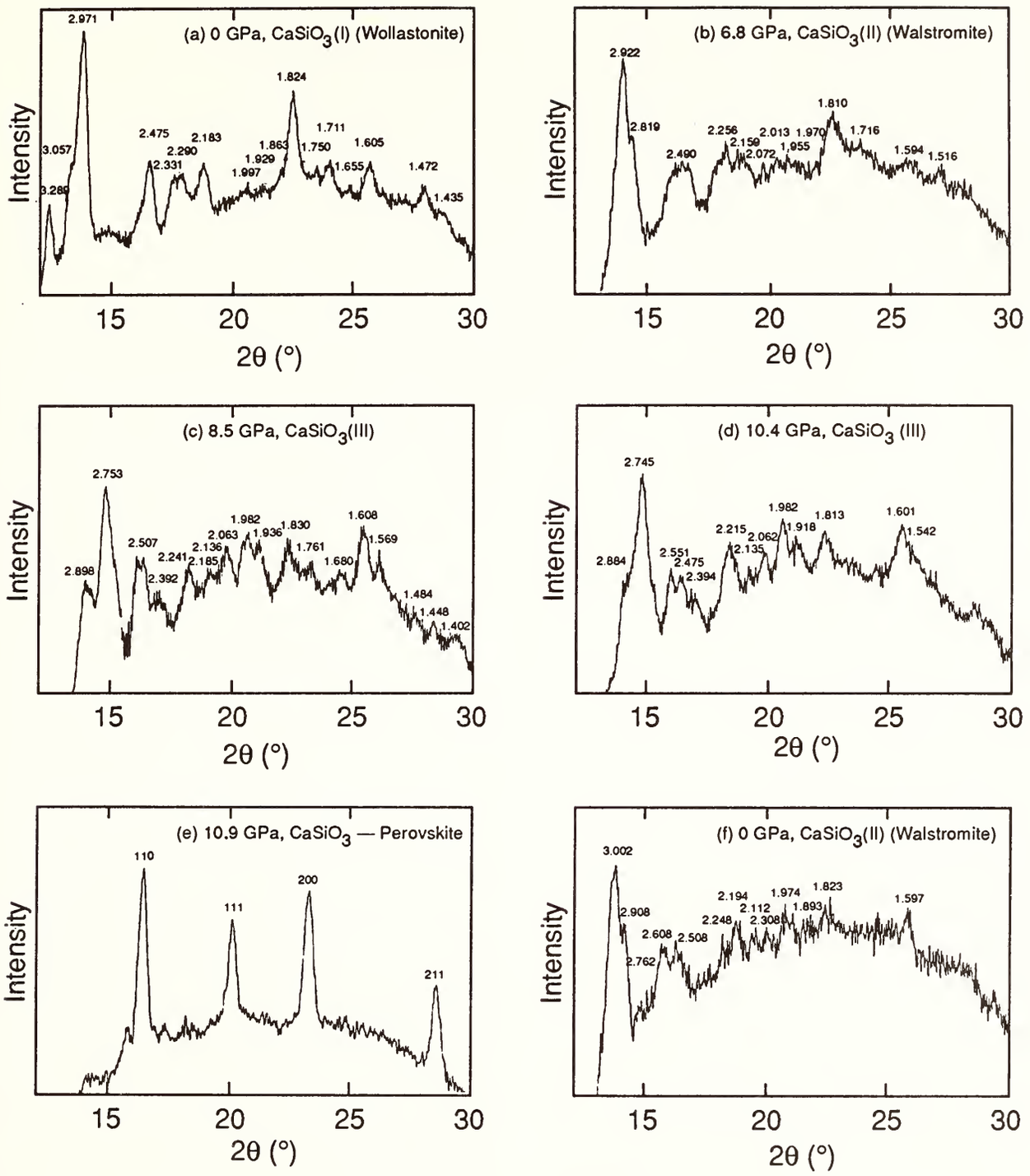

FIG. 61. Examples of x-ray diffraction patterns of $CaSiO_3$ as a function of pressure. The patterns were digitized from film with an automated densitometer.

walstromite-type $CaSiO_3$(II) is stable up to about 7 GPa at 300K. Above 8 GPa $CaSiO_3$(II) was observed to convert to a new non-quenchable phase named $CaSiO_3$(III) which is stable to 11 GPa. This phase converts to walstromite-type $CaSiO_3$(II) when quenched to ambient conditions. A list of the x-ray diffraction lines observed at 8.3 GPa and at ambient conditions is shown in Table 12. The simple cubic perovskite phase of $CaSiO_3$ appeared above 11 GPa. When the pressure was

TABLE 12. The *d*-spacings and relative intensities for $CaSiO_3$(III)

$CaSiO_3$(III) at 8.3 GPa		$CaSiO_3$(II) (Walstromite) at 0.1 MPa	
I	*d* (Å)	*I*	*d* (Å)
2	3.050		
10	2.916	10	3.002
9	2.750	5	2.889
1	2.692	1	2.762
5	2.560	3	2.608
5	2.478		
5	2.393	2	2.448
7	2.240	1	2.256
4	2.122	3	2.194
5	2.062	1	2.112
5	1.980	1	2.038
5	1.919	1	1.974
		1	1.893
7	1.831	4	1.823
7	1.606	4	1.644
2	1.571	4	1.597

released at room temperature, the perovskite structure remained at 0.8 GPa and disappeared at zero pressure. X-ray diffraction patterns of $CaSiO_3$(I), $CaSiO_3$(II), $CaSiO_3$(III) and $CaSiO_3$-perovskite formed at different pressures are compared in Fig. 61. Changes in the measured *d*-spacings for $CaSiO_3$ with increasing pressure are shown in Fig. 62.

In a second set of experiments, the perovskite phase was synthesized at about 17 GPa, the sample was examined by x-ray diffraction up to 40 GPa and on pressure release to ambient conditions. Pressure was again measured from ruby fluorescence. The sample was heated with the Nd-YAG laser after each pressure change in order to accelerate transformations in the material to reduce pressure inhomogeneity. Four diffraction lines of $CaSiO_3$-perovskite (110, 111, 200, and 211) were measured for each film. Because of the incompressibility of the perovskite phase, additional measurements at higher pressure were required to constrain the equation of state of this phase. These measurements also permitted us to examine possible polymorphic transformations in $CaSiO_3$ under lower mantle pressure and temperature.

A third set of experiments was therefore performed; these were similar to the first set except that 3% platinum black was added to the sample. Two x-ray diffraction lines from the platinum (111 and 200) were observed in addition to the four diffraction lines from $CaSiO_3$-perovskite. The plati-

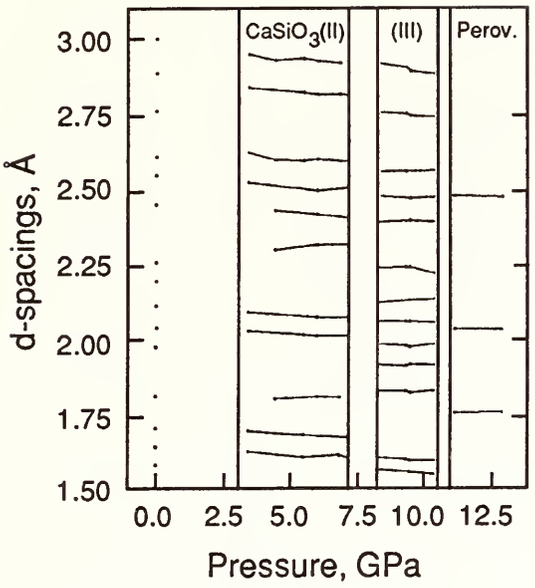

FIG. 62. Observed *d*-spacings of $CaSiO_3$ as a function pressure.

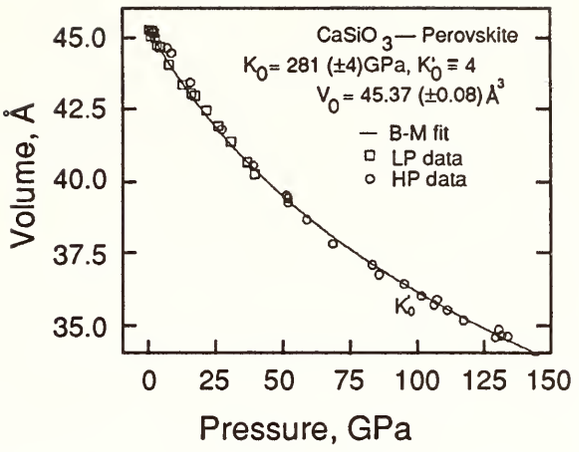

FIG. 63. Pressure-volume data for $CaSiO_3$-perovskite at 300K. Squares (LP): low and moderate pressure data. Circles (H): high-pressure data. Curve: Third-order Birch-Murnghan equation fit.

num diffraction served as an internal pressure standard; the new ultrahigh-pressure equation of state of platinum, recently developed by Lawrence Livermore Laboratory was used to calculate the pressure (Holmes, *et al.*, 1989). Again, the sample was laser-heated after each pressure change in order to drive possible high-pressure transformations. The maximum pressure reached in this set of experiments is 134 GPa, the pressure of the core-mantle boundary. The diffraction data indicate that $CaSiO_3$ is stable in the cubic perovskite over this entire pressure range.

The pressure-volume data from the low- and high-pressure x-ray diffraction measurements for the perovskite phase are plotted in Fig. 63. All data points were fitted with a third-order Birch-Murnaghan equation of state. The zero-pressure parameters are: V_o = 45.31 (±0.08) Å^3, K_o = 281 (±4) GPa, and K_o' = 4.3 (±0.2), density ρ_o = 4.258 (±0.008) g/cm^3.

Discussion

The pressure range of stability of the $CaSiO_3$ polymorphs identified in this study are indicated in Fig. 62. Above 8 GPa, walstromite-type $CaSiO_3$(II) converts to a new non-quenchable phase $CaSiO_3$(III) which is stable to 11 GPa. Tamai and Yagi (1988) have also obtained evidence for $CaSiO_3$(III), although they report its range of stability at 10 to 13.8 GPa. The diffraction patterns measured at high pressure indicate that the structure is complex and cannot be determined from the available powder diffraction data. Experimental determination of the density, structure, and elastic properties of this phase is essential in order to assess the possible role of this phase in the upper mantle. It is useful to note that recent single-crystal diffraction studies suggest that numerous upper mantle minerals may indeed have complex structures (Finger *et al.*, in preparation).

The perovskite-type of $CaSiO_3$ remains in the simple cubic structure up to at least 134 GPa. During pressure release, the perovskite remains metastable at pressures close to 0.1 MPa. It is also of interest to compare the densities of the mixed oxide assemblage of $CaO + SiO_2$ (stishovite) with that of $CaSiO_3$ (Richet *et al.*, 1988; Bass *et al.*, 1981). At ~80 GPa the density of the oxide assemblage exceeds that of $CaSiO_3$-perovskite. This result may indicate that the extrapolated equation of state of stishovite overestimates the densities at high pressure. Alternatively, the comparison may indicate that $CaSiO_3$-perovskite may disproportionate at pressures above 134 GPa (outside the range of the lower mantle).

Our results strongly suggest that cubic $CaSiO_3$-perovskite is a stable phase throughout the entire lower mantle. Under stable conditions, the $CaSiO_3$-perovskite exists in the lower mantle as a major separate phase with abundance only next to ferromagnesian silicate perovskite and probably to magnesiowüstite, depending on the chemical composition model (Anderson, 1989). Further, the cubic $CaSiO_3$-perovskite phase may also be significant as a reservoir for rare earth elements in the lower mantle (Mao *et al.*, this Report). The 300K equation of state of $CaSiO_3$-perovskite is close to that of $(Mg_{0.90}Fe_{0.10})SiO_3$-perovskite (Mao *et al.*, this Report). We also note that the ρ_o of $CaSiO_3$-perovskite, 4.26 g/cm^3, is in excellent agreement with the inferred 300K, zero-pressure density of the lower mantle. Hence, $CaSiO_3$-perovskite must be considered an "invisible" component, in terms of density and bulk modulus constraints, in the lower mantle.

References

Anderson, D. L., Composition of the Earth, *Science, 243*, 367-370, 1989.

Bass, J. D., R. C. Liebermann, D. J. Weidner, and S. J. Finch, Elastic properties from acoustic and volume compression experiments, *Phys. Earth Planet. Inter., 25,* 140-158, 1981.

Hemley, R. J., M. D. Jackson, and R. G. Gordon, Theoretical study of the structure, lattice dynamics, and equations of state of perovskite-type $MgSiO_3$ and $CaSiO_3$, *Phys. Chem. Minerals, 14*, 2-12, 1987.

Holmes, N. C., J. A. Moriarty, G. R. Gathers, and W. J. Nellis, The equation of state of platinum to 660 GPa (6.6 Mbar), *J. Appl. Phys.*, in press, 1989.

Liu, L. and A. E. Ringwood, Synthesis of a perovskite-type polymorph of $CaSiO_3$, *Earth Planet. Sci. Lett., 28,* 209-211, 1975.

Mao, H. K., T. Yagi, and P. M. Bell, Mineralogy of the Earth's deep mantle: quenching experiments on mineral compositions at high pressures and temperature, *Carnegie Instn. Washington Year Book, 76,* 502-504, 1977.

Mao, H. K., P. M. Bell, J. W. Shaner, and D. J. Steinberg, Specific volume measurements of Cu, Mo, Pd, and Ag and calibration of the ruby R_1 fluorescence pressure gauge from 0.06 to 1 Mbar, *J. Appl. Phys., 49,* 3276-3283, 1978.

Richet, P., H. K. Mao, and P. M. Bell, Static compression and equation of state of CaO to 1.35 Mbar, *J. Geophys. Res., 15*, 279-288, 1988.

Ringwood, A. E., and A. Major, Some high-pressure transformations of geophysical significance, *Earth Planet. Sci. Lett., 2,* 106-110, 1967.

Tamai, H., and T. Yagi, High-pressure and high-temperature phase relations in $CaSiO_3$ and CaMgSi2O6 and elasticity of perovskite-type CaSiO3, *Phys. Earth Planet. Inter., 54,* 370-377, 1989.

Trojer, F. J., The crystal structure of a high-pressure polymorph of $CaSiO_3$, *Z. Kristallogr., 130*, 185-206, 1969.

The Polarized Raman Spectra of Tourmaline

*Mingsheng Peng, Ho-kwang Mao, Liang-chen Chen, and Edward C. T. Chao**

Polarized Raman spectroscopy (PRS) has been used extensively for structural and compositional characterization of minerals, (White, 1975, Mao *et al.*, 1987, Hemley, 1988). The Raman spectra of minerals are generally analyzed in terms of factor group analysis (McMillan, 1985). For tourmaline with several structural groupings, a general assumption is that its Raman spectra are made of internal modes of each of the individual structural units in the crystal (Si_6O_{18}, BO_3, OH), plus lattice modes characteristic of the entire unit cell. Each structural unit, $[Si_6O_{18}]^{12-}$, $[BO_3]^{3-}$ and $(OH)^{1-}$, has its distinctive vibrational spectrum.

In this paper we present results of PRS of samples of tourmaline from three different geological occurrences in China, namely granite pegmatites, hydrothermal veins, and metamorphic skarns. Our interest is focussed on the correlation of the PRS to the compositional and structural differences among tourmalines, and the nature of order-disorder of the OH ions in the tourmaline structure in regards to the specific geological occurrences.

*U.S. Geological Survey, Mail Stop 929, Reston, VA 22920

Crystal Structure of Tourmaline and Description of Samples

Tourmaline is a complex borosilicate of aluminum varying considerably in composition with a general formula:

$$WX_3Y_6(BO_3)_3Si_6O_{18}(OH, F, Cl)_4.$$

where W= Na and Ca; X= Mg, Fe^{2+}, Mn, Al, and Fe^{3+}; and

Y= Al, Fe^{3+}, Cr, and V.

As shown by Buerger *et al.* (1962), tourmaline has rhombohedral symmetry, and is in the space group $R3m$ - C_3^v. The crystal structure is characterized by a layer of six nearly regular SiO_4 tetrahedra in hexagonal arrangement similar to that of a phyllosilicate sheet. The octahedral layer consists of three larger central octahedra containing X cations, six smaller peripheral octahedra containing Y cations, and three boron atoms. The three octahedra of X cations (mainly Mg) shares edges and forms a trigonal unit similar to a brucite $[Mg(OH)_2]$-like layer. The trigonal X octahedra unit also share edges with the six Y cations. Each of the boron atoms is in a 3-fold coordination of oxygens at the vertices of octahedra of this layer. The W cation and OH are located along the 3-fold axis of symmetry in the middle of the unit cell. The (OH) hydroxyl groups are confined to three $Mg(OH)_2O_4$ octahedra lying in the same layer as the three pairs of $Al(OH)O_5$ octahedra.

TABLE 13. Microprobe analysis of tourmaline of three different types

Types	Pegmatitic		Hydrothermal	Metamorphic	
Sample No	TO5	TO4	TO9	TO6	TO8
Color	Red	Lt. Green	Green	Blue	Deep Blue
SiO_2	37.60	37.05	35.33	34.37	35.1
TiO_2	0.22	0.50	0.61	0.32	0.21
Al_2O_3	33.30	31.63	33.09	29.83	32.89
FeO	2.19	4.89	4.79	5.43	6.43
MnO	3.30	0.23	0.37	0.18	0.43
MgO	3.65	3.95	8.76	10.05	7.03
CaO	2.37	2.58	0.29	3.36	4.11
K_2O	0.11	0.20	0.30	0.64	0.29
Na_2O	2.86	2.18	1.66	1.48	1.68
Total	85.6	83.21	85.20	85.66	88.17

The pegmatitic tourmaline samples are from Xinjiang Province in northwest China (samples no. TO5 and TO4). The associated minerals are beryl, columbite, and pollucite. The tourmaline crystals are almost of gem quality. Their color changes from rose-red to green and blue along the *c*-axis. Normal to the *c*-axis, color rings of the same color occurs. The tourmaline from the hydrothermal vein (TO9) came from Hunan province of China. It is associated with quartz and beryl. The tourmaline crystals exhibit prismatic habit. The color ranges from light green to dark green. The tourmalines from metamorphic skarn (TO6 and TO8) came from the tin deposit of Yunnan province of China. The tourmalines have the highest iron content among the three types of samples. The associated minerals are cassiterite, calcite, scapolite and diopside. Chemical compositions of tourmaline samples are listed in Table 13.

Characteristics of PRS of Tourmalines and Assignment of Spectral Peaks

Polarized Raman spectra of tourmaline samples are presented in Table 2. Raman peaks are observed in the regions of 0-1200 cm^{-1} and 3400-3600 cm^{-1}. Representative spectra are shown in Figs. 64 and 65.

The major peaks of the PRS in the 0-1200 cm^{-1} region are related to the $[Si_6O_{18}]^{12-}$ hexagonal rings (Table 14). Peak assignments are based on the analysis of Raman spectra of a powdered tourmaline sample by Griffith (1969). In the present study, intense Si-O stretching vibration peaks are observed at 1000-1200 cm^{-1}. Two symmetrical ring stretching peaks lie between 400 and 570 cm^{-1}. Two asymmetrical ring stretching peaks lie at 962-999 cm^{-1} and at 600-700 cm^{-1}. Two ring deformation stretching peaks are located between 220 - 380 cm^{-1}. These two ring deformation stretch-

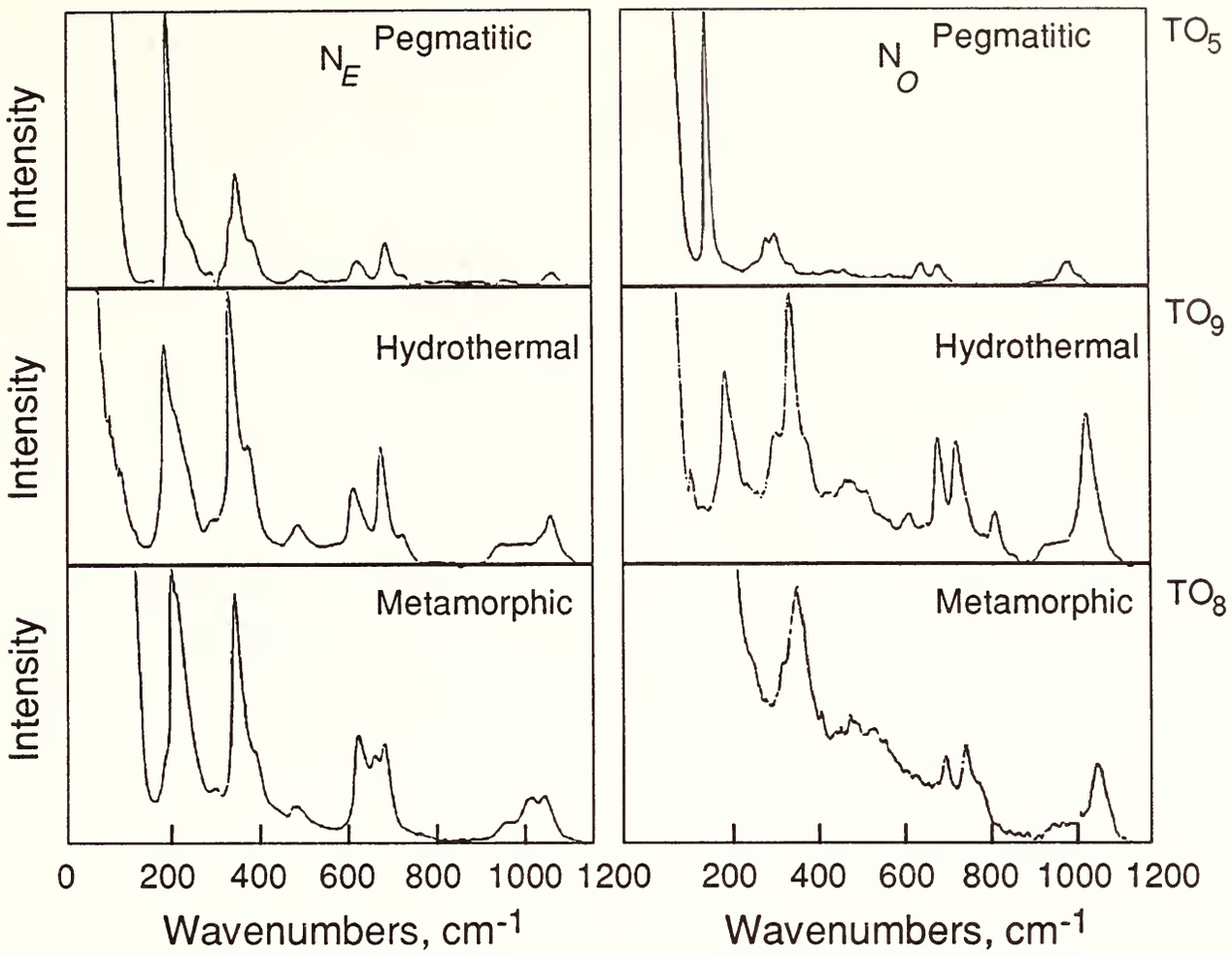

FIG. 64. Polarized Raman spectra of different types of tourmaline in N_e direction and in N_o direction,. The ring deformation stretching peaks of $[Si_6O_{18}]$ are very strong at 220-380 cm^{-1}. The PRS peak corresponding to the stretching of the B-O bond in BO_3 lies between 700-800 cm^{-1}.

ing peaks are very intense. At different polarization directions, the number of Raman peaks are the same, but the positions of the peaks shift, and the intensities of the peaks vary. The PRS in the N_e direction is much more intense than that of the N_o direction. In addition, as the iron content in the tourmaline increases, the spectral peak splits or distorts, so that the PRS from the granite pegmatite (Fig. 64; TO5) are clearly different from the PRS from the skarn metamorphic tourmaline (Fig. 64; TO8) along the N_o direction.

The PRS peak corresponding to the B-O bond in $[BO_3]^{3-}$ lies between 700 and 800 cm^{-1}. Brethous *et al.* (1981) studied Raman spectra of the synthetic system of B_2O_3 - SiO_2 - Li_2O. By holding the Li_2O content constant but varying B_2O_3 and SiO_2 content, they found that the intensity of the 760 cm^{-1} peak increased with increasing B_2O_3 content, and that the intensity of the peaks at 1040, 950, and 600 cm^{-1} increased with increasing SiO_2 content. Our finding regarding the ring vibrational peaks assigned to Si-O and B-O vibrational peaks is generally consistent with that of Brethous *et al.* (1981). However, the B-O vibration peaks

TABLE 14. Frequencies (cm^{-1}) of polarized Raman spectra of tourmaline in the N_e direction

Types	Pegmatitic		Hydrothermal	Metamorphic		Powdered Samples (Griffith, 1969)
Sample No.	TO5	TO4	TO9	TO6	TO8	
$[Si_6O_{18}]^{12-}$						
				1049	1048	
ν^s (Si-O)	1114	1115	1082(s)	1016(s)	1016(s)	1040(6)
Ring Stretches*						
	543	540	510	527	526	569(5)
		563				
	437	436	403	484	487	464(10)
	404(s)	404(s)				
Ring Stretches**						
	999	998	971	965	962	929(1)
	671	685	638	672	669	682
				633	634	
Ring deformation						
	304	342(s)	372(s)	363(s)	363(s)	353(5)
			314	306	306	340($1/_2$)
$[BO_3]^{3-}$						
	253(s)	255(s)	220(s)	228(s)	228(s)	
	744	775	746	764	764	
	734(s)	737(s)	703(s)	693(s)	692(s)	
$[OH]^{1-}$						
ν_2	3635	3636	3648	3629	3630	
ν_1	3573(s)	3551(s)	3589(s)	3562(s)	3555(s)	
		3577				
ν_3	3460	3472	3482	no	no	

* = symmetrical stretching vibration

** = asymmetrical stretching vibration

in tourmaline often split into two peaks. The main splitting is probably due to the variation of bond lengths between boron and adjacent oxygen ($B\text{-}O_2$ bond length is 1.375 , $B\text{-}O_8$ bond length is 1.358Å). The C_3 symmetry of the boron atom is reduced to C_{2v}, and thus the peak splits into two.

Raman peaks in the region between 3400 and 3600 cm^{-1} are assigned to OH stretching. The peak positions and multiplicities in this region are complicated due to the combined influence of octahedral site occupancies, in- and out-of-phase effects, Al/Si ordering, OH_1/OH_2 ordering, alkali cations (K, Na, Li), and the extent of Al substitution in octahedral and/or tetrahedral sites. The PRS in tourmaline structure peaks assigned to (OH) show clear differences parallel to N_o as compared to N_e. The intensities of the main (OH) band (ν_1) in tourmalines are particularly sensitive to the orientation of the sample.

The blue (Fig. 65; TO6) and deep blue (Fig. 65; TO8) tourmalines from metamorphic skarn have two $(OH)^{1-}$ stretching vibrational peaks. The most prominent feature in the spectrum of tourmaline is a sharp, intense peak ν_1 at 3550-3590 cm^{-1} and a weak peak ν_2 at 3630 cm^{-1}. For the blue tourmaline, the two (OH) peaks are located at 3562 (ν_1), and 3629 (ν_2) cm^{-1}). For the deep blue tourmaline, the two (OH) peaks are located at 3555 (ν_1), and 3630 (ν_2) cm^{-1}.

Based on the crystal structure of tourmaline, we know that the (OH) site is at the center of the hexagonal silicon tetrahedra and below the Na ion. The Na-OH bond is 3.285 Å long. The (OH) ion is surrounded by 3 Mg ions which form three octahedra of

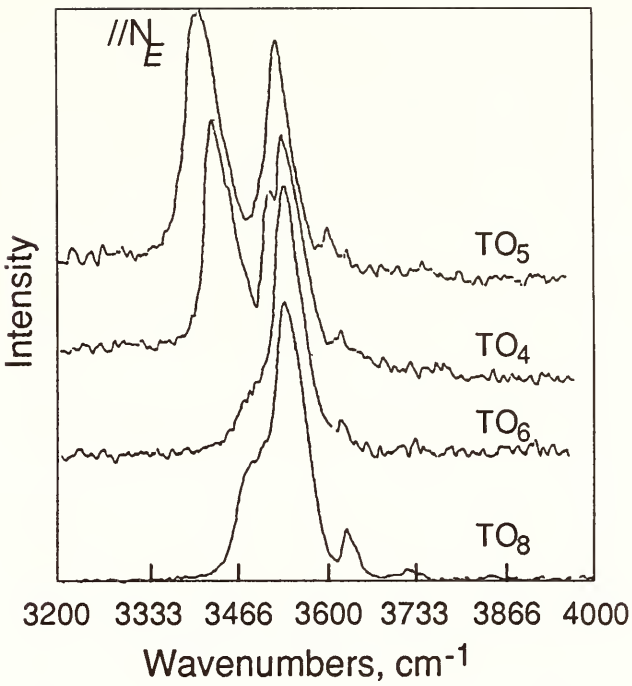

FIG. 65. PRS of $[OH]^{1-}$ groups in different types of tourmaline in N_e direction at 3400-3650 cm^{-1}. Spectra of tourmalines from metamorphic skarn (TO6 and TO8) and from pegmatite and hydrothermal vein (TO4 and TO5) are plotted.

$Mg(OH)_2O_4$. The Mg-OH bond length is 2.063Å. Thus the tourmaline structure contains brucite type (OH) groups.

The vibration peak assigned to (OH) in brucite is shown in Fig. 66 (brucite from U.S. National Museum No. 14390, courtesy of the Division of Mineralogy, U. S. National Museum). A very sharp single peak is observed at 3648 cm^{-1}. The singular peak is due to its high degree of symmetry of (OH) in the brucite structure. The OH group is surrounded by one type of cation (Mg) only. In tourmaline, although the (OH) ion has symmetry similar to that of brucite, the surrounding atoms varies. Thus its symmetry is reduced and the Raman peak splits into two. The deep blue and blue tourmaline of metamorphic skarn origin is high in Fe^{2+} content (Table 13). The Fe^{2+}

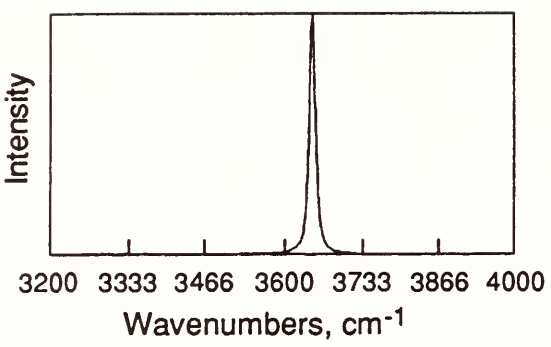

FIG. 66. Raman spectra of brucite [Mg $(OH)_2$].

replacement of Mg^{2+} in the $(Mg,Fe)(OH)_2O_4$ octahedra causes distortion of octahedra and splitting of the OH peak.

The PRS of tourmalines from the granitic pegmatite and from the hydrothermal vein have an additional OH peaks. There are three peaks attributed to (OH) stretching. The rose red Mn-bearing tourmaline has three (OH) peaks at 3460 (ν_3), 3570 (ν_1) and 3635 (ν_2) (Fig. 65; TO5). The three peaks may be accounted for if (OH) occupy two different sites. In addition to the one at the center of the unit all in the middle of the ring as mentioned earlier, (OH) may also substitute an oxygen which surrounds boron atoms, and form an $(OHBO_2)$ ion group. The location of this peak is similar to that of B-O stretching vibrational peak of $HOBO_2^{2-}$ ion (Grice *et al.*, 1986). The light green Fe-bearing tourmaline (Fig. 65; TO4) from the granite pegmatite has 4 peaks where the ν_1 peak splits into two. These four peaks are located at 3472 (ν_3), 3551 and 3577 (ν_1), and 3636 (ν_2).

Conclusion

Based on the PRS of single crystals of tourmaline, we are able to assign the vibrational spectra to $[Si_6O_{18}]^{12-}$, $[BO_3]^{3-}$, and $[OH]^{1-}$. The general feature of the polarized Raman spectra (PRS) of tourmaline in the ranges of 200-1200 and 3400-3600 cm^{-1} are presented. Strong peaks of tourmaline were observed at 1000-1200 and 200-400 cm^{-1}. They belong to Si-O stretching vibration and ring deformation vibration of $[Si_6O_{18}]^{12-}$. Strong peaks of $[BO_3]^{3-}$ vibration were measured at 700-800 cm^{-1}. PRS peaks of $[BO_3]^{3-}$ shift to higher frequencies in the N_o direction.

Strong peak of $(OH)^{1-}$ vibration occurs at 3550-3565 (ν_1) in the N_e direction. The (OH) vibration is strongly polarized. PRS of (OH) can only be detected in the N_e direction. The (OH) group in the metamorphic skarn tourmaline occupies a single site. The site occupancy is ordered. In hydrothermal and granitic pegmatite tourmalines, (OH) occupies two sites with disordered distribution. The (OH) vibrational can be used to characterize site occupancy, and are potentially indicative of the mode of geological occurrences of tourmaline.

References

Brethous, J. C., A. Levasseur, G. Villeneuve, P. Echegut, and P. Hagenmueller, Studies by spectroscopic Raman and by RMN of the glasses of the system B_2O_3 - SiO_2 - Li_2O, *J. Solid State Chem.*, *39*, 199-208, 1981.

Buerger, M. H., C. W. Burnham., and D. R. Peacor, Assessment of the several structures proposed for tourmaline, *Acta Crystallogr.*, 15, 583-590, 1962.

Grice, D. J., and J. V. Velthuigen, Moydite (Y. REE) $[B(OH)_3(CO_3)]$, a new mineral species from the evans-lou pegmatite, *Quebec Can.*

Min., *24*, 665-673, 1986.
Griffith, W. P., Raman studies on rock-forming minerals, Part I orthosilicates and cyclosilicates, *J. Chem. Soc. (A)*, 1372-1377, 1969.
Hemley, R. J., H. K. Mao, and E. C. T. Chao, Raman spectrum of natural and synthetic stishovite, *Phys. Chem. Minerals*, *13*, 285-290, 1986.
Mao, H. K., R. J. Hemley, and E. C. T. Chao, The application of micro-Raman spectroscopy to analysis and identification of minerals in thin section, *Scanning Microscopy*, *1*, 495-501, 1987.
McMillan, P., Vibration spectroscopy in the mineral sciences, *Rev. Mineral.*, *14*, Miner. Soc. Am., 9-63, 1985.
White, B. W., Structural interpretation of lunar and terrestrial minerals by Raman spectroscopy, in *Infrared and Raman Spectroscopy of Lunar and Terrestrial Minerals*, C. Karr, Jr., ed., Academic Press, New York, Chap. 13, pp. 325-356, 1975.

New Optical Transitions in Type Ia Diamonds at Very High Stresses

Russell J. Hemley and Ho-kwang Mao

The generation of ultrahigh pressures in the megabar range is now routine with the diamond-anvil high-pressure cell (Mao, 1988). One of the important features of the diamond-cell arises from the transparency of the diamond anvils to large regions of the electromagnetic spectrum, permitting spectroscopic characterization of materials at high pressures using ultraviolet, visible, and infrared radiation (Hemley *et al.*, 1987). Type Ia diamonds are used in ultrahigh pressure studies owing to the presence of nitrogen platelets which may enhance their strength (Mao *et al.*, 1979). The nitrogen impurities in these diamonds give rise to a variety of absorption and luminescence systems in the visible and ultraviolet at ambient pressures (Walker, 1979). In optical studies using the diamond-anvil cell, the absorption system at 3 eV in type Ia diamonds serves as an effective absorption edge, precluding most optical measurements at higher energies. Laser excitation in this region gives rise to a broad background fluorescence that can complicate optical measurements of samples within the cell. Further, the enhancement of this luminescence at very high pressure (above 200 GPa) can interfere with measurements of ruby fluorescence used for pressure determination (Mao *et al.*, 1978).

Recently, we performed a series of optical studies of hydrogen and a variety of materials compressed at pressures in the 200 GPa range (Mao and Hemley, 1989; Hemley and Mao, this Report). During the course of this work we discovered dramatic changes in the optical characteristics of the diamonds in the high stress regions (tips) of the anvils. Documenting these effects is essential for further optical studies of materials at pressures above 200 GPa. In particular, this work is a prerequisite for optical characterization of the pressure-induced insulator-metal transition in hydrogen and other systems.

In the present work optical measurements were performed on anvils with 25-50 mm diameter tips, 300-500 mm culets, and bevel angles of 8-10° (see Mao, 1988). As a result of their small tips, at a given load these diamonds generate higher stresses within the anvils than those used in previous spectroscopic studies. The spatial de-

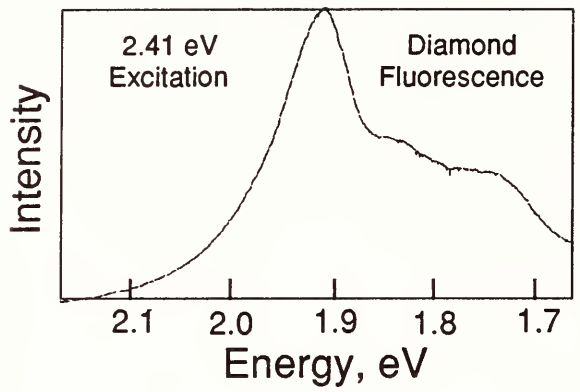

FIG. 67. Fluorescence spectrum of a type Ia diamond anvil at ultra-high pressure excited with 514.5 nm (2.41eV) Ar^+ laser line. The sample consisted of hydrogen and ruby at a peak pressure of 250 to 300 GPa.

pendencies of luminescence and Raman spectra within the anvils were measured using a ~135° scattering configuration with a 2 x 2 mm aperture and an argon-ion laser beam focused to 2-4 mm at the imaged spot within the diamond (Hemley *et al.*, 1987). An example of this fluorescence is shown in Fig. 67. With increasing stress (corresponding to sample pressures above 200 GPa) a fluorescence peak appears at 2 eV. At very high pressures the signal dramatically increases. The peak tends to shift toward lower energies with higher energy excitation. Absorption extending throughout the visible region of the spectrum, with a broad peak at 2.4 eV, is also observed.

These changes in the fluorescence and absorption spectra of the diamonds are accompanied by new Raman bands (Fig. 68). Changes in the Raman spectra have been documented with samples consisting of hydrogen, neon, ruby, NaCl, and SiO_2. Peak pressures were estimated from both the pressure profile determined from ruby fluorescence and from x-ray diffraction measurements on metal pressure standards. Fig. 68 shows the dependence of the Raman

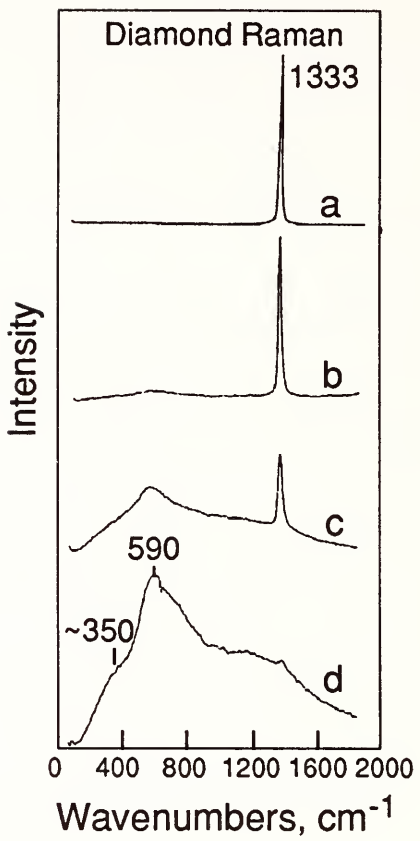

FIG. 68. Raman spectrum of a type Ia diamond anvil as a function of distance from a sample at ultrahigh pressure: (a) 30mm. (b) 20mm. (c) 10mm. (d) sample-diamond interface. The sample consisted of NaCl and ruby at a peak pressure of ~250 GPa.

spectrum on distance from the sample-anvil interface for a sample containing NaCl with 10-20% ruby. At the top of the diamond anvil the zone-center, Raman-active T_{2g} mode of the diamond at 1333 cm^{-1} is clearly visible, with no bands apparent at lower frequencies. The stress dependence of this band has been measured previously in diamond anvils under load (Sharma *et al.*, 1985; Hanfland and Syassen, 1985). As the tip of the diamond is approached a new feature at 590 cm^{-1} with a broad shoulder at ~350 cm^{-1} appears. In some runs, a sharper band at ~900 cm^{-1} was also observed. At the sample-anvil interface the intensity of the band overwhelms the diamond T_{2g} band.

Although the relative wavenumbers of the bands are independent of laser excitation wavelength (indicative of Raman transitions), they are superimposed on a structured fluorescent background, which is especially strong with 488.0 and 514.5 nm excitation. In addition, the intensities of the Raman bands showed a large degree of resonance enhancement with decreasing wavelength (e.g., 647.1 to 476.5 nm). The bands were found to be reversible on releasing the stress, although the 590 cm^{-1} peak can remain at low sample pressures (~ 30 GPa) before disappearing. The tips of the diamonds have been found to exhibit higher luminescence intensity upon unloading.

The present experiments demonstrate that significant changes in the electronic properties of type Ia diamonds occur at stresses in the 200 GPa range. The luminescence may be due to pressure-induced electronic changes in deep level impurity centers (Walker, 1980). If so, the Raman bands may be associated with localized vibrational modes at these centers. In this regard, we note that the N-V (nitrogen-vacancy) defects have an absorption band in this region (zero-phonon line at 1.95 eV at zero stress) with a fundamental vibrational interval in this range (n = 525 cm^{-1}, also at zero stress) (Davies and Hamer, 1978). Alternatively, the new bands may be associated with actual changes in the diamond structure. There is a close similarity between the new Raman features and the one-phonon density of states of diamonds which has a broad peak centered at 600 cm^{-1} (Dolling and Cowley, 1966). Such a correlation would imply a breakdown in crystalline selection rules, resulting perhaps from growth of defects at the anvil tips or macroscopic flow of the diamond (Mao *et al.*, 1979). Although a structural transformation in the diamond itself induced by nonhydrostatic stress also cannot be ruled out (Nielsen, 1986), our results indicate that such a transition must be reversible. Similar measurements carried out on different diamond types (type II, Ib, including synthetics) can be used to determine the extent to which the optical effects are associated with impurities or are intrinsic to diamond.

References

Davies, G., and M. F. Hamer, Optical studies of the 1.945 eV vibronic band in diamond, *Proc. Roy. Soc. London A, 348*, 285-298, 1978.

Dolling, G., and R. A. Cowley, The thermodynamic and optical properties of germanium, silicon, diamond, and gallium arsenide, *Proc. Phys. Soc. (London), 88*, 463-494, 1966.

Hanfland, M., and K. Syassen, A Raman study of diamond anvils under stress, *J. Appl. Phys., 57*, 2752-2756, 1985.

Hemley, R. J., P. M. Bell, and H. K. Mao, Laser techniques in high-pressure geophysics, *Science, 237*, 605-612, 1987.

Mao, H. K., Static compression of simple molecular systems in the megabar range, in *Simple Molecular Systems at Very High Densities*, P. Loubeyre, A. Polian, and N. Boccara, eds., Plenum, New York, pp. 221-236, 1988.

Mao, H. K., and R. J. Hemley, Optical studies of hydrogen above 200 gigapascals: evidence for metallization by band overlap, *Science, 244*, 1462-1465, 1989.

Mao, H. K., P. M. Bell, J. W. Shaner, and D. J. Steinberg, Specific volume measurements of Cu, Mo, Pd, and Ag and calibration of the ruby R_1 fluorescence pressure gauge from 0.06 to 1 Mbar, *J. Appl. Phys., 49*, 3276-3283, 1978.

Mao, H. K., P. M. Bell, K. J. Dunn, R. M. Chrenko, and R. C. Devries, Absolute pressure measure-

ments and analysis of diamonds subjected to maximum pressures of 1.3-1.7 Mbar, *J. Appl. Phys., 50*, 1002-1009, 1979.

Nielsen, 0. H., Optical phonons and elasticity of diamond at megabar stresses, *Phys. Rev. B, 34*, 5808-5819, 1986.

Sharma, S. K., H. K. Mao, P. M. Bell, and J. A Xu, Measurement of stress in diamond anvils with micro-Raman spectroscopy, *J. Raman Spectros., 16*, 350-352, 1985.

Walker, J., Optical absorption and luminescence in diamond, *Rep. Prog Phys, 42*, 1605-1659, 1979.

Premonitory Twinning in the High-Pressure Phase Transition of ZrO_2

*Yasuhiro Kudoh, Charles T. Prewitt, and Haruo Arashi**

At room temperature, a single crystal of the monoclinic phase of ZrO_2 with space group $P2_1/c$ transforms to a single crystal of the orthorhombic phase at 35 kbar (Fig. 69). At pressures higher than 130 kbar, a further phase transition to a different orthorhombic phase with the cotunnite-type structure is known. In this paper we report two observations of stress-induced twinning: the formation of 90° twin domains about the *c* axis in single crystal ZrO_2 of the orthorhombic phase, and formation of (111) twinning in a single crystal ZrO_2 of the tetragonal phase under the application of stress in a diamond-anvil cell at 298K. These observations provide direct evidence of ferroelastic behavior in ZrO_2 and further corroborate predictions of the occurrence of a displacive phase transition to a higher symmetry phase in this material at high temperatures and pressures.

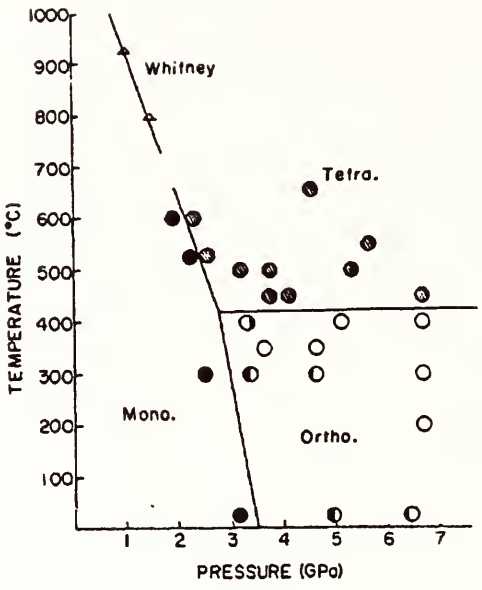

Fig. 69. *In situ* phase diagram for ZrO_2 deduced from diffraction measurements at high temperatures and pressures (after Arashi *et al.*, 1988).

Twinning in the orthorhombic phase with a tetragonal symmetry operation

A single crystal of ZrO_2 was pressurized up to 45 kbar with cedar oil as the fluid-pressure medium using a modified Merrill-Bassett type diamond-anvil pressure cell. After loading in the diamond-anvil cell, the pressure on the crystal was gradually increased up to 45 kbar at room temperature, exceeding the hydrostatic limit of cedar oil. The pressure was then reduced slowly back to ambient pressure and the sample removed from the cell. X-ray precession photographs were made on the crystal, both before and after pressure loading and at 45 kbar, using Mo$K\alpha$ radiation. Fig. 70 shows an x-ray precession photograph taken of

*Tohoku University, Research Institute for Scientific Measurements, Sendai, Japan

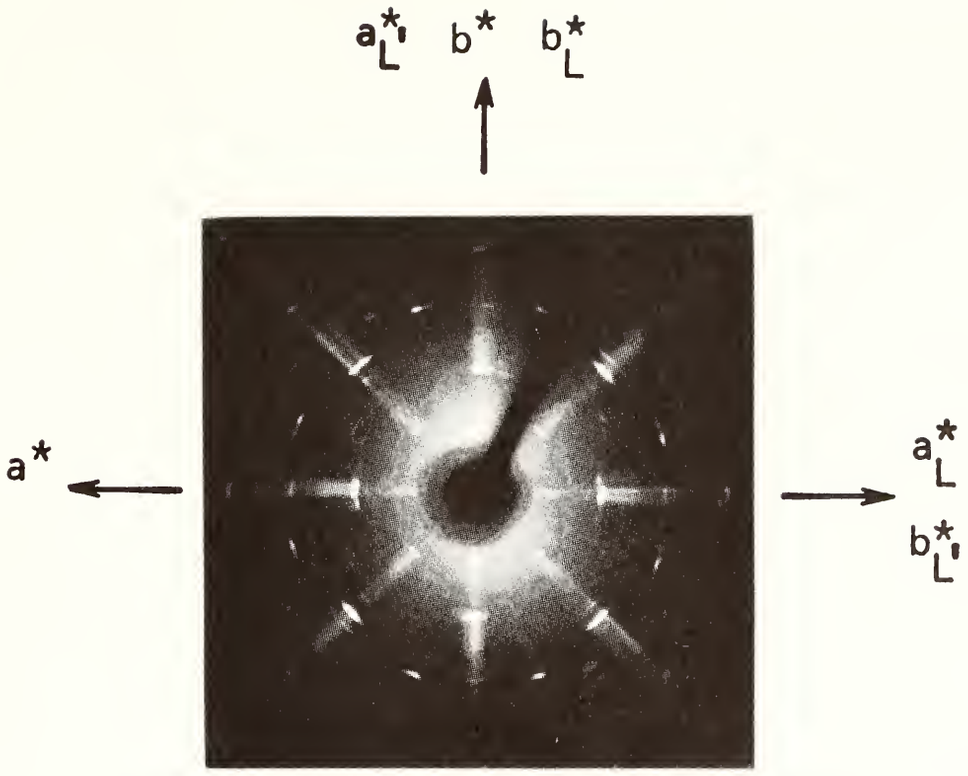

FIG. 70. X-ray precession photograph of ZrO_2 after pressure loading to 45 kbar. Twinning by a mirror plane parallel to the *b-c* plane [(100) twinning] is indicated by L. Twinning resulting from fourfold rotation about the *c* axis of the orthorhombic phase is indicated by L'.

the pressure-released specimen at ambient conditions. An analysis of the precession photograph indicates the presence of two types of twinning:

(1) Twinning by mirror plane parallel to the *b-c* plane [(100) twinning]. Reciprocal lattice axes resulting from these twin operations are indicated by L in Fig. 70. This type of twinning is known to occur in the monoclinic phase prior to transition to the orthorhombic phase (Kudoh *et al.*, 1986). The mechanism of this twinning can readily be interpreted by the slip system (100)<001>. In monoclinic ZrO_2 this slip system results in a 180° rotation of the axes about the *c* axis, such that the *b* axis in some domains lies parallel to the -*b* axis in others.

(2) Twinning by fourfold rotation about the *c* axis of the orthorhombic phase (L' in Fig. 70). This twinning is consistent with a unit cell rotation of exactly 90° about the *c* axis, such that the *a* axis in some domains lies parallel to the *b* axis in others. Because the pressure of 45 kbar exceeds the hydrostatic limit of the cedar oil, this twinning is thought to have occurred under a non-hydrostatic condition. Since the fourfold symmetry operation is included in the tetragonal or cubic class, this twinning is considered to be a premonitory phenomenon, suggesting the possible existence of a phase transition of the orthorhombic phase to tetragonal symmetry, which was confirmed by the experiment described below.

Twinning in the tetragonal phase with a cubic symmetry operation

Another single crystal of ZrO_2 was pressurized up to 550 kbar at room temperature. Pressure was generated using a lever-type diamond-anvil cell and measured by using the ruby fluorescence method. Distilled water was employed as the pressure transmitting medium. Details of the experimental procedure have been reported previously (Arashi *et al.*, 1989). The high pressure phase is quenchable to atmospheric pressure when the diamond anvil pressure cell is unloaded rapidly (Arashi *et al.*, 1989). After reducing the pressure to room pressure, the recovered crystal was examined by x-ray precession photography.

An analysis of the precession photograph indicates the presence of two crystallographically distinct orientations for the tetragonal ZrO_2 crystal, indicating the presence of twinning on (111). Because the pressure of 550 kbar exceeded the hydrostatic limit of distilled water, this twinning also occurred under a non-hydrostatic condition. Because the (111) mirror plane is not included in the tetragonal class, but is included in the cubic class, this twinning is probably a premonitory phenomenon, suggesting the possible existence of a transition of the tetragonal phase to cubic symmetry.

References

Arashi, H., O. Shimomura, T. Yagi, S. Akimoto, and Y. Kudoh, *P-T* Phase diagram of ZrO_2 determined by in-situ x-ray diffraction measurements at high pressures and high temperatures, in *Advances in Ceramics, Vol. 24, Science and Technology of Zirconia III,* The American Ceramic Society, Inc., Westerville, Ohio, 493-500, 1988.

Kudoh, Y. and H. Takeda, *In situ* determination of the crystal structure for high pressure phase of ZrO_2 using a diamond anvil and single crystal x-ray diffraction method, *Phys. Chem. Minerals, 13,* 233-237, 1986.

BIOGEOCHEMISTRY

NITROGEN ISOTOPE TRACERS OF HUMAN LACTATION IN MODERN AND ARCHEOLOGICAL POPULATIONS

Marilyn L. Fogel, Noreen Tuross, and Douglas W. Owsley#*

Variations in the stable isotope ratios of carbon ($\delta^{13}C$)** and nitrogen ($\delta^{15}N$)** are useful for paleodietary analysis of archaeologically-derived skeletal material (e.g., van der Merve, 1982; Schoeninger and DeNiro, 1984; DeNiro, 1986). Because plants and animals have distinctive isotopic signatures, the isotopic composition of humans can therefore be correlated with diets. For example, the C isotopic composition of corn is distinct from other crop plants, such as beans or squash. The difference in the $\delta^{13}C$ value is due to the operation of a different photosynthetic pathway (C-4 photosynthesis) that occurs in corn relative to that which is operational in most other higher terrestrial plants (C-3 photosynthesis). Accordingly, the introduction of corn (maize) into the diet of prehistoric North American Indians has been traced with stable C isotope ratios of the protein collagen preserved in fossil bones (van der Merve and Vogel 1977; Boutton *et al.*, 1983).

Nitrogen isotopes are useful tracers of an animal's diet primarily because isotopic fractionation occurs during the metabolism of dietary nitrogen and its incorporation into animal biomass. The protein in the tissue of an animal is enriched in ^{15}N relative to the diet of the animal by about +3 ‰ (Minigawa and Wada, 1983). The enrichment in the ^{15}N in the animal relative to the diet has been used to determine a variety of important features concerning prehistoric human diets such as the importance of marine-derived food sources, legumes, and meat (e.g., Schoeninger and DeNiro, 1984).

One of the major questions in anthropology is what effect did the introduction of horticulture have on weaning and birth intervals in prehistoric peoples? Some have hypothesized that, before agriculture, humans nursed their infants longer and concomitantly, birth intervals were longer (e.g., Buikstra *et al.*, 1986). They assume that with the introduction of agriculture, mothers weaned their babies onto alternative food sources at a younger age, and were thus able to give birth again in a shorter time interval. These hypotheses are difficult to test in modern populations, and seemingly would be impossible to test in prehistoric ones. In this paper, we investigate whether breast milk has a unique isotopic signature that can be used to trace lactation in humans. Infant nutrition in both modern and fossil populations was studied

** $\delta X = (R_{sample}/R_{standard} - 1)10^3$, where X refers to ^{13}C or ^{15}N, and R refers the ratio of the heavy to light isotope of either C ($^{13}C/^{12}C$) or N ($^{15}N/^{14}N$) in the sample or the standard.

* Conservation Analytical Laboratory, Smithsonian Institution, Washington, D.C., 20550

Department of Anthropology, Smithsonian Institution, Washington, D.C., 20550

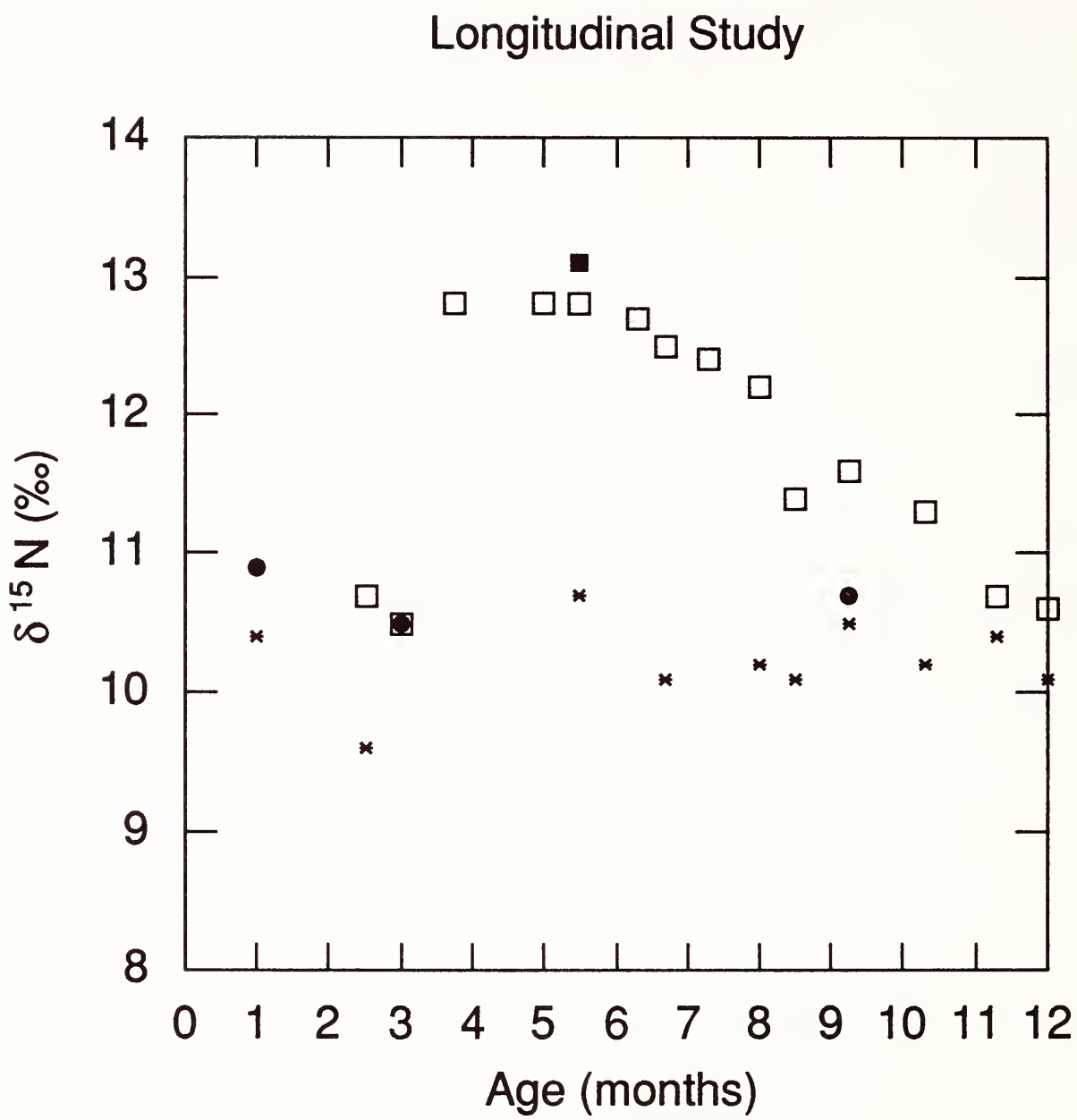

FIG. 71. Longitudinal study of the variation in $\delta^{15}N$ in the fingernail cuttings of a single mother (*) and infant pair (□). The time (months after birth) indicates when the fingernails were sampled. The infant's hair (■) and the father's fingernails (•) were also measured. The infant was exclusively breast fed until 5 months of age, when a bovine milk-based formula was introduced (100 ml/ day). Formula amounts increased with time to 500 ml/ day at 11 months. Dairy products were introduced at 7 months (100 g/ day). Fingernails (1-3 mg) were combusted at 900°C, as in Tuross *et al.*, (1988). The error of the analysis for $\delta^{15}N$ was ±0.2 ‰.

with carbon and nitrogen isotopic tracers. The hypothesis that nursing infants exist one trophic level up on the food chain from their lactating mothers, and thus protein from infant tissue should be enriched in ^{15}N relative to the mother's protein, was tested.

In our study of contemporary mothers and infants, fingernails were sampled and analyzed. Fingernails are a rapidly synthesized tissue easily obtainable from both infants and their mothers. Numerous studies on nail growth have documented that in

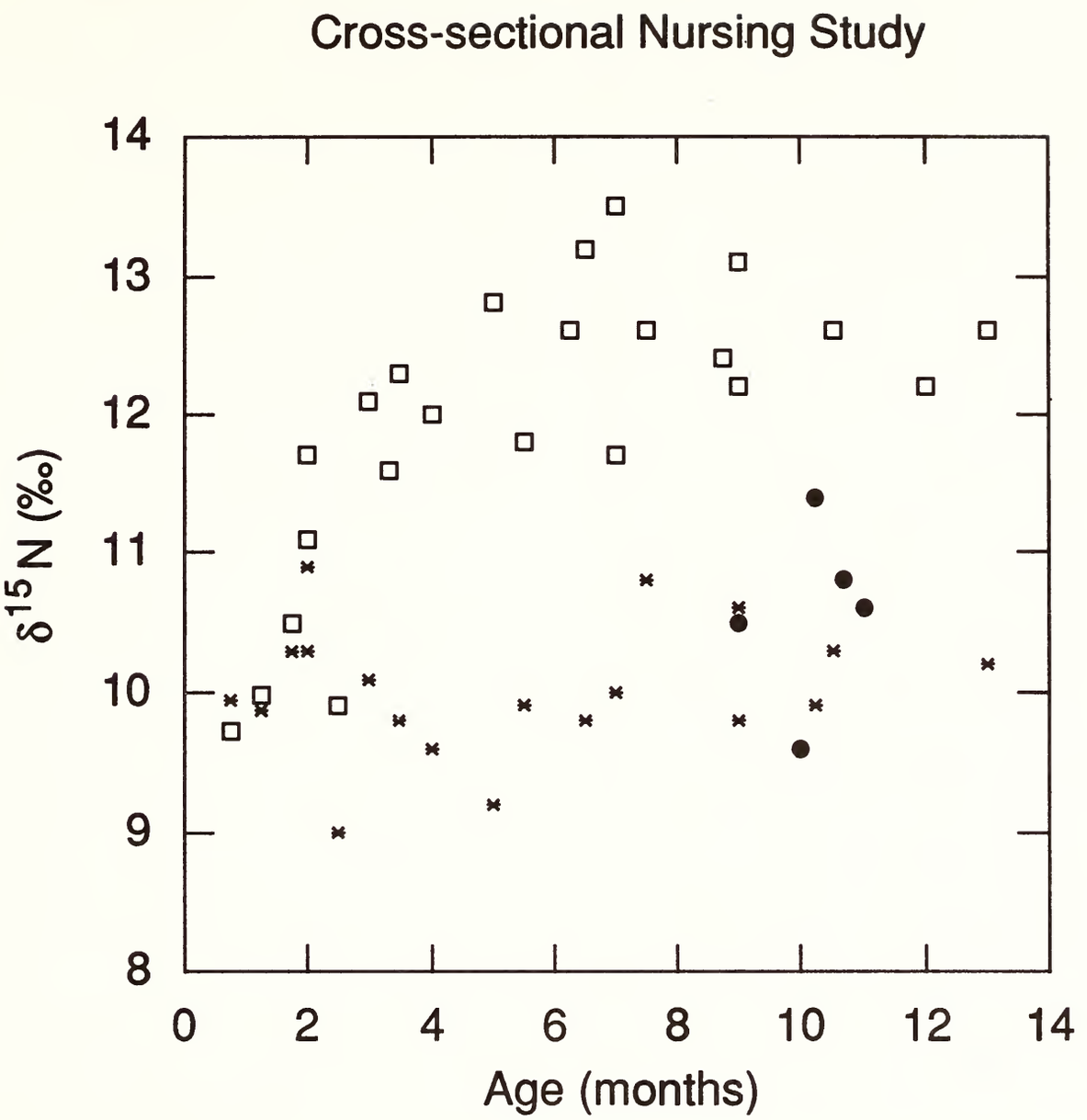

FIG. 72. Cross-sectional study of isotope variation in fingernail samples collected from 16 mother (*) and infant pairs (□). Several children were sampled at different times after birth. All infants were fully breast fed for at least three months. At approximately 3 months after birth a variety of substitute foods were introduced to their diets. Children who were totally weaned to milk or milk-formula are indicated with (•).

healthy, growing infants, fingernails require 2-3 months time to grow from cuticle to finger tip. We sampled one infant and her mother from birth to 15 months in a longitudinal study (Fig. 71), in addition to 16 separate mothers and their infants in a cross-sectional study (Fig. 72). In all cases, the isotopic composition of the nursing infants' fingernails was enriched in ^{15}N as compared to that of the mothers' over the age range from three months until several months after alternate food sources were introduced. A decrease in the infant $\delta^{15}N$ values toward those of their mothers correlates with the introduction of alternative nitrogen sources: infant formula, milk, dairy

products, and meat. Carbon isotopic compositions of infant fingernails (-17.5 ‰) were nearly identical to those of their mother and were not useful for tracing a human milk source.

Fingernails cut in the first three months of life were synthesized *in utero*. The increase in the ^{15}N content in the nursing infants' fingernails after 3 months corresponds to the introduction of breast milk at birth ($\delta^{15}N = +8.0$; n=4). After three months of age, each infant was enriched in ^{15}N by an average +2.4 ‰, when compared to the mother. Four babies who were totally weaned at 4-8 months of age to bovine milk-based formula ($\delta^{15}N = +4$) (n=3) or whole bovine milk (n=1) showed a decrease in the $\delta^{15}N$ of their fingernails 3-5 months after the dietary change. The other infants who were not given a milk substitute, or provided formula in limited amounts, maintained the enrichment of ^{15}N in their fingernails for the duration of the study. Thus, the natural abundance of stable nitrogen isotopes provides a measure of the nitrogen sources, especially breast milk, being utilized by a growing infant.

No attempt was made to control for the diet of the mothers, yet 14 females had an average $\delta^{15}N$ of $+10 \pm 0.6$ (1σ). In the longitudinal study, the woman had an average $\delta^{15}N$ of $+10.2 \pm 0.3$. The isotopic composition of three individual nails from different fingers sampled at one time from this mother and her baby had a standard deviation of ±0.4 ‰, which is larger than the mean of the adult isotopic signal. In a study of nine subjects from Chicago, Schoeller *et al.* (1986) reported an average $\delta^{15}N$ of +9.4. Given the diversity of nitrogen sources in current diets, and the range of $\delta^{15}N$ in these sources, the lack of variation is surprising. The difference in $\delta^{15}N$ between infants and their mothers (+2.4 ‰) is thus eight standard deviations away from the adult isotopic mean and provides a distinct tracer of lactation.

Whereas fingernails have a more clearly defined and straightforward turnover time in infants, collagen synthesis in bone and its relation to diet are more complex. Generally, the stable isotopic values obtained from fossil bone collagen are thought to reflect the dietary input over a long period of time, because the turnover time of collagen in adult bone is on the order of 10-20 years. In the modern American society, infants triple their birth weight by one year (Ryan and Martinez, 1987). Therefore, even without any resorption of the bone collagen present at birth, the one year old infant would be expected to have synthesized a minimum of two-thirds of its bone mass after birth.

To determine whether a nursing signal could be detected in skeletal remains, bone samples from infants, small children and adults were analyzed for age differences in $\delta^{15}N$ values of bone collagen. The samples are from archaeological contexts and represent pre- and post-horticultural populations. This contrast in subsistence patterns provides a test of the hypothesis that the time of weaning changed after agriculture became established. The pre-horticultural population sample (13 adults, 34 children) was comprised of skeletal remains from three Tennessee Valley Middle and Late Archaic period sites located in Benton County, TN: Cherry (40Bn74), Eva

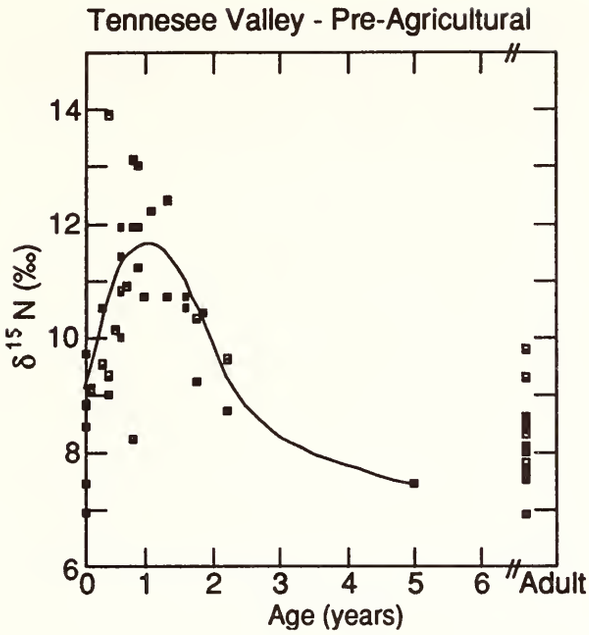

FIG. 73. Nitrogen Isotopic composition of bone collagen from the Tennessee Valley as a function of the age at the time of death of the individual. Horticulture was not practiced at this site.

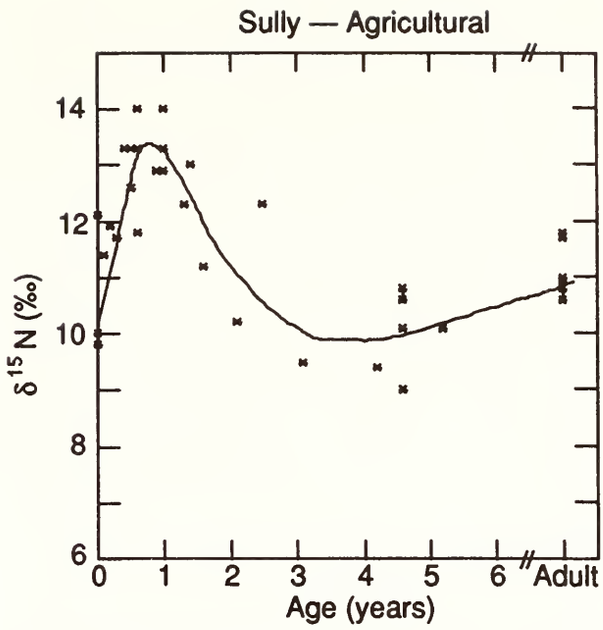

FIG. 74. Nitrogen isotopic composition of bone collagen from the Sully site, South Dakota, as a function of the age of the individual at the time of death. The Sully site is representative of a Plains Indian population that practiced maize agriculture.

(40Bn12), and Ledbetter (40Bn25) (Higgins, 1982; Magennis, 1977; Lewis and Kneberg, 1959; Lewis and Lewis, 1961). The subsistence pattern was based on hunting and gathering. There is no evidence for maize horticulture during this period, which dates from about 5500 B.C. until 2000 B.C. Permission to use the samples was granted by J. Chapman and M.O. Smith of the Frank H. McClung Museum of the University of Tennessee.

Rib bones from the Sully site (39S14), Sully Co., South Dakota, were obtained primarily from the Smithsonian collection and represent a population dependent on horticulture. This protohistoric North Plains Coalescent Tradition site dates to A.D. 1650-1700 (Owsley and Jantz, 1978). This population relied on a mixed subsistence economy, involving the hunting and collecting of wild foods, as well as horticulture with principal crops being corn, squash, beans, and sunflowers (e.g., Holder, 1970). A total of 12 adult and 27 children specimens were analyzed.

Age determination of infants and children in both populations were based on the dental calcification standards of Moorrees *et al.* (1963), as modified by Hyman (1987), and characteristic lengths of the long bones (Merchant and Ubelaker, 1977). Bone samples, usually rib fragments (1-2 g), were decalcified in either EDTA solution or 1 N HCl (Tuross *et al.*, 1988), and the isotopic ratio was determined as described therein.

An enrichment in ^{15}N of total collagen was measured in almost all of the bones tested from one year old infants (Figs. 73 and 74). Age determination of the humans at the time of death is a critical component of the study. If the infant age were off by 6 months to a year, the isotopic ratios would

be random. In the Tennessee samples, the difference between the babies and the adults at 1 year was +4 ‰, whereas at Sully it was +2.5 ‰. Both differences are similar to that measured between the isotopic ratio of modern infant and maternal fingernails. The $\delta^{15}N$ of bones from both archeological sites declined sharply at 18-20 months. The initial enrichment and subsequent depletion of the isotopic ratio of collagen is consistent with the establishment and preservation of a nursing signature in the younger group and a weaning pattern in the older group. The $\delta^{15}N$ of the newborns was variable but, on average, was almost identical with that of the adults. These children were probably too young to have expressed the *extra utero* nursing pattern, as was the case with the isotopic ratios in modern infants under 3 months of age.

From the modern data presented here, we conclude that a clear tracer of lactation is established in the protein of fingernails. In every sample tested, the isotopic ratio of a nursing infant was always more enriched in ^{15}N than that of its mother. The results from the analysis of prehistoric human populations demonstrate that when a suite of individuals with known ages are analyzed, then the $\delta^{15}N$ of collagen preserved in bone can be used as a tracer of infant nutrition: breast feeding, weaning, and the introduction of alternate food sources. Nursing and weaning practices in the pre- and post-horticultural Indian populations studied were not significantly different from one another. In both populations alternate food sources were introduced at 18-20 months, and breast milk became less important in the diet. Full realization of the application of this technique will require the analysis of well-characterized collagen from large skeletal populations.

References

Boutton T. W., P. D. Klein, M. J. Lynott, J. E. Price, and L. L. Tieszen, Stable carbon isotope ratios as indicators of prehistoric human diet, in *Stable Isotopes in Nutrition, ACS Symposium Series 258*, J. R. Turnland, P. E. Johnson, eds., American Chemical Society, Washington, D. C. pp. 191-204. , 1984

Buikstra, J. E., L. W. Konigsburg, and J. Bullington, Fertility and the development of agriculture in the prehistoric midwest, *Amer. Antiquity, 51*, 528-546, 1986.

DeNiro, M. J., Stable isotopy and archaeology, *Am. Sci., 75*, 182-191, 1986.

Higgins, Katherine F., The Ledbetter Site: A Study of Late Archaic Mortuary Patterning. Unpublished Master's thesis. Dept. of Anthropology, The University of Tennessee, Knoxville, Tennessee, 1982.

Holder, P., *The Hoe and the Horse on the Plains*, University of Nebraska Press, Lincoln, 1970.

Hyman, Suzanne A., The Relationship Between Dental Age and Long Bone Growth in Arikara Infants, Unpublished Master's thesis, The University of Tennessee, Knoxville, 1987.

Lewis, Thomas M. N. and Madeline Kneberg, The archaic culture in the middle South, *Am. Antiq., 25*(2), 161-183, 1959.

Lewis, Thomas M. N., and M. K. Lewis, Eva, *An Archaic Site*, University of Tennessee Study in Anthropology, Knoxville, Tennessee, 1961.

Magennis, Ann L., Middle and Late Archaic Mortuary Patterning: An Example from the Western Tennessee Valley, Unpublished Master's Thesis, Dept. of Anthropology, The University of Tennessee, Knoxville, 1977.

Merchant, Virginia L. and Douglas H. Ubelaker, Skeletal growth of the protohistoric Arikara, *Am. J. Phys. Anthropol., 46*(1), 61-72.

Minagawa, M. and E. Wada, Step-wise enrichment of ^{15}N along food chains, Further evidence

and the relationship between $\delta^{15}N$ and animal age, *Geochim. Cosmochim. Acta, 48*, 1135-1140, 1984.

Moorrees, Coenraad F. A., Elizabeth A. Fanning, and Edward E. Hunt, Jr., Formation and resorption of three deciduous teeth in children, *Am. J. Phys. Anthropol., 21,* 205-213, 1963a.

Owsley, D. W. and R. L. Jantz, Intracemetary morphological variation in Arikara crania from the Sully site (39SL4), Sully County, South Dakota, *Plains Anthropol., 23,* 139-147, 1978.

Schoeller, D. A., M. Minagawa, R. Slater, and I. R. Kaplan, Stable isotopes of carbon, nitrogen and hydrogen in the contemporary North American food web, *Ecol. Food Nutrition , 18,* 159-170, 1986.

Schoeninger, M. J., and M. J. DeNiro, Nitrogen and carbon isotopic composition of bone collagen from marine and terrestrial animals, *Geochim. Cosmochim. Acta, 48*, 625-639, 1984.

Ryan, A.S. and G.A. Martinez, Physical growth of infants 7 to 13 months of age, results from a national survey, *Amer. J. Physical Anthropol., 73*, 449-457, 1987.

Tuross, N., M. L. Fogel, and P. E. Hare, Variability in the preservation of the isotopic composition of collagen from fossil bones, *Geochim. Cosmochim. Acta, 52*, 929-935, 1988.

van der Merve, N. J., Carbon isotopes, photosynthesis and archeology, *Amer. Sci.,70*, 596-606, 1982.

van der Merve, N.J., Isotopic evidence for early maize cultivation in New York State, *Amer. Antiquity, 42*, 238-242, 1977.

Nitrogen Isotope Fractionation in the Uptake of Ammonium by a Marine Bacterium

Matthew P. Hoch, David L. Kirchman, and Marilyn L. Fogel*

Heterotrophic bacteria can contribute substantially to total biomass and biomass production in marine environments. On the order of 50% of primary production, in the form of dissolved organic matter (DOM), can be processed by heterotrophic bacteria in marine and freshwater environments (Ducklow, 1983). In marine nitrogen cycling, bacteria have traditionally been viewed as consumers of dissolved organic nitrogen (Fuhrman, 1987) and regenerators of ammonium (Hollibaugh, 1980). Contrary to this, recent studies have shown that ammonium is a significant source of nitrogen required for bacterial biomass production, and a large fraction of total ammonium uptake can be attributed to bacteria (Wheeler and Kirchman, 1986). For example, in the Delaware Estuary 4 - 30% of the total ammonium uptake can be attributed to bacteria (Hoch and Kirchman, in preparation).

The influence of heterotrophic bacteria in changing the isotopic composition of organic and inorganic pools of nitrogen in the water column has not been considered extensively (Altabet, 1988; Sigleo and Macko, 1985). *In situ* microbial processes can greatly influence the isotopic signature of nitrogen that enters the sedimentary records. Large isotope fractionation associated with microbial processes such as denitrification and nitrification (Mariotti *et al.*, 1981) can alter the isotopic composition of NO_3^-, NO_2^-, and NH_4^+, and therefore, particulate organic matter when this nitrogen is fixed. A large isotope fractionation associated with the assimilation of ammonium by heterotrophic bacteria would affect the ^{15}N abundance of the ammonium pool in addition to bacteria and phytoplankton.

* College of Marine Studies, University of Delaware, Lewes, DE 19958

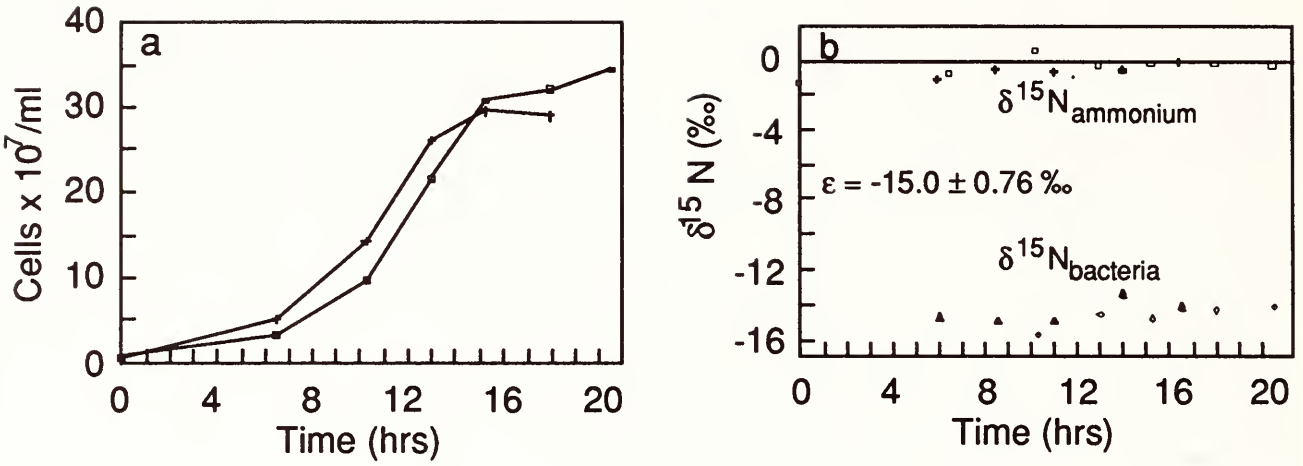

FIG. 75. Growth of *Vibrio harveyi* on 20 mM ammonium and 10 mM glucose; a) bacterial cell numbers over time, b) δ^{15}N of bacterial nitrogen and residual ammonium in the medium for replicate cultures (a, +, ▲; b, □, ◆).

In this study, the isotope fractionation between NH_4^+ and bacterial nitrogen has been determined for a common marine isolate, *Vibrio harveyi*, grown on ammonium as its sole nitrogen source. Bacteria have been shown to have two enzymatic pathways for NH_4^+ assimilation, which are regulated by the concentrations of this N source in the growth media. The hypothesis that the isotopic fractionation would correlate with a switch in the enzymatic pathway for the assimilation, from glutamate dehydrogenase to glutamine synthetase as ammonium concentration decreased, was tested.

Batch cultures of *Vibrio harveyi* were grown on a minimum nutrient media with ammonium and glucose as the sole source of nitrogen and carbon, respectively. Additions of glucose, to 10 mM, and ammonium, to either 20, 10, 5, 2, or 0.5 mM, were first filter sterilized through 0.22 μm *Millipore*™ membrane. Cell growth was followed by monitoring the absorbance at 660 nm and by cell abundance epifluorescent microscopy. Cultures were incubated at 25°C until stationary phase of the growth curve was reached.

Cultures were sampled for the measurement of their ammonium concentration and bacterial nitrogen content, and for isotopic analysis of ammonium and bacterial nitrogen. Bacterial biomass was collected on pre-combusted 25mm *Whatmann*™ GF/F glass fiber filters for analysis of nitrogen content with a *Hewlett Packard*™ 185B CHN Analyzer. Ammonium concentration of the medium was determined by the indophenol blue method (Solorzano, 1969). Bacteria for isotopic analysis were concentrated by centrifugation, washed with distilled water, freeze dried, and stored *in vacuo*. Filtrate collected for ammonium isotope analysis was frozen at -80°C until distillation. A *Labconco*™ Rapid Kjeldahl System, Rapid Still III was used for alkaline distillation of ammonium (Velinsky *et al.*, 1989). Bacterial biomass and zeolite with ammonium were converted to N_2 for mass spectral analysis by combustion

(Macko, *et al.*, 1987).

Specific activities for the bacterial enzymes glutamate dehydrogenase (GDH) and glutamine synthetase (GS) were measured in cultures of *V. harveyi* grown on 20, 10, 5, 2, or 0.5 mM ammonium and harvested at mid-exponential growth. Total GS activity was assayed using the g-glutamyltransferase assay of Bender *et al.* (1977). Activity of GDH was assayed by following the oxidation of NADH (Sanwal and Lata, 1961).

At high concentrations (20 and 5 mM) only a small fraction of ammonium (<0.05%) was assimilated by cultures that had grown to stationary phase (Fig. 75a). These conditions are characteristic of an open system, so the isotope enrichment (ε) approximates the difference between the δ^{15}N of the bacteria and that of ammonium:

$$\varepsilon \approx \delta^{15}\text{N bacteria} - \delta^{15}\text{N ammonium.} \quad (1)$$

For the 20mM NH_4^+ cultures, ε equaled -15 ‰ (± 0.78 ‰) (Fig. 75b).

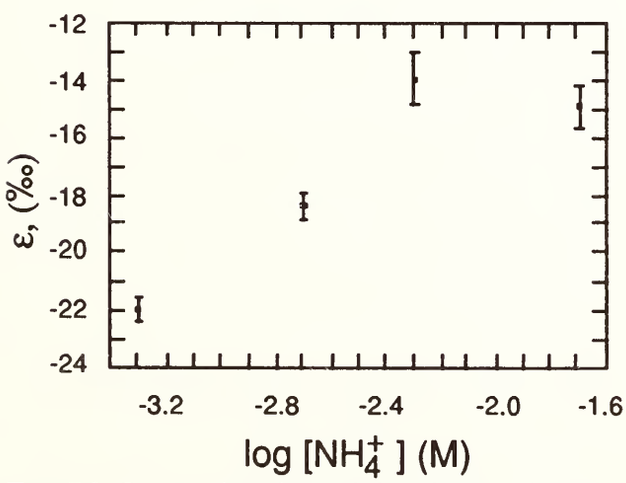

FIG. 76. Composite plots of the nitrogen isotope fractionations for *Vibrio harveyi* grown on 20, 5, 2, and 0.5 mM ammonium, plotted as the log of the molar ammonium concentration. One error bar equals one standard deviation.

All the ammonium was assimilated by the stationary phase in cultures with 2 and 0.5 mM NH_4^+ at the start of growth. The isotope ratio of NH_4^+ was determined at intervals before it was totally assimilated. In this case ε was calculated with equations described by Mariotti *et al.* (1981):

$$\varepsilon = 1000 \log (R/R_o) / \log f, \quad (2)$$

where f is the fraction of ammonium remaining, R is the ratio of $^{15}N/^{14}N$ in the initial NH_4^+ and R_o is the ratio in the sample at time (t_o). There is an inverse relationship between the ammonium concentration of the culture medium and the isotope fractionation (Fig. 76). *V. harveyi* grown on 5 and 20 mM NH_4^+ fractionated ammonium nitrogen by ca. -15 ‰. At the lowest concentration (0.5 mM) the isotope fractionation was the greatest, -22 ‰. In order to explain the change, the activity of the primary ammonium assimilatory enzymes

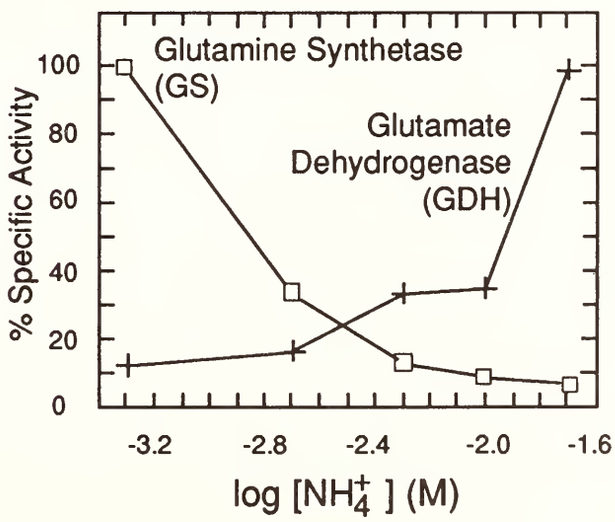

FIG. 77. Composite plot of percent specific activity of glutamine synthetase and glutamate dehydrogenase for *V. harveyi* grown on 20, 10, 5, 2, and 0.5 mM ammonium, plotted as the log of the molar ammonium concentration.

were assayed.

The highest specific activities for *V. harveyi* GDH and GS were in the cultures with 20 mM and 0.5 mM ammonium, respectively (Fig. 77). This relationship suggests that isotope fractionation is dependent on the enzymatic pathway for ammonium assimilation. At high ammonium concentrations, GDH is the dominant assimilatory enzyme for bacteria, and is responsible for catalyzing the reaction:

$$\text{2-oxoglutarate} + NH_3 + \text{NAD(P)H} \Leftrightarrow \text{L-glutamate} + \text{NAD(P)+} + H_2O. \quad (3)$$

At lower concentrations of ammonium, GS becomes dominant, and catalyzes the reaction:

$$\text{L-glutamate} + NH_3 + \text{ATP} \Leftrightarrow \text{L-glutamine} + \text{ADP} + P_i. \quad (4)$$

Nitrogen isotope fractionation associated with ammonium assimilation by other cultured organisms is about the same as that for *V. harveyi* (Table 15). When both algal and bacterial species were grown on millimolar concentrations of ammonium (3.5 to 70 mM), the nitrogen isotope fractionation ranges from -13.5 to -15 ‰. Pennock *et al.* (in preparation) measured fractionations within the range of -19 to -27 ‰ for a marine diatom, *Skeletonema costatum,* grown on 50 μM NH_4^+. These values for this diatom are similar to those for *V. harveyi* grown at 0.5 mM NH_4^+. Apparently, nitrogen isotope fractionation

TABLE 15. Isotope fractionation (ε) between NH_4^+ and organic matter for various organisms studied. Ammonium concentration of growth media are given in parentheses.

Organism	ε (‰) High [NH_4^+] (mM)	ε (‰) Low [NH_4^+] (μM)	
Vibrio harveyi (marine bacterium)	-15.0 (5,20)	-22.0 (500)	(present study)
Azotobacter vinelandii (soil bacterium)	-14.8 (70)	——	Delwiche and Steyn (1970)
Anabaena sp (cyanobacterium)	-13.6 (18)	——	Macko *et al.* (1987)
Skeletonema costatum (marine diatom)	——	-19 to -27 (100)	Pennock *et al.* (unpublished)
Phaeodactylum tricornutum (marine diatom)	-13.6* (3.5)	——	Wada and Hattori (1978)

* Recalculation of data from Wada and Hattori (1978) using equation 11 from Mariotti *et al.* (1981), and assuming f=0.6 and initial substrate $\delta^{15}N$ = -1.5 ‰ when phytoplankton biomass $\delta^{15}N$ is approximately -12 ‰.

associated with ammonium assimilation is not species specific. We conclude that the rate-limiting step in ammonium assimilation for high and for low ammonium concentrations is similar among different organisms.

Potential sites of an isotope effect (i.e., the rate-limiting step) for ammonium assimilation are depicted in Fig. 78. The equilibrium isotope effect between NH_4^+ and NH_3 is -19.2‰ at 25°C (Hermes *et al.*, 1985). The ^{15}N is concentrated in NH_4^+, whereas ^{14}N is enriched in the NH_3. In calculating the kinetic isotope effect of alanine and glutamate dehydrogenase from bovine liver. Weiss *et al.* (1988) corrected the observed values to account for equilibrium isotope effects during the deprotonation of NH_4^+, because the actual substrate for the enzyme is NH_3. Therefore, the isotope effects for alanine and glutamate dehydrogenase are inverse, +8‰ and +2‰(±1‰), respectively. Assimilation of ammonia with a $\delta^{15}N$ of -19 by these enzymes would yield $\delta^{15}N$ values for bacterial cells of -17.2‰ and -11.2‰, respectively. Isotope fractionation for *V. harveyi* grown on 20 mM NH_4^+ (ca. -15 ‰) is between these values. Alanine dehydrogenase may be involved in *V. harveyi* ammonium assimilation, however, its activity was not assayed in our cultures.

We are presently measuring the isotope fractionation by glutamine synthetase. Also inherent in determining the isotope fractionation of GS is the pre-equilibrium isotope effect between NH_3 and NH_4^+, because NH_3 is the species taken up by the enzyme. The rate controlling steps of many chemical reactions are preceded by rapid and

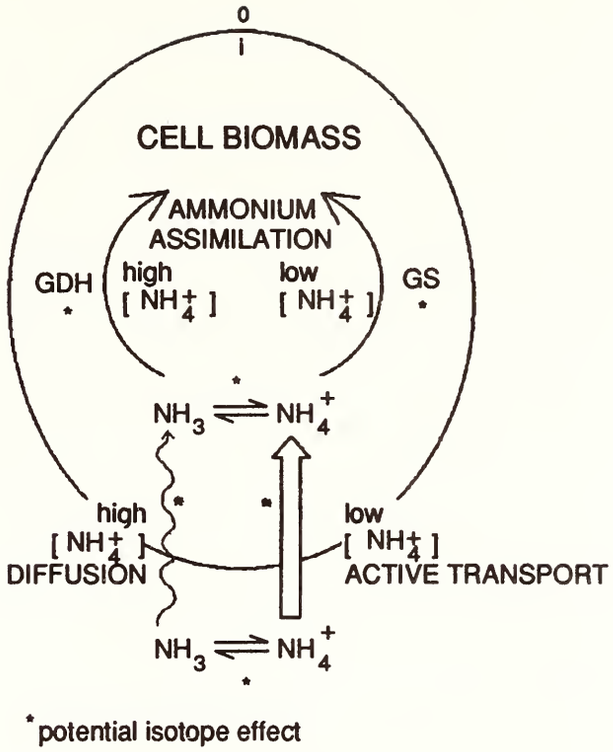

FIG. 78. Schematic diagram of the pathways for ammonium assimilation in a bacterial cell showing the potential sites of isotope effects. Values for isotope fractionation are explained in the text.

reversible pre-equilibria (Bigeleison and Wolfsberg, 1958). Glutamine synthetase was assayed at two pH values to determine the effect of this pre-equilibrium on the measured fractionation of the reaction. At pH 7.0, where less than 1% of the total N is NH_3, the isotope fractionation (ε) for both the pre-equilibrium step and the enzyme reaction itself is -8.0 ± 0.3 ‰ ($r^2 = 0.95$; n = 13). At pH 8.6, where a greater proportion of the total N is NH_3, the total fractionation is -12.3 ± 0.5 ‰ ($r^2 = 0.94$; n = 9). Accordingly, the fractionation by GS itself was determined by calculations modified from Bigeleison and Wolfsberg (1958):

$$\varepsilon_{\text{total}} - \varepsilon_{\text{equilibrium}} = \varepsilon_{GS}. \qquad (5)$$

At pH 7.0 and 8.6, respectively, inverse

isotope effects of +10.8 and +3.0 were calculated. Both values have a similar direction and magnitude as those measured by Weiss *et al.* (1988) for ADH and GDH.

Therefore, at lower ammonium concentrations the observed isotope fractionation for *V. harveyi* is a result of some other process involved in the ammonium assimilatory pathway. Bacteria obtain ammonium across cell membranes by physical diffusion of NH_3 or by active (i.e., energy dependent) transport of NH_4^+ (Kleiner, 1985). Nothing is known about isotope effects associated with active NH_4^+ transport, although Marotti *et al.* (1982) found no isotope fractionation during the active uptake of NO_3^- into plant cells. Conversely, the isotope effect during the diffusion NH_3 may be as large as -29 ‰ (See Hermes *et al.*, 1985). At low NH_4^+ concentrations, diffusion may be the rate-limiting step in assimilation.

The relatively large isotope fractionation associated with ammonium assimilation by heterotrophic marine bacteria can have a major influence on the nitrogen isotope ratio of suspended and sedimentary organic matter in estuarine and coastal environments. With our results, nitrogen isotopes may be useful in addressing ecological questions concerning the role of heterotrophic bacteria in marine nitrogen cycling.

References

Altabet, M. A.,Variations in nitrogen isotopic composition among particle classes: Implication for particle transformation and flux in the open ocean, *Deep Sea Res., 35,* 535-544, 1988.

Bender, R. A., K. A. Janssen, A. D. Resnick, M. Blumenberg, F. Foor, and B. Magasanik, Biochemical parameters of glutamine synthetase from *Klebsiella aerogenes*, *J. Bacteriol., 129 (2),* 1001-1009, 1977.

Biegeleison, J., and M. Wolfsberg, Theoretical and experimental aspects of isotope effects in chemical kinetics, in *Advances in Chemical Physics*, I. Prigogine, ed., Interscience Publishers, Inc., New York, 1958.

Delwiche, C. C., and P. L. Steyn, Nitrogen isotope fractionation in soils and microbial reactions, *Environ. Sci. Technol., 4,* 929-939, 1970.

Ducklow, H. W., Production and fate of bacteria in the oceans, *BioScience, 33(8),* 494-501, 1983.

Eppley, R. W., R. W. Holmes, and J. D. H. Strickland, Sinking rates of marine phytoplankton measured with fluorometer, *J. Exp. Mar. Biol. Ecol., 1,* 191-208, 1967.

Fuhrman, J. A., Close coupling between release and uptake of dissolved free amino acids in seawater studied by an isotope dilution approach, *Mar. Ecol. Prog. Ser., 37,* 45-52, 1987.

Hermes, J. D., P. M. Weiss, and W. W. Cleland, Use of nitrogen-15 isotope effects to determine the chemical mechanism of phenylalanine ammonium-lyase, *Biochem., 24,* 2959-2967, 1985.

Hollibaugh, J. T., A. B. Carruthers, J. A. Fuhrman, and F. Azam, Cycling of organic nitrogen in marine plankton communities studied in enclosed water columns, *Mar. Biol., 59,* 15-21, 1980.

Kleiner, D., Bacterial ammonium transport, *FEMS Microbiol. Rev., 32,* 87-100, 1985.

Macko, S. A., M. L. Fogel (Estep), P. E. Hare, and T. C. Hoering, Isotope fractionation of nitrogen and carbon in the synthesis of amino acids by microorganisms, *Chem. Geol. (IGS), 65,* 79-92, 1987.

Mariotti, A., J. C. Germon, P. Hubert, P. Kaiser, R. Letolle, A. Tardieux, and P. Tardieux, Experimental determination of nitrogen kinetic isotope fractionation, some principles; illustration for the denitrification and nitrification processes, *Plant and Soil., 62,* 413-430, 1981.

Mariotti, A., F. Mariotti, M.-L. Champigny, N. Amarger, and A. Moyse, Nitrogen isotope frac-

tionation associated with nitrate reduction activity and uptake of NO_3^- by pearl millet, *Plant Physiol., 69*, 880-884, 1982

Sanwal, B. D., and M. Lata, The occurrence of two different glutamic dehydrogenases in neurospora, *Can. J. Microbiol., 7*, 319-328, 1961.

Sigleo, A. C., and S. A. Macko, Stable isotope and amino acid composition of estuarine dissolved colloidal material, in *Mar. Estuar. Geochem.* A. C. Siegleo and A. Hattori, eds., Lewis Publishing Inc., Chelsea, Michigan, pp. 29-46, 1985.

Solorzano, L., Determination of ammonium in natural water by the phenol hypochlorite method, *Limnol. Oceanogr., 14*, 799-800, 1969.

Velinsky, D. J., L. A. Cifuentes, J. R. Pennock, J. H. Sharp, and M. F. Fogel., Determination of the isotope composition of ammonium-nitrogen at the natural abundance level from estuarine waters, *Mar. Chem.*, in press, 1989.

Wada, E., and A. Hattori, Nitrogen isotope effects in the assimilation of inorganic nitrogenous compounds by marine diatoms, *Geomicrobiol. J., 1(1)*, 85-101, 1978.

Wheeler, P. A., and D. L. Kirchman., Utilization of inorganic and organic nitrogen by bacteria in marine systems, *Limnol. Oceanogr., 31(5)*, 998-1009, 1986.

Weiss, P. M., C. Y. Chen, W. W. Cleland, and P. F. Cook, Use of primary deuterium and ^{15}N isotope effects to deduce the relative rates of steps in the mechanisms of alanine and glutamate dehydrogenases, *Biochemistry, 27*, 4814-4822, 1988.

Dissolved Nitrogen Isotopic Distribution in the Black Sea

*David J. Velinsky, Marilyn L. Fogel, and Bradley M. Tebo**

The Black Sea is the world's largest, present-day, anoxic marine basin (Fig. 79). As a result of intense water column stratification, the flux of oxygen to the bottom waters is not sufficient for the complete oxidation of surface-derived organic matter. Below approximately 200 m, bacteria use alternate electron acceptors, including iron and manganese oxides, nitrate and most importantly sulfate, to oxidize organic matter during respiration. Because sulfate is the most abundant oxidant after oxygen, microbial respiration is dominated by sulfate reduction in the deep waters and sediments of the Black Sea.

During the oxidation of organic matter coupled to sulfate reduction, organically bound nitrogen is converted to ammonium.

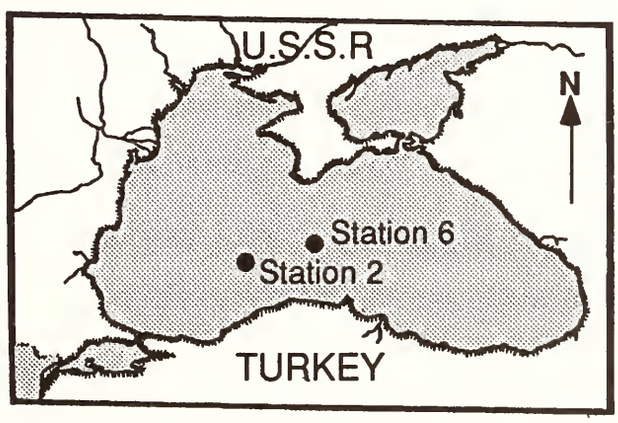

Fig. 79. Black Sea station location map.

* Scripps Institution of Oceanography, La Jolla, CA 92093.

Richards (1965) described a steady state stoichiometric model for the production of ammonium during anaerobic oxidation of organic matter (Table 16). These reactions, coupled with the sluggish mixing of Black Sea deep waters, result in the buildup of ammonium in the waters below approximately 100 m. As the ammonium diffuses upward in the water column across the oxygen-sulfide boundary, it undergoes important transformations that affect biological production and possibly also trace metal distributions. For example, ammonium can serve as an energy source for aerobic chemosynthetic production of organic matter (Brewer and Murray, 1973). In the process of nitrification, chemoautotrophic bacteria convert ammonium to nitrite and nitrate, which can subsequently be reduced to nitrogen gas via denitrification in tightly coupled reactions (Hattori, 1982). In addition, because of the broad zone of low oxygen concentration observed just above the oxygen/sulfide interface during the 1988 expedition to the Black Sea, it has been postulated that nitrate can serve as an electron acceptor for both ammonium and dissolved manganese oxidation (Murray *et al.*, 1989). Thus there are potentially both aerobic and anaerobic processes taking place near the interface that can consume ammonium and limit its availability as a nutrient in the overlying waters.

Isotope tracers at the natural abundance level have been used to determine the flow

TABLE 16. Steady-State Stoichiometric Model for the Oxidation of Organic Matter

1) Oxygen Respiration:

$$(CH_2O)_{106}(NH_3)_{16}H_3PO_4 + 106\ O_2 \Leftrightarrow 106\ CO_2 + 16\ NH_3 + H_3PO_4 + 106\ H_2O \quad (1)$$

Ammonia is oxidized to nitrate (i.e., nitrification):

$$16\ NH_3 + 32\ O_2 \Leftrightarrow 16\ HNO_3 + 16\ H_2O \quad (1a)$$

2) Nitrate Reduction and Denitrification:

$$(CH_2O)_{106}(NH_3)_{16}H_3PO_4 + 84.8\ HNO_3 \Leftrightarrow 106\ CO_2 + 42.4\ N_2 + 16\ NH_3 + H_3PO_4 + 148.4\ H_2O \quad (2)$$

Also, the NH_3 released can be oxidized by HNO_3:

$$5\ NH_3 + 3\ HNO_3 \Leftrightarrow 4\ N_2 + 9\ H_2O \quad (2a)$$

3) Sulfate Reduction:

$$(CH_2O)_{106}(NH_3)_{16}H_3PO_4 + 53\ SO_4^{2-} \Leftrightarrow 106\ CO_2 + 53\ S^{2-} + 16\ NH_3 + H_3PO_4 + 106\ H_2O \quad (3)$$

and reactions for both carbon and nitrogen in estuarine and open ocean environments (Cifuentes *et al.*, 1988a; Mariotti *et al.*, 1984; Altabet, 1988). Processes such as algal assimilation of nitrogen (e.g., NH_4^+, NO_3^-, and NO_2^-), nitrification, denitrification and possibly organic decomposition can be followed with stable isotope tracers. Overall, the isotopic composition of both the dissolved and particulate pool of nitrogen is determined by the isotopic composition of the source material and any related isotopic fractionation in its formation or decomposition. To understand better the reaction pathways of the nitrogen, particularly near the oxygen-sulfide interface in stratified waters, the stable N isotope composition ($\delta^{15}N$) of dissolved ammonium and nitrate were determined from water samples taken from the Black Sea. Along with particulate nitrogen isotopic data, the transformations of nitrogen can be further elucidated. This information is extremely important in the understanding of the isotope biogeochemistry of material formed in the oxic surface waters and deposited in euxinic environments like the Black Sea. Once the variability and processes related to the formation of the nitrogen isotopic composition of particulate matter are understood, a more thorough interpretation of the $\delta^{15}N$ distribution in the sedimentary record can be made (Rau *et al.*, 1987).

Samples for nitrogen isotopic composition of dissolved ammonium and nitrate were obtained during the 1988 Black Sea Oceanographic Expedition on leg 3 (June 3-16, 1988). Two stations (Fig. 79) were occupied and water samples were taken from the R/V *Knorr* for full water column chemistry, Station 2 (BS3-2; 42°50'N 32°00'E) and Station 6 (BS3-6; 43°04'N 34°00'E).

The method for the preparation and nitrogen isotopic determination of dissolved ammonium is described in Velinsky *et al.* (1989). Briefly, an aliquot of the sample is adjusted to *pH*>9 using 6 M NaOH and distilled with a rapid steam distillation apparatus. The distilled ammonia is collected in a dilute acid trap and removed from solution by ion-exchange onto a zeolite. The nitrogen isotopic composition of dissolved nitrate is accomplished by the method described by Mariotti and Letolle (1978) and Horrigan *et al.* (unpublished). Dissolved nitrate is reduced to ammonia using Devarda's Alloy (Cu-Al-Zn) in a basic solution. The ammonia generated is distilled with a conventional distillation apparatus, into a dilute acid and zeolite trap (Velinsky *et al.*, 1989). The zeolite and particulate N is analyzed for the nitrogen isotopic composition ($\delta^{15}N$) of both ammonium and nitrate by a modified Dumas combustion technique (Macko, 1981). The data are reported in the standard δ notation {i.e., $\delta^{15}N = [(R_{sample}/R_{standard})-1]10^3$; where $R = {}^{15}N/{}^{14}N$} and the ratios are reported against air ($\delta^{15}N = 0$). Precision of replicate samples for ammonium and nitrate isotopic analysis is approximately ± 0.5 ‰ and ± 1.0 ‰, respectively.

The concentration and isotopic composition of dissolved ammonium and nitrate varied with depth in the water column (Figs. 80 and 81). Ammonium concentrations (Fig. 80) in the surface waters (0-80 m) were close to the detection limit and

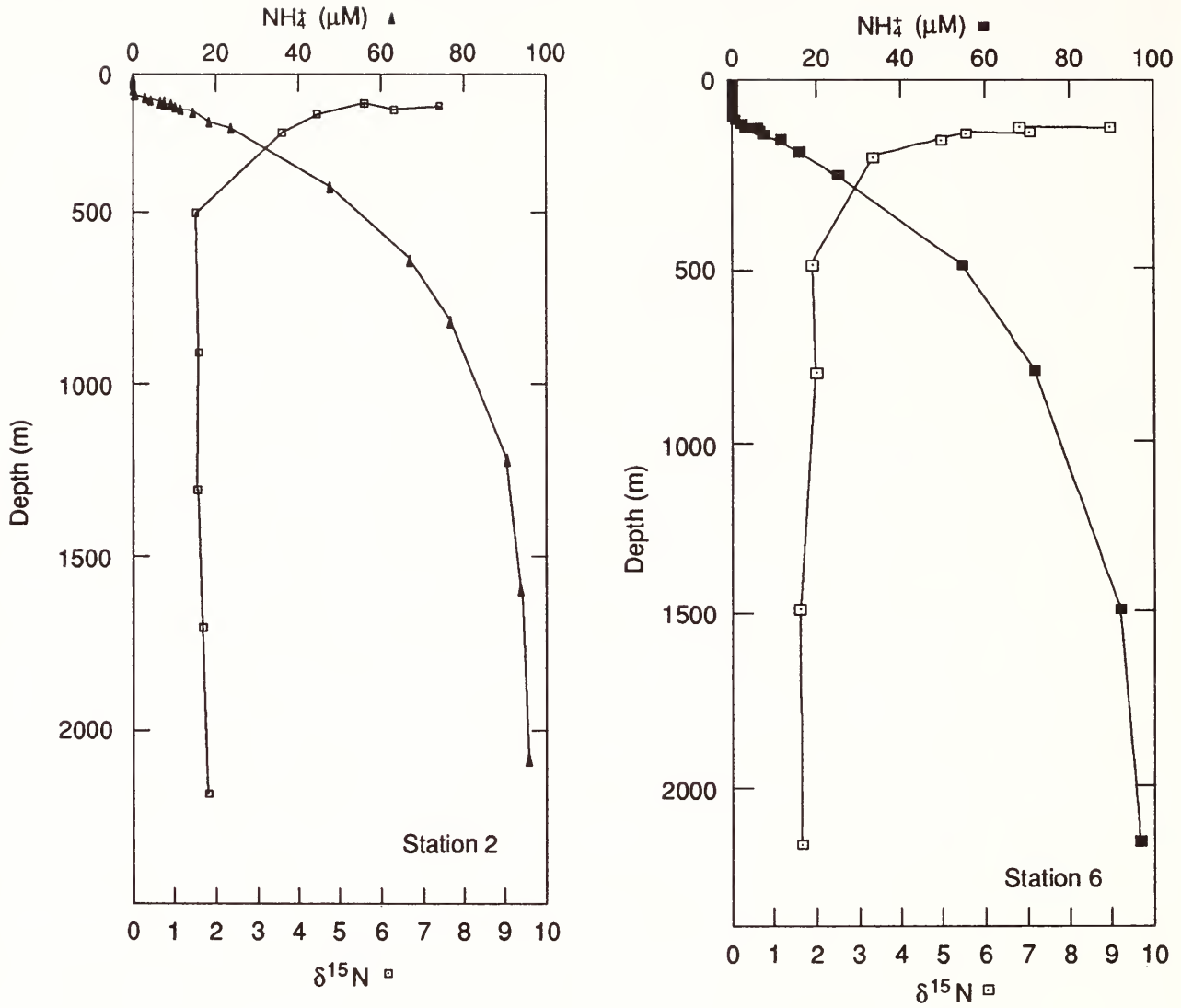

FIG. 80. Concentration and nitrogen isotopic composition of dissolved ammonium with depth in the Black Sea at Stations 2 and 6.

reflected biological uptake. Below 80 m, with the onset of sulfate reduction, ammonium concentrations increased from less than 0.2 to about 20 μM at 200 m and up to 90 μM by 2000 m. Nitrate concentrations exhibited a broad maximum of 6.5 μM near the middle of the sub-oxic zone (Fig. 81). A slight overlap between nitrate and ammonium distributions near 85 m was indicative of the oxidation of ammonium to nitrate. The presence of nitrite which is an intermediate in the oxidation of ammonium to nitrate during nitrification is further evidence for this process (Murray *et al.*, 1989a,b).

The distribution of isotopic ratios of ammonium and nitrate are presented in Figs. 80 and 81. The $\delta^{15}N$ of ammonium at depths greater than 500 m was uniform for both stations (1.71 ± 0.16 ‰, n=9). Above 500 m dramatic shifts occurred in the nitrogen isotopic composition of ammonium. As the concentration of ammonium decreased toward the interface, the $\delta^{15}N$ of ammonium increased. At station 6 for example, the $\delta^{15}N$ increased from ca. 1.9 ‰ at 500 m to 9.0 ‰ at 95 m. A similar distribution was observed at station 2. The

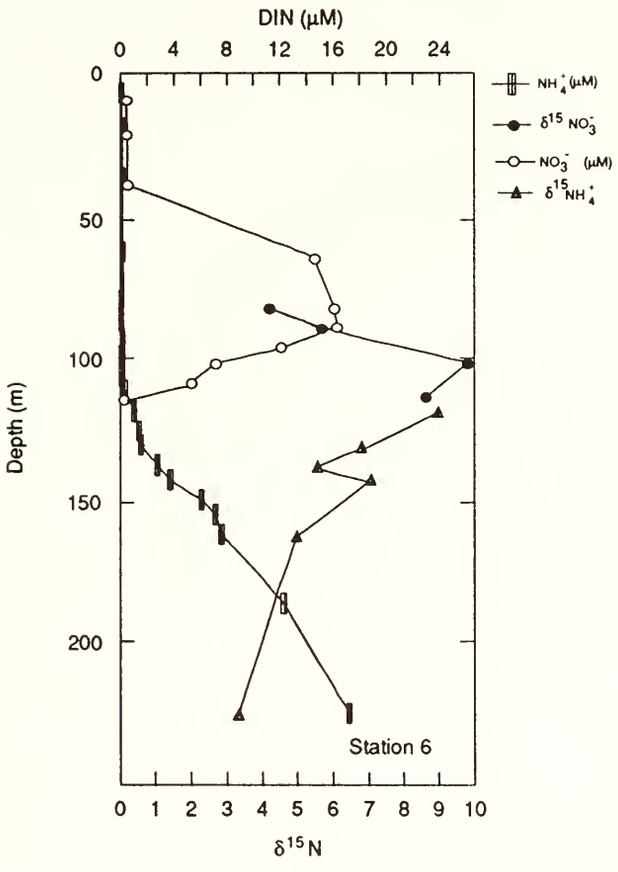

FIG. 81. Concentrations and nitrogen isotopic composition of dissolved ammonium and nitrate in the upper water column of the Black Sea at Station 6. (DIN = dissolved inorganic nitrogen)

more positive isotope ratios for ammonium are indicative of isotopic fractionation during the consumption or oxidation of ammonium (see below).

The $\delta^{15}N$ of nitrate also changed considerably with depth. At station 6, the $\delta^{15}N$ of nitrate increased with depth from 4.2 ‰ at 50 m to 9.8 ‰ just below the nitrate concentration maximum. Bazylinski *et al.* (1988) measured maximum denitrification rates below this maximum at station 2 during leg 2 (May 1988). The transformation of nitrate to N_2 by denitrification (Table 16) induces a large isotopic fractionation (ε; where $\varepsilon = (\alpha - 1)10^3$) of approximately -30 ‰ (Cline and Kaplan, 1975). Therefore, the residual nitrate should be enriched in ^{15}N. The more positive $\delta^{15}N$ values of nitrate below the nitrate concentration maximum could be explained by high denitrification rates at depth. Similar observations of $\delta^{15}N$ of nitrate and denitrification zones occurred at station 2 (data not shown).

An advection-diffusion model was used to calculate the consumption or production of ammonium in the water column of the Black Sea with a final goal of understanding isotope fractionation and biogeochemical processes in nitrogen cycling. This model is similar to that developed by Craig (1969) and Craig and Weiss (1970). Because the data set for station 6 is more complete, only this station was used for the advection-diffusion model.

The general equation for the advection, diffusion and reaction of a chemical species within a water system is (Craig, 1969):

$$K\partial^2 C/\partial z^2 - \omega\, \partial C/\partial z + J = 0. \qquad (1)$$

This particular form of the equation assumes steady state conditions where K is the vertical eddy diffusion coefficient, ω is the vertical advection velocity, J is the production or consumption of ammonium (C). It assumes only vertical water movement (i.e., where z is positive upward) and is valid only in the linear portion of the potential temperature-salinity profile. In this case, J [equation (1)] was fitted by an exponential term ($J = J_o e^{-\mu z}$), where μ is the decay constant for ammonium consumption or production with depth (z). The equation was first solved in terms of K/ω (Craig, 1969) for stable conservative elements (i.e., potential temperature and

salinity). K/ω is a mixing parameter for species that do not undergo any reaction during two end-member mixing. Once K/ω was determined, the model was solved for stable nonconservative species (i.e., ammonium) in terms of J_o/ω and μ. The use of this type of model and its limitations is discussed by Craig (1969), Craig and Weiss (1970) and Spencer and Brewer (1971).

The solution of equation (1), fitted to the salinity data, yielded a K/ω of 127 m, which is in excellent agreement with the results of Spencer and Brewer (1971). The model was run for a constant J and exponentially fitted J (see above) and both solutions gave similar results. The median J within our mixing interval (90 to 800 m) is $-3.8 \bullet 10^{-2}$ μM NH_4^+/kg yr, where $\mu = -2.80$ km^{-1}. The negative sign means that ammonium was being consumed. This median consumption rate occurs at a depth of 390 m below the surface. Fig. 82 shows the fitted data with an exponentially decreasing J and with a model run with $J = 0$. The consumption rate of $-3.8 \bullet 10^{-2}$ μM NH_4^+/kg yr was approximately three times lower than that derived by Brewer and Murray (1973). Station to station variability and different mixing intervals could be the reason for this difference (Spencer and Brewer, 1971; Murray *et al.*, 1989). In any case, the ammonium taken up in this interval, could be oxidized via nitrification or consumed by other chemoautotrophic or heterotrophic bacteria around the interface. Both of these processes are enzymatically mediated, thus a normal isotope effect (i.e., ^{14}N is taken up at a faster rate then ^{15}N) was expected.

Qualitatively, the ammonium in the mixing interval became more enriched in

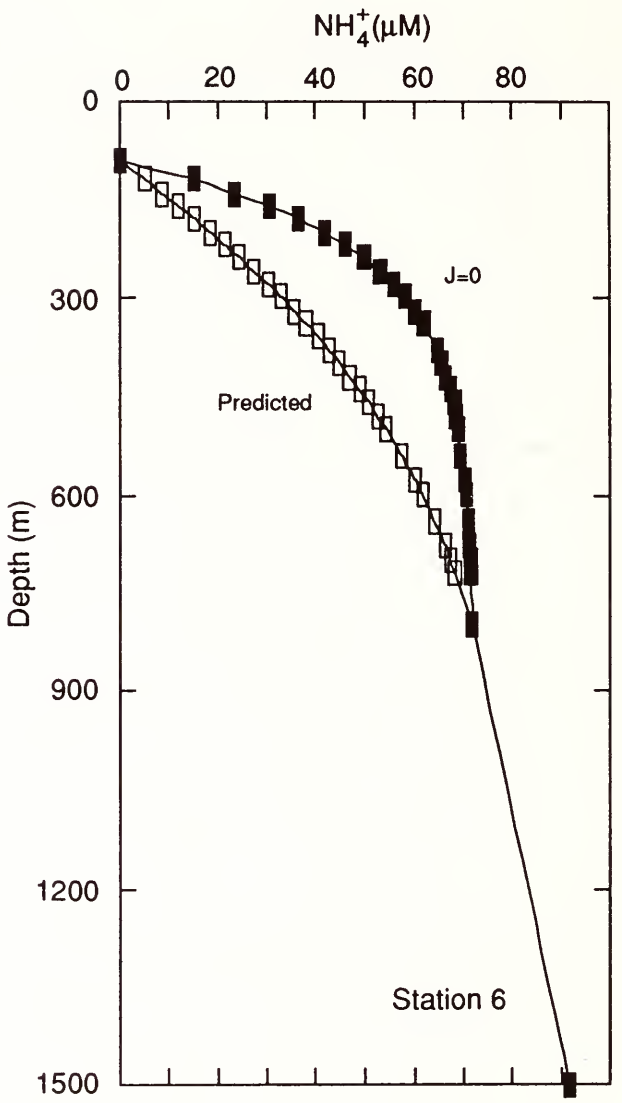

FIG. 82. Advection-diffusion model results for both predicted ammonium concentrations assuming J decreases exponentially with depth (predicted) and with no production or consumption ($J = 0$).

^{15}N compared to that in bottom waters (Fig. 80). In other words, as ammonium was consumed, the residual ammonium became enriched in ^{15}N. Isotopic fractionation by bacteria has been determined by Hoch *et al.*, (this Report) for the bacterium *Vibrio harveyi*. Fractionation values, ε, varied between -15 to -22 ‰ during growth on ammonium as the sole nitrogen source. Chemosynthetic uptake by bacteria of ammonium near the interface of the Black Sea (Brewer and Murray, 1973) is therefore

associated with a normal isotope effect because the residual ammonium becomes increasingly heavier as it was consumed. Our calculations, based on a closed system, yielded a fractionation, ε, of -3.7 ‰ between the mixing interval of 90 to 800 m. Closed system calculations will yield smaller isotope fractionations than those calculated from open system models, because ^{14}N is constantly diffusing upward and reacting faster (i.e., an open system) than ^{15}N. We are presently developing an advection diffusion model taking into account isotopic fractionation during the uptake of ammonium. This type of equation has been used to model the isotopic composition of nitrate in the low oxygen zone of the North East Pacific (Cline and Kaplan, 1975).

In summary, two distinct processes appear to be occurring near the interface (< 200 m) of the Black Sea; 1) denitrification and 2) chemosynthetic production of organic matter. Both processes result in distinct isotopic ratios for both ammonium and nitrate. Below the nitrate concentration maximum, the concentration of nitrate decreases due to denitrification. This is further evidenced by the increase in ^{15}N below the nitrate concentration maximum (Fig. 81). Ammonium concentrations start to increase because sulfate reduction and related ammonium production (Table 16) were faster then both transport and consumption. However, our model results show that there is a net consumption of ammonium most likely associated with bacterial chemosynthetic production near the interface. As the bacteria consume ammonium, the residual ammonium becomes increasingly enriched in ^{15}N.

The nitrogen isotope fractionation during the chemosynthetic uptake of dissolved ammonium was calculated using closed system assumptions. While the fractionation for closed system calculations yielded an ε of -3.7, calculations based on more realistic open system assumptions will yield a slightly greater fractionation value. It will be of interest to compare these results with model calculations from other anoxic environments such as the Framvaren Fjord and the Saanich Inlet. These data would help eventually determine the controls on the isotopic composition of material formed in the water column and eventually buried in anoxic marine environments.

References

Altabet, M. A., Variations in nitrogen isotopic composition between sinking and suspended particles: implications for nitrogen cycling and particle transformation in the open ocean, *Deep Sea Res.*, *35*, 535-554, 1988.

Bazylinski, D. A., B. L. Howes, and H. W. Jannasch, Denitrification, nitrogen fixation and nitrous oxide concentrations through the Black Sea oxic-anoxic interface, *EOS*, *69*, 1241, 1988.

Brewer, P. G., and J. W. Murray, Carbon, nitrogen and phosphorus in the Black Sea, *Deep Sea Res.*, *20*, 803-818, 1973.

Cifuentes, L. A., J. H. Sharp, and M. L. Fogel, Stable carbon and nitrogen isotope biogeochemistry in the Delaware estuary, *Limnol. Oceanogr.*, *33*, 1102-1115, 1988a.

Cifuentes, L. A., M. L. Fogel, J. R. Pennock, and J. H. Sharp, Seasonal variations in the stable nitrogen isotope ratio of ammonium in the Delaware Estuary, *Annual Report of the Director of the Geophysical Laboratory, Carnegie Instn. Washington, 1987-1988,* Geophysical Laboratory, Washington, D. C., 114-121, 1988.

Cline, J. D., and I. R. Kaplan, Isotopic fractionation of dissolved nitrate during denitrification in the eastern tropical North Pacific Ocean, *Mar. Chem.*, *3*, 271-299, 1975.

Craig, H., Abyssal carbon and radiocarbon in the Pacific, *J. Geophys Res.*, *74*, 5491-5506, 1969.

Craig, H., and R. F. Weiss, The Geosecs 1969 intercalibration station: Introduction, hydrographic features, and total CO_2-O_2 relationships, *J. Geophys. Res.*, *75*, 7641-7647, 1970.

Macko, S. A., Stable nitrogen isotope ratios as tracers of organic geochemical processes, Ph. D. dissertation, Univ. of Texas at Austin, 1981.

Mariotti, A., C. Lancelot, and G. Billens, Natural isotopic composition of nitrogen as a tracer of origin for suspended organic matter in the Scheldt Estuary, *Geochim. Cosmochim. Acta*, *48*, 549-555, 1984.

Mariotti, A. and R. Letolle, Analyse isotopique de l'asote au niveau des abondances naturelles, *Analusis*, *6*, 421, 1978.

Murray, J. W., H. W. Jannasch, S. Honjo, R. F. Anderson, W. S. Reeburgh, Z. Top, G. E. Friederich, L. A. Codispoti, and E. Izdar, Unexpected changes in the oxic/anoxic interface in the Black Sea, *Nature*, *338*, 411-413, 1989a.

Murray, J. W., and E. Izdar, The 1988 Black Sea oceanographic expedition: Overview and new discoveries, *Oceanography*, *1*, 15-21, 1989b.

Rau, G. H., M. A. Arthur, and W. E. Dean, $^{15}N/^{14}N$ variations in Cretaceous Atlantic sedimentary sequences: implications for past changes in marine nitrogen biogeochemistry, *Earth Planet. Sci. Lett.*, *82*, 269-279, 1987.

Richards, F. A., Anoxic basins and fjords, in *Chemical Oceanography*, J. P. Riley and G. Skirrow, eds., pp. 1-41. Academic Press, New York, 1965.

Spencer, D.W., and P. G. Brewer, Vertical advection diffusion and redox potentials as controls on the distribution of manganese and other trace metals dissolved in waters of the Black Sea, *J. Geophys. Res.*, *76*, 5877-5892, 1971.

Velinsky, D. J., J. R. Pennock, J. H. Sharp, L. A. Cifuentes, and M. L. Fogel, Determination of the isotopic abundance of dissolved ammonium-nitrogen from estuarine waters at the natural abundance level, *Mar. Chem*, *26*, 351-362, 1989.

Mineralogical and Oxygen Isotope Analyses of Manganese Oxides Precipitated by Spores of a Marine Bacterium

Kevin W. Mandernack, Marilyn L. Fogel, Bradley M. Tebo, and Jeffrey Post***

Manganese(II) [Mn(II)] oxidation in the environment is generally catalyzed by bacteria (Nealson *et al.*, 1988). The mechanism of this process, however, is poorly understood, as are the products of microbial Mn oxidation. In recent experiments, Hastings and Emerson (1986) utilized the catalytic properties of spores of a marine bacillus (SG-1) to perform laboratory Mn (II) oxidation experiments under environmentally significant conditions of pH and Mn (II) concentration. They concluded that the concentration of Mn (II) in seawater and the oxidation state of marine Mn oxides are controlled by the rapid precipitation of hausmannite (Mn_3O_4), which can be microbially mediated. The Mn_3O_4 rapidly undergoes abiotic disproportionation to MnO_2 because of low Mn(II) concentrations typically found in the marine environment.

Hastings and Emerson's (1986) work supports the model of Hem and Lind (1983) in which manganese oxidation is believed to occur in two steps (Fig. 83). In the laboratory at 25°C, the initial product is hausmannite, which can spontaneously protonate to manganite, γ-MnOOH (Murray *et*

* Scripps Institution of Oceanography, La Jolla, CA 92093

** Smithsonian Institution, Washington, D. C. 20550

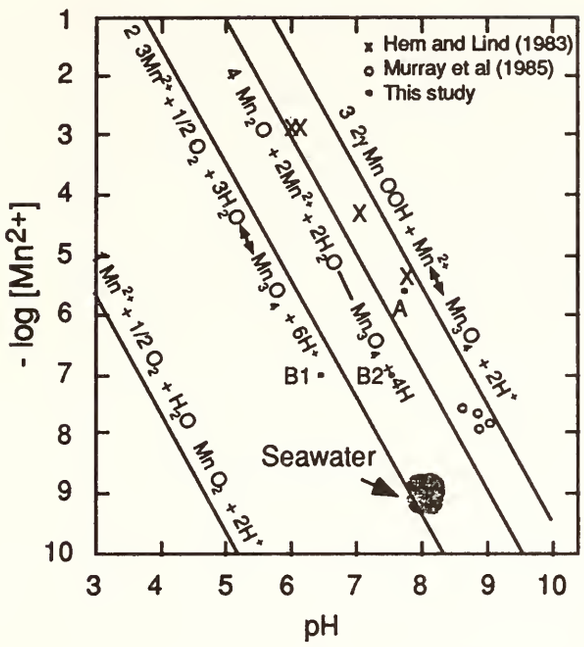

FIG. 83. [Taken from Hastings and Emerson, 1986]. Dissolved Mn^{2+} activity - *pH* equilibrium relationships in aerated solutions (based on the work of Hem and Lind, 1983). Each line represents the equilibrium for the reaction written. Based on these lines and with Mn and pH values, it is possible to predict which Mn phase is thermodynamically stable. A solution with Mn and *pH* values to the right of line 2 would be expected to precipitate Mn_3O_4. Data points from Hem and Lind (1983), Murray *et al.*, 1985 and Hastings and Emerson (1986; referred to this figure as "this study") are shown as well as the field which represents typical seawater Mn concentration and *pH*.

al., 1985; Piper *et al.*, 1984). Theoretically, MnO_2, which has an oxidation state of 4+, results from a disproportionation of Mn_3O_4. In laboratory experiments that lasted up to 9 months, however, the highest oxidation state observed was 3+ except under more extreme conditions of high temperature or *pH* (Murray *et al.*, 1985). This fact is rather enigmatic considering that manganese in the oceans is usually highly oxidized (Kalhorn and Emerson, 1984; Murray *et al.*, 1984; Piper *et al.*, 1984). Hastings and Emerson (1986) suspected that more oxidized phases did not form in their experiments because of high concentrations of dissolved Mn(II).

Representative strains of bacteria that could be responsible for Mn oxidation in the ocean have been observed to precipitate high-oxidation state manganese oxides (≥3+), even at high dissolved Mn(II) concentrations in solution (Tebo, unpublished results). Because of the uncertainties that persist in the mechanisms of Mn oxide formation by these bacteria, we examined these processes with oxygen isotope tracer and x-ray powder diffraction studies on an array of oxides precipitated by SG-1 spores.

The oxygen isotopic composition of dissolved atmospheric oxygen is very different from that of water. Thus, the relative proportions of these two oxygen sources to Mn oxides can be traced. Molecular oxygen in air has a $\delta^{18}O$ of +23.5, whereas seawater has a $\delta^{18}O$ value of around 0 ‰ (Kroopnick and Craig, 1976). The percentage of oxygen in Mn oxides derived from both H_2O and O_2 can be predicted depending on the mechanism that is proposed for manganese oxide formation. The model of Hem and Lind (1983), for example, predicts that 25% of the oxygen in hausmannite should come from dissolved O_2. In contrast, MnO_2 minerals formed by direct precipitation from seawater without an intermediate would be expected to have 50% of the oxygen from dissolved O_2, as in the following equation:

$$Mn^{2+} + 1/2\ O_2 + H_2O \Leftrightarrow MnO_2 + 2H^+. \quad (1)$$

In this paper preliminary results of mineralogical and stable oxygen isotope investigations of Mn oxides produced by

SG-1 spores in buffered seawater or deionized distilled water with varying Mn concentration and temperature are presented. The dual approach is useful for (1) establishing the identity of the mineral phase formed under given conditions, and (2) determining the portion of the oxygen atoms in the Mn oxide product that is derived from either dissolved oxygen or water

The marine bacillus bacterium SG-1 is unique since only spores, a dormant nonmetabolic resting stage in the life cycle of the bacterium, are capable of oxidation while the growing vegetative cells are not (Nealson and Ford, 1980; Rosson and Nealson, 1982). SG-1 is able to oxidize Mn(II)

TABLE 17. Mineralogy of Mn Oxides Produced by SG-1 Spores

	[Mn (II)]	3°C	RT	50°C	70°C
Seawater	10 μM	todorkite(?)	ND	ND	ND
	100 μM	buserite→ birnessite	buserite → birnessite	todokorite(?)	todorokite(?)
	1 mM	todorokite(?)	todorokite(?)	todorokite(?)	hausmannite
	10 mM	U	manganite,	manganite & feitknechtite(?),	hausmannite, trace manganite &
			$MnCO_3$(?)	hausmannite	trace $MnCO_3$
Distilled H_2O	10 μM	birnessite(?) 8.9Å phase	ND	ND	ND
	100 μM	buserite → birnessite	buserite → birnessite	U (10Å phase)	hausmannite
	1 mM	ND	feitknechtite(?), manganite	hausmannite	hausmannite
	10 mM	feitknechtite → manganite, groutite (?)	manganite > hausmannite	hausmannite trace manganite	hausmannite

RT = Room temperature
ND = Not determined
U = Unknown phase
? = Tentative identification
→ = Process that apparently occurred upon drying

over a wide range of temperatures (2-80°C) and Mn concentrations (10 nM to 10 mM), in both seawater and distilled water. The use of SG-1 spores as a catalyst permitted sufficient amounts of manganese oxides to form within a short time frame so that the objectives of this study could be met. SG-1 was grown to a fully sporulated state in a 20 mM HEPES buffered (*pH* 7.5) seawater medium containing 0.5 g yeast extract and 2 g peptone per liter and 100 μM $MnCl_2$. The spores were harvested by centrifugation and purified to remove any remaining vegetative cells and cell debris.

The SG-1 produced Mn oxides were prepared in 0.22 μm filtered seawater (SW) or in deionized-distilled water (DW). Additions of 1 M $MnSO_4$ and 1 M HEPES buffer (20 mM final concentration, pH 8.0) were followed by inoculation with SG-1 spores (Table 17). The oxides were prepared during 2 week incubations. The oxides that were formed were collected by centrifugation and washed with DW. They were stored wet and frozen until analysis.

Powder x-ray diffraction patterns were collected for the oxides at the Smithsonian Institution on a *Scintag*™ automated diffractometer with copper K_α radiation. The oxides were analyzed wet because drying can change the crystal structure of certain manganese oxides (Paterson *et al.*, 1986).

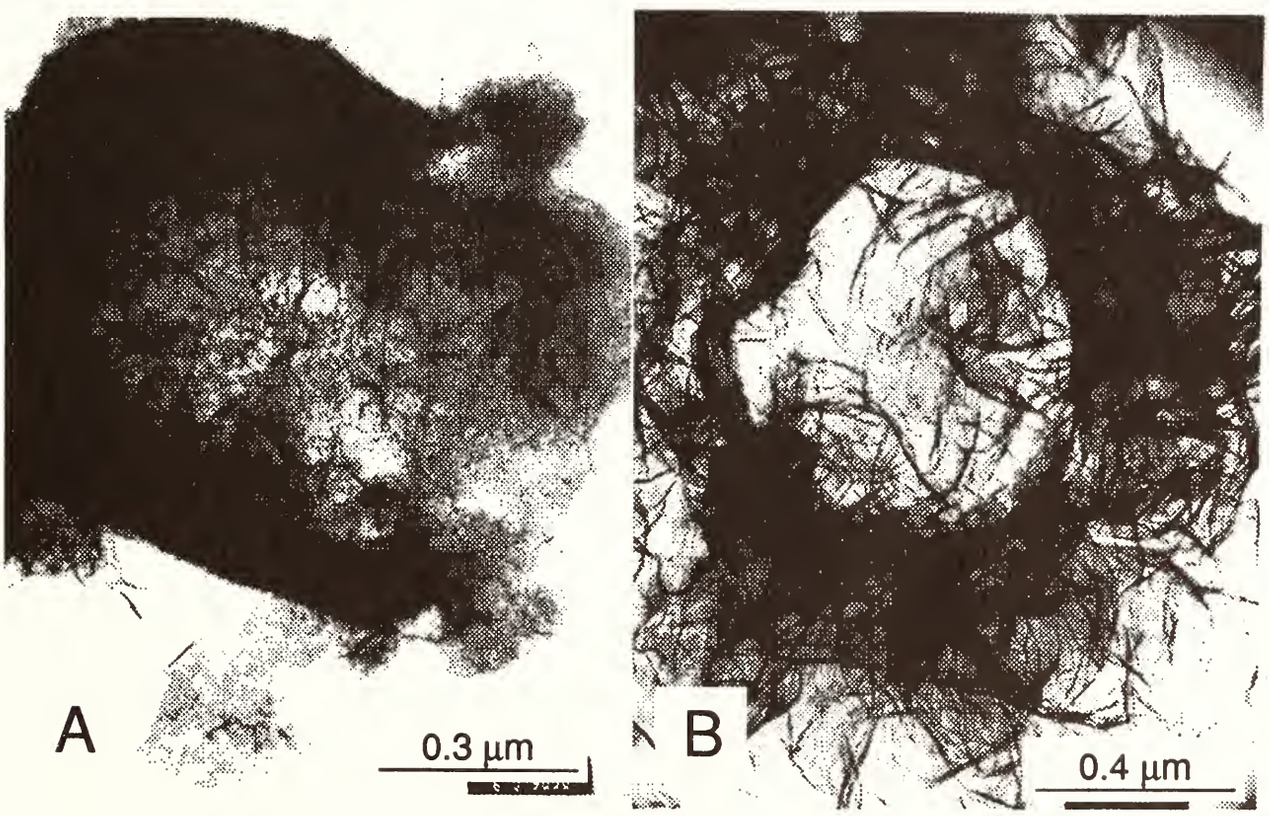

FIG. 84. Transmission electron micrographs of spores before (A) and after (B) organic matter extraction. Spores in Figure 84a were grown at 3°C in 10mM Mn. Spores in Figure 84b were grown at 25°C in 100μm Mn. Note the amorphous Mn minerals coating the spore wall. In Figure 84a, two different types of Mn minerals are present: wavey sheets and granular material.

Some of the oxides were finely crystalline or poorly ordered, and consequently could not be positively identified. Table 17 shows the inferred mineralogy based on the XRPD results and the conditions under which the oxides formed. Transmission electron microscopy was performed on several of the samples at the Department of Earth Sciences, Johns Hopkins University, by Jill Banfield (Fig. 84).

The microbially-produced oxides were extracted to remove organic material prior to $\delta^{18}O$ determination. The method that proved the most efficient without altering the isotopic composition of the oxides was a modification of a DNA purification procedure, followed by hypochlorite treatment at 4°C. Frozen cells with oxide coatings were sequentially extracted with phenol, chloroform, and methanol with a final wash with DW. This final residue was treated with dilute (3%) hypochlorite overnight at 4°C. The oxide was washed extensively with DW and dried *in vacuo* at 50°C.

The fluorination method with BrF_5 was used for determining the $\delta^{18}O$ of silicates

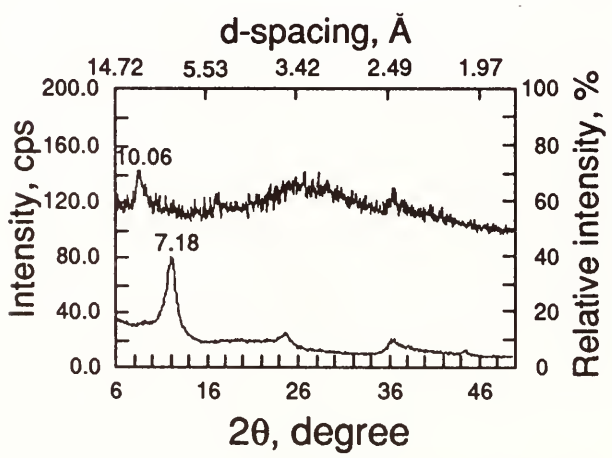

FIG. 85. X-ray powder diffraction pattern of manganese mineral before (10Å peak) and after (7Å peak) drying. Spores were cultured in distilled water at 3°C in 0.1 mM Mn

(Clayton and Mayeda, 1963). For most analyses duplicate samples of 3 to 7.5 mg of Mn oxide were reacted at 600°C for ≥ 18 hr for the highest yields. The error of the analysis for the $\delta^{18}O$ of technical grade MnO_2 was ±0.5 ‰.

Broad interpretations can be made from Table 17 regarding Mn oxide mineral formation. In general, hausmannite formed at high temperatures and higher Mn concentrations in both DW and SW. Subsamples collected from the 10 mM DW and SW preparations after 4 days incubation at 50 and 70 °C were essentially completely composed of hausmannite (data not shown). Conversely, those that incubated for 2 weeks usually contained a significant amount of manganite (Mn(III)). The shift in mineral structure with time may indicate that the hausmannite was protonating to manganite as indicated in reaction 2. Protonation may occur faster at lower temperatures, as the oxides from 10 mM solutions at room temperatures were composed mostly of manganite.

In general, higher oxidation state oxides were observed to form under conditions of lower Mn concentration and lower temperature. Qualitatively, this is what would be predicted from thermodynamics (Fig. 83). Buserite was evidently precipitated at 100 μM Mn at 3°C and room temperature in both waters. The XRPD patterns for these samples showed the characteristic collapse of a 10Å peak to 7Å upon drying (Fig. 85). The 7Å phase is presumed to have a birnessite-type structure.

Manganese minerals from the seawater incubations appeared as buserite or re-

TABLE 18. Isotope Ratios of Manganese Minerals Precipitated from SG-1 Spores

[Mn]	Medium	T °C	$\delta^{18}O$ H_2O	$\delta^{18}O$ O_2	$\delta^{18}O$ Min	$\%H_2O$	$\%O_2$
				Hausmannite			
1 mM	DW	50	-9.5	23.5	-10.3	100	0
10 mM	DW	70	-9.5	23.5	-11.9	100	0
1 mM	SW	70	0.0	23.5	2.5	89	11
				Birnessite			
1 mM	DW	25	-9.5	23.5	-0.2	72	28
				Todorokite			
100 µM	SW	25	0.0	23.5	7.7	67	33
1 mM	SW	50	0.0	23.5	8.9	62	38

sembled a disordered todorokite with a fixed d-spacing near 10Å. Todorokite was tentatively identified based on the characteristic 10Å peak both before and after drying. Todorokite-like phases were only observed in the seawater incubations, and therefore the interaction with the other cations in seawater may be significant in the mineral formation.

Spores were cultured in distilled water or seawater with air as the source of oxygen. The source of the oxygen to the manganese minerals and therefore, the mechanism of formation, was elucidated using the following mass balance equation:

$$(\delta^{18}O\ H_2O)(\%\ O\ \text{from}\ H_20) + (\delta^{18}O\ O_2)(\%\ O\ \text{from}\ O_2) = \delta^{18}O\ \text{Mn oxide} \quad (2)$$

The determination is approximate as there is a ±0.5 ‰ uncertainty in the isotopic analysis of the Mn oxide. The calculation also assumes negligible isotopic fractionation in the incorporation of both water and dissolved O_2. Studies with slightly ^{18}O-enriched water and oxygen in comparable minerals gave similar results with the same equation (Tebo *et al.*, 1987).

The percentage of H_2O-derived oxygen in the minerals decreased with increasing oxidation state (Table 18). The $\delta^{18}O$ of hausmannite was always slightly more negative than that of the water in which the precipitation occurred. Based on equation (1), all of the oxygen in the mineral must have originated from water, unless the mineral freely exchanged its oxygens with water. The possibility of rapid and total

exchange of the isotopic signature in the manganese minerals was tested previously (Tebo *et al.*, 1987). Only 10% of the oxygens in manganite exchanged after 12 months. One hausmannite sample containing manganite yielded a $\delta^{18}O$ that was +2.5 more positive than that of the water. Tebo *et al.* (1987) had previously measured the isotopic composition of synthetic manganite, and concluded that approximately 75% of its oxygen came from water and the remaining portion from dissolved O_2.

The higher oxidation state oxides contain between 62 to 72% oxygen from water and the remainder from dissolved oxygen (28-38%). Because no dissolved oxygen signal was measured in the Mn_3O_4, the reaction mechanism for Mn oxidation must be different from that proposed by Hem and Lind (1983) and Hastings and Emerson (1986). Equation (1) and the following equation are closer representations of the reaction mechanism indicated by isotopic analysis:

$$Mn^{2+} + 1/4\ O_2 + 3/2\ H_2O \Leftrightarrow Mn(III)OOH + 2H^+. \qquad (3)$$

The minerals formed by the spores were commonly mixtures of mineral phases (Table 17). Accordingly, the variability in the isotopic results for a particular set of growth conditions is most likely the byproduct of the analysis of these mixtures.

In summary, both x-ray powder diffraction and isotopic tracer studies confirm that manganese oxides are precipitated by a different mechanism from that proposed previously for chemical precipitates and for spore catalyzed oxides. No traces of hausmannite or manganite were found in minerals precipitated at low Mn concentration. If hausmannite were the initial product in the formation of the higher oxidation state oxides, oxygen bonds in the crystal lattice must be broken and reformed during the rearrangement of structure to buserite or todorokite. The involvement of molecular oxygen is indicated by isotopic ratios of these two oxides, rather than in the initial formation of hausmannite itself. With better quantitative mineral identification we should be able to determine whether Mn oxidation mechanisms for chemically driven systems are the same as those catalyzed by living organisms.

References

Clayton, R. N., and T. K. Mayeda, The use of bromine pentafluoride in the extraction of oxygen from oxides and silicates for isotopic analysis, *Geochim. Cosmochim. Acta, 27,* 43-52, 1963.

Hastings, D., and S. Emerson, Oxidation of maganese by spores of a marine Bacillus: kinetic and thermodynamic considerations, *Geochim. Cosmochim. Acta, 50,* 1819-1824, 1986.

Hem, J. D., Redox coprecipitation mechanisms of manganese oxides: particulates in water, in *Advances in Chemistry, Series No. 189,* M. C. Kavanaugh and J. O. Lecke, eds., American Chemical Society, Washington, D. C., pp. 45-72, 1980.

Hem, J. D., and C. J. Lind, Nonequilibrium models for predicting forms of precipitated manganese oxides, *Geochim. Cosmochim. Acta, 47,* 2037-2046, 1983.

Kalhorn, S., and S. Emerson, The oxidation state of manganese in surface sediments of the Pacific Ocean, *Geochim. Cosmochim. Acta, 48,* 897-902, 1984.

Kroopnick, P. and H. Craig, Oxygen isotope frac-

tionation in dissolved oxygen in the deep sea, *Earth Planet. Sci. Lett., 32*, 375-388, 1976.

Murray, J. W, L. S. Balistrieri, and B. Paul, The oxidation state of manganese in marine sediments and ferromanganese nodules, *Geochim. Cosmochim. Acta, 48,* 1237-1247, 1984.

Nealson, K. H., and J. Ford, Surface enhancement of bacterial manganese oxidation: Implications for aquatic environments, *Geomicrobiol. J., 2,* 21-37, 1980.

Nealson, K. H, B. M. Tebo, and R. A. Rosson, Occurrence and mechanisms of microbial oxidation of manganese, *Adv. Appl. Microbiol., 33,* 279-318, 1988.

Paterson, E, J. L. Bunch, and D. R. Clark, Cation exchange in synthetic manganates: I. alkylammonium exchange in a synthetic phyllomanganate, *Clay Minerals, 21,* 949-955, 1986.

Piper, D. Z, J. R. Basler, and J. L. Bischoff, Oxidation state of marine manganese nodules, *Geochim. Cosmochim. Acta, 48*, 2347-2355, 1984.

Rosson, R. A., and K. H. Nealson, Manganese binding and oxidation by spores of a marine bacillus, *J. Bacteriol., 151,* 1027-1034, 1982.

Tebo, B. M, M. L. Fogel, A. T. Stone, and K. W. Mandernack, Oxygen isotope tracers of manganese oxide precipitation, *EOS, 68*, 1702, 1987.

Separation and Purification of Phosphates for Oxygen Isotope Analysis

Ellen K. Wright and Thomas C. Hoering

Oxygen isotope analysis of biogenic, marine phosphates is a potentially powerful tool for determining the temperature of ancient oceans because phosphates are more resistant towards isotope exchange during diagenesis than the conventionally-used carbonates. However, published temperatures deduced from analyses of phosphates indicate several problems. Some of these are clearly extrinsic such as unknown isotopic composition of the ocean water through time. However, others may be inherent in the analytical methods and these problems will be discussed here.

There are stringent requirements for an analytical method designed to measure stable oxygen isotope ratios in geological materials. First, all steps must be either quantitative, in order to avoid isotope fractionation due to incomplete yields, or else a reproducible fraction of the sample must be converted. Second, there must be no addition of extraneous oxygen through contamination, memory effects, or isotope exchange induced during the analysis. Three, the final product to be introduced into the mass spectrometer must be free of spectral contaminants. These criteria were used in the design of an analytical method for the isotopic analysis of phosphates. As will be seen below, requirements one and three are probably met, but two presents difficulties.

A published method (Tudge, 1960) involves bringing the phosphate into solution with nitric acid and then oxidizing any organic matter with potassium permanganate. This is followed by three successive purification steps wherein the sample is first precipitated as ammonium phosphomolybdate which is filtered, dissolved and precipitated as magnesium ammonium phosphate. This compound is dissolved and finally precipitated as bismuth phosphate, which is heated to remove water of crystallization. Oxygen is extracted from anhydrous bismuth phosphate by reaction with bromine pentafluoride at 250°C. The

oxygen is then converted to carbon dioxide for analysis in the mass spectrometer.

This method can be considerably simplified by substituting the lengthy precipitation and dissolution steps with an ion exchange separation method and then precipitating non-hydrating silver phosphate instead of bismuth phosphate. In the first step, 30 to 60 mg of a calcium phosphate sample (~200 μM PO_4) is dissolved in 2 ml of 2 molar HF (digestion time ~24 hours). Calcium ions are precipitated as calcium fluoride and are removed by centrifugation. The resulting solution is pipetted off, and the residue is rinsed in 2 ml distilled water, centrifuged again, and the rinse water pipetted off and added to the solution.

The solution is neutralized with potassium hydroxide ~ 2.2 ml of 2 molar solution) and added to a disposable ion exchange column (6 ml volume) packed with a strong base anion exchange resin in the hydroxide form [*Amberlite*™ IRA-400(OH)]. The column is rinsed with distilled water until neutral and free of fluoride ions. Then the phosphate is eluted with 20-30 ml 0.5 Molar ammonium nitrate. The eluate is added to an ammoniacal solution of silver nitrate and precipitated as silver phosphate according to the method of Firsching (1961).

The phosphate concentration in the eluate was monitored by the method of Parsons *et al.* (1984a). Collecting fractions of eluate from a 200 µM PO_4 sample showed peak concentrations of phosphate ions between 1 and 12 ml eluate and only traces after 14 ml eluate. Care should be taken that all fluoride ions are removed from the column in the rinse step as fluoride interferes with formation of the blue color, which is used to monitor the phosphate concentration.

A large sample of potassium dihydrogen phosphate, KH_2PO_4 (> 99.97% pure) has been reserved as a oxygen isotope reference material. This compound is not hygroscopic and does not form a hydrate. Oxygen isotope analyses were done first on the potassium dihydrogen phosphate, then on silver phosphate precipitated directly from potassium dihydrogen phosphate, then on silver phosphate precipitated from potassium hydrogen phosphate processed through the anion exchange column, and finally on bismuth phosphate precipitated directly from potassium hydrogen phosphate. Each of these compounds was reacted with an excess of bromine pentafluoride at 300°C according to the procedure of Clayton and Mayeda (1963) to yield oxygen. The oxygen was converted to carbon dioxide by reaction with hot graphite. Also several samples of National Bureau of Standards phosphate standards (NBS 120b and NBS 120c) were processed through the columns and the isotopic values compared with the published values of Shemesh *et al.* (1983).

Results

The results are shown in Table 19. A sample of quartz, that had been analyzed previously in several laboratories, was used as a control. The published value for $\delta^{18}O$ of this material is +7.18 ‰ relative to Standard Mean Ocean Water. The value shown in Table 19 agrees within the precision of

measurement, proving that the extraction system and the mass spectrometry are functioning properly. The mean $\delta^{18}O$ of the potassium dihydrogen phosphate reference material (11.91 ‰) was higher than the mean $\delta^{18}O$ values of several batches of silver phosphate (11.76 to 10.05 ‰) and bismuth phosphate (10.55 ‰) precipitated directly from this reagent. The standard deviation of the potassium dihydrogen phosphate (0.2 ‰) was comparable with a standard deviation of 0.2 ‰ for the quartz run on the same extraction system. However, the standard deviation increased for the secondary precipitates (0.3 and 0.4 ‰ for the silver phosphates and 0.5 ‰ for the bismuth phosphate) and was highest for the column processed silver phosphates (0.6 to 1.0 ‰). The mean $\delta^{18}O$ of the column processed NBS 120b standard was 19.81 ‰ with a standard deviation of 0.8 ‰. The published values of Shemesh *et al.* (1983) are 20.1 ‰ and a standard deviation of 0.3 ‰.

The decrease of $\delta^{18}O$ values and the increase in the variance of the the silver phosphate precipitated from the potassium dihydrogen phosphate reference material may be caused by contaminants. Silver phosphate precipitated from phosphate ions purified by the ion exchange column has a different color (greenish or brownish yellow) and smaller crystal size than silver phosphate precipitated directly in an

TABLE 19. Summary of means and standard deviations of $\delta^{18}O$ of silver phosphate, bismuth phosphate, and quartz.

Compound	Yield(%) precipitate	mean δ^{18}(O‰)	Yield(%) CO_2	s.d.(‰)	N
KH_2PO_4	-	11.91	102	0.2	7
Ag_3PO_4*	100	11.76	104	0.4	8
Ag_3PO_4*	100	11.21	104	0.3	7
Ag_3PO_4* (silica free)	100	10.75	103	0.4	7
Ag_3PO_4* (column)	98	11.55	104	0.7	6
Ag_3PO_4* (column)	98	10.05	103	1.0	8
$BiPO_4$*	99	10.55	105	0.5	8
Ag_3PO_4 (from NBS 120b)	98	19.81	100	0.8	12
Ag_3PO_4 (from NBS 120c)	98	19.94	101	0.6	7
SiO_2 •		6.99	101	0.2	21

$\delta^{18}O = \{^{18}O/^{16}O_x/^{18}O/^{16}O_{std} - 1\}$ x 1000 where the subscript x refers to the unknown sample and std refers to standard Mean Ocean water.

* denotes that the compound is derived from the KH_2PO_4 isotope reference material.

• the published value for $\delta^{18}O$ of quartz is +7.18 ‰

ammoniacal solution from pure potassium dihydrogen phosphate. Possible contaminants are small inclusions of silver chloride and coatings of organic matter and silica on the silver phosphate crystals. The chloride ions stem from the ion exchange resin. The *Amberlite*™ IRA-400(OH) resin is mainly in the hydroxide form. However, a small amount of chloride ions is present, and attempts to eliminate it by flushing the resin with potassium hydroxide solution caused decomposition of the resin before complete elimination of the chloride.

The organic coatings stem from unavoidable decomposition of the anion exchange resin. Combustion of a silver phosphate sample that was derived from a column processed NBS 120c sample showed the presence of 0.3 weight percent carbon. The $\delta^{13}C$ of the carbon was -31 ‰. This low value is indicative of petrochemicals that were used to manufacture the exchange resin, and not of sedimentary carbonates contained in the NBS 120c sample, or from dissolved carbon dioxide co-precipitated as silver carbonate. Traces of silica were detected by microprobe analysis in some batches of silver phosphate. This contaminant would yield oxygen upon reaction with bromine pentafluoride. Silica was detected in the ammonium hydroxide used in the final precipitation step by the colorometric method of Parsons *et al.* (1984b). Silica-free ammonium hydroxide was produced by dissolving ammonia gas from a cylinder into distilled water and storing the solution in a *Teflon*™ bottle. Microprobe analysis of column processed and directly precipitated silver phosphate samples showed no detectable silica levels when silica-free ammonium hydroxide was used in the precipitation step.

Discussion

The silver phosphate procedure for analyzing oxygen is promising, although several problems remain to be solved. It is definitely easier and more rapid than previous methods and more amenable to processing large numbers of samples. The precision of measurement has steadily improved until it now rivals that of the bismuth phosphate method, although there seems to be a constant bias between the two methods. The procedure fulfills two of the three criteria described in the introduction. The wet chemistry steps are monitored by a sensitive and specific colorometric method. No losses of phosphate were detected in any of them. Firshing's (1961) method for precipitating silver phosphate is quantitative and accurate. The bromine pentafluoride method of Clayton and Mayeda (1963) has been used on silicates for many years and found to be completely reliable. Quantitative yields of carbon dioxide are obtained from pure silver phosphate by this method. The reproducible results on the control sample of quartz are encouraging.

The source of of the variance is most likely due to small and variable amounts of contaminants that are precipitated with the silver phosphate and yield oxygen on reaction with bromine pentafluoride. Future work will focus on finding the source of this contamination and methods for eliminating it. Reasons for the systematic differ-

ences between the silver phosphate and the bismuth phosphate will be sought.

It is unlikely that the problem is due to isotopic exchange of phosphate with water during the course of the analysis. Keisch *et al.* (1958), Bunton *et al.* (1961), and Tudge (1960) have shown that the phosphate ion is inert to exchange under all of the conditions used in this study.

References

Bunton, C. A., D. R. Llewellyn, C. A. Vernon, and V. A. Welch, The reactions of organic phosphates. Part IV. Oxygen exchange between and water and orthophosphatic acid, *J. Chem. Soc.* London, 1636-1640, 1961.

Clayton, R. N., and T. K. Mayeda, The use of bromine pentafluoride in the extraction of oxygen from oxides and silicates for isotopic analysis, *Geochim. Cosmochim. Acta., 27*, 43-54, 1963.

Firsching, F. H., Precipitation of silver phosphate from homogeneous solution, *Anal. Chem., 33*, 873-87, 1961.

Keisch, B., J. W. Kennedy., and A. C. Wahl, The exchange of oxygen between phosphoric acid and water, *J. Amer. Chem. Soc., 80*, 4778-4782, 1958.

Parsons, T. R., Y. Maita, and C. M. Lalli, Determination of phosphate, in *A Manual for Chemical and Biological Methods for Seawater Analysis*, Pergamon Press, New York, 22-25, 1984a.

Parsons, T. R., Y. Maita, and C. M. Lalli, Determination of silica, in *A Manual for Chemical and Biological Methods for Seawater Analysis,* Pergamon Press, New York, 25-28, 1984b.

Shemesh, A., Y. Kolodny, and B. Luz, Oxygen isotope variations in phosphate of biogenic apatites, II. Phosphorite rock, *Earth Plan. Sci. Let., 64*, 405-416, 1983.

Tudge, A. P., A method of analysis of oxygen isotopes in orthophosphates - its use in the measurement of paleotemperatures, *Geochim. Cosmochim. Acta., 18*, 81-83, 1960.

Scientific Highlights of the Geophysical Laboratory 1905-1989

H. S. Yoder, Jr.

Table of Contents

1. Introduction

The concept of a geophysical laboratory was initiated by Clarence King at the U. S. Geological Survey in 1882. The laboratory was placed under the direction of Carl Barus, and continued until government funds were cut off in 1892. Work was resumed in 1900 under the direction of George F. Becker, a field geologist with a background in physics and mathematics, and some support for its staff was obtained in 1904 from the newly formed Carnegie Institution of Washington (CIW). An Advisory Committee in Geophysics had been set up in the Institution in 1902, mainly at the instigation of Charles D. Walcott, then Director of the U. S. Geological Survey, who also served as Secretary of the Executive Committee of the Board of Trustees of CIW. Charles R. Van Hise, who had drawn up the plan for the work of the U.S.G.S. geophysics group, served with T. C. Chamberlin, Carl Barus, A. A. Michelson, C. D. Walcott and R. S. Woodward (Chairman) on the Advisory Committee.

A proposal for an independent, privately endowed geophysical laboratory was hastily prepared for the Committee by Becker. A subcommittee was formed in July, 1902, consisting of Chamberlin, Van Hise, and Woodward to prepare a more detailed report on the problems to be investigated from both physical and chemical viewpoints. Van Hise and Becker were sent to Europe in 1903 to consult their colleagues on the continent about forming a new laboratory. In addition to the reports of Van Hise and Becker, the Trustees received a detailed outline of suggested geophysical investigations on 1 October 1903 from Frank D. Adams, Whitman Cross, Joseph P. Iddings, James F. Kemp, Alfred C. Lane, Louis V. Pirsson, H. S. Washington, and John E. Wolff. (That outline eventually served as the charge to the new laboratory). Because Becker's plan required a large proportion of the CIW budget, the more modest plan of Van Hise, focusing on geochemical and petrological research, was deemed more acceptable. As a result, Becker's deputy, Arthur L. Day, was asked to submit a proposal whereby small grants could foster programs from which a larger scale endeavor might evolve.

Day received a grant in 1904 to enlarge his studies on petrogenesis at the U.S.G.S., and a grant was made to Becker for the analysis of the strain relations in the flow and rupture of rocks. These two tests of the practicability of experimental solutions to geological problems proved successful. Later that year, R. S. Woodward, a member of the geophysics subcommittee, succeeded to the presidency of CIW, and he urged the Board of Trustees to approve the construction of a geophysical laboratory. On 12 December 1905, Woodward, with the help of Walcott, succeeded in getting the Trustee's approval, and within a few months, Day was named as its first Director.

The news of the authorization did not please Mr. Andrew Carnegie, who believed the exceptional investigator should be supported in his own environment. Others were equally unhappy with the proposed specific program of work. The physicochemical study of mineral solutions at high temperatures was considered by Becker a mere "detail" in the general need to under-

stand the behavior of matter under the extreme conditions in the earth. Nevertheless, the following broad program outlined in 1902, reviewed and rededicated by Day in 1927, has served the Geophysical Laboratory well for over 80 years.

> "The crust of the lithosphere has thus far been the chief field of geology in the narrower sense, since it contains the rock record of the earth's past; and geological studies have been directed chiefly to reading and mapping this record, but the record needs to be interpreted on broader and deeper lines based on a profounder knowledge of physical laws. To this end the data of geology need to be correlated and unified under these laws on an experimental basis ....
>
> "Some of the salient problems of the outer lithosphere are the origin and maintenance of the continental platforms . . . and a whole group of intricate questions of a chemical and chemico-physical nature, including the flow of rocks, the destruction and genesis of minerals, the functions of included water and gases, the internal transfer of material, the origin of ore deposits, the evolution and absorption of heat, and other phenomena that involved the effects of temperature, pressure, tension and resultant distortion upon chemical changes and mineralogical aggregations.
>
> "These questions of the earth's outer part are inseparably bound up with those of the interior, and here the problems involve the most extreme and the least known conditions and make their strongest demand for experimental light. The themes here are the kinds and distribution of the lithic and metallic materials in the deep interior; the states of matter; the distribution of mass and of density, and the consequent distribution of pressure; the origin and distribution of heat; . . . the secular redistribution of heat within the earth and its loss from the surface; the possible relations of redistribution of internal heat to vulcanism and to deformation and similar profound problems.
>
> "A series of specific laboratory questions arise from these, e.g., the effect of pressure on the melting point of rocks carried to as high temperatures and pressures and through as wide range of materials as possible to develop the laws of constancy or of variation; the effect of temperature and pressure on thermal conductivity as indicated above, and on elasticity, especially as involved in the transmission of seismic tremors."

In subsequent years all of the recommended areas of geophysical research have been investigated by the staff.

The land for the new building in the Azadia area of the District of Columbia was obtained in March of 1906, construction began in June of that year from plans prepared in 1904, and the building was occupied on 7 June 1907. The design of the massive structural walls resulted from Day's experience at the Physikalisch-Technische Reichanstalt in Berlin, where passing streetcars caused the galvanometers to vibrate. Another innovative feature was the erection of the machine shop on a floating slab independent of the building.

The staff was recruited primarily from the U.S.G.S. At the end of the first year of operation in the new building, the staff consisted of 3 physicists (A. L. Day, J. K. Clement, W. P. White), a chemist (E. T. Allen), 2 physical chemists (E. S. Shepherd, G. A. Rankin), and 2 petrologists (F. E. Wright, E. S. Larsen, Jr.). Grants were also made by CIW to G. F. Becker (U.S.G.S.) and F. D. Adams (McGill Univ.) in geophysics and to T. C. Chamberlin (Univ. of Chicago) and H. S. Washington (Locust, N. J.) in geology.

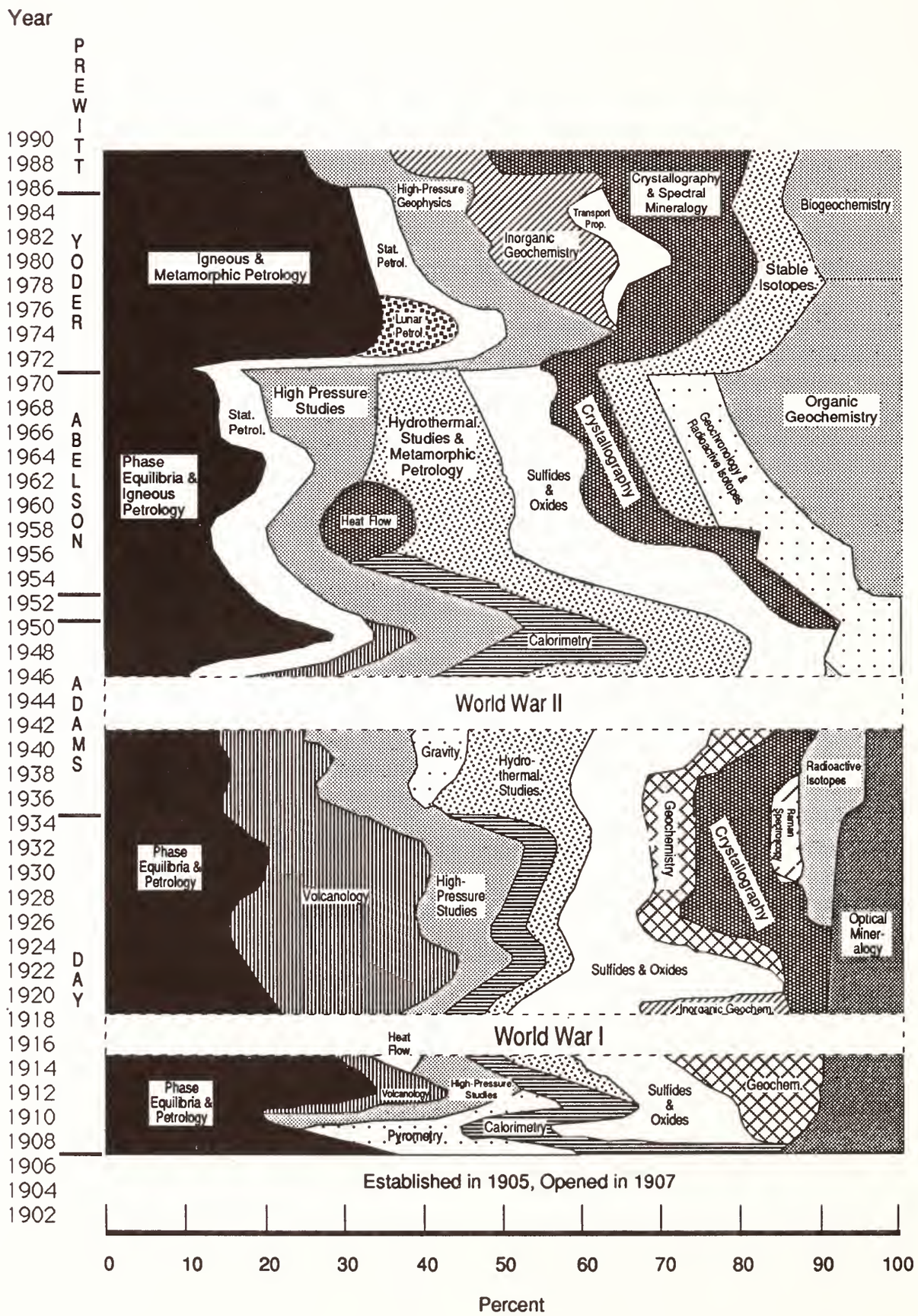

FIG. 1. Change in proportional effort of regular Geophysical Laboratory staff (not including Fellows or Visiting Investigators) in various fields of research with time and directorship. (George W. Morey served as Acting Director, 1952-1953; Robert B. Sosman served as Acting Director, 1918-1920, for Arthur L. Day).

Over the years, more than 2100 papers have been issued from the Geophysical Laboratory, but this represents only one measure of the contribution of the staff. The ebb and tide of the focus of the work has indeed been great. Figure 1 gives a crude picture of the change in effort of the regular staff throughout the years. The effort assigned to various fields is somewhat arbitrary in view of the overlap and integration of the fields. The designated fields, however, serve as focal points on which to summarize the following highlights of the work. It is evident the Geophysical Laboratory has responded dynamically to the needs of the science, developing the most rewarding directions as they evolved. It is also evident that it is the individual staff members who have made the concept of interdisciplinary research so successful. In accord with the original wishes of Mr. Andrew Carnegie, the support of exceptional individuals has resulted in a record of discovery and invention that is extraordinary.

2. Experimental Petrology

Igneous Petrology

The charter for the Geophysical Laboratory, as recorded in the report of the Advisory Committee on Geophysics, clearly stated the need to unify geological field observations under physical and chemical laws on an experimental basis. They believed geologists wanted to know:

> "...the melting points of rocks, the temperatures at which rocks crystallize from magma, the relative specific gravities of melted and crystallized rocks, the effects of slow cooling upon the crystallization of rocks with and without pressure, the solution of one kind of rock in another, and, in short, all the phenomena which concern the transformation of magma to crystallized rock and of crystallized rock to magma."

That statement appeared in Year Book No. 2 of CIW for 1903, which included a detailed plan of investigation (pp. 195-201). It has served as the principal guideline for the core program of the Geophysical Laboratory for 84 years.

The experimental approach to those goals was immediately beset with problems of the most fundamental nature. There was no generally acceptable temperature scale above 200°C and standard calibration points had not been established even though several boiling and melting points were commonly used up to about 1100°C (Sosman, 1952). Primary pressure calibration was available only to 2 kbar. There was, however, considerable knowledge about the composition of rocks and the ten most important oxides had been identified by chemical analyses. The main advantage lay with the incredible intuition and perception of the geological advisors who had acquired a remarkable qualitative sense about how rocks were formed.

The most abundant mineral in the crust of the earth is plagioclase, and the Ab-An system had been selected for study at the U.S.G.S. in the formative years of a geophysical laboratory. That first step in a

much broader scheme of investigation of the common rock-forming minerals was undertaken by Day **(1906-1935)**[1], Allen **(1907-1932)** and Iddings (Univ. of Chicago) with the financial support of CIW. The results were published in 1905 as paper No. 1 of the new Geophysical Laboratory. The liquidus was determined by the heating curve method from An_{100} to $An_{26.1;}$ the remainder of the now classical solid solution loop was deduced as Roozeboom's Type I. The temperature calibration was based on the Reichsanstalt scale for the melting of Cd, Zn, Hg, and Cu. Platinum-Rhodium thermocouples were employed with a Pt-wound resistance furnace. Because of the great difficulty in determining the exact temperature of complete melting, Shepherd **(1904-1946)** and Rankin **(1907-1916)** devised a new method in 1909 for the $CaO\text{-}SiO_2$, $MgO\text{-}SiO_2$, and $Al_2O_3\text{-}SiO_2$ systems in which the liquid was quenched from a known temperature to a glass and examined optically for crystals. The new technique was applied in a reexamination of the plagioclase system in 1913 by N. L. Bowen **(1910-1919; 1920-1937; 1947-1952)**, who proved that the solid solution loop was indeed as deduced. He also showed that the depression and rise of the melting temperatures of the endmembers An and Ab, respectively, were in close agreement with Raoult's Law of vapor pressure. Thus, plagioclase may be considered an ideal solution, however, the conditions under which it deviates from ideality remains a principal focus of today. The new Geophysical Laboratory temperature scale (discussed at the end of this section), calibrated with lithium metasilicate, diopside and anorthite, was applied in those experiments.

In the short time of seven years, Bowen had at his disposal the data for Ne-An,[2] Ab-An, Di-Fo-Qz, An-Fo-Qz (Anderson, **1912-1918,** 1915), Di-Ab-An, and $CaO\text{-}Al_2O_3\text{-}SiO_2$ (Rankin and Wright, **1906-1944**, 1915). From these few data and a large measure of genius Bowen produced "The later stages of the evolution of the igneous rocks." In 1922, he published "The reaction principal in petrogenesis," which Pentti Eskola **(1921)** of Finland later called "the most important contribution to petrology of the present century." With only the additional information in $CaO\text{-}MgO\text{-}Al_2O_3$ (Rankin and Merwin, **1906-1946,** 1916), $MgO\text{-}Al_2O_3\text{-}SiO_2$ (Rankin and Merwin, 1918), $CaO\text{-}MgO\text{-}SiO_2$ (Ferguson, **1912-1919,** and Merwin, 1919); Ak-Geh (Ferguson and Buddington, **1919-1920,** 1920) and the immiscibility studies of Greig **(1922-1960**, 1927) in $FeO\text{-}Fe_2O_3\text{-}Al_2O_3\text{-}SiO_2$, Bowen assembled all his previous petrological discussions in a set of Princeton lectures published in 1928 as "The Evolution of the Igneous Rocks." Although Bowen expressed his great prejudice for the well established theory of crystal fractionation as the guiding principle in accounting for the diversity of rocks, he also

[1] Numbers in bold-face type are the years during which the Staff Member or Fellow officially served the Geophysical Laboratory. The single years in text type is for a reference or an Annual Report citation, most of which are listed in the "Indices of the Annual Reports of the Director of the Geophysical Laboratory" and the "Publication List of the Geophysical Laboratory."

[2] Bowen's Ph.D was granted in 1912 by the Massachusetts Institute of Technology in part for his study of Ne-An at the Geophysical Laboratory between 1910 and 1912. He appears to have been the Laboratory's first "Predoctoral Fellow."

provided the theory for testing alternative views. No other book has had a greater influence on the course of petrology. On the fiftieth anniversary of Bowen's book, a review of the same questions raised by Bowen was made (Yoder, **1948—,** 1979), and it was evident that he had indeed discussed the critical issues still relevant today.

Most of the other staff members not as geologically inclined as Bowen and his associates chose to pursue a plan whereby oxide systems, rather than mineral systems were investigated. By taking each of the principal oxides alone, then two at a time, successively adding other components, the melting behavior of the multicomponent rock can be ascertained. Because there are about 10 oxides essential to rocks, there would be 45 binary, 120 ternary, 210 quarternary, and 252 quinary systems. Clearly judicious choices were necessary, because not all of these systems are pertinent to rock-forming processes. Some systems were of exceptional industrial importance, however, and a few staff members deviated from the principal goals initially set. It was fortunate indeed they did, because some of the studies resulted in the establishment of the optical glass industry in the U. S. (see section on Wartime Studies), solution of the clinker problem in Portland cement, increased metal yields in the steel industry by adjusting the slag compositions, and others have been important to the high-temperature refractories industry.

During the first thirty years, there was a special effort to deal with the oxidation states of iron, starting with Sosman **(1908-1928)** and his associates. In experiments on the Na_2O-Fe_2O_3-SiO_2 system involving acmite and hematite, Bowen *et al.* (1930) pointed out that the liquids actually contained some FeO. From this experience, Bowen and Schairer **(1927-1970)** set out to ensure that equilibrium was obtained on FeO-SiO_2 (1932). The successful breakthrough in dealing with iron came as a result of using an iron crucible held in a purified stream of nitrogen. The equilibria were well defined as long as native Fe was present, even though the Fe_2O_3 content of the liquids varied in a systematic way. With this new technique, reproducible results were obtained by them, with the help of Posnjak **(1913-1947)**, on Ln-Fa, CaO-FeO-SiO_2, MgO-FeO-SiO_2, Ab-Fa, and Ne-FeO-Qz. Later, Schairer (1942) completed a major portion of the very complex system CaO-FeO-Al_2O_3-SiO_2, for which he invented the summary "flow sheet" to describe the major courses of fractionation of liquids. As will be seen in the section on Hydrothermal Studies, the next breakthrough at the Laboratory in controlling the oxidation state of iron was through the oxygen buffer technique devised by Eugster **(1952-1958,** 1957). A major tool for petrologists was provided by Lindsley **(1960-1970)** who calibrated the coexisting pairs of Fe-Ti oxides for use as thermometers and oxygen barometers. Because the oxidation state of iron has a profound influence on the differentiation trend of a magma, the quantitative measure of the partial pressure of oxygen with minerals of wide spread occurrence has been of exceptional value. For systems requiring only Fe_2O_3, Huckenholz **(1966-1973)** and Yoder (1971) mixed PtO_2 in the starting materials held in Pt

tubes to ensure an excess of oxygen for the study of andradite and ferridiopside at high pressures. Another method for maintaining the partial pressure of oxygen, developed elsewhere (Darken and Gurry, 1945) was the use of mixtures of gases, such as CO_2-H_2. Eventually it was possible to define the Mg-Fe fractionation trends for the major rock-forming phases as a function of $f(O_2)$ and T.

Characterization of the principal rock-forming minerals and investigation of their stability relations has been an ongoing program of the Geophysical Laboratory. After the determination of Ne-Ks-Qz, "petrogeny's residua system," by Schairer and Bowen in 1935, the course of phase equilibria research was set for years to come. Systematically, Schairer and colleagues added the endmembers of each of the phases formed early in magma (e.g., forsterite, anorthite, diopside, and enstatite) to the relevant joins in the residua system. The ternary feldspars required considerable effort because of their complex stability relations at various pressures and even more complex structural changes. The sluggish growth problems were overcome when suitable hydrothermal pressure vessels were developed.[3] The Ab-Or-H_2O system was studied by Bowen and Tuttle (**1947-1953,** 1950) in preparation for their classic work on the granite system. The ternary feldspars were investigated by Yoder, Stewart (**1955-1957**) and Smith **1954-1957**) (1957) at $P(H_2O)$ = 5 kbar to avoid the incongruent melting of sanidine and to achieve a suitable rate of reaction. In the course of that work a direct method was established for obtaining the water content of the liquid as defined by the phase equilibria. The melting relations of Ab-An were worked out by Lindsley (1968) at 10 and 20 kbar after Bell (**1964-1989**) and Roseboom (**1956-1959**) (1965) provided the P-T diagram for Ab up to 50 kbar while Hays (**1965-1966,** 1967) was investigating the P-T diagram for An and related phases up to 35 kbar. It became evident that plagioclase was not a stable phase at pressures above about 32 kbar.

In a similar way, the stability regions of the olivines, pyroxenes, spinels, melilites, and an array of feldspathoids were mapped out by many staff members and their associates at atmospheric pressure as well as at mantle pressures. Those phases found to be stable only at high pressures, e.g., jadeite, pyrope, sodium melilite, provided new constraints on the origin of rocks in which they occur, particularly in solid solution. It was essential that the stability relations of each of the major mineral groups be well defined before their interrelationships as assemblages in rocks could be tackled. (Space does not permit a detailed account of the investigations of each of these major mineral groups even though staff members played leading roles in defining their stability relations.) Impatience, however, usually led to somewhat premature ventures into the study of more complex assemblages. One successful venture is given in the following example.

After extensive experimental experience with feldspars and pyroxenes, the time was considered appropriate to put these two major mineral groups together as

[3] The development of techniques and apparatus is given in the following sections on Hydrothermal Techniques and High-pressure Apparatus.

they are found in basalt. Study of the multicomponent system one component at a time would require an unreasonable amount of time. For this reason a less rigorous approach was taken in which the natural igneous rock, presumed to have been at one time all liquid, could be treated as a single bulk composition in the multicomponent system. On this basis Yoder and Tilley **(1931, 1955-1967)** examined various natural basalt types and their high pressure analogues. The results were published in 1962 under the title "Origin of basalt magmas: an experimental study of natural and synthetic rock systems." According to the Institute for Scientific Information, it was the most quoted paper in 43 core earth science journals in the period 1961-1980. Their model, the generalized basalt tetrahedron, still serves as a guide for testing other theories of basalt magma generation.

Attention turned to the petrology of the mantle in the 40-200 km depth range when the Boyd-England **(1926-1971)** high-pressure apparatus was developed. During the very active period 1960-1970, Boyd **(1953—)** and colleagues determined the melting curves for Di, Ab, En, Fo, and Jd. In addition, the stability fields of pyrope, coesite, and jadeite were defined in early studies. The transformation of basalt to eclogite was outlined by Yoder and Tilley in 1961. O'Hara **(1962-1963)** worked out the melting relations of natural garnet peridotite at 30 kbar and B. T. C. Davis **(1962-1965)** provided the liquidus for Di-Py-Fo at 40 kbar. The critical observation that eclogite (equivalent to basalt) was at the minimum melting composition of omphacite-garnet was based on O'Hara's study of that join at 30 kbar with purified natural minerals and B. T. C. Davis' work on Di-Py at 40 kbar. The solvus on the Di-En join was measured by B. T. C. Davis and Boyd (1966) at 30 kbar, and they applied it as a geothermometer to the pyroxenes in nodules from kimberlites. A particularly important phase diagram was published by Boyd (1970) for the system Wo-En-Cor in which the alumina content of orthopyroxene was later (1973) calibrated as a geobarometer. During this time, the limits of alumina content of diopside were defined on the solvus of the join Di-Jd by Bell and B. T. C. Davis (1969) who had earlier determined the melting relations of that system. All of these studies and related investigations had indeed generated a new outlook on the origin of magmas, the depths of metamorphism, and placed constraints on the plethora of earth models that erupted with the rise of plate tectonics.

The lower mantle and core captured the attention of some of the staff and a large number of Postdoctoral Fellows and Guest Investigators when the diamond-anvil cell became a practical tool. The phase stabilities and equations of state of the metals and major oxide components of the earth were studied first, some to pressures near the center of the inner core. Next, combinations such as $CaSiO_3$- and $(Mg,Fe)SiO_3$-perovskite were investigated, and then Al_2O_3 was added to the system. The samples were heated with a YAG[4] laser at each pressure increment to accelerate the phase transitions. Phase diagrams were generated for

[4] The yttrium aluminum garnet (YAG) was first synthesized by Yoder and M. L. Keith **(1947-1950)** in 1949 at the Geophysical Laboratory in a study of spessartite-yttrogarnet.

MgO-FeO-SiO_2 up to 700 kbar by T. Yagi (**1976-1978**), Bell, and Mao (**1972—**, 1979). The partitioning of Mg and Fe between the various solid solutions placed great constraints on the geochemical models of the earth. When the equations of state of the various structures were fitted to similar equations inferred from seismic data (Preferred Reference Earth Model), it became evident that the lower mantle was dominated by two perovskite structures, mostly an orthorhombic ferromagnesian silicate perovskite and a cubic calcium silicate perovskite ($CaSiO_3$) as a minor phase. After the sharp phase transition between spinel and perovskite + magnesiowüstite was discovered, Mao (1988) proposed a model wherein the 670-km seismic discontinuity is a phase-transition-driven, chemical-composition boundary. Because magnesiowüstite strongly partitions iron relative to silicate perovskite, Mao, Bell and T. Yagi constructed a new fractionation model of the earth whereby the magnesiowüstite would sink toward the center and lose some of its iron to the core by chemical reduction or disproportionation. The excitement generated by these difficult and laborious experiments on the interior of the earth rivals that of the returned lunar samples.

Although much of the emphasis was placed on understanding the interrelationships of the crystalline phases, their melting behavior was, from a thermodynamic point of view, highly dependent on the character of the liquid. For this reason, characterization of the liquid became a major focus. The techniques for the measurement of density, viscosity, thermal expansion compressibility, refractive index, and heat contents were developed, but understanding why they varied with composition required knowledge of the liquid structure. With the advent of spectroscopic tools, the local short-range structure of the "amorphous" liquid could be ascertained. The structural units were identified and simple coordination rules developed. A model emerged that could be used to rationalize the chemical, physical and thermodynamic properties of melts. The model was achieved by systematically examining the melt structure of simple systems. The work of B. O. Mysen (**1972—**) and D. Virgo (**1971—**) and associates on systems with the common rock forming oxides, with and without volatiles, resulted in a book by Mysen (1988) on the "Structure and Properties of Silicate Melts."

Temperature Scale. The very first practical problem to be faced by the staff of the Geophysical Laboratory was the calibration of a temperature scale above about 1100°C, there being no internationally accepted scale in 1905. Because of Day's experience at the Physikalisch-Technische Reichanstalt in Berlin, the first apparatus installed was the nitrogen-gas thermometer. With a new design for improved accuracy of measurement, Day and Sosman gave accurate data for a scale from 300° to 630°C with a direct determination of the boiling point of sulfur. The scale was then extended by them in 1910 to the palladium melting point of 1549.2°C. The fixed points were corrected from the constant-volume nitrogen scale to an absolute thermodynamic scale and expressed by Johnston

(1908-1916) and Adams **(1910-1952)** (1914) as an e.m.f. for copper-constantan and platinum-rhodium thermocouples from 0° to 1755°C. The principal fixed points for gold, copper, diopside, and palladium became known as the Geophysical Laboratory scale,[5] and it is still used today. The melting point of platinum, 1755°C, was based on the incremental difference of optical pyrometer measurements of the Bureau of Standards between palladium and platinum.

After WWI, an international conference met and the International Temperature Scale of 1927 was adopted. Silver was set 0.3° higher; gold, 0.4° higher, palladium, 5.5° higher, and the major change was that platinum became 1773°C. In spite of these recommendations, the scientists at the Geophysical Laboratory retained their own scale because of their belief in its thermodynamic foundation and for consistency with their previously published phase diagrams. In the meantime, physicists noted certain discrepancies in the physical constants related to the International Temperature Scale. A new international committee met in 1939, but WWII intervened and their results were not published until 1948. The changes nearly restored the fixed values below 1550°C to those of the Geophysical Laboratory scale. One significant change related to the extrapolation to the melting point of cristobalite which would require a change from 1713°C to 1723°C. Nevertheless, the values for diopside (1391.5°C) and pseudo-wollastonite (1544±2°C), anorthite (1553±2°C), and cristobalite (1713±5°C) have all been retained by the Geophysical Laboratory as calibration points not only for consistency but also because they are within the errors of experimental determination of the International Temperature Scale, which is still subject to change. It would be useful to ascertain in the near future the melting point for the important endmember mineral forsterite that is still known only as 1890±20°C. The corrections to the e.m.f. of thermocouples used at high pressures, recently studied but subject to debate, also remain an important subject for reinvestigation. In principle, the triple points of mineral phase changes may serve as an adequate *P-T* scale for interlaboratory comparisons.

[5] The fixed boiling and melting points below gold are listed by Sosman (p. 522, 1952).

Metamorphic Petrology

Prior to WWII there were only a few studies concerned with metamorphism at the Geophysical Laboratory, even though an extensive program had been laid out by the Advisory Committee. Van Hise had already completed his enormous (1286 pages) "Treatise on Metamorphism" for the U.S.G.S. in 1904 and was well prepared to advise the CIW. Some of the thermodynamic principles were stated by Johnston and Niggli **(1912-1913)** (1913), and Eskola (1922) described the sequence of metamorphic rocks at a limestone-granite contact. A major mapping study of the metamorphic zones of Dutchess Co., N. Y,. was made by Barth **(1929-1936,** 1936). He demonstrated that the rocks were apparently at equilibrium because the assem-

blages accounted for the bulk composition at each stage of the metamorphism of the argillaceous sediments.

The principal delay in tackling experimentally the metamorphic facies of Eskola as well as Bowen's petrogenetic grid was the lack of apparatus to contain the hydrous minerals. That problem was subsequently solved (see next section) by Bowen and Tuttle (1949) who published the first systematic study on the *P-T* stability of some of the critical metamorphic minerals in $MgO\text{-}SiO_2\text{-}H_2O$. Shortly thereafter a series of papers appeared on systems defining the stability fields of chlorite, cordierite, muscovite, biotite, chloritoid, staurolite, garnets, and especially the Al_2SiO_5 polymorphs.

Serious objections to the facies and isograd concepts were raised by Yoder (1952) in a study of $MgO\text{-}Al_2O_3\text{-}SiO_2\text{-}H_2O$ in which representatives of all the then defined facies were found to be stable at the same *P* and *T*. He also raised the issue of the role of water in metamorphism (Yoder, 1955) in regard to its presence in excess as a free phase or where it was "deficient" relative to the most hydrous assemblage. The open *vs.* closed system with volatiles became the major issue of the day. A significant contribution to the problem was made by H. J. Greenwood **(1959-1963)** from experiments on analcite-H_2O-Argon, Ct-Qz-H_2O, and others. The influence of $P(H_2O)$ less than P_{total} was clearly demonstrated for those simple but highly informative reactions.

The apparent loss of large volumes of water during the metamorphism of some sediments and the gain of water by other rocks, implied an active flow of fluids. Oxygen isotopic evidence and phase analysis led D. Rumble **(1969-1971; 1973—)** and associates to estimate that the volume of fluid that flowed through a calc-silicate bed at Beaver Brook, N. H., was from 1.5 to 4.0 times the rock volume. Their paper (1982) emphasized the process of rock-fluid interaction, but the proportions of fluid to rock are still being debated vigorously. The concept of reaction progress variables espoused by J. M. Ferry **(1975-1977)** have been helpful in understanding the process. More recently, the flow of fluids has been related to structure by C. P. Chamberlain **(1985-1987)**. The transport of heat with fluid was documented by comparing the isotherms deduced from the metamorphic reactions with the oxygen isotopic data. The mapping of channeled, hot, fluid-flow regions is potentially a valuable tool for ore prospecting.

The extensive studies on the amphiboles at the Geophysical Laboratory pertain to both metamorphic and igneous rocks. In general, the role of amphibole in metamorphism is confined to low $P(H_2O)$ and relatively low temperatures, whereas most amphiboles appear on the liquidus above a few kbar $P(H_2O)$ Although Allen and Clement **(1904-1907)** (1908) found water to be a component in tremolite, its structural role deduced by Schaller (1916) was confirmed by Posnjak and Bowen (1931), and a previous report of its formation from a dry melt was withdrawn. A few years later, fluoroamphiboles were formed inadvertently when NaF was used as a flux to grow orthopyroxenes. (That study laid the groundwork for a later extensive program

at the U. S. Bureau of Mines for the possible production of synthetic asbestos.) The first systematic *P-T* studies of tremolite and pargasite were made by Boyd (1954). A complex hornblende was produced from a tholeiite basalt by Yoder and Tilley (1956), and its stability field outlined up to 10 kbar. The study by staff and associates of most of the critical endmember amphiboles followed: magnesioriebeckite, arfvedsonite, glaucophane, ferropargasite, richterite, ferrorichterite, K-richerite, anthophyllite, cummingtonite, and aluminous anthophyllite. The breakdown of amphibole at high pressures (20-30 kbar) was first suggested from thermodynamic calculations by Greenwood (1963), but it was several years before the general concept was demonstrated experimentally by others. The possible storage of water in the mantle then shifted from the amphiboles to the micas and hydrous forms of commonly anhydrous minerals (e.g., hydrogarnets).

3. Hydrothermal Techniques

Before 1900 some 80 mineral species had been synthesized, but not under controlled and reproducible conditions. The devices used for synthesis were generally gun barrels closed by brazing, welding, or a screw on cap. A pressure vessel having a screw-on-cap fitted with a flat metal washer, made in about 1900, was brought to the Geophysical Laboratory by E. T. Allen from the U. S. Geological Survey. Few experiments were tried before WWI because the devices were unreliable even at low pressures. The review of hydrothermal mineral formation by G. W. Morey (**1912-1957**) and Paul Niggli in 1913, however, registered the strong interest in pursuing those experiments. Further stimulus was provided by the analyses of gases at Kilauea volcano, Hawaii, by Day and Shepherd who found H_2O a principal component. In 1917 Morey and Earl Ingerson (**1935-1947**), no doubt inspired by the demonstration by Day and Shepherd of H_2O in the gases of Kilauea, designed a pressure vessel with a contained copper or silver washer that would retain reliably pressures somewhat over 1 kbar. With that apparatus Morey and C. N. Fenner (**1910-1937**) investigated the K_2SiO_3-SiO_2-H_2O system up to 1000°C and about 340 bar by the isothermal polybaric saturation method. Their detailed exposition of theory and experimental methods recorded a major advance in hydrothermal studies. There followed a series of experiments in the "Morey bomb" on the simple oxide systems with H_2O.

The next breakthrough came with the F. H. Smyth (**1919-1925**) and L. H. Adams (1923) device in which 1400°C and 1 kbar could be sustained with a CO_2-gas medium. With the same device, R. W. Goranson (**1926-1951**) achieved the first systematic results on the melt curves of the rock-forming silicates, albite-H_2O and sanidine-H_2O, as well as the melting curve for granite-H_2O. These dramatic experiments would appear to be the last major developments in experimental apparatus prior to WWII. Fortunately, Morey had also described a new design for his pressure vessel that was to lay fallow throughout the war. He adapted P. W. Bridgeman's unsupported-area principle to the closure and connected

a H_2O pump directly to the Morey bomb, thereby controlling the water pressure independently of the temperature.

A review of the Geophysical Laboratory's programs after WWII by the staff and a large host of external colleagues greatly emphasized the need to pursue hydrothermal systems. An inventive and imaginative investigator employed at the Laboratory during the war under an Office of Scientific Research and Development contract, O. F. Tuttle, was hired to help Morey and N. L. Bowen carry out this mission. The hot-seal apparatus, eventually called the Tuttle apparatus, and the cold-seal pressure vessels soon were developed by Tuttle, using alloys found superior for machine gun barrel liners during WWII research at the Geophysical Laboratory (see section on War-time Studies). The cold-seal, pressure vessels, also called "rod bombs" or "test-tube bombs" depending on their position in, or orientation of, the furnace, remain the most widely used vessels for hydrothermal investigation today. A simple, cold-seal, pressure-vessel bench employing an intensifier was built by Yoder for operation to 850°C, and 5 kbar for runs of one month or more duration. The sealed-platinum-tube technique, first introduced at the Laboratory by P. Eskola in 1922, was used for a wide range of gases in addition to H_2O.

Because of the inherent limitations of the *externally*-heated pressure vessels, Yoder constructed in 1949 an *internally*-heated, gas-media pressure vessel that could sustain 1650°C and 10 kbar for months. These conditions were adequate for the entire range of temperatures and pressures in the continental crust within which 99% of the rocks observed crystallized. With the experience gained from investigations on pure mineral systems, Yoder and C. E. Tilley initiated in 1956 a study of natural igneous rocks with and without water. In the same apparatus, sulfur-bearing systems were studied in gold tubes by Kullerud and Yoder.

Other new techniques were developed rapidly thereafter. For examples, the control of oxygen fugacity by a series of mineral buffers was demonstrated by Eugster in 1956. The buffers initially consisted of iron oxides whose stability had been determined by Darken and Gurry (1945). For pairs of oxides in equilibrium, the $P(O_2)$ is fixed for a given temperature and pressure. By surrounding a sample contained in Pt, a metal that is permeable to hydrogen, with water and a pair of oxides held in an outer gold tube that is relatively impermeable to hydrogen, the oxygen pressure can be maintained. Eugster's first demonstration of the technique was in determining the stability of the iron-rich endmember mica, annite, between 0.5 and 2 kbar. The technique was adopted rapidly worldwide and continues to be a principal method for investigating redox reactions with a large range of buffers. The equilibrium established through the Pt membrane is of a restricted type because the gas phase over the buffer has a different composition that than over the sample. Nevertheless, the simplicity of the technique and wide range of application have had a major impact on igneous and metamorphic petrology. In 1976, J. D. Frantz **(1972-)** redesigned the Shaw apparatus for controlling the H_2 fu-

gacity. The influence of gas mixtures, such as CO_2 and H_2O, on metamorphic reactions was outlined by H. J. Greenwood, after he resolved the gas-mixing problem that frustrated previous attempts to measure these effects.

With the above-described devices it was then possible to establish the stability ranges of most of the common rock-forming minerals that contained a volatile component. The Postdoctoral Fellows carried these techniques to other parts of the world, and hydrothermal studies evolved exponentially. The attainment of those conditions to be found in the mantle and core required new concepts and these are outlined in the next section.

4. High-Pressure Apparatus

The effect of pressure on the melting "point" of rocks has been a high priority question since the inception of CIW. The compressibility studies of T. W. Richards and W. N. Stull (1903) at Harvard University were supported by CIW, probably on the recommendation of C. Barus, a member of the Advisory Committee on Geophysics. [Barus (1893) was the first to obtain an estimate of the change of melting "point" of diabase with pressure from measurements of the volume change, melting temperature, and heat of melting.] In 1906 P. W. Bridgman began his experiments at Harvard on a range of materials to ascertain the change of physical properties with pressure. About the same time, John Johnston began to develop apparatus for sustaining both high temperature and high pressure for geological applications at the Geophysical Laboratory. The limits obtained were 400°C at 2 kbar, and Johnston and L. H. Adams (1911) were able to report on the melting point changes with pressure of Sn, Bi, Cd, and Pb. The study of the compressibility of major rock-forming minerals and rocks, however, remained of central interest. The measurements on dunite and basaltic glass were especially pertinent to theories of the constitution of the mantle. By 1923 Smyth and Adams had achieved 1400°C at 1 kbar, and the range was later extended in the same apparatus to 940°C and 3.7 kbar by Goranson. In this time period, the manganin pressure gauge and its calibration was perfected by Adams and his colleagues as well as valves and other high-pressure fittings critical to the success of high-pressure experiments. Nevertheless, the trial-and-error stage of testing metals and packings continued. The availability of an on-site machine shop and direct accessibility to imaginative instrument makers contributed immeasurably to the development of new high-pressure techniques.

After WWII, Yoder sustained 1650°C and 10 kbar by 1949 in an internally-heated, gas-media apparatus. In 1956 substantial increases in pressure and temperature were achieved by F. R. Boyd, Jr. and J. L. England who had adapted the Griggs and Kennedy design of Bridgman's (1935) carbide-piston "squeezer". They attained 800° at 10 kbar and 600° at 50 kbar, illustrating the breakdown of nepheline to jadeite and an unidentified phase.

The exciting announcement of Loring Coes (Norton Co., Worcester, MA) that he

had synthesized a large number of "high-pressure" minerals others had struggled unsuccessfully to obtain, came in 1953. He had devised a solid-media, high-pressure apparatus in which a hot-pressed Al_2O_3 core supported by steel bands and tungsten carbide pistons were used. His experiments were made up to 1000°C and 45 kbar in that device. Because of its obvious applicability to many geological questions, the Coes apparatus was the basis for an improved chamber assembly designed by Boyd and England (1958, 1960) that could sustain 1750°C and 50 kbar. The main breakthroughs were in fitting a thermocouple up to the sample and in providing adequate support for a reuseable tungsten carbide core. Immediately after the announcement of the details of diamond synthesis by the General Electric Co. in 1959, Boyd and England successfully made diamonds in their apparatus. That highly successful design has been used by hundreds of investigators around the world on mineralogical and petrological problems in the mantle. Extension of the range to 100 kbar was accomplished by them through a two-stage device in which the piston was supported by a substance such as KBr, that undergoes a phase change, thereby maintaining the support pressure at the phase change.

On the basis of Bridgman's anvil concept, Weir *et al.* (1959) at the National Bureau of Standards patented a miniature device in which the sample is squeezed between two opposing diamond anvils, for pressures up to 160 kbar at relatively low temperatures (< 175°C). Substantial improvements by H-k. Mao and P. M. Bell in 1978 led to the production of 1.72 Mbar, verified by three different methods of calibration. In subsequent years, pressures beyond those in the center of the earth (3.5 Mbar) were achieved and the current record is 5.5 Mbar. The observation of plastic flow in diamond during one super pressure experiment raised an array of theoretical questions. The sample in the high-pressure, diamond-anvil cell can be heated to 3500°C with an appropriate laser beam to which diamond is transparent. The transparency of the diamond was a great advantage for observing absorption, scattering, and diffraction by the sample at pressure with Mössbauer, x-ray diffraction, Raman, optical, infrared and other spectral devices. The versatility of the Mao-Bell diamond cell has resulted in an explosion of studies on specific materials in the earth at ambient conditions and generated a host of opportunities for the chemist and physicist.

In spite of the availability of equipment that reproduces the entire range of *P-T* conditions in the earth, their exploitation in general systematic studies of phase equilibria have been slow in the geological community. The current trend toward development of large-volume devices for sustaining high pressures and high temperatures appears to be driven by the desire to understand those properties of the earth's mantle and core that require measurement of larger volume specimens. For examples, measurement of sound velocity, rheology, partitioning in multiphase assemblages, single crystals for structural study, and particularly those measurements requiring a constant and uniform temperature currently require larger volumes than can be

accommodated in the diamond-anvil cell without special facilities.

Pressure calibration has been a difficult problem in itself. The primary calibration of force per unit area is dependent on an evaluation of the friction on the piston. A rotating, free piston loaded with weights was used at the Laboratory for many years up to 10 kbar. Secondary calibrations were usually dependent on abrupt volume changes in a simple material. The melting of ice VI to water at room temperature was given as 9630 bar at 25°C by Adams (1931). The freezing pressure of Hg at 0°C was taken as 7492 bar, and the transformation pressure of CCl_4 I $\rightarrow$ II was taken as 3326 bar (Bridgman, 1911, 1914). As higher pressures were developed the transformation of Bi I $\rightarrow$ II (25.2 kbar at 25°C) was employed by Boyd and England. The transition of Tl II $\rightarrow$ III (37.15 kbar at 29°C) was also used by Boyd and England (1958) indirectly by measuring its abrupt change in electrical resistence in a silver chloride cell.

When the pressure range exceeded 50 kbar, the limit of the tungsten carbide core, it was necessary to turn to still other methods. The shift in the lattice constants of certain metals (Au, Ag, Cu, Mo, Pd, Pt) was used as the primary pressure calibration. The shift of the ruby R_1 fluorescence line became the new secondary calibration in the diamond-cell apparatus. Because the ruby fluorescence weakened above 1 Mbar, it was necessary to return to the primary method of using force per unit area, with a substantial loss in accuracy, or to the multiple use of calibrated metals. It is likely that new calibrations will be required as the investigation of certain ranges of pressure involved with major seismic discontinuities in the earth progresses.

The leadership of the Geophysical Laboratory in developing high-pressure techniques has been maintained throughout its existence. Although geology is often described as an applied science, the geologists at the Laboratory have provided the basic physics and chemistry in the extreme regions of pressure and temperature for use in other sciences. Challenges to existing theory have been proposed by experimentation under the core and mantle conditions in the earth, and the feedback to the basic sciences has been rewarding. The analysis of a geological problem by isolating and evaluating the effect of each significant variable appears to be an effective way to understand multivariate natural phenomena.

5. Ore Petrology

The plans submitted in 1903 by Dr. C. R. Van Hise for a geophysical laboratory included the need for

> "experimental studies on underground solutions and the artificial reproduction of natural minerals [that] will lead to correct theories of ore deposition and also give results of practical value, the magnitude of which cannot now be estimated."

Although Van Hise championed but one of the several schools of ore deposition, the recommendation was clear. Within a few years of the opening of the laboratory building, papers appeared on the characteriza-

tion of sulfides, the analytical procedures for determining sulfur, and on the physical chemistry of sulfide systems. For example, the chemistry of the secondary enrichment of copper sulfides was unraveled by E. G. Zies **(1913-1949)**, E. T. Allen, and H. E. Merwin in 1916. The studies of Allen and Zies (1919) on the chemistry of hot springs was applied by Fenner (1933) to ores derived from igneous origins. In the same year, Bowen (1933) proposed that the heavy metals would be concentrated in the residual fractions of a differentiating magma. It became evident that hot springs were an end product of ore deposition as well as indicators of volcanic activity.

A benchmark paper on the Cu-Fe-S system by Merwin and Lombard **(1915-1927)** appeared in 1937. They laid out the technique for holding synthetic and natural samples at a defined vapor pressure of sulfur (455 mm) and temperature in silica-glass (vitreosil) tubes. The phase diagram was of great importance to economic geologists because it helped to constrain the temperatures and pressures of ore formation. With continued investigation, the system has been found to be exceptionally complex, and it remains one of the most intensively studied systems even today. The concept of buffers was clearly defined even though the "equilibrium" obtained was of a restrictive type, the buffer and sample being at different temperatures.

Merwin and Lombard had recognized many of the problems arising from the inability to quench the run products. The unmixing of solid solutions in the FeS-ZnS system had been determined quantitatively as a function of temperature by Kullerud **(1954-1970)**. After he joined the Geophysical Laboratory he applied this important principle of geothermometry to other systems and to the estimation of the temperature of formation of natural ores. During a highly inventive period, techniques were evolved by Kullerud (1971) for dealing with sulfur and selenium systems, beyond the limitations of silica-glass tubes, up to 1400°C. Kullerud and his colleagues showed that essentially all sulfide and selenide systems exhibited liquid immiscibility. The first high-pressure-temperature diagram for a sulfide, pyrite, was achieved by Kullerud and Yoder (1959). Their observation of incongruent melting in pyrite clearly showed that it could not be a magmatic phase in either basalts or rhyolites. A similar conclusion was reached for pentlandite in a study by Kullerud (1963). The phase diagram for the economically important system Cu-Fe-Ni-S was established by J. R. Craig **(1965-1967)** and Kullerud (1969).

The systematic study of the synthetic sulfide systems have yielded information on the stability of mineral assemblages in a wide range of ore bodies. Not infrequently, the discovery of synthetic phases preceded their discovery as minerals in the ore body! The temperature gradients in the ore bodies, as determined by sulfide geothermometry, have been especially useful in exploration. The rapid response of some of the sulfides to changes in temperature in the laboratory have brought special insight into the metamorphism of ore bodies, a concern of Van Hise as early as 1900. Re-equilibration to temperatures as low as 200°C for some sulfides has been useful in generating

a scale of closure for determining the kinetics of the cooling of the ore body (Kullerud, 1967).

The interrelationships of sulfides and silicates, the essence of ore petrology, did not get underway until the early 1960's. Kullerud and Yoder, after considering the zones around the Bodenmais, Bavaria, ore body, reacted sulfur with fayalite and obtained pyrrhotite, magnetite, and quartz. From these and other experiments with various iron-bearing silicates, the concept of sulfurization emerged that helped explain the apparent high-grade metamorphic aureoles around low-temperature ore bodies. This concept was also demonstrated and applied to the interrelationship of sulfides and carbonates as well as sulfides and oxides. In the latter case, Kullerud and colleagues produced a new type of omission solid solution in magnetite when reacted with sulfur.

The magmatic ores, especially those occurring in the layered igneous intrusions, have been of more recent concern. With an exceptionally wide range of experience in the layered intrusions of the world, Irvine **(1972—)** and his colleagues characterized the Pt-Pd ores of the Stillwater Complex of Montana. The detailed analyses of the J-M reef illustrated how magma mixing and double diffusive convection play a major role in the deposition of ores high in the layered sections of silicate rocks.

6. X-ray Crystallography

The program in crystal structure determination was initiated at the Geophysical Laboratory in 1919, just seven years after Laue's discovery of x-ray diffraction, by Ralph W. G. Wyckoff **(1919-1927)**, who had been invited to the Laboratory by Day during a visit to Cornell. Atomic arrangements were initially deduced intuitively and then tested by the few measured reflections. Wyckoff derived a complete analytical expression of Schoenflies space group theory to define all the possible arrangements and used the x-ray information to select the correct structure. In this way he worked out the relatively simple structures of the calcite group, dolomite, aragonite, periclase, quartz, wüstite, and zircon. The first structure to be determined at high temperature from powder x-ray-diffraction data was high cristobalite (Wyckoff, 1925). With the help of Wyckoff, C. J. Ksanda **(1914-1940)**, a Swiss-trained instrument maker, designed the twin-gas tubes for x-ray generation. Wyckoff joined with Eugene Posnjak **(1913-1947)** to prove the validity of Werner's coordination theory. When Wyckoff departed to work at the Rockefeller Institute on organic crystals, T. F. W. Barth joined the staff in 1929. He worked with Posnjak on the spinel problem, which resulted in their recognition in 1931 of "variate atom equipoints" - that is, crystallographically equivalent sites that could be occupied by chemically different atoms. It was the key idea in understanding many crystal structures, especially the aluminosilicates.

According to Donnay *et al.* (Yearbook 68, pp. 278-283), only the Geophysical Laboratory and Caltech had x-ray crystallography programs carried on continuously from 1919 to 1969. This activity continues

at the Geophysical Laboratory and Caltech in 1989.

The sulfide minerals were the focus of attention of George Tunell **(1925-1947)**. He determined the structures of tenorite, calaverite, sylvanite and krennerite. He also derived the Lorenz correction factor for equi-inclination Weissenberg films, essential for use of the intensities of diffracted x-rays. The Patterson-Tunell stencils were a very popular aid for the computation of Fourier synthesis prior to the computer era.

With the arrival of the powder x-ray diffractometer in 1949, the identification and characterization of synthetic mineral phases, primarily carried out under the microscope, was supplemented by the use of comparative powder patterns. The cell dimensions and volumes of the alkali feldspar solid-solution series were determined and the existence of a high-order transition established by Gabrielle Donnay **(1950-1952;1955-1960;1963-1970)** and L. H. Adams. The first applications of generalized symmetry to magnetic-structure determinations were made by J. D. H. Donnay (Visiting Investigator) with colleagues at the Brookhaven National Laboratory. The Donnays were especially successful in relating morphology to structure, which led to additional generalizations of the Law of Bravais. These studies were followed with the discovery of the relationship between crystallographic axes and morphological features of the calcite skeleton, termed biocrystals, in Echinodermata.

During his tenure as a Postdoctoral Fellow, J. V. Smith **(1951-1954)** pursued crystallographic studies of paracelsian, melilite, and alkali feldspars, much of the latter in collaboration with W. S. MacKenzie **(1951-1952; 1953-1957).** Smith also provided the theoretical and structural basis for polymorphism in the micas with Yoder. Although a staff member for only a brief period, Charles W. Burnham **(1963-1966)** refined the structures of sillimanite, kyanite, and mullite. He compared in detail the crystal structures of orthoferrosilite, clinoferrosilite, and ferrosilite III, and pointed out differences in these polymorphs that have not yet been fully explained. In addition, he provided several computer programs whose successors are still being used in crystallographic studies. A wide range of crystal structures among the common rock-forming minerals were refined by L. W. Finger **(1967—)**. He also developed computer reduction programs for the electron microprobe, automated the x-ray diffractometer, and contributed many techniques for resolving the more complex mineral structures. Finger and R. M. Hazen **(1976—)** initiated single-crystal, diamond-cell techniques that resulted in the accurate measurement of both compressibility (to 200 kbar) and thermal expansion (to 1000°C). From these techniques the concepts of cation polyhedral analysis as a function of pressure and temperature evolved.

Current studies include the adaptation, initially by Finger, A. Jephcoat **(1982-1989)**, and H-k. Mao, of synchrotron radiation to structure determination of very small single crystals held at pressure in the diamond cell and the characterization, primarily by Finger and Hazen, of the structures of phases with high-temperature superconducting

properties. C. T. Prewitt (**1986—**) joined the Laboratory as Director and collaborated with Finger and Hazen on a variety of projects including the first structure determinations of high-temperature superconductors and high-pressure silicate structures containing octahedrally-coordinated silicon that were synthesized in the cubic-anvil apparatus at SUNY Stony Brook. As part of his involvement in the superconductor research, Hazen wrote a book, "The Breakthrough", which gives an account of the discovery of the 1-2-3 high-T_c superconductor and subsequent attempts by different research groups to develop the discovery.

In addition to their individual pioneering efforts, the hallmark of the crystallographers at the Geophysical Laboratory has been their cooperative response to the needs of other staff members in characterizing the common rock-forming minerals and especially the minute synthetic phases produced. The determination of crystal structure at a range of conditions and its relationship to physical and chemical properties constitutes a major and essential contribution to the success of the Geophysical Laboratory's mineralogical investigations.

7. Spectral Mineralogy

The field of mineral physics at the Geophysical Laboratory evolved mainly from initial efforts in mineral optics, arc-Raman, and x-ray crystallography, followed in the 1970's by Mössbauer, laser-Raman and infrared spectroscopy, and in the 1980's by the entire array of spectral tools of modern day physics and chemistry.

An early pioneer in the U. S. in the application of microscopy to mineralogical and petrological problems was F. E. Wright. His design of a petrographic microscope was adopted by a leading U. S. manufacturer and his improvements substantially advanced its use. His book on "The methods of petrographic-microscope research" in 1911 had great influence in promoting the quantitative measurement of the optical properties of crystals. Another major contributor to crystal optics was H. E. Merwin. He developed with E. S. Larsen (**1907-1909**) special immersion media of unusually high refraction using mixtures of amorphous sulfur and selenium. His dispersion method for measuring refractive indices of grains in immersion liquids is still widely used. Because of his demonstration of the relationship of index of refraction, density, and composition of glasses, he contributed to many of the phase equilibria studies of the Laboratory.

Some of the earliest studies of the Raman effect, discovered in 1928, were carried out in the U. S. by J. H. Hibben (**1928-1939**). He provided detailed treatises on inorganic compounds in 1933 and on organic compounds in 1939. His principal successes were in the speciation of organic compounds, and he made a special effort to apply the technique to the petroleum industry. The low intensity of the Raman effect using an arc lamp and photographic plates was eventually enhanced with the advent of laser light sources and photoelectric cell recording of the spectra. Applications to

the common rock-forming minerals and their melts did not begin until the arrival of Postdoctoral Fellow S. K. Sharma **(1977-1980)** who installed a modern Raman spectrometer and a variety of laser sources with the help of his colleagues J. D. Frantz and D. Virgo. Another Raman system fitted with a microscope was added, and a multichannel detector was introduced by Mao, Bell and Hemley **(1984—)**. These refinements led to the techniques of single-crystal, micro-Raman spectroscopy as well as ultra high-pressure optical spectroscopy. An outpouring of highly innovative studies at pressures in the megabar range yielded an array of studies of crystallized gases, new mantle-phase structures, as well as coordination changes in common minerals. The crystallized gases became the "hydrostatic" media for subsequent diamond-anvil experiments and initiated the race to make metallic hydrogen. With these new instruments for sustaining record pressures, the winning of that race by Hemley and Mao appears to have been achieved in 1988 and documented above 2.5 Mbar.

The application of Mössbauer techniques to atom site preference problems was carried out by D. Virgo. Landmark studies of the Fe-Mg ordering in olivines (with L. Finger) and anthophyllite (with F. A. Seifert, **1973-1974**) included an important estimate of the kinetics of the process over a range of pressure and temperature. The resulting time-temperature-transformation plots are useful in defining the later stages of the cooling path of a metamorphic rock.

One of the ultimate goals of vibrational spectroscopy is in deriving the thermodynamic properties of crystals that can be used in calculating their phase relations. A major step forward was taken in 1985 by Hofmeister **(1983-1987)** and colleagues in modifying a Fourier-transform, far-infrared spectrometer with a beam condenser, an He-cooled bolometer, and a diamond cell in order to obtain high-pressure spectra. From the data collected in the modified apparatus, combined with the data from the Raman active bands, the heat capacity and the Grüneisen parameters could be obtained. The equation of state for the Mg-Fe olivines in particular will be at hand when the temperature effects are investigated.

Brillouin scattering from a five-pass, interferometer was used by Mao, Bell, and other colleagues to obtain the pressure dependence of longitudinal- and transverse-acoustic velocities and refractive index in solid hydrogen and deuterium for the purpose of obtaining its equation of state. These techniques can now be applied to the principal mantle phases to obtain their elastic parameters that are so important to the seismologist.

The important problem of heat transfer by radiation in the earth was examined by S. P. Clark, Jr. **(1957-1962)**. The strong onset of photon absorption in natural olivine appeared to be an important process that influenced the thermal regime in the earth. With dual-beam, crystal-field spectra H-k. Mao and P. M. Bell showed that the radiation window broadened with pressure, but the shift of the absorption edge with pressure blocked the radiative transfer.

Because of the enormous advantage of the intense, parallel x-rays from a synchrotron source, Mao, Hemley, and colleagues

have developed the appropriate devices for carrying out diffraction at high pressures at the National Synchrotron Light Source at the Brookhaven National Laboratory, Upton, NY. The intense beam, properly collimated, is ideal for high-resolution, low-atomic-weight elements, and small sample diffraction. The determination of the crystal structures of solid hydrogen and helium, for example, has been a major contribution to fundamental physics. The structures of oxides and silicate-perovskites, critical in the mantle, and those of iron and nickel-iron alloys at core pressures have also been ascertained in the diamond cell. These impressive experiments have been acclaimed by the entire scientific community.

The assembly in the 1970's and 1980's under one roof of the wide range of tools described, supplemented by the use of electron spin resonance, nuclear magnetic resonance devices, and transmission electron microscopes at other institutions, have resulted in a major revolution at the Geophysical Laboratory and in the field of mineralogy. The quantitative approach to mineralogy in which mineral properties are characterized in order to obtain thermodynamic parameters is of critical importance in understanding materials under the extreme range of conditions in the earth, particularly where the direct measurement of thermodynamic parameters is not yet possible. Theoretical computational methods for predicting structural, thermodynamic, and elastic properties has been developed by Hemley for minerals under these extreme conditions. In combination with the on-going experimental mineral physics research, a sound theoretical basis for interpreting condensed phase behavior is developing.

8. Field Petrology

Throughout the years, field measurements have been an integral part of the experimental program. Most staff members have collected their own samples to test new concepts, but the help of colleagues, especially in the U. S. Geological Survey, has also been vital. The generosity of museum curators has also been essential in obtaining materials with the appropriate properties for meaningful experiments.

Some staff members have relied heavily on detailed mapping for the development of ideas. The analytical work of H. S. Washington **(1912-1934)** and E. G. Zies, for examples, was guided by first hand experience in the field. The classic studies of Fenner at Gardiner River, Yellowstone National Park, Wyoming, and Katmai, Alaska, are still highlighted. No doubt his work was well remembered by some of the officials of Yellowstone National Park, who watched with "considerable apprehension" as Fenner began drilling operations in 1929 several hundred feet west of Old Faithful geyser. The study of that core as well as one from Norris Basin recorded the rock alteration, which correlated well with the results of Allen's analyses of the discharge waters.

Fenner's papers gave rise to an extended debate on the roles of assimilation and magma mixing. He was a strong advocate of superheat, and he believed that an adequate heat content was necessary in the magma for assimilation to be a major proc-

ess. Bowen, on the other hand, assigned a minor role to assimilation because he did not believe superheat prevailed. Perhaps the more widely known Fenner-Bowen debate was in regard to the fractionation trends of magmas. Whereas Fenner's field studies led him to believe iron was concentrated in intermediate liquids, Bowen was persuaded on experimental grounds that iron was removed continuously through the stages of fractionation. The iron-enrichment trend through ferrogabbro became labelled the Fenner trend, and the basalt → andesite → dacite → rhyolite series was designated as the Bowen trend. Later work by E. F. Osborn **(1938-1945; 1973-1977)** in which iron oxidation was taken into account, has shown that both trends can result depending on the conditions.

A major contribution to the granite problem resulted from the extensive collections of granites by F. Chayes **(1947-1986)**. His techniques of modal analysis provided critical evidence that related the mineralogical composition of these rocks to the minimum melting diagram of Tuttle and Bowen (1958). The persuasive argument that liquid was involved in the generation of rhyolites and granites was made, but whether they arose by partial melting or fractionation depended on other criteria. Various granites have been distinguished by both modal and chemical analyses, yet attempts to relate the pyroxene-, pyroxene-amphibole-, amphibole, mica-amphibole-, mica-, two-mica-bearing granites have not been rewarding. The search for chemically equivalent granites having different mineralogy has not as yet been successful, so the question of heteromorphism in granites remains open.

Layered intrusions have provided critical tests for many theories purporting to relate magmas. Careful field observations by T. N. Irvine have yielded many new ideas. Before arriving at the Geophysical Laboratory, he had made detailed studies of layered intrusions on Duke Island (Alaska) and Muskox (N.W.T.), Canada. Subsequent studies included Skaergaard, Stillwater, Bushveld, and other classic areas. As a result of these experiences he characterized the processes resulting from new magma influxes, side-wall accumulation, mass slumping, density currents, troughs, double-diffusive convection, and accounted for compaction effects, metasomatic exchange, replacement reactions, and the products of magma mixing. Debate has been vigorous, but the thoroughness of his documentation, supported by laboratory model experiments, have stimulated efforts in field studies by others.

The collection and identification of ultrabasic xenoliths from alkaline rocks has been a major interest of F. R. Boyd. On the basis of many thousands of electron microprobe analyses of coexisting minerals in nodules collected from kimberlite pipes in southern Africa, Boyd and associates were able to define the depth and temperature of origin of the nodules. From these data and the constraints of high-pressure experimental studies, Boyd was able to construct a section of the mantle under the Kaapvaal Craton and adjoining younger rocks. The model illustrates the lithosphere-astheno-

sphere boundary at about 150 km with a root zone extending to 200 km under the craton. The root zone extended into the stability field of diamond and is also marked by the presence of low-Ca garnets. From these field and mineralogical studies extending over twenty-years, a unique structural and chemical model has emerged that will no doubt be further supported as the great variety of nodules are characterized. The metasomatic effects, recrystallization, deformation, and kinetic responses to the dynamics of eruption of the nodules are currently under investigation.

The classical studies of T. F. W. Barth in 1936 on the "metamorphism" of paleozoic sediments in Dutchess Co., N. Y., resulted in the definition of a new class of rocks called "syntectic". His detailed mineralogical and petrological studies outlined the passage of sediment → slate → schist → gneiss → augen gneiss → intrusive granite. During these events the rocks were "heated and stewed in liquids of magmatic and anatectic origin". The role of fluids became an important aspect of the mapping by Rumble and associates of metamorphic rocks of New Hampshire. He developed a dynamic model for the flow of fluids through rocks during metamorphism from stable isotope data. His recognition of hydrothermal graphite as the core marker of fluid transport generated a wide variety of investigations.

The staff members of the Geophysical Laboratory are convinced that experiments derived from, guided by and tested with field relations result in principles of lasting value. The field-laboratory-field process is reiterated until an acceptable interpretation of the geological field observations is obtained.

9. Statistical Petrology

Four years were required for H. S. Washington to compile the "Chemical Analyses of Igneous Rocks" that had been published during the period 1884-1913. He personally recalculated all the CIPW (*C*ross, *I*ddings, *P*irsson, *W*ashington) norms of the rocks. The monumental work appeared in 1917 with the statement that rock analyses were "indispensable", and "the study of igneous rocks is in large part the study of silicate solutions and their equilibria, often complicated by the presence of volatile components, and is thus regarded as essentially a special branch of physical chemistry". The CIPW norms contributed greatly to the classification of igneous rocks, but more importantly reduced the chemical analysis of a rock to simple endmember components that could be experimentally investigated. The normative system incorporates an enormous amount of petrologic intuition and perceptiveness derived from field experience. The assignment of the analyzed constituents was made in an order that reflected field knowledge of the physicochemical behavior of rocks not yet demonstrated experimentally in 1902!

A "Manual of the Chemical Analyses of Rocks" was also published by Washington in 1904, revised through three subsequent

editions, with due acknowledgment of the advice of his friend W. F. Hillebrand, a chemist at the U. S. Geological Survey at that time. That manual served a generation of analysts in the production of high quality rock analyses.

The explosion of analytical data after WWII presented a challenge of the first order that was met primarily by the remarkable developments in electronic data storage and retrieval at first confined to numerical data. An early compilation of over 16,000 analyses of Cenozoic volcanic rocks by Felix Chayes, a petrologist, proved extremely useful both in research and as a guide to further work. As soon as it became apparent that large quantities of *non*-numerical data could be effectively stored, sorted, and selectively retrieved in digital form, Chayes turned his efforts to systematic development of a world data base for igneous petrology. He developed a suitable international organization for the construction and maintenance of such a base. Currently, the International Geological Correlation Project 263 and a Subcommission of the International Union of Geology share responsibility for the base, version 2 of which is distributed by World Data Center A.

Current estimates of the number of published rock analyses range from 65,000 to over 100,000. It is evident that a more intensive effort will be required to use the information now available. The eventual correlation of phase assemblage (mineralogy) with chemical composition, not yet done for a single rock type, is essential for the future progress of petrology. The least-squares approximation technique pioneered by W. B. Bryan **(1967-1970)**, Chayes and Finger (1969) was a major contribution to the estimation of these important relationships.

Another important problem, still largely unresolved, results from ratio formation, in particular, the percentage form of statement used in reporting rock analyses. For example, the closure resulting from dividing the amount of each constituent by the sum of all imparts special properties to the interrelationships of the constituents. Chayes summarized these properties in a manual for students called "Ratio Correlation" in 1971. Chayes' extensive experience in the modal analysis of rocks, mentioned in the section of Field Petrology, was recorded in "Petrographic Modal Analysis" (1956) in which he showed that the point-counting of minerals in thin sections gave an accurate estimate of their volumes in rocks, and he provided experimental evaluation of the number of points and sections required to achieve appropriate precision.

10. Extraterrestrial Petrology

Meteorites

The nickel-iron core of the Earth was at one time believed to be surrounded by a zone of mixed iron and silicate, pallasite. Because of the supposed similarity between some meteorites and the interior of the earth, the pallasites were studied both for their structure and range of composition by Adams and Washington (1924). The

meteorites also contribute to an understanding of the origin and history of the solar system. For this reason S. P. Clark, Jr. and Kullerud undertook a study of Fe-Ni-S and Fe-Ni-P to establish a buffered system of taenite and kamacite with troilite or schreibersite in order to derive the temperature of formation of the meteorites. While in residence, P. Ramdohr **(1960-1962, 1964)** examined over 340 polished sections of stony meteorites to characterize in a systematic way the mineralogy of the opaque phases. In typical fashion, he discovered many new minerals as well as previously described minerals hitherto not previously observed in meteorites. The Fe-Cr-S system was studied by El Goresy **(1967-1968)** and Kullerud to account for the Cr-bearing compounds in meteorites. They found the sulfides responded more readily to shock impact than silicates thereby explaining their disequilibrium relations.

Over the years the Allende carbonaceous chondrite received the special attention of the staff because of its potential applications to the early evolution of planets of alleged chondritic composition. The P-T diagram for the Allende meteorite up to 30 kbar with and without H_2O was investigated by Kushiro **(1962-1965, 1968-1969, 1971-1976, 1978-1987)** and M. G. Seitz **(1971-1974)**. They demonstrated that separation of the phases would yield the layered structure presumed for the earth. Other experiments dealt with the partitioning of elements between the metal, oxide and silicate portions. The amino acids were identified by Cronin **(1974-1975,** 1975) and some notion of the process whereby abiotic organic compounds could be formed from the precursor compounds in the meteorite. The partitioning of boron was achieved through an etching technique that revealed the spallation recoil tracks in whitlockite. The high concentration of boron and other volatile elements in a meteorite alleged to have formed at high temperatures remains a mystery. The fassaite of the Allende meteorite was interesting because it was found to be iron free and contain trivalent titanium, confirmed by high-resolution optical spectra. The chemical incompatibility of its oxidation state with other minerals in the meteorite, such as metallic iron and andradite, was evident.

Meteorites frequently contain minerals formed at high pressures through shock. For this reason they are important in understanding the phase changes that take place at depth in the earth's mantle. The discovery of ringwoodite, the spinel form of olivine, indicated to N. Boctor **(1977-1980)**, Mao and Bell that the pressure was between 100 and 225 kbar during impact metamorphism. The presence of majorite in association with ringwoodite suggested to them that a large pressure gradient existed in the order of 100 kbar to > 300 kbar. Other features such as veins of inhomogeneous glass from incipient melting, fracturing, undulatory extinction, and mosaicity are also indicative of high shock pressures.

Lunar Samples

The return of the successful Apollo missions with samples of the moon beginning in 1969 provided one of the most

exciting scientific opportunities for the following decade. The incredibly fresh and unaltered character of the rocks greatly facilitated their study, but the fine grain and shock metamorphism of the minerals were the principal challenges. The characterization of the fine-grained material generated a new array of techniques and the unique conditions of rock formation on the moon led to the new field of comparative petrology. Needless to say, the daily excitement of discovery has not been equaled by the arrival of any other set of specimens. The initial stages of inquiry were predominantly detailed mineralogical studies, followed by experimental studies of both the natural samples and synthetic analogues, and then the testing of various models of the moon's composition and structure. The entire array of sample types (rocks, breccias, glass fragments, and soils), was investigated by the staff members.

Because of the special skills of the staff, the opaque minerals received detailed attention. Ilmenite was the major opaque phase, but members of the chromite-ulvöspinel series, the newly discovered armalcolite series, as well as troilite and metallic iron alloy were studied. (Armalcolite was also discovered independently by several laboratories, and subsequently named by combining the initial letters of the names of the astronauts *Arm*strong, *Al*drin, and *Co*llins.) Haggerty **(1968-1971)** found that the spinels were bimodal at some sites, but other samples exhibited a complete series of solid solutions. A new pyroxenoid was discovered by Lindsley, which he then prepared synthetically at high pressures. The new phase, pyroxferroite, is apparently metastable and had persisted in that state for at least 3 b.y.! The olivines also appeared to be bimodal in some samples. The Cr content of olivine was more than twice that of earth olivines, and more importantly, was in a reduced state (Haggerty *et al.*, 1970). The first demonstration of Fe-Mg ordering in any olivine was made by Finger on the lunar material.

The pyroxenes were studied in exceptional detail by Boyd, whose electron microprobe data clearly reflected their chaotic crystallization behavior. The zoning of the pigeonites and oscillatory augite rims, for example, suggested cooling and mixing with new magma batches. Two distinct rate-determining steps were found by Virgo in the cooling of two lunar pigeonites. A steady state of Fe-Mg ordering was achieved at about 810°C involving a few hours of time, then an exceptionally slow rate to about 480°C below which no further annealing was possible. (The ^{57}Fe resonance spectroscopy technique for determining valence state and geometrical configuration of iron in a crystal structure had been previously proved useful in kinetic studies of terrestrial pyroxenes). The plagioclases contained Fe^{2+} and its site preference was determined by Finger. The range of shock features in the plagioclase were particularly impressive. The lunar glasses were studied with the new high-resolution, optical-spectra apparatus of Bell and Mao. Some of the glasses were igneous in origin and others formed from the meteorite impacts. Various colored glasses were found to result from the reduced states of Fe and Ti. A particularly exciting event, although

short lived, was the discovery of "rust" (goethite and akaganéite) on some of the lunar specimens, eventually attributed to accidental contamination in the earth's atmosphere. The event was not only an exhibit of the great care taken by the observers, but also of the advanced state of the art of characterizing fine materials.

The experimentalists also contributed to the understanding of the formation on the moon of the principal rock types, called basalts and anorthosites even though they were quite different in composition and mineralogy from their earth-bound namesakes. Because of the extreme rarity of the lunar samples, Muan and Schairer (1969) made a synthetic analogue and studied its behavior at a series of temperatures in iron crucibles. This "basalt" composition yielded pyroxene on the liquidus at 1185°C and had a solidus between 1075°-1090°C with plagioclase and ilmenite. These values are not greatly different from those of some earth basalts. Later, as more material became available, lunar samples themselves were studied at a range of P and T by Kushiro and Hodges **(1973-1974)**. Of the three models of lunar composition they tested, the model composition of Ganapathy and Anders (1974) appeared to fit the observations best. A most interesting observation of Bell and Mao in support of the high-pressure experiments was recognition that a spinel + two-pyroxene symplectite in olivine had the bulk composition of garnet. The reaction of garnet and olivine to the symplectite assemblage had been previously demonstrated to be a high-pressure reaction. Another set of pioneering experiments was performed by M. G. Seitz. He was concerned about the chemical fractionation that resulted from the volatization of materials during the impact events. He showed in a vacuum furnace that all of the alkalies and some of the iron was lost by volatilization in short heating events. These experiments were precursory to the major program of study, described below, most pertinent to the origin of the solar system.

Condensation Petrology

An understanding of the evolutionary processes of the solar system require data on the P, T, and composition at various times and places as the solar nebula collapses. The fundamental issue is whether the minerals formed by direct condensation from a gas or by crystallization from an intermediate liquid phase of the proto-solar system. Experiments conducted at the Geophysical Laboratory by Mysen, Virgo, and Kushiro bear on these processes. The materials found in meteorites are believed to be representative of the oldest solar system material. For this reason, they worked on the very low-pressure region of stability for minerals such as akermanite, diopside, corundum, spinel, and hibonite, found in the carbonaceous chondrites. By means of a Knudsen-cell technique, in a high-vacuum, high-temperature furnace, they established the P-T curves separating the crystal, vapor, and liquid regions. From the experimental results, they suggest that for the solar-gas composition, the pressure would have to exceed 10^{-2} bar for liquid to form, increasing with decreasing oxygen fugacity. In general, it appears that the

early solar nebula resulted from gas-crystal reactions in the absence of melting at pressures below 10^{-4} bar and at an $f(O_2)$ at least 3 orders of magnitude below that of the iron-wüstite buffer. In short, these dramatic experiments place severe constraints on the collapse of the solar nebula and emphasize the systematic chemical differences between the terrestrial planets as a function of their distance from the sun.

Other constraints are placed on the gaseous planets by experiments in a totally different realm. Materials that are normally gaseous condense to form liquids and crystals at high pressures. Studies up to 5.5 Mbar are particularly pertinent to the early evolution of the solar system as well as the interior of Jupiter, for example. The *P-V* curves for crystalline hydrogen, deuterium, argon, neon, xenon, and oxygen have been determined, and, in some cases, their crystalline structure determined with synchrotron-generated radiation. The first single-crystal structure determination of n-H_2 at 54 kbar by Hazen *et al.* (1987) with conventional x-ray diffraction was of fundamental interest to condensed-matter and planetary physicists. In addition, methane and water, important in the Giant Planets were also studied. In this way Mao, Hemley, and a large number of colleagues were able to set limits on the conditions required to collapse these gases in the nebula.

11. Volcanology

In 1902, when the CIW was only five months old, the city of St. Pierre, Martinique, was destroyed by the eruptions of Mount Pelée. The event no doubt helped persuade the Board of Trustees of the need for a geophysical laboratory that would investigate the phenomena of volcanic eruption. Field and analytical investigations of the rocks from an active volcanic region by H. S. Washington (1906) were promptly supported by CIW. His monograph on "The Roman Comagmatic Region" (≈Italian petrographic province) presented a detailed description of the many rare lavas characterized by the presence of leucite. In 1911 the Hawaiian Volcano Observatory was founded by T. A. Jaggar (MIT) in collaboration with R. A. Daly (Harvard), the Volcano Research Association of Hawaii, and the Geophysical Laboratory. The measurement of the temperature of the lava lake in Kilauea and the role of gas in the flowing lavas were undertaken by E. S. Shepherd and F. A. Perret that year. These epoch-making studies involved the collection, via a cable across the lava lake, of an iron bucket dip sample of the lava and immersion of a thermocouple pipe in the bubbling lake itself. In the summers of 1911 and 1912, Day and Shepherd collected and analyzed the gases in the active part of the Halemaumau crater of Kiluaea. They clearly demonstrated that water was an original component of the lava, contrary to the prevailing view of the nonaqueous quality of magmatic gases. Furthermore, they attributed the loss of gas as the reason for the structural change from Pahoehoe lava to Aa lava.

Day and Allen next turned to Lassen Peak, CA., after its catastrophic outbreak in May of 1915, the first eruption from a volcano within the continental boundaries

of the U. S. in the memory of then living men. In addition to the description of the eruptive activity, they focused on the types of hot springs and fumeroles with field and laboratory measurements. The change from springs of acid character transporting pyrite, to those of alkaline character was attributed to the interaction of the hot waters with the silicate rocks.

In the meantime, Mount Katmai, Alaska, had erupted during June, 1912, but it was 1916 before an expedition, organized by R. F. Griggs and supported by the National Geographic Society, reached the area. On that and subsequent expeditions to the Valley of Ten Thousand Smokes were C. N. Fenner, E. G. Zies, and E. T. Allen, who collected rocks, fumerole encrustations, measured the temperature of the hot springs, aspirated exhalations for the "insoluble" gases, and helped in the geologic mapping. They concluded that the vast sheet of siliceous rocks were not lavas but were of pyroclastic origin, ejected as rhyolitic pumice through the fractured valley floor. The fumeroles (100°-650°C) were, therefore, of deep seated origin and decreased in temperature with time. Through successive observations, the mineralogy of the encrustations changed as the temperature dropped, and because many economic minerals were formed, a relationship of ore deposits to volcanic exhalations was established. The analyses of the gases collected showed the highest contents of HCl and HF that had ever been detected. The hybrid nature of the rocks (also found at Lassen Peak) led Fenner to believe that a superheated rhyolite magma melted fragments of old andesitic lavas and incorporated them into the erupted pumice and ash. The detailed analytical work, tied closely to the mineralogy and geology, established the value of a multidisciplinary approach to geologic problems.

In the course of these studies, Morey (1922) provided a new theory for the increase in pressure of a cooling hydrous magma, based on the continuity and univariancy of the crystal + liquid + gas curve in the KNO_3-H_2O system. Some forty years later Yoder (1965) pointed out that most magmas were not saturated or univariant and that explosive volcanism resulted from an incremental drop in pressure when gas was liberated from an initially undersaturated magma. This concept arose out of an experimental study of the synthetic basalt system diopside-anorthite-H_2O at 5 and 10 kbar.

Four major studies in volcanology by F. A. Perret, an associate of the Geophysical Laboratory, were supported by the CIW. Detailed descriptive monographs were published on the Vesuvius eruption of 1906, the eruptions of Mt. Pelée, the volcano-seismic crises at Montserrat, and finally, because Perret was obliged to stay in the U. S. during WWII, a compendium of his studies of volcanoes around the world. These unique contributions record the observations of one of the world's most perceptive students of volcanic activity.

The remarkable hydrothermal activity of Yellowstone National Park was described in another classic study by Allen and Day (1935), in which is recorded the physical and chemical changes of the fumeroles, geysers and thermal springs over a period of seven years. The relationship of hot

springs to fumeroles was defined and the differences in rock alteration from the acid, mixed, and alkaline types contrasted. They identified superheated water up to 138°C, which gave rise to violent effervescence, and they contributed to the problem of discharge and its relation to rainfall.

A further contribution to the study of hot springs and geysers was made by T. F. W. Barth who carried out the laboratory study of samples collected in Iceland. The work was done during the summers of 1934 and 1937, but publication was held up for eight years while Barth was detained in occupied Norway.

Note should be made of the extensive field and chemical investigation by E. G. Zies of the domes of the active volcano Santiaguito and its ancient edifice Santa Maria in Guatemala. Unfortunately, failing health prevented him from bringing those studies, mentioned in a series of nine abstracts, to the publication stage. The combination of Zies' analytical skills and H. E. Merwin's keen microscopy had generated a detailed picture of the mixing of magmas and the digestion of individual crystals.

The last major work on volcanic activity supported in part by the Laboratory was F. R. Boyd's study of the welded tuffs and flows in the rhyolite plateau of the Yellowstone National Park, Wyoming. Boyd mapped the plateau, determined its stratigraphy, and, most importantly, discovered the Yellowstone caldera. His thermodynamic analysis combined with experimental evidence showed that tuffs can have temperatures of emplacement sufficiently high for them to weld.

More pages have been written by the staff on volcanology than any other field of endeavor. Other projects on active volcanoes have been undertaken by the staff in recent years, but the field studies have been primarily for the purpose of keeping touch with the principal problems uncovered by other workers. Field work has always been encouraged at the Geophysical Laboratory in order to investigate experimentally the significant problems whose solution may be applied broadly.

12. Geophysics

Although the name of the Geophysical Laboratory implies that a large component of the work would involve geophysics, the classical fields of endeavor now included under the term have played a small role over the years. For brief periods, however, gravity, heat flow, electrical conductivity, thermal conductivity, density, magnetism, tectonophysics, oceanography and seismology, have all been investigated. Some of these studies were cooperative with the Department of Terrestrial Magnetism, which was established in 1903. It initially dominated the field of magnetism, complementary to the national bureaus, and was a pioneer in explosion seismology after WWII.

Gravity

One of the many interests of F. E. Wright was the difference in gravity between the earth and moon and the resulting differ-

ences in geomorphology and isostatic compensation. Pursuing this interest, he persuaded F. A. Vening Meinesz in 1928 to install his pendulum for making gravity determinations at sea on a U. S. submarine. From subsequent measurements, they concluded that some oceanic deeps were uncompensated whereas the Mississippi delta was practically compensated in spite of the enormous load of sediment laid down each year. Inspired by the facility of occupying a large number of stations at sea, Wright and J. L. England developed an improved torsion gravity meter mounted on a truck so that twenty or more stations could be occupied in a day. Although most of the stations occupied were in the eastern U. S., the apparatus was set up in 1940 on an active volcano in Guatemala to assess the changes in the magma chamber in conjunction with other geophysical measurements.

Heat Flow

An early attempt (1912) to measure the thermal gradient in the crust was made by J. Johnston and L. H. Adams. They used both mercury thermometers and an electrical resistance thermometer in wells as deep as 5230 feet. It was believed that such measurements might also have economic importance in identifying layers rich in coal or oil, indicated by a higher temperature gradient. An opportunity for measuring heat flow in long tunnels occurred in the construction of the Arlberg and Taverin tunnels in Austria. With the underground temperature observations and the laboratory measurement of thermal conductivity of the various rocks, S. P. Clark, Jr. found that relatively high geothermal fluxes extend into the eastern Alps. More recently the relatively high heat flow (2.2 mcal/cm^2sec) in Arizona was investigated by Bell and R. F. Roy (Harvard), who related the results to the gravity and seismology data of the region.

Geotherm

The problem of the cooling of a primitive earth was undertaken by L. H. Adams (1924) after the revealing calculations of Holmes (1916) and Jeffreys (1924). He generated a "most probable" geotherm down to 300 Km, assuming the age of the earth was 1.6 b.y., the generation of radioactive heat was constant, and the earth was covered with a substantial molten layer. Urry (1949) also calculated the geotherms for the earth at various times taking into account the exponential decay of radioactive elements and the variation of surface heat flow with time. Later, Clark (1961) derived geotherms as a function of time for various models calculated with the aid of a digital computer. He concluded that the distribution of radioactivity cannot be inferred from the near surface heat flow. Furthermore, the variability of heat flow cannot be attributed to different degrees of concentration of radioactivity in the outer few hundred kilometers of an initially homogeneous earth. An innovative approach to the geotherms was found by F. R. Boyd, Jr. by applying the pyroxene geobarometer and geothermometer. On the basis

of the composition of coexisting pyroxenes in nodules from kimberlites, he obtained a quantitative measure of the geotherm. In general, the geotherm derived from the nodules substantiates the geophysical estimates based on surface heat flow. His results also showed that cratons have been cool relative to oceanic plates for at least 3 b.y. One surprising result was an inflection in the geotherm under northern Lesotho that may be attributed to a region of partial melting.

Tectonophysics

Prior to the opening of the Geophysical Laboratory and during its formative period, grants were made to F. D. Adams **(1902-1912)** by CIW to study the flow of rocks. A 120-ton press was set up at McGill University to investigate the deformation of marble, granite, diabase, and other rock types at temperatures up to 1000°C. One of the goals was to understand the origins of crystalline schists, a subject of special concern to Van Hise who served on the CIW Advisory Committee in Geophysics. A theoretical interpretation of the flow in stressed solids by R. W. Goranson, using thermodynamic potential relations for different physical conditions, was corroborated by experimental studies. Those experiments were not published, presumably because of Goranson's assignments during WW II, but support for his theory was provided by the more detailed laboratory studies of D. Griggs (Harvard). For a five-year period, two Postdoctoral Fellows from Yale undertook a field and experimental program relating the conditions of flow to the resultant plastic strain. On the basis of these and other studies, E. Hansen **(1964-1968)** developed the concept of "strain facies" recorded in a book with that name.

Oceanography

The discovery of the high radium content of ocean bottom samples collected by the auxiliary brigantine *Carnegie* led C. S. Piggot **(1925-1947)** to develop a device for coring ocean bottom sediments in 1935. Using a gun-fired sample tube and hoisting gear built at the Geophysical Laboratory, he obtained cores with the cooperation of the crews on the ship *Atlantis* (Woods Hole Oceanographic Institution). Cores up to ten feet in length were recovered from depths as great as 2700 fathoms. Changes in the orientation of the earth's magnetic field with depth in those cores were studied at DTM.

Magnetism

The pressure effect on the critical temperature of magnetization of iron was found to be negligible up to 3.6 kbar by L. H. Adams and J. W. Green (1931). They concluded that the nickel-iron core had little influence on the earth's magnetic field because the core temperature was well above the Curie point! The Curie point was investigated for a large number of materials by Posnjak during 1936-1937, and the effects of solid solution on the magnetic properties of spinels were the subject of investigation for many years to follow.

Seismology

Of special significance was the theoretical contribution of L. H. Adams and E. D. Williamson **(1914-1923)** in 1923 when they deduced a formula that related the compressibility and density of rocks to the seismic velocities of the longitudinal and shear waves. In this way the laboratory measurement of the density and compressibility of rocks and minerals constrained the kinds and proportion of phases in earth where the seismic velocities were known. Observational seismology had been recommended by the Van Hise Committee as early as 1903 and proposed on numerous occasions thereafter. The Director of the Geophysical Laboratory, A. L. Day was appointed chairman of the CIW Advisory Committee in Seismology in 1921. On his Committee's recommendation, a program of study was outlined and a Seismology Laboratory built in Pasadena, California, in 1926 in cooperation with the California Institute of Technology. The studies were administered by the Committee until 1 Jan 1937 when the Seismological Laboratory was turned over to Caltech. That Laboratory was primarily concerned with natural earthquakes; however, following WWII, the DTM initiated a cooperative program in explosion seismology. Three members of the Geophysical Laboratory staff, J. W. Greig, J. L. England, and G. L. Davis **(1941-1978)**, helped select the seismometer sites for their geological advantages and on occasion occupied those sites to receive signals from quarry blasts and the destruction of old military explosives, for examples. In another more recent cooperative project with DTM, the velocity of transmission of both longitudinal and shear waves in partially molten peridotite was measured directly up to 10 kbar by T. Murase **(1976-1980)** and colleagues.

13. Geochemistry

In the formative stages of the Geophysical Laboratory, the major debate about its program of work concerned physical measurements, promoted by G. F. Becker, and chemical measurements, advocated by C. R. Van Hise. A compromise resulted in physical chemistry, with the emphasis on chemistry, a position strongly supported by C. D. Walcott who was Director of the USGS and Secretary of the CIW Board of Trustees. There was no disagreement on the great need for application of the quantitative principles of physics and chemistry to the science of geology. Although, geochemistry, loosely defined, pervades most aspects of geology, the following highlights of the work of the Geophysical Laboratory are restricted to only a few investigations highly dependent on chemistry.

Element Partitioning

The accuracy and precision of the analysis of the minutest amounts of an element has reached an exceptionally high state with the wide variety of techniques available. Nevertheless, the analysis of a mineral, a unique combination of elements,

still requires research—it is not a routine matter. The data produced are of a most fundamental character in determining *P, T*, time, and reaction path of the mineral and its host rock. Analytical chemistry, however, has greatly outstripped the *calibration* of those data in defining the conditions endured by the rock.

Phase equilibria studies have defined limits of solid solution for a large number of the common rock-forming minerals. Some of those studies have already been mentioned in the section on Experimental Petrology; however, the minor and trace elements would appear to be a more accurate measure of conditions because they tend to obey the thermodynamic laws of dilute solution. The emphasis, therefore, has been on the partitioning of elements such as Ni, Cr, Ti, alkali metals, alkaline earths, and various rare earths for crystal-liquid, crystal-vapor, as well as crystal-crystal equilibria. The major productive period was 1970-1980, and perhaps the principal reason for the diminution of interest after 1980 can be attributed to the realization that the partitioning coefficients were much more sensitive to bulk composition than previously envisaged. The enormity of the task of calibrating trace elements then acquired dimensions beyond the scope of a small laboratory dedicated to pioneering ventures.

In 1953, Eugster and colleagues initiated some experiments on the partitioning of Cs, Tl, and K between sanidine and a fluid phase at a series of temperatures from 500° to 800°C and 1 and 2 kbar. Cesium, for example, more readily entered the sanidine structure at high temperatures than at low temperatures when Cs/K was 0.0002 to 0.01, but the enrichment was much less than observed in nature. Eugster attributed the difference to the great enhancement that results from fractional crystallization. These experiments appear to be the first direct determination of the distribution factors of minor elements in silicates.

The technique that facilitated the measurement of crystal-liquid partition coefficients was fission-track mapping on muscovite or on emulsions, which when developed revealed the concentration of the radioactive element. Seitz described the method in 1973 for the partitioning of ^{235}U and ^{230}Th between diopside and a liquid in Di-Ab-An, a simple basalt system. He used less than 30 ppm of the spikes and concluded that the activity coefficients were independent of concentration. In another series of experiments he examined the partitioning of ^{151}Sm between diopside and the simple basalt liquid to compare with the previous results of Kushiro and Masuda (1970) on clinopyroxene in a natural basaltic liquid. He found that the coefficients in synthetic systems were considerably lower than those in the natural system. Although he indicated that chemical and physical conditions affect the measurements, he also attributed the higher values in the natural system to non-equilibrium conditions.

Subsequent detailed studies by Mysen (1976) and his associates clearly demonstrated that the concentration range of Henry's law behavior was limited, and the partition coefficients became compositionally dependent. In the course of a few years, it was shown that the partition coefficients were dependent on pressure, tem-

perature, bulk composition, presence of other phases, and on the available sites in a crystal for specific trace elements. Even the structure of the melt was found by Mysen and Virgo (1980) to influence the partition coefficients. To all those factors can be added the influence of $f(O_2)$ and $f(S_2)$ on the partitioning of Ni between olivine and iron sulfide melt. The calibration of any partition coefficient indeed required careful control of all the variables.

Throughout the productive period, a wide range of natural rocks were melted at various conditions to determine specific partition coefficients in an empirical approach to defining their conditions of formation. Some of the rock types investigated included basalt, kimberlite, peridotite, komatiite, and other ultramafic rocks, primarily for the purpose of relating presumed source rocks to their partial melts. It became evident that the partial melts, as represented by the alkali basalts, were much too enriched in the light rare earths to have been generated from such sources by even small degrees of melting (Harrison, **1977-1979,** 1979). That conclusion gave strong support to the concept that metasomatism plays an important role in the mantle.

Aside from the many experiments on crystal-crystal partitioning, two ingenious investigations on liquid-liquid and crystal-vapor partitioning must be mentioned. In 1975, Watson **(1975-1977)** measured the partitioning of spiked elements in coexisting immiscible liquids in the K_2O-Al_2O_3-FeO-SiO_2 system. The compositions of the quenched glasses were determined by electron microprobe. From these data, he concluded that deviations from Henry's law were confirmed for several of the elements; there are cation interaction effects; and that there are distinct differences between the ways various cations are accommodated in the acid melt relative to the iron-rich melt. The results provided a useful test of speculations on the origin of mafic-felsic associations such as basalt and rhyolite.

The partitioning of elements between a water-rich vapor and the constituent minerals of a garnet peridotite was investigated by Mysen (1978). With the beta-track technique he measured the partition of Ce, Sm, and Tm in its minerals and obtained the trace element content of the coexisting vapor by mass balance. He demonstrated that the REE patterns were highly pressure dependent. In summary, it was clear that the REE content of the crystals are similar to the depleted nodules from the mantle and that the metasomatizing fluid in the mantle was, therefore, probably similar to that observed in the experiments.

Mineral Solubility

The initial studies on the solubility of minerals were carried out in 1915 on KNO_3 and KCl by L. H. Adams, who was interested in freezing point depression in dilute solution. He used an interferometer, rather than the customary refractometer, to achieve higher precision in the analysis of the solutions. About the same time, Johnston and Williamson, paying particular attention to the species dissolved in the solution, investigated the solubility of calcite. During the depression years and up to WWII, consid-

erable efforts were made in studying the simple systems NaCl-H_2O, K_2SO_4-H_2O, B_2O_3-H_2O, and KCl-H_2O, with emphasis on obtaining thermodynamic properties. With the development of high-pressure equipment, *P-V-T* data were developed for common salt solutions. One significant breakthrough was the study by Goranson (1936) of Ab-H_2O in which he determined the solubility of water in silicate melt, that is, the high-temperature end of the three-phase solubility curve. Other staff members focussed on the $CaSO_4$-H_2O system with various salts in order to understand the deposition of gypsum and anhydrite in salt water. Posnjak (1941) came to the conclusion that gypsum was most likely to be deposited from ocean water and might be converted to anhydrite after deposition.

During those years attempts were made to resolve the experimental problems of determining solubility at high *P* and *T* by developing a stirring and filtering device (Morey and Burlew **1936-1952**, 1938) so that the fluid could be quenched independently of the crystals. The increase in solubility with water pressure was of special interest, and in one study the weight of solids dissolved in the fluid reached almost half. Much of the theory for the solubility curves had already been worked out, however, a paper by Morey and Niggli (1913) was instrumental in guiding the laboratory research. It was not until 1940 that Morey and Fleischer **(1936-1938)** provided the background for two-volatile systems, such as K_2O-SiO_2-CO_2-H_2O, that are so important to the entire range of geological problems. Some of the stimulus for the study of the solubility of minerals in aqueous solutions no doubt came from the detailed studies of other staff members on the study of sublimates around fumeroles and volcanoes.

After WWII and with the development of many new tools for generating *P* and *T* and characterizing products, attention again turned to the *P-V-T* of simple aqueous solutions. Morey was then able to study Na_2O-SiO_2-H_2O, which exhibited retrograde solubility: The solubility of sodium disilicate fell to almost zero at the first critical end point, but became important again at the upper part of the solubility curve. The determination of the solubility of quartz in steam up to 600°C and 2 kbar was of practical importance in relation to the fouling of turbine blades as well as in the understanding of the formation of quartz veins. Morey and Hesselgesser **(1949-1953)** demonstrated that the solubility of some minerals was incongruent in the vapor phase - a property that became of special significance in metasomatism. In this post war period, Yoder (1958) studied the melting curves of Ab-H_2O, Sa-H_2O, Di-H_2O, An-H_2O, Ne-H_2O and Qz-H_2O up to 10 kbar, but none of the systems showed a second critical end point on the solubility curve.

The next major thrust was on the solubility of ore minerals in aqueous solution. A new apparatus was developed by H. L. Barnes **(1956-1960)** in which he could sample and analyze the gas phase from a reaction vessel at *P* and *T*. In this way, he obtained quantitative solubility measurements of sphalerite (ZnS) in H_2S-saturated water. In addition, he found evidence that a bisulfide complex was the most probable

transport mechanism for sphalerite. Barnes also observed that adding NaOH to the ZnS-H_2S-H_2O system did not change the phase relations significantly; however, in a study with Ernst, it was demonstrated that NaOH lowered the stability of brucite, for example, in a major way.

After an almost ten-year hiatus, solubility work again resumed in the new diamond-anvil, high-pressure cell. By direct, visual observation, the solubility of gypsum was measured up to 8 kbar by A. Van Valkenburg **(1975-1980)** and his colleagues Mao and Bell. They also observed the phase $CaCO_3 6H_2O$, ikaite, which had been found in a carbonatite deposit submerged in arctic waters.

With the development of infiltration models for mass transport in hydrothermal rock systems, the need for mineral solubility data became acute. Because fluid inclusions in many ore deposits contained chlorides, geothermal well waters are often brines, and evaporate minerals are associated with copper porphyry deposits, Frantz and his colleagues investigated simple systems in the presence of HCl. Study of the reaction of HCl with talc, hausmannite, albite and hematite resulted in the conclusion that the metals were dominantly associated, e.g., $MgCl_2°$, above 400° to 600°C at 1 and 2 kbar. With knowledge of the associated species, accurate solubility information could be calculated for those minerals investigated and a host of others.

In view of the above importance of ionization behavior of electrolytes, Frantz joined with W. L. Marshall (Oak Ridge National Laboratory) to measure the electrical conductance of salt solutions as a function of pressure and temperature. A large array of simple systems were investigated, including carbonates, hydroxides, and fluorides. The results were immediately applicable to steam-generated corrosion in nuclear power plants in addition to their fundamental importance to the principles of element concentration in ore deposits. Current research is focusing on the determination of the PVT properties of mixed volatiles in which synthetic, fluid-inclusion techniques are used. Methods are being developed for the accurate analysis of *individual* fluid inclusions in the silicates coexisting with ore minerals with new sophisticated microanalytical techniques. Concurrently, a high-pressure cell has been designed to examine the Raman spectra of solutions at 600°C and 4 kbar to ascertain the species transporting the various metals important in ore deposits.

14. Thermodynamics and Calorimetry

The first director, A. L. Day, while attending Yale occupied an office in the same building as J. Willard Gibbs, and presumably Gibbs influenced Day's scientific focus. Later, on returning from Germany, Day served as the personal emissary of the Berlin Physical Society, advising Gibbs of his election as president of the Society, which Gibbs declined for reasons of age. It is no wonder, therefore, that thermodynamics became a major factor in the work of the Geophysical Laboratory. Intensive study sessions were conducted by members of the staff, and several members achieved international recognition for their

interpretation and application of thermodynamic principles. After a series of papers on laws of chemical equilibria, heterogeneous equilibria, and phase rule problems, G. W. Morey (1912-1957) was asked to contribute an article to the "Commentary on the Scientific Writings of J. Willard Gibbs." Another major contributor to thermodynamics was George Tunell, renown for his careful exposition and explicit derivations, particularly in regard to open systems.

The definition of activity, chemical potential, and related thermodynamic quantities, especially their variation with temperature and pressure was the principal area of expertise of L. H. Adams. A treatise on the "Thermodynamic relations in multicomponent systems" by R. W. Goranson was published by CIW. He, too, was involved in the thermodynamic treatment of activity as it applied to solutions. But for the practical PVT relations in solutions, whether they were organic or inorganic, one turned to R. E. Gibson **(1924-1946)**. Experimentalists consulted Morey for application of Schreinemaker's principles, especially the Morey-Schreinemaker's coincidence theorem, in the solution of their phase diagrams.

It was N. L. Bowen who led the way in using the phase diagram to derive thermodynamic properties. The diopside-anorthite system is often used to illustrate those principles, and his diopside-albite-anorthite system is the current model for describing thermodynamic functions. The *theoretical* guidance of thermodynamic principles was evident throughout all the work of the Geophysical Laboratory.

The *experimental* determination of thermodynamic properties was at various times a significant part of the work of the Laboratory. The construction of a calorimeter was in the hands of W. P. White **(1904-1935)**, who was best known for the White double potentiometer adopted by the leading manufacturer of precision electrical measuring devices. White was greatly concerned with the factors that resulted in high precision and accuracy, and his monograph in the American Chemical Society Series on "The Modern Calorimeter" records detailed analysis of each facet of the experiment. He provided specific heats for the various forms of silica and some silicates, including the feldspars, in which a drop calorimeter was used.

Calorimetry was considered a high priority subject of investigation after WWII. A hydrofluoric-acid-solution calorimeter was built by F. C. Kracek **(1923-1956)** and his colleagues T. G. Sahama **(1947-1949)** and K. J. Neuvonen **(1948-1950)**, with improvements on the successful Bureau of Mines (Berkeley, CA) design. At that time jadeite was under intense study from both a theoretical and experimental viewpoint, so the thermodynamic data for the critical reaction nepheline + albite $\rightarrow$ jadeite were obtained. With the newly determined heats of formation as well as the determination of the other relevant parameters by other workers at the Laboratory, L. H. Adams was able to calculate the pressure-temperature curve of stability for jadeite, as yet not synthesized in the laboratory. In short order, the heats of formation of the plagioclases, alkali feldspars, olivines, and the hypersthenes followed. One of the divi-

dends of the calorimetry program not recorded, was the large number of purified mineral separates prepared that were valuable in related studies.

With the material and financial help of the Geophysical Laboratory, T. G. Sahama was able to build his own calorimeter at the University of Helsinki and continue mineralogical studies with K. J. Neuvonen. In more recent years the determination of thermodynamic properties has been carried out by calculation from more fundamental parameters. The elegant work of A. H. Hofmeister (1983-1987), who used the spectral methods of mineralogy, is outlined in the section on Mineral Physics. The thermochemical properties of silicate glasses and liquids was of special interest to Pascal Richet **(1983-1984)** in collaboration with his colleague in France, Y. Bottinga.

15. Heat and Mass Transport and Kinetics

In all of the phase equilibrium studies carried out at the Geophysical Laboratory, much effort was expended in achieving equilibrium conditions. The products of such reproducible experiments were to be applied to rocks, which were assumed to approach closely equilibrium in the earth. In addition, if the end products of an equilibrium process were known, the non-equilibrium paths could be deduced. It is fortunate that rocks retain some of their non-equilibrium features, thereby revealing the path to their present state of closure. Some of the factors that provide evidence of path, such as heat and mass transport properties as well as process rates, have been investigated by the staff. For convenience, the studies are grouped under diffusion, reaction kinetics, crystal growth and dissolution, metasomatism, and heat transfer.

Diffusion

One of the earliest measurements of diffusion in silicate liquids was made by Bowen (1921). He studied the interdiffusion against gravity (to avoid convection) between a buoyant layer of plagioclase liquid over a denser diopside liquid at about 1500°C. After holding the liquids for a period of time, they were quenched, and the compositions of glass were determined at various levels by measuring their refractive indices, which had been previously calibrated with mixtures of known composition. From the diffusion profiles an "average diffusivity" was calculated. Bowen concluded that the formation of border phases of large bodies of igneous rocks by diffusion could not be considered possible in the time available for a cooling magma. On the other hand, the formation of reaction rims about inclusions could be attributed to diffusion.

A similar experiment was carried out by Yoder (1973) between liquids of basalt and rhyolite compositions at 1200°C and $P(H_2O) = 1$ kbar. The gradients of the major elements after quenching were determined by electron microprobe. He noted the strong coupling of the fluxes of major components and suggested that the structural units in the liquid were related to subspecies of

the minerals.

The self diffusion of ^{45}Ca in diopside at one atmosphere (McCallister **1973-1975, 1978-1979**, Brady **1978-1979**, and Mysen, 1979) and up to 30 kbar (Watson, 1979) were especially informative experiments in regard to exsolution and homogenization processes in pyroxenes. The study of the coupled diffusion of Mg and Fe in olivine by Misener (**1971-1972,** 1972) was carried out at a series of temperatures for the purpose of relating diffusion to the creep rate. The interdiffusion coefficient was found to be sensitive to composition and crystallographic orientation. With the available creep data, Misener was able to demonstrate that the rate-controlling step was not the volume diffusion of cations. Similar coupled diffusion experiments were done by Boctor and Brady (1979) involving S in HgSe (tiemannite).

The diffusion of those elements used in geochronology received considerable attention. For example, the discordant ages that fit a chord across the concordia curve in a plot of $^{207}Pb/^{235}U$ *vs* $^{206}Pb/^{238}U$ were attributed by Tilton (**1956-1965**) to the continuous volume diffusion of Pb from the minerals measured. The paradox of lead loss at the same time on all continents from rocks of the same age was thereby resolved. Other studies included the gain and loss of argon in albite (Laughlin and Yoder, 1971) and the disequilibrium distribution of Th in diopside (Seitz, 1974). The technique of preparing fission-track maps developed by Seitz was successful in obtaining data on the diffusion of Th, U, and O in diopside and fluorapatite. In cooperative studies with DTM, the diffusion of Sr in basalt liquid, studied by Hofmann (1974), was especially pertinent to the small scale heterogeniety of the mantle as well as to applications to Rb-Sr geochronology of magmatic rocks.

Reaction Kinetics

The compositions of exsolved pyroxenes place limits on their conditions of formation and give valuable information on the cooling history of the host rock. In a laboratory study of a synthetic solid solution of Di-En, McCallister measured the rate of exsolution between 1225°C and 1300°C. The observed changes in textures suggested to him that nucleation and growth occur above 1300°C, whereas spinodal decomposition, dependent solely on interdiffusion kinetics, is the appropriate mechanism at lower temperatures. Additional annealing experiments yielded the useful observations, substantiated by bright-field micrographs, that rapid exsolution produces irregular lamellae (spinodal decomposition), whereas slow exsolution has regular lamellae that lie within the coherent solvus.

Another major contribution to the cooling rate problem was made by Seifert and Virgo (1975). By determining the Mg-Fe distribution with Mössbauer spectra in anthophyllite at $P(H_2O)$=2 kbar, 400°-720°C, and various times, they were able to calibrate the order-disorder parameters. In this way the cooling rates of natural anthophyllites could be ascertained. These experiments were seminal to a large range of studies on the rates of metamorphic events.

Other studies included the influence of Zn and Pb on the transformation rates of

metacinnabar to cinnabar (Boctor and McCallister, 1979), the influence of porosity on the reaction rate of periclase and quartz to form forsterite (Brady, 1979), and the rate of homogenization of zoned garnets from metamorphic zones (Muncill, **1983-1989,** and Chamberlain, 1986). The latter study is being applied in New England in order to obtain the cooling rates after peak metamorphism.

Crystal Growth and Dissolution

In 1916 Becker and Day demonstrated by experiment the linear force of growing crystals. They refuted earlier failures by showing that the load increased crystal solubility, so it was necessary to maintain supersaturation for growth. A crystal-growth apparatus was designed by Hostetter **(1912-1919)** in 1919 in which separate thermostats held the source fluid at a higher temperature than the growing crystals. Whereas the growing of crystals under equilibrium conditions was the essence of obtaining phase equilibria diagrams, the growing of large crystals was only undertaken in regard to special measurements.

The persistence of staff members in obtaining phases that are difficult to grow is the source of many legends. One example, is the incredible patience of J. F. Schairer in determining the melting point of albite. The liquid of appropriate composition has to be prepared at a temperature high enough to dissolve the Al_2O_3, but not too high to volatilize the Na. The liquid is quenched to a glass, crushed to homogenize, and remelted at successively lower temperatures. The process of "acclimating" the liquid structure to that close to crystalline albite results in a glass that will produce the appropriate crystalline structure just below the melting point. Only after a five-year effort, was Schairer satisfied that he knew the exact melting point of albite! In the difficult synthesis of pyrope, Boyd and England (1959) resorted to seeding, and its field of stability at high pressures was accurately delineated. Similarly, iron cordierite was grown in the system FeO-Al_2O_3-SiO_2, where previous attempts failed, merely by crushing a natural iron cordierite in the same room, thereby providing inadvertently sufficient dust for seeds!

A highly sophisticated apparatus has recently been assembled by Muncill (1988) for the exact measurement of growth rates of crystals in melt. He measured the isothermal growth kinetics of plagioclase in a haplogranodiorite melt at $P(H_2O)$=2 kbar. The growth rate curves were well modeled by a modification of the theory of Muncill and Lasaga (1987) for a simple system, and the endmember mineral growth curves can now be used to calculate growth rates in multicomponent systems. One of the dividends of the study was a videotape that shows the *in situ* growth and melting of plagioclase and other minerals that led to a visual appreciation of the generation of textures in igneous rocks.

The dissolution of crystals in melt is important to the process of assimilation and provides a test of theories of disequilibrium melting. Minerals were separated from a spinel lherzolite and ground into spheres by Scarfe **(1978-1980)**, E. Takahashi **(1979-1981)** and Yoder (1980) and held in an alkali basalt melt at high

pressures and temperatures. By measuring the change in diameter of the spheres it was found that the rate of dissolution of Gr > Cpx > OPx > Sp > Ol at the range of conditions examined. In general, the rate of dissolution was inversely proportional to the enthalpy of melting. The results are pertinent to the digestion of mantle xenoliths by basaltic magmas during their rapid ascent to the surface. In another series of experiments by Muncill and Dingwell **(1984-1986)** the minerals stable in granitic melts dissolved much more slowly under anhydrous conditions than when volatiles were present.

Metasomatism

The rocks that result from the transport of various volatile and nonvolatile components are usually explained by the diffusion of components through a *static* solvent. For example, mineral textures at metamorphic isograds are often accounted for in this way. A different model, first proposed by Korzhinskii (1936) involves the transport of material by the *flow* of a solvent in response to gradients of fluid pressure. To obtain quantitative information on such infiltration mass transport, J. D. Frantz and A. Weisbrod **(1972-1973)** studied the K_2O-Al_2O_3-SiO_2-H_2O-HCl system in 1973 to identify the sequence of zones of assemblages, the nature of the boundaries or "fronts", and calculate the relative rates of progression of those fronts. They showed that infiltration metasomatism was adequate for long distance transport if there was an adequate fluid pressure gradient, which may remain unchanged regardless of the thickness of the reaction zones. These elegant computations were particularly instructive in predicting reaction paths and the relative velocities of the fronts and hence the relative thickness of the zones. Frantz and Weisbrod took into account the important volume term, introducing a porosity factor, and concluded that unless the rock expands, the infiltration process stops when the pores are filled. Although the infiltration theory is usually applied to metamorphic rocks, Irvine (1980) described the same process for postcumulus magmatic metasomatism to account for the observed compositional variations in the cyclical units of the Muskox intrusion.

In contrast to the graphical solution of Frantz and Weisbrod, a general mathematical model for mass transfer by both infiltration and diffusion was considered by Frantz and Mao (1974) for a multicomponent system. As a demonstration of their theory, the system MgO-SiO_2-H_2O-HCl was examined analytically by them using new and published values of the solubility of the phases and taking porosity, tortuosity, and diffusion coefficients into account. The calculations yielded zone sequences and thicknesses for various times. Further work included the more complex system CaO-MgO-SiO_2-H_2O-CO_2 in which they were able to calculate the sequence of zones and the modal abundance of each of the phases in each zone with the diffusion-infiltration model.

In an attempt to deal with the multicomponent natural systems, R. C. Fletcher and R. J. Vidale (now Buden) **(1974-1975)** proposed in 1975 a finite-difference model

for combined diffusion-infiltration metasomatism. The results were applicable to a wide variety of reactions between fluid-filled cracks and country rock and between incompatible rock assemblages.

Heat transfer

One of the important modes of heat transfer, resulting in metamorphism or magma generation, is from an external planar source. To obtain quantitative information on the rates of heat transfer that determine the width of metamorphic zones and the rate of magma production, Yoder devised an apparatus for measuring, during a constant heat flux, the heat transfer properties in advance of melting and during the partial-melting process for a binary system. Detailed temperature profiles were obtained as a function of time. It was found that the melting process was decoupled from the rapid establishment of the thermal gradient. No evidence was observed for convection even though the properties of the system closely approached those of natural magmas except for linear scale. The results were well represented by a theoretical model, deduced by Finger and Muncill, from which the effective thermal diffusivities could be calculated. The challenge of future experiments is to evaluate quantitatively the combined heat and mass transfer, but that project awaits a suitable theory for guidance.

16. Geochronology

The determination of the age of minerals by the ratio of lead to uranium and thorium was a well established principle by 1928, but a number of difficulties in analysis remained. Methods for the chemical analysis of these elements was given in detail by C. N. Fenner. In the following year, he and C. S. Piggot enlisted the help of F. W. Aston (Cambridge), in making the first calculation of a mineral (thorian uraninite) age on the basis of the specific isotopes of lead determined by mass spectroscopy. The discrepancy between the Pb-U age and Pb-Th age, however, led them to believe that the assumed U-Th equivalence factor may be in error. Although the radioactivity of ocean sediments became a major interest of C. S. Piggot and of W. D. Urry **(1938-1949)**, the age determination of minerals was dominated by others until after WWII.

A program for the determination of the age of minerals was initiated as a collaborative effort with DTM in 1950. The goal was to develop techniques and equipment for determining the age of several common minerals in the same rock for which different methods could yield completely independent ages. Granites of Precambrian age were chosen from which almost a dozen major and accessory minerals were extracted. The methods focused on the accurate measure of the naturally occurring radioactive elements having long half-lives. The parent and daughter elements were concentrated from each separated mineral by ion-exchange resins after spiking the sample with a known amount of a tracer isotope and digesting it in acid. In this way the absolute concentration of the isotopes in the mineral could be ascertained by analysis in a mass spectrometer. The mineral separation and solution chemistry was performed by Davis at the Geophysical

Laboratory and the mass spectrometry was carried out mainly by others at DTM (Aldrich, Wetherill, Tilton). In 1956 Tilton transferred from DTM to the Geophysical Laboratory, and the close cooperation of both groups, with a growing tide of Post-doctoral Fellows and Guest Investigators, was even more effective.

During the 1950-1955 period efforts were concentrated on methods. With the increased sensitivity of the isotope dilution technique, the decay scheme of ^{87}Rb to ^{87}Sr was applied successfully to the Li-bearing micas. The $^{40}K/^{40}Ca$ and $^{40}K/^{40}Ar$ clocks were slowly being developed. The discrepancies between the various clocks were attributed to radiation damage in the zircons, differential leaching in acids, and the transfer of Pb between minerals. These problems were investigated in great detail. The highest ages appeared to be given by the Rb-Sr clock, whereas the lowest age was found by the Th-Pb method. It was deduced that the Rb half-life used in the calculation was apparently too low, so a new half-life was found by assuming the U-Pb age was correct in a mineral giving concordant ages from six locations having a range of ages. Values of the half-life were calculated from the $^{87}Rb/^{87}Sr$ from Rb-bearing minerals at the same localities. The new Rb half-life so determined geologically, eliminated some of the previous discordance, and it remains the present-day value.

With improved techniques, it became possible to begin applying the results to the solution of geological problems. In 1957, after discovering large groups of ancient rocks, the concept developed that the oldest rocks were the "nucleus" of a continent and younger belts of rocks were subsequently added on. Because of the different responses of specific minerals to metamorphism, it became possible to identify the age of the critical events in the geologic history of a region. In 1958 a major problem among discordant age values was resolved. Wetherill (1956) had shown in a plot of $^{206}Pb/^{238}U$ *vs.* $^{207}Pb/^{235}U$ that the various measurements could be related by a line of "concordia". The line was interpreted by Tilton as the locus of apparent ages resulting from the continuous loss by diffusion of Pb. It was this discovery that cleared the way for geological application on a grand scale. Subsequently, the zones of various ages mapped for the U. S. and Canada were confirmed, and the concept of the slow accretion of a continent began to take shape.

Discordant ages continued to plague the analysts, but each time the cause of the discordancy was resolved greater insight into geologic processes emerged. Studies of contact aureoles and eventually regional metamorphic grades illustrated that temperature affected the diffusion of radioactive daughter elements. The apparent ages could then be used for mapping thermal zones in a metamorphosed region.

When the amphiboles and pyroxenes became useful indicators of age, a new range of petrological problems could be tackled. For example, the exceptionally low concentration of U in dunites and websterites suggested that the heat flow in the oceans had to arise from another source rock; eclogite appeared to be adequate. On the other hand, the hornblende-bearing peridotites in some of the islands had enough K to yield the appropriate heat flow. In

addition, the isotopic analysis of Pb indicated that the basalts of the oceanic islands were from heterogeneous sources.

With the arrival of T. Krogh (**1966-1975**) the major thrust of the work turned to the Grenville controversy. The value of analyzing the whole rock as a closed system instead of individual minerals became appreciated. As belts of ages were identified, the region appeared to have analogues with the modern-day, island-arc volcanic zones. The Grenville front was interpreted as an ancient plate boundary where a major metamorphic event took place 1500-1800 m.y. ago with a second major dislocation about 1000 m.y. ago.

In the next ten years (1968-1978) at least three major improvements in technique took place. Krogh invented a new dissolution method for zircons in which a teflon-lined pressure vessel was used at 220°C. X-ray fluorescence became a standard tool for ascertaining the suitability of samples for Rb-Sr analysis. The production and purification (Krogh and Davis, 1975) of the ^{205}Pb spike (with the help of the Holifield National Laboratory) greatly improved the precision of the clocks based on lead. [The use of the ^{205}Pb spike was apparently developed independently at the same time by Tera and Wasserburg (1975)]. With these improvements the ages of zircons in kimberlites were measured by Davis. The African diamond pipes were found to be around 90 m.y. old and two groups of pipes at Yakutsk, U.S.S.R., were 402-443 m.y. and 360-344 m.y. Other studies included the dating of many other geologically significant formations .

With the resignation of Krogh in 1975 and the retirement of Davis in 1978, the geochronology program was reevaluated. It was evident that the Geophysical Laboratory had served its role in pioneering new methods and contributing new concepts to the solution of geologic problems dependent on knowledge of accurate isotopic compositions. The existence of more than 50 laboratories in the U. S. devoted to the dating of rocks and minerals, many headed up by past associates, indicated the field was well established, and it was appropriate for the Laboratory to invest its limited resources in new opportunities.

17. Stable Isotopes

The stable isotopes of the five elements sulfur, carbon, hydrogen, oxygen, and nitrogen (the SCHÖN, or "beautiful" system) provide a special set of tools to investigate both organic and inorganic processes in the earth. The stable isotope program at the Geophysical Laboratory evolved after the arrival of T. C. Hoering (**1959—**). In a very short time, he built a mass spectrometer, with the help of colleagues at DTM, and began applying the C and O isotopes to the solution of organic problems. (The apparatus, with several stages of improvement, served the staff well for exactly 30 years!)

Carbon

The fractionation of C by algae was studied by Abelson (**1953-1971**) and Hoer-

ing (1959) and found to be consistent with the general observation that $^{13}C/^{12}C$ has a lower ratio than carbonate or CO_2 in the environment. They examined a large array of separated, *individual* amino acids with marked isotopic differences, which they attributed to the different biosynthetic pathways by which its constituents are incorporated into the algae. Fatty acids are the precursors of petroleum, which is depleted in ^{13}C relative to whole modern organisms. That depletion was correlated with the low ^{13}C in the fatty acids of living organisms (both plants and animals) examined by Parker **(1961-1963)**. In a study of the organisms of a Texas bay, Parker produced one of the first investigations of an ecosystem in which isotopes were used as tracers of complex food webs. Even the reduced carbon in Precambrian sediments had relatively low ratios of $^{13}C/^{12}C$, according to Hoering's studies. From then on, isotopes became a common tool in studying the processes in living and fossil organic material.

Oxygen

Hoering set out to evaluate the effects of T, P, and X on the isotopic fractionation of oxygen. The solubility of CO_2 in H_2O, for example, resulted in fractionation. Pressure, on the other hand, was found not to be an important variable up to 4 kbar. This systematic study was soon set aside because of the demand to resolve igneous petrological problems. The lavas of Iceland, Snake River Plain, and rocks from the Island Arcs were examined for evidence of sediment contamination and their reaction with meteoric waters, which result in ^{18}O enrichment and depletion, respectively. These results led to a study of the exchange of oxygen between silicates and CO_2 and O_2 by Muehlenbachs **(1971-1974)** and Kushiro. The value of oxygen isotope analysis was rapidly recognized by the metamorphic petrologists, and experiments were designed to test the control of fluid composition by the buffering effects of local mineral assemblages in metamorphic rocks. Even the exchange of oxygen between fossils and minerals in metamorphic rocks were measured (Rumble, Hoering, and Boucot, 1978). The oxygen isotopes were then used to test the permeability of rocks during metamorphism, and eventually in the mapping of the principal hydrothermal pathways in a region. With an ever growing demand for data on a host of problems another mass spectrometer devoted to both carbon and oxygen was acquired, and the oldest machine was modified to investigate nitrogen isotopes. A dramatic new development by Z. Sharp **(1987-1989)** in technique for liberating the oxygen in a mineral on a microscale by laser heating will bring a new dimension to the application of oxygen isotopes to geological problems.

Hydrogen

The second mass spectrometer to be acquired was a special type dedicated to measuring hydrogen and deuterium. Beginning in 1977, Estep (now Fogel, **1977—**) and Hoering studied the fractionation of hydrogen isotopes in cultures of microalgae. They discovered several bio-

logical processes governing the isotope effect when a cell converts water in the medium to organic matter. Such information was necessary for interpreting hydrogen isotopes in the organic matter of sedimentary rocks. For example, marine organisms produce a larger effect than freshwater forms, therefore the source of organic matter in a sediment may be identified. Hydrogen isotopes in lipids were shown to be particularly promising in tracing the sources of plant matter contributed to sediments and petroleum.

Nitrogen

In many parts of the ocean, nitrogen is a limiting nutrient and determines the amount of growth. Variations of $^{15}N/^{14}N$ can be used as tracers in the biogeochemical cycle. Hoering and Ford (1960) studied the isotope fractionation during the fixation of N_2 for four species of bacterium cultured in the laboratory, and they could account for the depletions in the heavy isotope in natural populations. After a hiatus of almost twenty years, the processes of nitrate assimilation and reduction by blue-green algae attracted the attention of Macko **(1981-1983)** and colleagues. Whereas the fractionation of isotopes was small in the fixation of molecular nitrogen, the effect was large by contrast when the source of nitrogen available was in the form of a nitrate. In a collaborative effort of all the members of the Biogeochemical Group, individual amino acids were separated from cultured microorganisms in order to determine the isotopic effects during biochemical synthesis. Hare and Estep (now Fogel) (1983) later explored these differences in biosynthesis to trace metabolism of diets and subsequent diagenesis of modern and fossil animal bones.

In a broad survey of coastal and estuarian sediments, nitrogen isotopes were used to track the mixing and recycling of organic matter in the nearshore environments. Although the processes are indeed complex, Cifuentes **(1984-1988)** and colleagues were able to correlate some of the changes with the processes that tended to consume nitrogen. These results spurred the search for more details on the course of nitrogen in the diets of living organisms. In addition, the value of using several isotope systems was recognized as each system contributed to the definition of the environmental conditions. The multiple use of isotopes was applied on a grand scale in a study of the Delaware estuary. The continuing study has already documented the dramatic seasonal changes that take place in the waters and sediments of the estuary.

Sulfur

New technique usually opens the door to new opportunities, and the use of sulfur isotopes is exemplary. Sabels **(1962)** and Hoering in 1963 found that S could be liberated as SF_6 with the halogen fluorides, and its isotopes measured in the mass spectrometer. The precision in the available mass spectrometer was not sufficient to warrant a major study on the ore minerals. In 1983, however, in a new mass spectrometer fitted with four detectors, Hoering was able to measure the four stable isotopes of S (^{32}S, ^{33}S, ^{34}S, and ^{36}S) simultaneously.

The first applications were to metamorphic rocks in which the alteration of pyrite to pyrrhotite could be studied The flow of fluids from a nearby igneous body were believed to be responsible for the desulfurization process.

Hoering determined the isotopic composition of the sulfur in sedimentary barites ($BaSO_4$) and pyrite from the Archean of southern India. The values for the barite contrast sharply with that of contemporary seawater and appeared to fall in the range for igneous rocks. The values of the coexisting pyrite were even more anomalous. One of the factors Hoering thought might be important in explaining the results, prior to the emergence of the sulfur-reducing bacteria about 2.8 b.y. ago, was the role of atmospheric oxygen in the nonbiological oxidation of reduced sulfur molecules. Other isotopic systems are now being applied to resolve this fascinating paradox in ancient environments.

It is anticipated that any future study will require the use of all the pertinent stable isotope systems, whether the problem be in sedimentary, igneous, or metamorphic rocks. The advantage in having several dedicated mass spectrometers under one roof at the Geophysical Laboratory means there is no impediment to examining the same sample with all the appropriate isotopic systems, and to integrating all the observations by one or several investigators.

18. Biogeochemistry

The application of organic chemistry to geological problems at the Geophysical Laboratory arose out of the research interests of the newly arrived Director, Philip H. Abelson **(1953-1971)**. He used paper chromatography to demonstrate that fossils as old as 300 million years retained amino acids from some of their original proteins. Abelson also determined that the breakdown of amino acids in fossils could be simulated in the laboratory by substituting elevated temperatures for geological time, thereby demonstrating their potential as stratigraphic markers and geochronometric tools. These "chemical fossils" complemented the classical methods of paleontology. The book "Biochemistry of Amino Acids," edited by P. E. Hare **(1963—)**, T. C. Hoering, and F. King, Jr. **(1970-1974)**, has been the definitive work on the subject.

All the amino acids in proteins exist in two configuration that are mirror images, or optical isomers, designated D and L. Hare was successful in separating these isomers with gas chromatography and high-pressure liquid chromatography. He learned that biologically produced amino acids, which are dominantly L, transformed spontaneously to D abiologically as a function of time. Hare developed these observations into a method for dating fossils as old as 20 million years.

From the early paper chromatography, the techniques have evolved to very-high-resolution capillary gas chromatography, high-pressure liquid chromatography and eventually to a combination of gas-chromatographic and mass spectrometric methods. A field-portable, liquid chromatograph was made by Hare to measure amino stratigraphic sections on site. The fluorescent derivatives of NH_2 groups were used

by Hare to analyze for amino acids, peptides, and proteins at an unprecedented low concentration. With this technique he set a limit of less than one part per trillion of amino acids in the returned lunar soil. That method was not only useful in the analysis of fluid inclusions in igneous and metamorphic rocks, but also in the characterization of blood.

The study of amino acids in fossils was followed by investigations of the fatty acids, fatty alcohols, humic acids, prophyrins, kerogen and steranes by Hoering. Of special interest was the demonstration in the laboratory of the reaction of glucose and amino acids to produce melanoidin, a product closely related to humic acid, a significant fraction of the organic material in Holocene sediments. The work outlined the pathway whereby organic matter is effectively removed from the biological carbon cycle and preserved without further metabolization by micro-organisms.

The organic compounds in mildly metamorphosed Precambrian rocks were studied by Hoering. He discovered with the use of $^{13}C/^{12}C$ that the *extractable* organic compounds could be attributed to biological origin. The *insoluble* fraction, kerogen, yielded similar carbon isotope ratios, but the relationship of soluble to the insoluble fractions remained obscure because of potential contamination by modern organisms. Subsequent laboratory experiments on the thermal breakdown of kerogen provided a mechanism for the production of the high-molecular weight components found in petroleum (Hoering, 1984). The hydropyrolysis of shales and other rocks resulted in a method, now standard in the petroleum industry, for evaluating their potential for petroleum generation.

As a result of Hoering's skills in mass spectrometry, the Laboratory has developed dedicated facilities for measuring the stable isotopes of C, H, O, N, and S. For example M. Fogel traced the food chains with hydrogen isotopes. The specific algae on which a snail had been feeding could be identified in confirmation of the adage "you are what you eat." In another important study, Fogel showed with stable isotopes that modern blue-green algae and bacteria growing in CO_2-rich hot springs exhibited the same depletion in ^{13}C as in Precambrian stromatolites formed by the same types of organisms. She demonstrated that the atmosphere in Precambrian times was, therefore, probably enriched in CO_2 by several percent relative to the present day atmosphere.

In an unprecedented collaboration between the Geophysical Laboratory and the Carnegie Institution of Washington's Department of Plant Biology at Stanford, Fogel and Joseph Berry solved one of stable-isotope geochemistry's oldest problems, the "Dole Effect", that was identified in 1936. Atmospheric oxygen is anomalously enriched in the heavy isotope, ^{18}O, and previous studies could not account for this effect. Berry and Fogel discovered that a large isotope fractionation occurred during the uptake of O_2 in photorespiration, a process that accompanies the photosynthesis reaction, and thus they could account for the isotope enrichment.

The presence of a group in biogeochemistry in a geophysical laboratory has yielded many unanticipated dividends. The stable

isotope facilities initially developed by them have been applied to a wide range of problems in sedimentary, igneous, and metamorphic petrology. Their techniques and cooperation have contributed to the understanding of ore deposits, meteorites, and an unusual array of mineralogical problems. They are indeed exemplary of the outstanding results that can be achieved through the Carnegie concept of supporting scholars in fields of their own choice.

19. War-time Studies

World War I

Before hostilities began in 1914, it became evident that the U.S. would be cut off from the European sources of optical glass. Five American companies undertook to make optical glass but the quality was not satisfactory by the time the U.S. entered the war. Because of the critical need for high quality optical glass for military fire-control instruments, methods for its manufacture on a large scale had to be developed. The Council of National Defense appealed to the Geophysical Laboratory for help because it had been engaged for many years in the study of silicate liquids, similar to optical glass, at very high temperatures. It was the only organization in the country with a staff trained in the fundamentals necessary for the manufacture of optical glass.

In April 1917 groups of staff members were sent to the various plants and assigned the responsibility for their operations, whereas others remained at the Laboratory to deal with specific problems. The cooperative attitude of the companies and the direct liaison with the Army through the commissioning of F. E. Wright greatly facilitated the task. The expenses incurred were covered by CIW and no compensation was ever received for their work. The Director, A. L. Day, was eventually designated as "in charge of optical glass production, War Industries Board." After the armistice, the records show that 95% of all optical glass manufactured in the U.S. during the war had been made under the supervision of the staff of the Laboratory.

The manufacturing problems were eventually resolved by putting the secretive cook-book glass making methods on a scientific base. Formulae were devised so that glasses of the appropriate index of refraction or other optical constants could be prepared from the necessary constituents with a minimum of trial and error. Even the barium-rich glasses for aerial camera lenses were made on short notice. Most important contributions were made by Adams and Williamson (1919), who deduced the laws for relieving stress in glass by annealing, and Roberts (**1917-1947,** 1919), who by direct experiment was able to formulate cooling schedules for the glass pots. Sosman (1925) had investigated some of the principles governing the corrosion of the fire clays used in the pots by the molten glass. Other problems such as high dispersion due to successive iron content, stones from the digestion of unsuitable clay pots, cords and striations arising from poor stirring, and strain from rolling were all investigated. Over 20 papers were published by the staff on glass making for the benefit of the future U.S. glass

industry. Of these, the monograph on the properties of glass by G. W. Morey (1938) revised in 1954, remains a standard reference work. Although none of the 20 scientifically-trained staff had previous experience with the manufacture of glass, all used their basic knowledge of silicates to put this new U.S. industry on a sound basis.

The skills of the chemists at the Laboratory were also put to use on the fixation of nitrogen for the manufacture of explosives. Experimental work on the Bucher-cyanide process and the Haber-process were begun in the summer of 1918, and, therefore, had not proceeded far before the end of the war. As repugnant as the task may have been, the Laboratory also investigated some of the physical constants of mustard "gas" in response to a military request.

World War II

The president of CIW, Vannevar Bush, helped establish the National Defense Research Committee in 1940 and served as its chairman. On the 28 June 1941 Bush became Director of the Office of Scientific Research and Development (OSRD) that organized and directed most of the research efforts during the war. In that summer a comprehensive program of defense research was organized to be centered at the Geophysical Laboratory. Some of the staff began to collect information from military and other sources for delineating the lines of research. After the declaration of war in December, the entire staff, supplemented by thirty temporary employees, and all of the resources of the Laboratory were devoted to the tasks ahead.

The Director, L. H. Adams, was appointed chairman of the committee for investigating the erosion of gun barrels due to high-pressure, hot, propellant gases released on firing. As the research proceeded, studies were concentrated on the caliber-50, rapid-fire, aircraft gun where means to counteract severe swaging of the lands and thermal expansion of the barrel became the principal focus. The systematic studies included analysis of the corrosion products of the steel barrels and the propellant gases. By means of isotopically labeled nitrogen in the explosive charge and use of the National Bureau of Standards mass spectrometer, tracer studies revealed the depth of penetration of the gases. Experiments were carried out in high-pressure vessels on controlled explosions to ascertain the internal ballistics and chemical products. Metal with high, hot-hardness, as well as resistance to gas erosion were inserted as short liners in barrels at the origin of rifling. The liners were then tested on a firing range on the Potomac River or in firing ranges installed under the tennis courts (now volley ball court) behind the Laboratory. The superior metal was found to be the cobalt-based alloy, stellite, and it became a most useful material for making hydrothermal pressure vessels after the war.

Another group was concerned with the electroplating of chromium inside the barrel after the liner, in cooperation with the electroplating group at the National Bureau of Standards. Because it was not practical to machine a taper in the large number of barrels required, a method was designed to taper the plating, with increasing thickness of the plate toward the muzzle.

In this way, constriction of the bore compensated for the thermal expansion of the barrel during firing. The increased life and accuracy was documented by test firing on the Geophysical Laboratory ranges. The barrel adapted for military use, still being manufactured today, contains a short stellite liner and a chrome-plated, tapered bore.

Several of the staff members were also helpful at DTM in the development of the proximity fuze for artillery shells. That device was considered to be "the most important technical improvement in weaponry to come out of World War II."

Almost five years of the life of the Geophysical Laboratory were devoted to the war work. The regular staff was paid by CIW; however, the costs of the temporary employees and extra expenses were provided by the government. In 1946 the war work was phased out, the reports written, and a comprehensive review undertaken of the scientific programs in the light of the irreversible changes brought about by World War II.

20. Closing Remarks

The most important factor in the generation of new ideas at the Geophysical Laboratory has been the freedom of choice to follow whatever the staff member believes to be important in the solution of a geological problem. The scientist's overriding goal was to achieve an understanding of the problem so that the critical variables could be recognized, evaluated, and formulated into general concepts useful in solving other problems. The intent, therefore, was to seek knowledge that has broad application to the major problems of the earth. Because no researcher can predict how a fundamental discovery might be applied to future societal needs or problems, there is no test for relevance or applicability applied to the work at the Geophysical Laboratory as is made in industrial organizations. That freedom to follow whatever is critical to the solution of problems is why the Geophysical Laboratory has remained unique among research organizations. The price of such a generous measure of scientific freedom is greater personal responsibility to produce and greater accountability. Although peer review provides for continual testing, the responsibility to produce was self generated and was expressed by the high motivation and involvement of the staff.

Addendum

Most histories record the biased views of a single observer moderated by the written records and evaluations of others. It is difficult to subdue the enthusiasm, admiration and pride the author has for the Geophysical Laboratory and its past and present staff members. Having known almost all of the early staff members and experienced directly slightly more than half of the life of the Laboratory, the author might be forgiven for any excessive claims of discovery attributed to the staff. All science is built on the discoveries of others, and it is not always evident who arrives at the pinnacle of an idea first, demonstrates its proof, applies the solution to a geological problem, or capitalizes on its promotion. The

personal satisfaction of contributing to the growth of science is adequate reward in itself.

The scientific history presented above was prepared on short notice, with a minimum of time for reflection, preparatory to the departure of the staff from the Geophysical Laboratory building on 2801 Upton St., N. W., Washington, D. C. to a new building on the DTM campus. It is anticipated that a more detailed, documented history will be prepared in the future.

PUBLICATIONS

Reprints of the numbered publications listed below are available, except where noted, at no charge from the Librarian, Geophysical Laboratory, 2801 Upton St., N.W, Washington, D.C. 20008-3898, U.S.A. Please give reprint number(s) when ordering.

Angel, R. J., High-pressure structure of anorthite, *Am. Mineral., 73*, 1114-1119, 1988 (G.L. Paper 2089).

Angel, R. J., and L. W. Finger, Polymorphism of nickel sulfate hexahydrate, *Acta Crystallogr., Sect. C, 44*, 1869-1873, 1988 (G.L. Paper 2094).

Angel, R. J., T. Gasparik, and L. W. Finger, Crystal structure of a Cr^{2+}-bearing pyroxene, *Am. Mineral., 74,* 599-603, 1989 (G.L. Paper 2123).

Angel, R. J., S. A. T. Redfern, and N. L. Ross, Spontaneous strain below the $I\bar{1}$-$P\bar{1}$ transition in anorthite at pressure, *Phys. Chem. Minerals, 16*, 539-544, 1989 (G. L. Paper 2122).

Angel, R. J., L. W. Finger, R. M. Hazen, M. Kanzaki, D. J. Weidner, R. C. Liebermann, and D. R. Veblen, Structure and twinning of single-crystal $MgSiO_3$ garnet synthesized at 17 GPa and 1800°C, *Am. Mineral., 74*, 509-512, 1989 (G.L. Paper 2120).

Arashi, H., O. Shimomura, T.Yagi, S. Akimoto, and Y. Kudoh, *P-T* phase diagram of ZrO_2 determined by *in situ* X-ray diffraction measurements at high pressures and high temperatures, in *Advances in Ceramics, Vol. 24: Science and Technology of Zirconia III,* The American Ceramic Society, Inc., Westerville, Ohio, pp. 493-500, 1988 (No reprints available from Geophysical Laboratory).

Boctor, N. Z., and G. Kullerud, Phase relations in the mercury-selenium sulfur system at 200° to 700°C, *J. Solid State Chem.,* in press.

Boyd, F. R., Where do we go from here?, in *Kimberlite and Related Rocks, Proceedings of the Fourth International Kimberlite Conference, Perth, Australia, August, 1986,* J. Ross, ed., Geological Society of Australia, Special Publication No. 14, Vol. 2, Blackwell Scientific Pubns, Carleton, Victoria, Australia, pp. 1239-1251, 1989 (G.L. Paper 2142; no reprints available for distribution).

Boyd, F. R., Compositional distinction between oceanic and cratonic lithosphere, *Earth Planet. Sci. Lett.,* in press.

Chamberlain, C. P., P. H. Zeitler, and M. Q. Jan, The dynamics of the suture between the Kohistan Island arc and the Indian plate in the Himalaya of Pakistan, *J. Metamorphic Geol., 7,* 135-149, 1989.

Chamberlain, C. P., and M. Q. Jan, Petrologic constraints on the tectonic development of the Nanga Parbut - Haramosh Massif, Himalayas, *Spec. Pap. - Geol. Soc. Amer.,* in press.

Chamberlain, C. P., and D. Rumble, Thermal anomalies in a regional metamorphic terrane: An isotopic study of the role of fluids, *J. Petrol., 29,* 1215-1232, 1988 (G.L. Paper 2129).

Chamberlain, C. P., and D. Rumble, III, The influence of fluids on the thermal history of a metamorphic terrane, New Hampshire, USA. *J. Geol. Soc. London* (Spec. Issue), in press.

Chayes, F., The Delesse relation in a concentrically zoned sphere. I. The section-number bias, *Math. Geol., 21*, 319-329, 1989 (G.L. Paper 2134).

Cifuentes, L. A., J. H. Sharp, and M. L. Fogel, Stable carbon and nitrogen isotope biogeochemistry in the Delaware Estuary, *Limnol. and Oceanogr., 33*, 1102-1115, 1988 (G.L. Paper 2095).

Day, H. W., and C. P. Chamberlain, Implications of thermal and baric structure for controls on metamorphism in northern New England, *J. Geol. Soc. London*, in press.

Dingwell, D. B., The structures and properties of fluorine-rich magmas: a review of experimental studies, in *Recent Advances in the Geology of Granite-Related Mineral Deposits,* Proceedings of the CIM Conference on Granite-Related Mineral Deposits, Halifax, Canada, September, 1985, R. P. Taylor and D. F. Strong, eds., *CIM Bull. Spec Vol. 39,* pp. 1-12, The Canadian

Institute of Mining and Metallurgy, Montreal 1988 (G.L. Paper 2098).

Dymek, R. F., S. C. Brothers, and C. M. Schiffries, Petrogenesis of ultramafic metamorphic rocks from the 3800 Ma Isua Supracrustal Belt, West Greenland, *J. Petrol., 29,* 1353-1397, 1988.

Finger, L. W., R. M. Hazen, and R. J. Hemley, $BaCuSi_2O_6$: A new cyclosilicate with four-membered tetrahedral rings, *Am. Mineral., 74,* 952-955, 1989 (G.L. Paper 2131).

Fogel, M. L., E. K. Sprague, A. P. Gize, and R. W. Frey, Diagenesis of organic matter in Georgia salt marshes, *Estuarine, Coastal Shelf Science, 28,* 211-230, 1989 (G.L. Paper 2115).

Frantz, J. D., Y. G. Zhang, D. D. Hickmott, and T. C. Hoering, Hydrothermal reactions involving equilibrium between minerals and mixed volatiles. 1. Techniques for experimentally loading and analyzing gases and their application to synthetic fluid inclusions, *Chem. Geol.,* in press.

Guy, R. D., J. A. Berry, M. L. Fogel, and T. C. Hoering, Differential fractionation of oxygen isotopes by cyanide-resistant and cyanide-sensitive respiration in plants, *Planta, 177,* 483-491, 1989 (G.L. Paper 2138).

Hare, P. E., Chiral mobile phases for the enantiomeric resolution of amino acids, in *Chromatographic Chiral Separations,* L. J. Crane and M. Zief, eds., Marcel Dekker, New York, pp. 165-177, 1988 (G.L. Paper 2105).

Hare, P. E., and P. A. St. John, Detection limits for amino acids in environmental samples, in *Detection in Analytical Chemistry: Importance, Theory, and Practice,* L. A. Curie, ed., ACS Symposium Series 361, American Chemical Society, Washington, D.C., Chapt. 15., pp. 275-285, 1988 (G.L. Paper 2106; no reprints available for distribution).

Hare, P. E., Detection limits in amino acid analysis: An overview, in *Methods in Protein Sequence Analysis,* (Proceedings of the 7th International Conference, Berlin, July 3-8, 1988), B. Wittman-Liebold, ed., Springer-Verlag, New York, Chapt. 1.1, pp. 2-9, 1989 (G.L. Paper 2141; no reprints available for distribution).

Hazen, R. M., A useful fiction: polyhedral modeling of mineral properties, *Am. J. Sci.,* Special ("Wones") Volume, *288-A,* 242-269, 1988 (G.L. Paper 2059).

Hazen, R. M., Understanding perovskites of benefit to science and industry - an interdisciplinary approach, *Earth in Space, 1,* No. 3,.8-10, 1988 (G.L. Paper 2112; no reprints available for distribution).

Hazen, R. M., and Z. D. Sharp, Compressibility of sodalite and scapolite, *Am. Mineral., 73,* 1120-1122, 1988 (G.L. Paper 2088).

Hazen, R. M., and L. W. Finger, High-pressure crystal chemistry of andradite and pyrope: Revised procedures for high-pressure diffraction experiments, *Am. Mineral., 74,* 352-359, 1989 (G.L. Paper 2114).

Hazen, R. M., L. W. Finger, and D. E. Morris, Crystal structure of $DyBa_2Cu_4O_8$: A new 77 K bulk superconductor, *Appl. Phys. Lett., 4,* 1057-1059, 1989 (G.L. Paper 2113).

Hazen, R. M., *The Breakthrough: The Race for the Superconductor,* Summit Books, New York, 1988; Ballantine/Science, New York, 1989. Foreign editions: *Superconductors: The Breakthrough,* Unwin Hyman Ltd., London, 1988; *La Course Aux Supraconducteurs,* Librairie Plon, Paris, 1989; *De Dag Dat de Wetenschap Wild Werd,* Uitgeverij Lannoo, Tielt, The Netherlands, 1989 (G.L.Paper 2073; obtainable by purchase only from the publishers).

Hemley, R. J., R. E. Cohen, A. Yeganeh-Haeri, H. K. Mao, D. J. Weidner, and E. Ito, Raman spectroscopy and lattice dynamics of $MgSiO_3$-perovskite at high pressure, in *Perovskite: A Structure of Great Interest to Geophysics and Materials Science,* A. Navrotsky and D. J. Weidner, eds., American Geophysical Union, Washington, D. C., pp. 35-53, 1989 (G.L. Paper 2111).

Hemley, R. J., A. P. Jephcoat, C. S. Zha, H. K. Mao, L. W. Finger, and D. E. Cox, Equation of state of solid neon from X-ray diffraction measurements to 110 GPa, in *International AIRAPT Conference, XIth, Kiev, USSR, July 12-17, 1987, Vol. 3.* High Pressure Science and Technology: Proceedings, N. V. Novikov and Ye M. Chistyakov, eds., Naukova Dumka, Kiev, pp. 211-217, 1989 (G.L. Paper 2135; no reprints available for distribution).

Hemley, R. J., L. C. Chen, and H. K. Mao, New transformations between crystalline and amorphous ice, *Nature, 338,* 638-640, 1989 (G.L. Paper 2124).

Hemley, R. J., C. S. Zha, A. P. Jephcoat, H. K. Mao, L. W. Finger, and D. E. Cox, X-ray diffraction and equation of state of solid neon to 110 GPa, *Phys. Rev. B, 39*, 11820-11827, 1989 (G.L. Paper 2118).

Hickmott, D. D., and N. Shimizu, Trace element zoning in garnets from the Kwoiek area, British Columbia: Possible influence of interface kinetics in metamorphism, *Contrib. Mineral. Petrol.*, in press (No reprints will be available from Geophysical Laboratory).

Hoering, T. C., Isomers of the monomethyl, acyclic hydrocarbons in the Messel shale and in petroleums, *Cour. Forsch. Senkenberg, 107*, 79-87, 1988 (G.L. Paper 2116).

Hofmeister, A. M., J. Xu, H. K. Mao, P. M. Bell, and T. C. Hoering, Thermodynamics of Fe-Mg olivines at mantle pressures: Mid- and far-infrared spectroscopy at high pressure, *Am. Mineral., 74*, 281-306, 1989 (G.L. Paper 2097).

Irvine, T. N., A global convection framework: Evidence for symmetry and stratification in the Earth's convection system, *Econ. Geol.*, in press.

Kubicki, J. D., and A. C. Lasaga, Molecular dynamics of SiO_2 melt and glass: Ionic and covalent models, *Am. Mineral., 73*, 941-955, 1988 (No reprints available from Geophysical Laboratory).

Kudoh, Y., E. Ito, and H. Takeda, High-pressure structural study on perovskite-type $MgSiO_3$ - A summary, in *Perovskite: A Structure of Great Interest to Geophysics and Materials Science*, A Navrotsky and D. J. Weidner, eds., Geophysical Monograph 45, American Geophysicial Union, Washington, D. C., pp. 33-34, 1989 (No reprints available from Geophysical Laboratory).

Kushiro, I., Density of basalt magmas at high pressures and its petrological application, in *Advances in Physical Geochemistry*, "Physical Chemistry of Magma", L. L. Perchuk and I. Kushiro, eds., Springer-Verlag, New York, in press.

Kushiro, I., and B. O. Mysen, Experimental studies of the system Mg_2-SiO_4-H_2 at pressures 10^{-2}-10^{-10} bar and temperatures to 1650°C: Application to condensation and vaporization processes in the primitive solar nebula, in *Advances in Physical Geochemistry*, L. L. Perchuk, ed., Springer-Verlag, New York, in press.

Luth, R. W., Natural versus experimental control of oxidation state: Effects on the composition and speciation of C-O-H fluids, *Am. Mineral., 74*, 50-57, 1989 (G.L. Paper 2110).

Luth, R. W., and G. E. Muncill, Fluorine in aluminosilicate systems: Phase relations in the system $NaAlSi_3O_8$-$CaAl_2Si_2O_8$-F_2O_{-1}, *Geochim. Cosmochim. Acta*, in press (G.L. Paper 2136).

Luth, R. W., D. Virgo, F. R. Boyd, and B. J. Wood, Ferric iron in mantle-derived garnets: Implications for thermobarometry and for the oxidation state of the mantle, *Contrib. Mineral. Petrol.*, in press.

Mao, H. K., Static compression of simple molecular system in the megabar range, in *Simple Molecular Systems at Very High Density, Vol. 186*, Proceedings of a NATO Advance Research Workshop/European Society Workshop, March 28-April 6, 1988, Les Houches, France, A. Polian, P. Loubeyre, and N. Boccara, eds., Plenum Publ. Corp., New York, pp. 221-236, 1989 (G.L. Paper 2100).

Mao, H. K., R. J. Hemley, Y. Wu, A. P. Jephcoat, L. W. Finger, C. S. Zha, and W. A. Bassett, High-pressure phase diagram and equation of state of solid helium from single crystal X-ray diffraction to 23.3 GPa, *Phys. Rev. Lett., 60*, 2649-2652, 1988 (G.L. Paper 2083).

Mao, H. K., and R. J. Hemley, Optical studies of hydrogen above 200 gigapascals: Evidence for metallization by band overlap, *Science, 244*, 1462-1465, 1989 (G.L. Paper 2130).

Mao, H. K., L. C. Chen, R. J. Hemley, A. P. Jephcoat, Y. Wu, and W. A. Bassett, Stability and equation of state of $CaSiO_3$-perovskite to 134 GPa, *J. Geophys. Res.*, in press.

McMillan, P., and N. Ross, The Raman spectra of several orthorhombic calcium oxide perovskites, *Phys. Chem. Minerals, 16*, 21-28, 1988 (No reprints available from Geophysical Laboratory).

Morris, D. E., J. H. Nickel, J. Y. T. Wei, N. G. Asmar, J. S. Scott, U. M. Scheven, C. T. Hultgren, A. G. Markelz, J. E. Post, P. J. Heaney, D. R. Veblen, and R. M. Hazen, Eight new high-temperature superconductors with the 1:2:4 structure, *Phys. Rev. B, 39*, 7347-7350, 1989 (G.L. Paper 2127).

Muncill, G. E., and A. C. Lasaga, Crystal growth kinetics of plagioclase in igneous systems: Isothermal H_2O-saturated experiments and

extension of a growth model to complex silicate melts, *Am. Mineral., 73*, 982-992, 1988 (G.L. Paper 2087).

Mysen, B. O., and D. Virgo, Redox equilibria, structure, and properties of Fe-bearing aluminosilicate melts: Relationships among temperature, composition, and oxygen fugacity in the system Na_2O-Al_2O_3-SiO_2-Fe-O, *Am. Mineral., 74*, 58-76, 1989 (G.L. Paper 2108).

Mysen, B. O., Relations between structure, redox equilibria of iron, and properties of magmatic liquids, in *Advances in Physical Geochemistry*, L. L. Perchuk and I. Kushiro, eds., Springer-Verlag, New York, in press.

Mysen, B. O., Volatiles in magmatic liquids, in *Progress in Physico-Chemical Petrology* (D. S. Korzhinskii Memorial Volume), L. L. Perchuk, ed., Cambridge University Press, New York, in press.

Mysen, B. O., Distribution of aluminum between structural units in peralkaline aluminosilicate melts in the systems Li_2O-Al_2O_3-SiO_2, Na_2O-Al_2O_3-SiO_2 and K_2O-$A1_2O_3$-SiO_2, *Am. Mineral.*,in press.

Powell, E. N., A. Logan, R. J. Stanton, Jr., D. J. Davies, and P. E. Hare, Estimating time-since-death from the free amino acid content of the mollusc shell: A measure of time averaging in modern death assemblages? Description of the technique, *Palaios, 4*, 16-31, 1989 (G.L. Paper 2140; no reprints available for distribution).

Prewitt, C. T., *Annual Report of the Director of the Geophysical Laboratory, Carnegie Instn. Washington, 1987-1988*, Geophysical Laboratory, Washington, D.C., 1988 (G.L. Paper 2102).

Richet, P., J. A. Xu, and H. K. Mao, Quasi-hydrostatic compression of ruby to 500 Kbar, *Phys. Chem. Minerals, 16*, 207-211, 1988 (G.L. Paper 2071).

Richet, P., H. K. Mao, and P. M. Bell, Static compression and equation of state of CaO to 1.35 Mbar, *J. Geophys. Res., 93*, B12, 15279-15288, 1988 (G.L. Paper 2099).

Richet, P., H. K. Mao, and P. M. Bell, Bulk moduli of magnesiowüstites from static compression measurements, *J. Geophys. Res., 94, B3*, 3037-3045, 1989 (G.L. Paper 2109).

Ross, N. L., and A. Navrotsky, Study of the $MgGeO_3$ polymorphs (orthopyroxene, clinopyroxene, and ilmenite structures) by calorimetry, spectroscopy and phase equilibria, *Am. Mineral., 73*, 1355-1365, 1988 (No reprints available from Geophysical Laboratory).

Ross, N. L., and R. M. Hazen, Single crystal X-ray diffraction study of $MgSiO_3$ perovskite from 77 to 400 K, *Phys. Chem. Minerals, 16*, 415-420, 1989 (G.L. Paper 2119).

Ross, N. L., J. Ko, and C. T. Prewitt, A new phase transition in $MnTiO_3$: $LiNbO_3$ perovskite structure, *Phys. Chem. Minerals,* in press (G.L. Paper 2137).

Rumble, D., III, and C. P. Chamberlain, Graphite vein deposits of New Hampshire, in *New England Intercollegiate Geological Conference Guidebook, 80th Annual Meeting*, W. A. Bothner, ed., University of New Hampshire, Durham, NH, pp. 241-255, 1988 (G.L. Paper 2104; no reprints available for distribution).

Rumble, D., III, C. P. Chamberlain, D. K. Zeitler, and B. Barriero, Hydrothermal graphite veins and Acadian granulite facies metamorphism, New Hampshire, USA, in *Fluid Movements, Element Transport, and the Composition of the Crust,* D. Bridgwater, ed., Kluwer Academic Publ., Dordrecht, in press (G.L. Paper 2128).

Schiffries, C. M., Liquid-absent fluid inclusions and phase equilibria in the system $CaCl_2$ - NaCl - H_2O, *Geochim. Cosmochim. Acta, in press,* 1989.

Schiffries, C. M., and D. M. Rye, Stable isotope systematics of the Bushveld Complex: I. Constraints in magmatic processes in layered intrusions, *Am. J. Sci., in press,* 1989.

Schiffries, C. M., amd D. M. Rye, Stable isotope systematics of the Bushveld Complex: II. Constraints on hydrothermal processes in layered intrusions, *Am. J. Sci., in press,* 1989.

Sharp, Z. D., G. R. Helffrich, S. R. Bohlen, and E. J. Essene, The stability of sodalite in the system $NaAlSiO_4$-NaCl, *Geochim. Cosmochim. Acta,* in press (G.L. Paper 2133).

Sheng, Z. Z., A. M. Hermann, D. C. Vier, S. Schultz, S. B. Oseroff, D. J. George, and R. M. Hazen, Superconductivity in the T1-Sr-Ca-Cu-O system, *Phys. Rev. B, 38*, 7074-7076, 1988 (G.L. Paper 2103)

Spear, F. S., D. D. Hickmott, and J. Selverstone, The metamorphic consequences of thrust emplacement, Fall Mountain, New Hampshire, *Geol.Soc. Am. Bull.*, in press (No reprints will be

available from Geophysical Laboratory).

Stafford, T. W., Jr., and R. A. Tyson, Accelerator radiocarbon dates on charcoal, shell, and human bone from the Del Mar site, California, *Am. Antiq., 54*, 389-395, 1989 (G.L. Paper 2125).

Stafford, T. W., Jr., Extraction of organic fractions from fossil bones for radiocarbon dating and stable isotope analysis, *J. Archaeol. Sci.* , in press.

Stathoplos, Linda, and P. E. Hare, Amino acids in planktonic foraminifera: Are they phylogenetically useful? in *Origin, Evolution, and Modern Aspects of Biomineralization in Plants and Animals, Proceedings of the Fifth International Symposium on Biomineralization,* R. E. Crick, ed., Plenum Publ. Co., New York, in press.

Ulmer, P., The dependence of the Fe^{2+}-Mg cation-partitioning between olivine and basaltic liquid on pressure, temperature, and composition: An experimental study to 30 kbars, *Contrib. Mineral. Petrol., 101*, 261-273, 1989.(G.L. Paper 2139).

Velinsky, D. J., J. R. Pennock, J. H. Sharp, L. A. Cifuentes, and M. L. Fogel, Determination of the isotopic composition of ammonium-nitrogen at the natural abundance level from estuarine waters, *Marine Chemistry*, in press (G.L. Paper 2126).

Wood, B. J., and D. Virgo, Upper mantle oxidation state: Ferric iron contents of lherzolite spinels by ^{57}Fe Mössbauer spectroscopy and resultant oxygen fugacities, *Geochim. Cosmochim. Acta, 53*, 1277-1291, 1989 (G.L. Paper 2121).

Yoder, H. S., Jr., The great basaltic "floods," *South African J. Geol., 91* (Alex. L. du Toit Memorial Lectures, No. 20), 139-156, 1988 (G.L. Paper 2085).

Zhang, Y. G., and J. D. Frantz, Experimental determination of the compositional limits of immiscibility in the system $CaCl_2$-H_2-O-CO_2 at high temperatures and pressures using synthetic fluid inclusions, *Chem. Geol., 74*, 289-308, 1989 (G.L. Paper 2107).

PERSONNEL

July 1, 1988 to June 30, 1989

Research Staff

Charles T. Prewitt, Director
Peter M. Bell[1]
Francis R. Boyd, Jr.
Larry W. Finger
Marilyn L. Fogel
John D. Frantz
P. Edgar Hare
Robert M. Hazen
Russell J. Hemley
Thomas C. Hoering
T. Neil Irvine
Ho-Kwang Mao
Bjorn O. Mysen
Douglas Rumble III
David Virgo
Hatten S. Yoder, Jr.

Keck Earth Sciences Research Scholar

Gregory E. Muncill[2]

Postdoctoral Associates

Liang-chen Chen[3]
Ming Sheng Peng[4]
Jinfu Shu
Ellen K. Wright

Research Associates

David Velinsky
Nick Oliver[5]

Postdoctoral Fellows

Ross Angel[6]
Luis Cifuentes[7]
Donald Hickmott
Andrew P. Jephcoat[8]
Yasuhiro Kudoh[9]
Robert W. Luth[10]
Nancy Ross[11]
Craig Schiffries
Zachary Sharp[12]
Peter Ulmer[13]
Yi-gang Zhang[14]

Predoctoral Fellows

Constance Bertka
Yingwei Fei
Matthew Hoch[16]
Kevin Mandernack[17]
Linda Stathoplos[18]

Research Interns

Brad Herman[19]

Virginia Mattingly[20]
William Merrill[21]

Supporting Staff

Andrew J. Antoszyk, Shop Foreman
Bobbie Brown, Instrument Maker[22]
Stephen D. Coley, Sr., Instrument Maker
Roy R. Dingus, Instrument Maker[23]
David J. George, Electronics Technician
Christos Hadidiacos, Electronics Engineer
Marjorie E. Imlay, Assistant to the Director
Lavonne Lela, Librarian
Harvey J. Lutz, Technician
Mabel B. Mattingly, Department Secretary
Mary Moore, Word Processor Operator—Receptionist
Lawrence B. Patrick, Maintenance Supervisor
David Ratliff, Jr., Maintenance Technician
Pedro J. Roa, Maintenance Technician
Susan Schmidt, Coordinating Secretary
John M. Straub, Business Manager
Mark Vergnetti, Instrument Maker[24]

Visiting Investigators

Ronald E. Cohen, Naval Research Laboratory
David H. Freeman, University of Maryland
Jaidong Ko, SUNY, Stony Brook
James Kubicki, Yale University
Julie Kokis, George Washington University
Yali Su, University of Maryland
Bradley Tebo, Scripps Institution of Oceanography
Noreen Tuross, Smithsonian Institution
Donald J. Weidner, SUNY, Stony Brook

Emeritus

Hatten S. Yoder, Jr., Director Emeritus
Felix Chayes, Petrologist Emeritus

---

[1]Retired June 30, 1989.
[2]Expiration of Keck Fellowship Arpil 30, 1989.
[3]To June 30, 1989.
[4]From July 1, 1988.
[5]To June 1, 1989.
[6]To September 30, 1988.
[7]To September 1, 1988.
[8]To February 28, 1989.
[9]From September 1, 1988.
[10]To September 30, 1988.
[11]To October 30, 1988.
[12]To June 30, 1989.
[13]To September 30, 1988.
[14]From July 1, 1988 to June 30, 1989.
[15]From July 1, 1988 to June 30, 1989.
[16]From July 1, 1988.
[17]From July 1, 1988.
[18]To June 30, 1989.
[19]From June 1, 1989.
[20]From June 1, 1989.
[21]From June 1, 1989.
[22]From July 1, 1988.
[23]Transferred to D.T.M. February 1989.
[24]From April 1, 1989.